A QUANTUM FIELD THEORETIC FORMULATION OF ATOM-BOSON INTERACTIONS

A thesis submitted in partial fulfilment
of the requirements for the Degree of
Doctor of Philosophy in Physics
in the University of Canterbury
Christchurch New Zealand

by

B.J. McKenzie

University of Canterbury
1978

CONTENTS

To

Jane

ACKNOWLEDGMENTS.

Special thanks are due to my Supervisor, Dr. Geoff. E. Stedman, for his friendship, interest and encouragement during the course of this work. I would also like to thank Professor B.G. Wybourne for his sincere interest in my progress, especially during my Supervisor' study leave.

Many staff and fellow research students have given me encouragement and advice but special mention is due to Steven H. Payne who often acted as a "sounding board" for new ideas.

The New Zealand University Grants Committee provided a Post Graduate Scholarship and a Shirtcliffe Fellowship for which I am grateful.

Finally I would like to thank Mrs. Mary Boswell for typing this thesis and my wife, Jane, for her understanding and help in preparing the text for typing.

ABSTRACT

The results from the application of quantum field theoretic techniques to a number of problems in quantum optics are presented. We firstly evaluate the relative convenience of three possible mappings of spin operators to fermion operators that enable the usual Feynman diagram approach to be used. These were the drone, quasi-spin and iso-spin mappings which were compared by applying each to an analysis of the coupled spin-phonon modes problem. Using the iso-spin mapping we derive methods useful in applications to ionic level systems. These are then used to develop diagram formulations of: the single-ion absorption spectrum, absorption pair spectra and single-ion Raman spectra. The present work on the single-ion absorption spectrum extends the results of previous workers while the pair spectrum formalism is a new approach enabling a straightforward analysis of Kramers ion pairs to be presented. The formalism for Raman scattering is applicable to both time-dependent and steady-state situations and also to both the near-resonant and for far from resonant regimes.

CHAPTER 1: INTRODUCTION

1.1 Diagram technique

The method of quantum field theory with its associated Feynman diagrams as applied to many-body systems is a powerful and general technique for the investigation of a wide range of effects. In this work we have used this method to formulate a description of a number of phenomena in the field of optical absorption and scattering from impurity ions in crystals with special regard to the role of phonon processes in the host crystal. We have concentrated on obtaining expressions for the resulting spectral lineshapes and developing approximation schemes allowing analytic results to be obtained from these.

One of the most useful aspects of the technique is the ability to represent perturbation expansions in terms of Feynman diagrams. This enables the manipulation, identification and separation of terms to be achieved with greater ease than would be possible with the corresponding algebraic expressions. Furthermore, the diagrams enable group-theoretical simplifications and calculations to be performed using the diagram rules given by Stedman (1974, 1976b).

The generality of the method is an obvious advantage which includes for example the ability to include all modes of the phonon field simultaneously. The complexity that results from more fundamental approaches to quantum optics often restricts the coupling of the atomic system to only one or two reservoir modes which can result in qualitative errors (e.g. Abou-Ghantous *et.al.* 1974).

1.2 Structure of this work

The background notation and results of the diagram technique are presented in Chapter 2. This includes a discussion of the relative merits of three possible descriptions of the ionic system and a calculation of coupled spin-phonon modes. A formalism that describes the

single-ion absorption spectrum is presented in Chapter 3 and the resulting spectrum calculated. This work is extended in Chapter 4 to describe the pair or two-ion absorption spectrum with special emphasis being given to a Kramers ion system. In Chapter 5 we develop a formalism for the description of Raman scattering from impurity ions with the steady-state and time dependent spectrum being calculated in Chapters 6 and 7 respectively. Chapter 9 is devoted to a numerical study of a model three level system to investigate the accuracy of various approximation schemes and to give a feeling for the type of lineshape obtained when these approximations are relaxed. General conclusions of the work are presented in Chapter 9 and the appendices are devoted to the derivation of various equations in an attempt to improve the readability of the main text.

CHAPTER 2: FIELD THEORETIC FORMULATION

2.1 General overview

This chapter is devoted to a general introduction to the diagram method of many-body theory presenting the basic results and our notation. The method arose from the field of relativistic quantum field theory (Q.F.T.) developed in the late 1940's by workers such as Feynman (1949a, b) and Dyson (1949a,b). These techniques were first adapted to many-body theory at finite temperatures by Matsubara (1955) and were extended by Martin and Schwinger (1959), Galitskii and Migdal (1958) and Abrikosov *et.al.* (1959). Three excellent general references on the method are the books by Schultz (1964), Abrikosov *et.al.* (1963) and Fetter and Walecka (1971).

To particularize we take a system of fermions described, in second quantization formalism, by the Hamiltonian

$$\mathcal{H}_f^0 = \sum_n \varepsilon_n \, a_n^\dagger \, a_n \qquad (2.1.)$$

where $a_n^\dagger$, a_n are fermion operators that satisfy the commutation relation $[a_n, a_{n'}^\dagger] = \delta_{nn'}$, which respectively create, annihilate a fermion with energy ε_n. Further suppose that these fermions are interacting with a phonon bath satisfying

$$\mathcal{H}_{\text{phonon}}^0 = \sum_k \omega_k \, b_k^\dagger \, b_k \qquad (2.2)$$

where $b_k^\dagger$, b_k are boson operators, satisfying $\{b_k, b_{k'}^\dagger\} = \delta_{kk'}$, which respectively create, annihilate a boson with wavevector[1] $\underline{k}$ and energy ω_k.

[1] The parameter k is to be regarded as representing both wavevector and polarization index. E.g.

$$k \equiv \underline{k}j$$

$$-k \equiv (-\underline{k})j$$

$$\sum_k \equiv \sum_{\underline{k}} \sum_j$$

The interaction between the two systems is described by the Hamiltonian

$$\mathcal{H}^{int} = \sum_{k} \sum_{mn} V^{k}_{mn} a^{\dagger}_{m} a_{n} \phi_{k} \qquad (2.3)$$

where $\phi_k = b_k + b^{\dagger}_{-k}$. We can regard each term in this sum as describing the destruction of a fermion with energy ε_n and creation of a fermion with energy ε_m along with *either* the destruction *or* creation of a phonon with energy ω_k. The coupling coefficient V^k_{mn} is a measure of the strength of the interaction between the systems.

2.1.1 Greens Functions

The basic element of this approach to many-body theory is the thermal Greens function (G.F.). This is because it is possible to relate basic experimental observables such as spectra, dielectric constants, dispersion relations to one-, two- or multi-particle G.F.'s. Elementary accounts of these principles can be found in Stedman (1968) and the humorous book by Mattuck (1976).

The one-particle GF is defined by

$$G_{mn}(\tau) = - \langle T_{\tau} \{ a_m(\tau)\ a^{\dagger}_{n}(0) \} \rangle \qquad (2.4)$$

where $\langle \cdots \rangle$ denotes the average $\mathrm{Tr}(e^{-\beta\mathcal{H}} \cdots)/\mathrm{Tr}(e^{-\beta\mathcal{H}})$, $\beta = (k_B T)^{-1}$ with T being the temperature of the system, (assumed to be in thermal equilibrium), and T_τ is the time ordering operator which orders the operators it acts on in order of decreasing time (i.e. τ) with a factor (-1) for each pair of fermion operators commuted. For example

$$T_{\tau}\{a(\tau_1)b(\tau_2)\} = \begin{cases} a(\tau_1)b(\tau_2) & \tau_1 > \tau_2 \\ \pm b(\tau_2)a(\tau_1) & \tau_2 > \tau_1 \end{cases} \qquad (2.5)$$

+ or - being for bosons and fermions respectively. The time dependence of $O(\tau)$ is defined as $e^{\mathcal{H}\tau} O e^{-\mathcal{H}\tau}$.

Similarly the two-particle fermion G.F. is defined by

$$G_{mnst}(\tau_1,\tau_2,\tau_3) = \langle T_\tau\{a_m(\tau_1)a_n(\tau_2)a_s^\dagger(\tau_3)a_t^\dagger(0)\}\rangle \qquad (2.6)$$

and so on for higher order G.F.'s while the one-particle boson G.F. is defined by

$$\mathcal{D}_{kk'}(\tau) = -\langle T_\tau\{\phi_k(\tau)\phi_{k'}(\tau')\}\rangle \ . \qquad (2.7)$$

These G.F.'s have a formal periodicity

$$G_{mn}(\tau+\beta) = -G_{mn}(\tau) \qquad 0>\tau>-\beta \qquad (2.8)$$

enabling them to be given a Fourier representation

$$G_{mn}(\tau) = \beta^{-1}\sum_{q=-\infty}^{+\infty} e^{-i\omega_q\tau}\, G_{mm}(i\omega_q) \qquad (2.9)$$

with the Fourier coefficients satisfying

$$G_{mn}(i\omega_q) = \int_0^\beta e^{i\omega_q\tau}\, G_{mn}(\tau)d\tau \qquad (2.10)$$

where $i\omega_q = i(2q+1)\pi/\beta$ (and $= i2q\pi/\beta$ for $D_{kk'}(i\omega_q)$. Defining the zero-order G.F. by

$$G^0_{mn}(\tau) = -\langle T_\tau\{a_m(\tau)a_n(0)\}\rangle_0 \qquad (2.11)$$

where $\langle\cdots\rangle_0 = \mathrm{Tr}(e^{-\beta\mathcal{H}^0}\cdots)/\mathrm{Tr}(e^{-\beta\mathcal{H}^0})$, we obtain the result

$$G^0_{mn}(\tau) = \begin{cases} -\delta_{mn}\, e^{-\varepsilon_n\tau}(1 - f_D(\varepsilon_n)) & \tau \geqslant 0 \\ \delta_{mn}\, e^{-\varepsilon_n\tau} f_D(\varepsilon_n) & \tau < 0 \end{cases} \qquad (2.12)$$

where $f_D(x) = (e^{\beta x}+1)^{-1}$ is the Fermi-Dirac function. This gives

$$G^0_{mn}(i\omega_n) = \frac{\delta_{mn}}{i\omega_n - \varepsilon_n} \qquad (2.13)$$

and similarly we obtain

$$\mathcal{D}^0_{kk'}(i\omega_n) = \delta_{kk'}\frac{2\omega_k}{(i\omega_n)^2 - \omega_k^2} \ . \qquad (2.14)$$

The G.F. $G_{mn}(i\omega_n)$ is only defined at the points in the complex plane $z = (2q+1)i\pi/\beta$ with $q = 0, \pm 1, \cdots$. It is possible to specify a

complex function that is defined everywhere in the complex plane and is equal to $G_{mn}(i\omega_n)$ at these points on the imaginary axis. Baym and Mermin (1961) have shown that this analytic continuation can be performed by simply replacing the $i\omega_n$ in the function $G_{mn}(i\omega_n)$ by z, giving the complex function $G_{mn}(z)$, provided all factors $\exp(\beta i\omega_n)$ have firstly been reduced to -1, ((+1) for boson propagators). A clear account of these points is given in Fetter and Walecka (p297, 1971). For example the analytic continuation of $G^0_{mn}(i\omega_n)$ is

$$G^0_{mn}(z) = \frac{\delta_{mn}}{z - \varepsilon_n} \tag{2.15}$$

which has a simple pole at $z = \varepsilon_n$ on the real axis. This illustrates an important point; the poles of the G.F. determine the eigenvalues of the Hamiltonian, and hence knowledge of the G.F. gives the energy spectrum. (P59 of Abrikosov *et.al.* 1963).

2.1.2 Wick's Theorem

The formal step that enables the evaluation of $G_{mn}(i\omega_n)$ is the relationship given by Wick (1950). It is possible to show that one can evaluate traces using the expression (p104 of Abrikosov *et.al.* 1963)

$$\langle T_\tau\{a_m(\tau)a_n(0)\}\rangle = \frac{\langle T_\tau\{a_m(\tau)a_n(0)S(\beta)\}\rangle_0}{\langle S(\beta)\rangle_0} \tag{2.16}$$

where $S(\beta) = T_\tau \exp\{-\int_0^\beta \mathcal{H}^{int}(\tau')d\tau'\}$. This generates a perturbation expansion of both the numerator and denominator involving zero-order Hamiltonian averages over products of time-ordered operators. It is precisely with these that Wick's theorem deals and enables these products to be reduced to products of traces over paired or contracted operators (p108 of Arbrikosov *et.al.* 1963). For example with four operators

$$\langle T_\tau\{a(\tau_1)a(\tau_2)a^\dagger(\tau_3)a^\dagger(\tau_4)\}\rangle_0$$

$$= \langle T_\tau\{a(\tau_1)a^\dagger(\tau_4)\}\rangle_0 \langle T_\tau\{a(\tau_2)a^\dagger(\tau_3)\}\rangle_0 \qquad (2.17)$$

$$\pm \langle T_\tau\{a(\tau_1)a^\dagger(\tau_3)\}\rangle_0 \langle T_\tau\{a(\tau_2)a^\dagger(\tau_4)\}\rangle_0$$

where the +, - apply to boson, fermion statistics respectively. It will be noted that we have reduced these averages to products of one-particle GF's. It is this important theorem that will later motivate our choice of mapping from ion levels to operators.

2.1.3 Diagram Expansion

Each term in the resulting perturbation expansion of the numerator and the denominator can be represented by a Feynman diagram, (Feynman 1949 a,b), defined by explicit rules such as those in Fetter and Walecka (1971 p.242). By taking Fourier transforms (2.10) we obtain a simpler series of diagram rules (e.g. p.247 of Fetter and Walecka 1971) giving frequency space rather than coordinate space diagrams. The leading diagrams corresponding to the numerator and denominator are given in figure 2.1. All labels on internal propagators are to be summed and at each vertex the algebraic sum of incoming energies ($i\omega_n$) must vanish. (cf Kirchoff laws in electrical circuit theory).

2.1.4 Linked Cluster Theorem and Dyson's Equation

The expansion of figure 2.1 exhibits two classes of diagrams: *connected* diagrams consisting of only one part and *disconnected* diagrams containing a number of distinct parts. The properties of the expansion are such that the numerator factors into a product of sums over connected and disconnected diagrams and the disconnected diagrams cancel exactly with the denominator. (figure 2.2). This property is referred to as the linked cluster theorem. (L.C.T.).

There is another important property of the remaining diagrams that was discovered by Dyson (1949 a,b). Each diagram in the series after

Figure 2.1

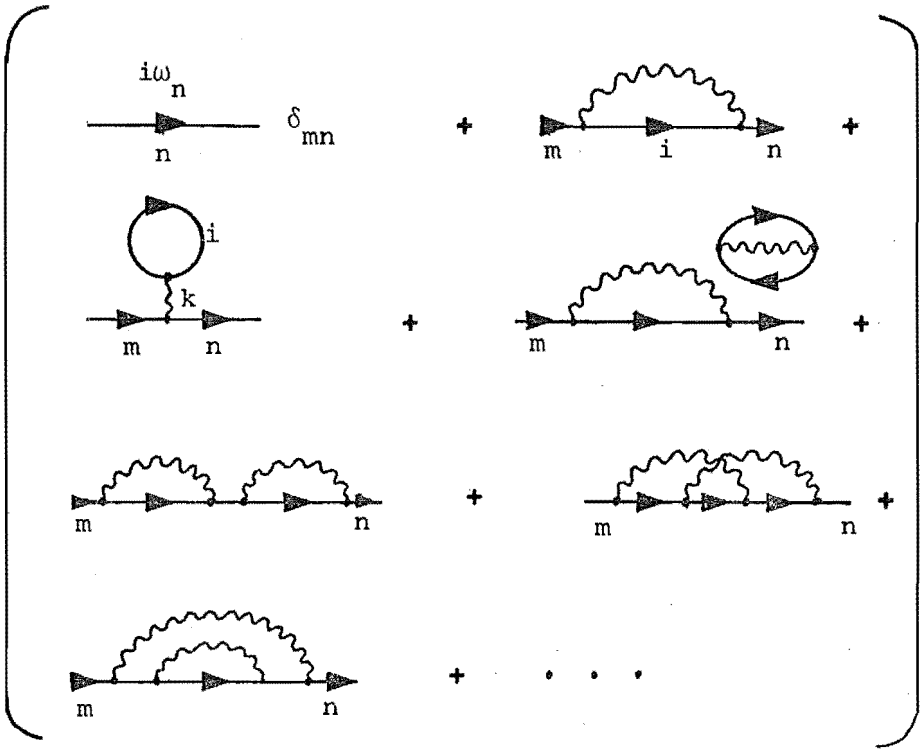

$G_{mn}(i\omega_n)$ =

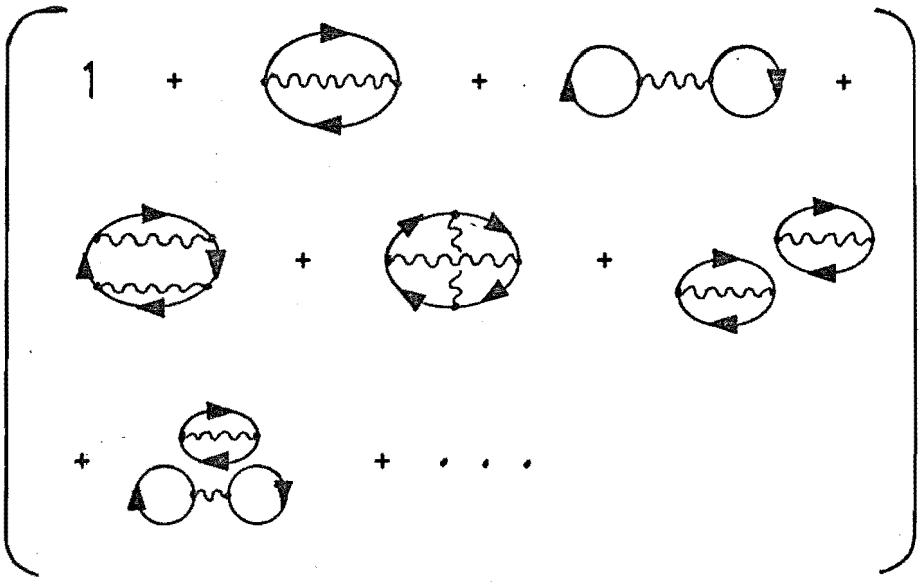

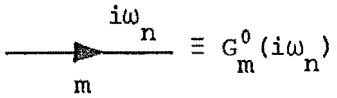

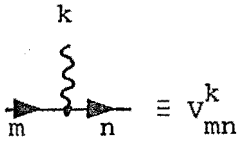

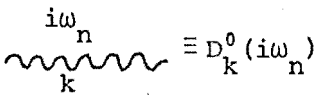

Figure 2.2

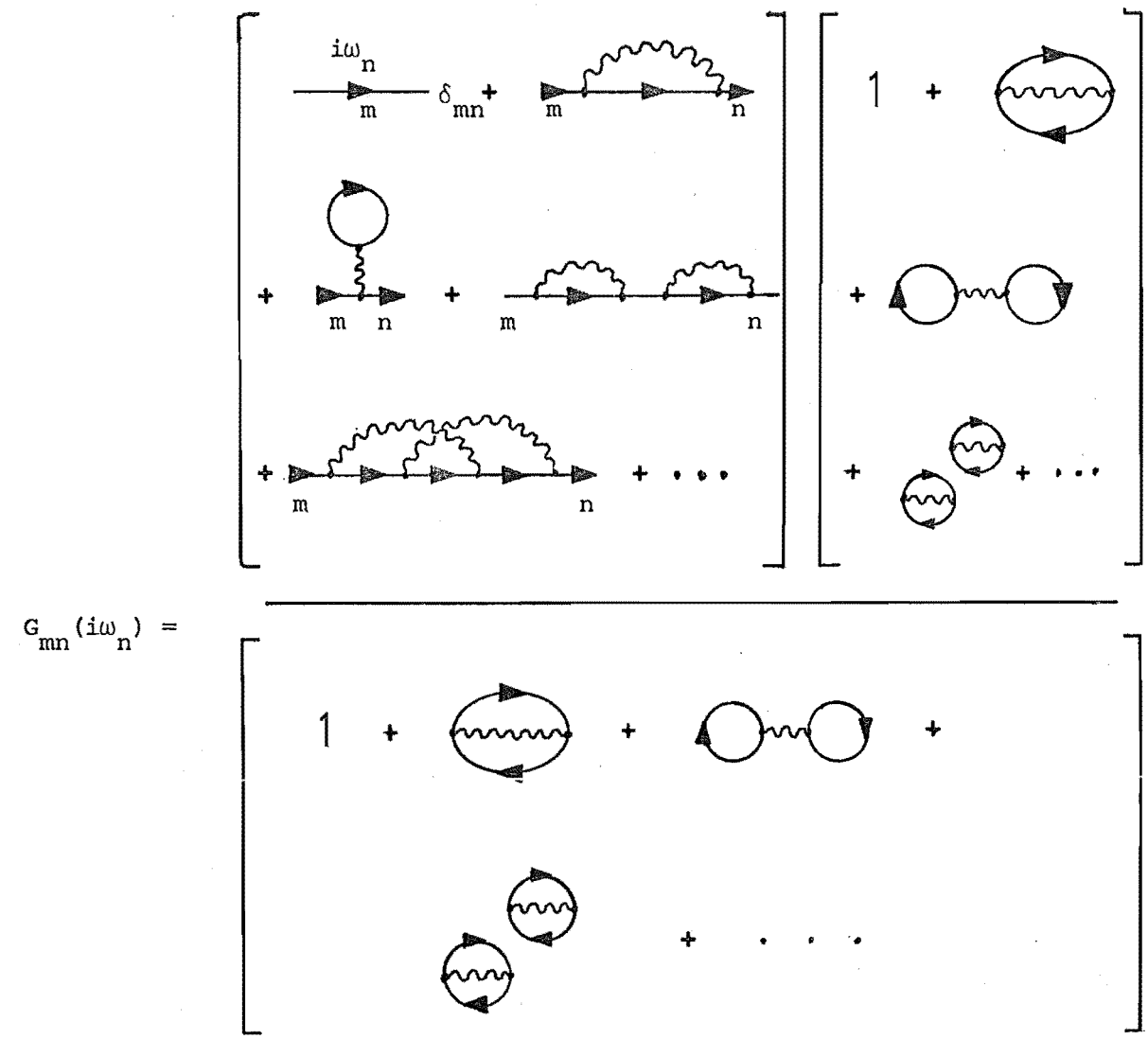
$G_{mn}(i\omega_n)$ =
$i\omega_n$
m
δ_{mn} +
m
n
1 +
+
m n
m
n
+ . . .
m
n
+
+
+ . . .
1 +
+
+
+ . . .
=
$i\omega_n$
m
δ_{mn} +
m
n
+
m
n
+ . . .
≡
$i\omega_n$
m
n

the first contains exactly three parts: a G^0 propagator (single line), then some part that cannot be disconnected by severing only one propagator and finally another part which is identical to some previous diagram contribution. Diagramatically this is indicated in figure 2.3.

Figure 2.3

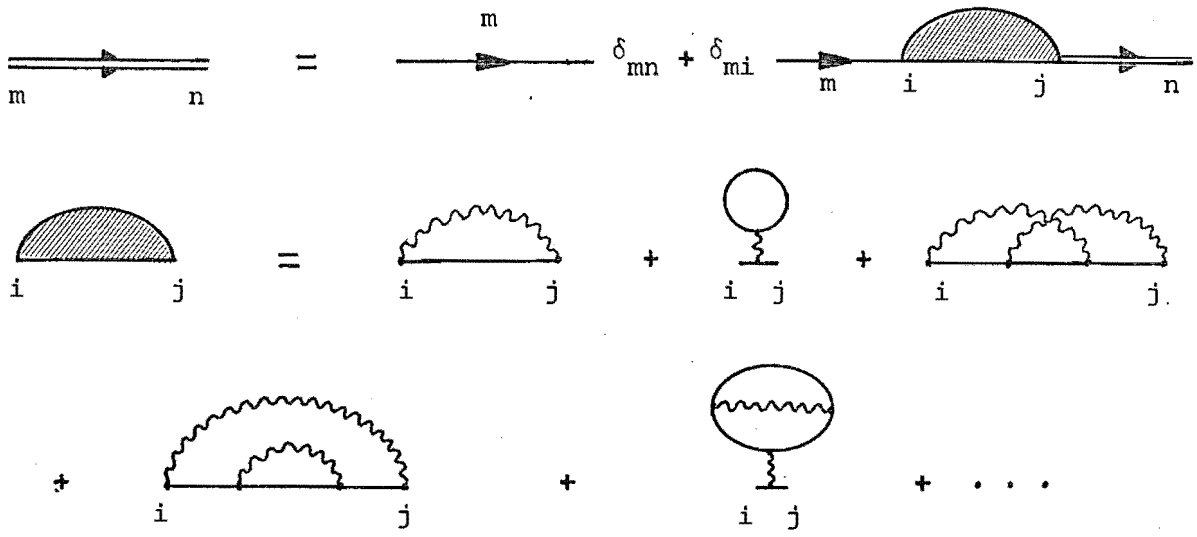

Algebraically this can be stated as

$$G_{mn}(i\omega_n) = G^0_m(i\omega_n)\delta_{mn} + \sum_{ij}(\delta_{mi}G^0_m(i\omega_n))\sum_{ij}(i\omega_n)\,G_{jn}(i\omega_n)$$

which can be regarded as a matrix equation, where for example $G_{mn}(i\omega_n)$ is the m^{th}, n^{th} matrix element of a matrix GF $G(i\omega_n)$.

$$G(i\omega_n) = G^0(i\omega_n) + G^0(i\omega_n)\,\Sigma(i\omega_n)G(i\omega_n) \qquad (2.18)$$

This can be rewritten in the more useful form

$$G^{-1}(i\omega_n) = (G^0(i\omega_n))^{-1} - \Sigma(i\omega_n)\ . \qquad (2.19)$$

If the self-energy function is assumed to be diagonal then this gives a diagonal $G(i\omega_n)$ and allows us to rewrite Dyson's equation in the form

$$G_m(i\omega_n) = G^0_m(i\omega_n) + G^0_m(i\omega_n)\,\Sigma_m(i\omega_n)\,G_m(i\omega_n) \qquad (2.20)$$

where $G_i = G_{ii}$, $\Sigma_i = \Sigma_{ii}$. By including diagrams such as those of figure 2.4 in the self energy function which are able to be disconnected by severing one propagator (i.e. labelled b) and hence are not included

Figure 2.4

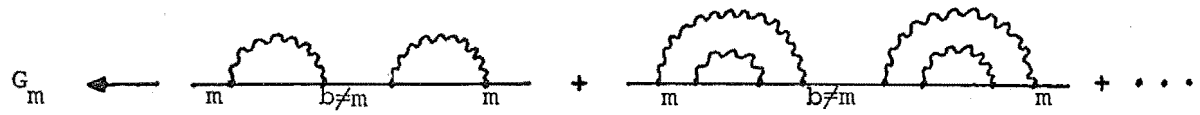

in the original definition, we are able to correct for some of the diagrams that would otherwise be left out by the diagonal assumption. Using (2.13) we obtain from (2.20) the simple expression

$$G_m(i\omega_n) = \frac{1}{i\omega_n - \varepsilon_m - \Sigma_m(i\omega_n)} \tag{2.21}$$

Upon analytically continuing $\Sigma_m(i\omega_n)$ to the whole of the complex plane, $\Sigma_m(z)$, it can be shown that this function is regular except on the real axis and has the property

$$\Sigma_m(z) = \Delta_m(z) \pm i\Gamma_m(z) \qquad \mathrm{Im}(z) \gtrless 0 \tag{2.22}$$

and hence (p.149 of Abrikosov *et.al.* 1963)

$$G_m(z) = \frac{1}{z - \varepsilon_m - \Delta_m(z) \mp i\Gamma_m(z)} \qquad \mathrm{Im}(z) \gtrless 0. \tag{2.23}$$

Great care needs to be taken with these analytic properties of the G.F. if correct results are to be obtained.

In the following section we shall redevelop the theory for the situation where the fermion system is replaced by a spin (or level) system indicating the points of departure from the usual theory.

2.2 Possible Spin Mappings

The general theory presented in the previous section applied to a system of fermions, (described by fermion creation and annihilation operators), interacting with a phonon bath. In the remaining chapters

however we shall apply these techniques to systems consisting of impurity ion levels interacting with the phonons of a host crystal (and also with an external electromagnetic field).

Stedman (1971a) has shown that such a system of N ionic levels can be described by an effective-spin Hamiltonian such as

$$\mathcal{H}^0 = \sum_{r=0}^{N-1} C_r (S^z)^r$$

$$\mathcal{H}^{int} = \sum_{r,s,k=0}^{N-1} d_{rsk} \{ (S^z)^r (S^+)^s + (S^-)^s (S^z)^r \} \phi_k \ .$$

The application of QFT techniques to spin systems has been hampered by the lack of a Wick's theorem for time ordered traces of spin operators. (cf McKenzie and Stedman (1976), §2.1.2). The usual Wick's theorem is not available because it requires either boson or fermion commutation relations to be obeyed by the operators, which is of course not satisfied by spin operators.

One possible approach is to continue to deal with spin operators but develop analogues of Wick's theorem and the diagram rules. (e.g. Giovannini 1965, Doniach 1966, Keiter 1968, Witschel 1971, Matlak 1973a,b, 1975, Wöger and Zittartz 1973, Yang and Wang 1974, 1975, Subramanian and Devanathan 1974, Buckbinder and Westwanskii 1975 and Care and Tucker 1976). This approach however tends to result in diagram rules that are complex and unwieldly and we shall use an alternative method.

This involves transforming the spin operators to combinations of boson and/or fermion operators and hence enables the use of the standard Wick's theorem and diagram rules. (e.g. boson mappings: Holstein and Primakoff 1940, Dyson 1956a,b, Maleev 1957, Schwinger 1965, Wang and Callen 1966, Trimper 1973, Lindgård and Danielsen 1974, 1976, Witschel 1975 and Biegala 1976. Fermion mappings : Mattis 1965, Schultz and Shapero 1973 and Haberlandt and Künrel 1973). In a spin or ionic level system, one and only one level is occupied at any time while the statistics of fermions or bosons are such that this restriction does not apply. This can result

in the need for a projection operation to remove the effects of any unphysical states that may arise as a result of the spin to fermion/boson transformation. In this section we investigate three such mappings referred to as the drones, quasi-spin and iso-spin mappings. These are the simplest such mappings known to us and we investigate each of them with the aim of finding the most convenient for the description of our ionic level system.

2.2.1 Drones, Quasi-spin or Iso-spin?

The *drone* mapping was introduced by Mattis (1965) and has been extended by the work of Spencer (1968) and Barnes (1972). The method has been applied to various systems by Fidler and Tucker (1970a,b, 1971), Sheard and Toombs (1973a,b), Toombs and Sheard (1973) and Tucker (1971, 1972, 1973a,b). The mapping is defined by

$$\begin{aligned} S_j^z &= \sum_{\mu=1}^{2S} (d_{j\mu}^\dagger d_{j\mu} - \tfrac{1}{2}) \\ S_j^+ &= \sum_{\mu=1}^{2S} d_{j\mu}^\dagger (e_{j\mu} + e_{j\mu}^\dagger) \end{aligned} \qquad (2.24)$$

where d,e obey fermion commutation relations.

The *quasi-spin* mapping, (Lipkin 1965), has not previously been used to generate a many-body diagram expansion but has been applied to superconductivity (Anderson 1958), atomic physics (Judd 1967) and crystal field theory (Wybourne 1973). The mapping is

$$\begin{aligned} S_j^z &= \sum_{\mu=1}^{2S} \tfrac{1}{2} (f_{j\mu}^\dagger f_{j\mu} + g_{j\mu}^\dagger g_{j\mu} - 1) \\ S_j^+ &= \sum_{\mu=1}^{2S} f_{j\mu}^\dagger g_{j\mu}^\dagger \end{aligned} \qquad (2.25)$$

where both f,g obey fermion commutation relations.

The *iso-spin* mapping has been used in nuclear and particle physics, (Lipkin 1965), and was introduced to many-body theory by Abrikosov (1965, 1968a,b) and hence is often referred to as the Abrikosov mapping. This

method has been the most popular in this field, (especially as applied to the Kondo problem), having been used by Barnes (1974), Fogedby (1972), Keiter (1968, 1971), Larson (1972), Murata (1972), Oppermann (1973), Schultz and Kwok (1972), Schultz and Shapero (1973), Stedman (1971a,b) Verwoerd (1973, 1974a,b), Yolin (1965) and Zawadowski (1969). The mapping is

$$S_j^z = \sum_{\mu=-s}^{+S} \mu \; a_{j\mu}^\dagger \; a_{j\mu}$$

$$S_j^+ = \sum_{\mu=-s}^{+S} [S(S+1) - \mu(\mu+1)]^{\frac{1}{2}} \; a_{j\mu+1}^\dagger \; a_{j\mu} \qquad (2.26)$$

It is easily shown that each of the transformations (2.24) - (2.26) satisfy the spin commutation rules

$$[S_i^+, S_j^-] = 2\delta_{ij} S^z$$

$$[S_i^z, S_j^+] = \delta_{ij} S_i^+ \qquad (2.27)$$

where S_i^z refers to the z component of the spin at site $\underline{r_i}$.

2.2.2 Projection Operators

Drones

The operators (2.24) act on the product states

$$\prod_{\mu=1}^{2S} |n_d \; n_e\rangle_\mu$$

where n_d, n_e are the eigenvalues of the number operators $d_\mu^\dagger d_\mu$, $e_\mu^\dagger e_\mu$ respectively which take the two values 0 or 1.

For example the $s = \frac{1}{2}$ operators

$$S^z = d_1^\dagger d_1 - \frac{1}{2}$$

$$S^+ = d_1^\dagger (e_1^\dagger + e_1)$$

act on the four basis states $|00\rangle_1$, $|01\rangle_1$, $|10\rangle_1$ and $|11\rangle_1$. The action

of these operators for $s = \frac{1}{2}$ is summarized in table 2.1 and allows the identification of the pairs $|00\rangle_1$, $|11\rangle_1$ and $|01\rangle_1$, $|10\rangle$ as two spin $\frac{1}{2}$ systems $|\frac{1}{2} - \frac{1}{2}\rangle$, $|\frac{1}{2} + \frac{1}{2}\rangle$.

TABLE 2.1

State	s^z eigenvalue	s^+	s^-	$s^2 = (s^z)^2 + (s^+s^- + s^-s^+)/2$ eigenvalue
$\|00\rangle_1$	$-\frac{1}{2}$	$\|11\rangle_1$	0	$\frac{1}{2}(\frac{1}{2} + 1)$
$\|01\rangle_1$	$-\frac{1}{2}$	$\|10\rangle_1$	0	$\frac{1}{2}(\frac{1}{2} + 1)$
$\|10\rangle_1$	$\frac{1}{2}$	0	$\|01\rangle_1$	$\frac{1}{2}(\frac{1}{2} + 1)$
$\|11\rangle_1$	$\frac{1}{2}$	0	$\|00\rangle_1$	$\frac{1}{2}(\frac{1}{2} + 1)$

$$|00\rangle,\ |01\rangle \equiv |\tfrac{1}{2} - \tfrac{1}{2}\rangle$$

$$|10\rangle,\ |11\rangle \equiv |\tfrac{1}{2} + \tfrac{1}{2}\rangle.$$

The operators (2.24) for general spin are just a sum over 2s $s = \frac{1}{2}$ operators and Barnes (1972) pointed out they can be regarded as acting on a product space

$$\prod_{\mu=1}^{2s} |\tfrac{1}{2} \pm \tfrac{1}{2};\ \mu\rangle \ .$$

Denoting a product space by $S^L \otimes S^{L'}$ where L and L' are the spin values associated with the spin spaces and using $(\otimes S^L)^n$ to denote $S^L \otimes S^L \otimes \ldots S^L$ he showed how these spin $\frac{1}{2}$ product spaces can be decomposed into a direct sum of higher spin spaces.

eg. $$(\otimes S^{1/2})^2 = S^1 \oplus S^0$$

$$(\otimes S^{1/2})^3 = S^{1/2} \otimes (S^1 \oplus S^0) = S^{3/2} + 2S^{1/2}$$

(This can be shown by constructing a table like table 2.1 or using the

the standard result $S^a \otimes S^b = S^{|a-b|} \oplus \ldots . \oplus S^{a+b}$).

It is possible to invert these decompositions to enable an arbitrary spin manifold to be written as a direct sum of powers of $S^{1/2}$ and S^0. The lowest order decompositions are

$$\begin{aligned} S^1 &= (\otimes S^{1/2})^2 \ominus S^0 \\ S^{3/2} &= (\otimes S^{1/2})^3 \ominus 2S^{1/2} \end{aligned} \tag{2.28}$$

($\ominus$ is defined as the inverse of $\oplus$).

From the rule that the trace of a direct sum is equivalent to the sum of the individual traces we obtain the following expressions for an arbitrary spin operator O.

$$\begin{aligned} \langle O \rangle_{s=1} &= Y_{s=1} \langle O \rangle_2 \\ \langle O \rangle_{s=3/2} &= Y_{s=3/2} \{ \langle O \rangle_3 - 2f^+ f^- \langle O \rangle_{s=1/2} \} \end{aligned} \tag{2.29}$$

with the notation $Y_s = [Z_s (f^+ f^-)^{s}]^{-1}$,

$$f^{\pm} = [\exp(\pm \omega_s \beta) + 1]^{-1}$$

and $\langle O \rangle_{s=3/2}$ or $\langle O \rangle_n$ being the thermal average over the $s = 3/2$ states or the states of the product space $(\otimes S^{1/2})^n$ respectively. Z_s is the true partition function for the spin=S space and $(f^+ f^-)^{n/2}$ the partition function for the $(\otimes S^{1/2})^n$ product space.

Barnes then noted that any Feynman diagram will consist of a number of closed drone-fermion loops, each loop labelled denoting the product space and site label with which it is associated. Barnes stated that for a given product space n, and considering the labelling of ℓ loops of the diagram, (having already fixed the site labels), that there would be $(n)^{\ell}$ ways of performing such a labelling. Noting that the value of a diagram is independent of such labelling he obtained an expression relating the value of a diagram for general spin S to the equivalent $S = \frac{1}{2}$ diagram

$$\langle \text{diagram} \rangle_s = K_s(\ell) K_s(m) \ldots \langle \text{diagram} \rangle_{s=1/2} \tag{2.30}$$

there being a $K_s(\ell)$ factor for each *distinct* lattice site with ℓ drone-fermion loops. The values of the $K_s(\ell)$ factors are found using (2.29) and the $(n)^\ell$ labelling factor above. For example

$$K_{s=\frac{3}{2}}(\ell) = Y_{s=\frac{3}{2}}\{(n=3)^\ell - 2f^+f^-(n=1)^\ell\} . \qquad (2.31)$$

However the types of interaction Hamiltonian we shall consider can result in more than one product space label to a diagram loop. (e.g. figure 2.7). This means that Barnes' $(n)^\ell$ factor is no longer applicable. While we might expect for the situation where there were two labels per loop a factor of $(2n)^\ell$ this is not quite correct because not all labels of a loop are 'free' to be summed over. The generalization is a factor $\prod_{i=1}^{\ell}(n)^{p_i}$ where p_i is the number of 'free' labels for loop i. This can be expressed as n^p where $p = \sum_{i=1}^{\ell} p_i$ is the sum over the loops, (with the same site label), of the number of free product space labels. With this understanding of p we regain (2.30) - (2.31) but with ℓ replaced by p.

e.g. $$K_{s=1}(p) = Y_{s=1}(n=2)^p \qquad (2.32)$$

$$K_{s=\frac{3}{2}}(p) = Y_{s=\frac{3}{2}}\{(n=3)^p - 2f^+f^-(n=1)^p\}$$

This analysis corrects the statements on p189 of McKenzie and Stedman (1976) where p was not defined exactly and the equation $K_1(\ell,p)=Y_1(2)(\ell)^p-4Y_1(1$ is in error in that $(\ell)^p$ should be 2^p. Furthermore the factors $K_s(\ell,p)$ really depend on ℓ implicitly through the $p(\ell)$ making the ℓ label unnecessary. However this does not affect the results of this paper as the rest of the work was performed using the correct relationships. We refer to the process of converting an $s = \frac{1}{2}$ diagram to a general spin diagram by the multiplication by various K factors as a *projection* operation.

Quasi-spin

Our analysis for quasi-spin will follow closely that of Barnes for drones. The $s = \frac{1}{2}$ operators at any site, (i.e. $f_1^\dagger, f_1, g_1^\dagger, g_1$), generate a

two-dimensional space spanned by the basis vectors $|11\rangle$, $|10\rangle$, $|01\rangle$ and $|00\rangle$ where the first and second labels are the eigenvalues of the number operators $f_1^\dagger f_1$ and $g_1^\dagger g_1$ respectively. Writing S^z and $S^2 = (S^z)^2 + (S^+S^- + S^-S^+)/2$ in terms of the fermion operators (2.25), their action on these states is summarized in table 2.2.

TABLE 2.2.

	S_z	S^2 (eigenvalues)
$\|11\rangle$	$\frac{1}{2}$	$\frac{1}{2}(\frac{1}{2}+1)$
$\|10\rangle$	0	0
$\|01\rangle$	0	0
$\|00\rangle$	$-\frac{1}{2}$	$\frac{1}{2}(\frac{1}{2}+1)$

This table enables the identification of both $|10\rangle$ and $|01\rangle$ with the spin 0 state $|S=0\ m_s=0\rangle$ and $|11\rangle$, $|00\rangle$ with the spin $\frac{1}{2}$ states $|S=\frac{1}{2}\ m_s=\frac{1}{2}\rangle$, $|S=\frac{1}{2}\ m_s=-\frac{1}{2}\rangle$ respectively. Thus the fermion space is the direct sum of a spin $\frac{1}{2}$ subspace and two spin 0 subspaces, written

$$\tilde{S}_{1/2} = S_{1/2} \oplus 2\, S_0 \tag{2.33}$$

where the tilde denotes a fermion space representation. The direct product of two $\tilde{S}_{1/2}$ states, written $\tilde{S}_{1/2} \otimes \tilde{S}_{1/2} \equiv (\otimes \tilde{S}_{1/2})^2$, is given by

$$\begin{aligned}(\otimes \tilde{S}_{1/2})^2 &= (S_{1/2} \oplus 2\, S_0) \otimes (S_{1/2} \oplus 2\, S_0) \\ &= (S_{1/2} \otimes S_{1/2}) \oplus 4(S_{1/2} \otimes S_0) \oplus 4(S_0 \otimes S_0) \\ &= S_1 \oplus 4S_{1/2} \oplus 5S_0 \ .\end{aligned} \tag{2.34}$$

This agrees with the identifications obtained from a study of the action of S^z, S^2 on the basis vectors $|n_1n_2n_3n_4\rangle$, $(n_i=0,1)$, which generate

the 4 dimensional product space. We find that $|1111\rangle$, $\frac{1}{\sqrt{2}}\{|0011\rangle + |1100\rangle\}$, $|0000\rangle$ form a triplet; $|1110\rangle$, $|0001\rangle$; $|1101\rangle$, $|0010\rangle$; $|1011\rangle$, $|0100\rangle$; $|0111\rangle$, $|1000\rangle$ correspond to four doublets while $\frac{1}{\sqrt{2}}\{0011\rangle - |1100\rangle\}$, $|1010\rangle$, $|1001\rangle$, $|0110\rangle$ and $|0101\rangle$ correspond to five singlets.

Proceeding in this manner to form higher products $(\otimes \tilde{S}_{1/2})^n$ and then solving these for the S_n we obtain the relations

$$S_{1/2} = \tilde{S}_{1/2} \ominus 2S_0$$

$$S_1 = (\otimes \tilde{S}_{1/2})^2 \ominus 4\tilde{S}_{1/2} \oplus 3S_0 \qquad (2.35)$$

$$S_{3/2} = (\otimes \tilde{S}_{1/2})^3 \ominus 6(\tilde{S}_{1/2})^2 \oplus 10\tilde{S}_{1/2} \ominus 8S_0 \ .$$

Again using the properties of traces over direct sums we obtain the relations

$$\langle 0\rangle_{s=1/2} = Y_{1/2}(1)\ \langle 0\rangle_{\tilde{1}}$$

$$\langle 0\rangle_{s=1} = Y_1(2)\ \langle 0\rangle_{\tilde{2}} - 4\ Y_1(1)\ \langle 0\rangle_{\tilde{1}} \qquad (2.36)$$

$$\langle 0\rangle_{s=3/2} = Y_{3/2}(3)\ \langle 0\rangle_{\tilde{3}} - 6Y_{3/2}(2)\ \langle 0\rangle_{\tilde{2}} + 10Y_{3/2}(1)\ \langle 0\rangle_{\tilde{1}}$$

where $Y_s(n) = \mathrm{Tr}_{\tilde{n}} \exp(-\beta\mathcal{H}_s)/\mathrm{Tr}_s \exp(-\beta\mathcal{H}_s)$ and we have used the notation of (2.29). If the zero-order Hamiltonian is of the form

$$\mathcal{H}_s = \omega_0 \sum_j S_j^z \qquad (2.37)$$

then these factors are of the form $Y_s(n) = [(f^+f^-)^n Z_s]^{-1}$ where f^+, f^- and Z_s are defined as for drones if we take $\omega_s = (\omega_0/2)$. For a given Feynman diagram the labelling takes the same form as for drones and we obtain an expression for a general spin diagram in terms of the equivalent $S = \frac{1}{2}$ diagram,

$$\langle \text{diagram}\rangle_s = K_s(p)\ K_s(q)\ \ldots . \langle \text{diagram}\rangle_{s=1/2} \qquad (2.38)$$

there being a factor $K_s(p)$ for each distinct site with p defined as for (2.32). The $K_s(p)$ factors are to be found from (2.36) and they take the

form

$$K_{s=1}(p) = Y_1(2)(2)^p - 4Y_1(1)(1)^p \qquad (2.39)$$

$$K_{s=3/2}(p) = Y_{3/2}(3)(3)^p - 6Y_{3/2}(2)(2)^p + 10Y_{3/2}(1)(1)^p$$

Iso-spin ($S = \frac{1}{2}$)

Whereas for drones and quasi-spin the $s = \frac{1}{2}$ case required no $K_s(p)$ projection operations, this is not the situation for $s = \frac{1}{2}$ iso-spin. This arises because the spin mapping defined by (2.26) has the unpleasant effect of introducing unphysical states (Abrikosov 1965). Labelling the basis vectors $|n_{-\frac{1}{2}}\, n_{+\frac{1}{2}}\rangle$ where $n_{-\frac{1}{2}}$, $n_{+\frac{1}{2}}$ are the eigenvalues of the number operators $a^\dagger_{-\frac{1}{2}} a_{-\frac{1}{2}}$, $a^\dagger_{+\frac{1}{2}} a_{+\frac{1}{2}}$ respectively, the $s = \frac{1}{2}$ operators (from 2.26)

$$\begin{aligned} S^z &= -\tfrac{1}{2} a^\dagger_{-\frac{1}{2}} a_{-\frac{1}{2}} + \tfrac{1}{2} a^\dagger_{+\frac{1}{2}} a_{+\frac{1}{2}} \\ S^+ &= a^\dagger_{\frac{1}{2}} a_{-\frac{1}{2}} \\ S^- &= a^\dagger_{-\frac{1}{2}} a_{\frac{1}{2}} \end{aligned} \qquad (2.40)$$

act on the space $|00\rangle$, $|01\rangle$, $|10\rangle$ and $|11\rangle$. The action of these operators on this space is presented in table 2.3.

TABLE 2.3

	$\|00\rangle$	$\|10\rangle$	$\|01\rangle$	$\|11\rangle$
S^z	0	$-\frac{1}{2}\|10\rangle$	$\frac{1}{2}\|01\rangle$	0
S^+	0	0	$\|10\rangle$	0
S^-	0	$\|01\rangle$	0	0

This enables the identification of the states $|10\rangle$ and $|01\rangle$ as the spin $\frac{1}{2}$ states $|s = \frac{1}{2}\ m_s = -\frac{1}{2}\rangle$ and $|s = \frac{1}{2}\ m_s = +\frac{1}{2}\rangle$ respectively but the vacuum $|00\rangle$, and $|11\rangle$ state have no physical identification. When a thermal average $\langle\cdots\rangle = \mathrm{Tr}\{e^{-\beta\mathcal{H}}\cdots\}/\mathrm{Tr}\{e^{-\beta\mathcal{H}}\}$ is evaluated the traces must be taken over physical states only. However to be able to use

Wick's theorem it is necessary to include the unphysical states to retain fermion statistics. The approach used is to evaluate averages using all states and then act on this with some projection operator that removes the effect of the unphysical states on the trace. Any physical quantity must be constructed from sums and products of the spin operators S^x, S^y and S^z and Yolin (1965) noted that these operators give zero when they act on the unphysical states. To correct a trace containing reference to n distinct spins then it is necessary to multiply the trace by a factor Y^n where Y is the ratio of the partition functions when the trace is taken over all states to that when it is taken only over the physical states. Taking the zero-order Hamiltonian (2.37) we obtain

$$Y = \frac{1 + \cosh(\beta\omega_0)}{\cosh(\beta\omega_0)} \qquad (2.41)$$

Isospin ($s \neq \frac{1}{2}$) : Single spin.

Because the isospin space for general spin is not a power of a $s = \frac{1}{2}$ spin space we require a distinctly different approach to this case. For a single spin at site $j = 1$ and general spin S, the operators (2.26) act on a $2S + 1$ dimensional vector space. This space is spanned by the basis kets

$$|n_{-s}\ n_{-s+1} \ldots\ldots\ldots n_s\rangle\ , \qquad (2.42)$$

where n_i is the eigenvalue of the number operator $a_{1i}^{\dagger} a_{1i}$ and takes the values 0 or 1. By considering the action of the spin operators S^z, $S^{\pm}$ on these states as was done for $s = \frac{1}{2}$ in table 2.2 we find that only $2s + 1$ of these vectors correspond to the physical spin states $|sm\rangle$ $(-s \leqslant m \leqslant s)$. Defining the total number operator for ion 1 by

$$N_1 = \sum_{i=-s}^{+s} a_{1i}^{\dagger} a_{1i} \qquad (2.43)$$

then the physical states are those whose eigenvalues are in unity with respect to this operator. (i.e. they contain a single one and 2S zero's in (2.41)). The unphysical states include the vacuum state, $|00\ldots.0\rangle$

with eigenvalue zero and those states with eigenvalues in the range two to 2s + 1.

The projection operation required to remove the effects of these unphysical states to any average was supplied by Abrikosov (1965). The first step in the procedure is to add a term λN_1 to the zero-order spin Hamiltonian (2.1) which corresponds to a trivial shift of the energy levels.

$$\mathcal{H}_0^1 \rightarrow \mathcal{H}_0^\lambda = \mathcal{H}_0^1 + \lambda N_1 \quad . \tag{2.44}$$

As a result of this transformation the operator average

$$\langle V_1(\tau_1) \cdots V_m(\tau_m)\rangle_0 = \frac{\mathrm{Tr}_{\text{all states}} \{e^{-\beta\mathcal{H}_0^1} V_1(\tau_1) \cdots V_m(\tau_m)\}}{\mathrm{Tr}_{\text{all states}} \{e^{-\beta\mathcal{H}_0^1}\}} \tag{2.45}$$

becomes

$$\langle V_1(\tau_1) \cdots V_m(\tau_m)\rangle_0^\lambda = \frac{\mathrm{Tr}_{\text{all states}} \{e^{-\beta\mathcal{H}_0^\lambda} V_1^\lambda(\tau_1) \cdots V_m^\lambda(\tau_m)\}}{\mathrm{Tr}_{\text{all states}} \{e^{-\beta\mathcal{H}_0^\lambda}\}} \tag{2.46}$$

where $V_i^\lambda(\tau_i) = e^{\mathcal{H}_0^\lambda \tau_i} V_i\, e^{-\mathcal{H}_0^\lambda \tau_i} = e^{\lambda N_1 \tau_1} V_i(\tau_i) e^{-\lambda N_1 \tau_i}$.

If V_i is either independent of, or a function of, real spin then $[V_i, N_1] = 0$ giving $V_i^\lambda(\tau_i) = V_i(\tau_i)$ and (2.46) differs from (2.45) only by the factor $e^{-\beta\lambda N_1}$ in each trace. This has the effect of weighting each term in the trace by a factor of unity for the vacuum state, $e^{-\beta\lambda}$ for the physical states and $e^{-\beta\lambda n}$ $(n \geqslant 2)$ for the remaining unphysical states. The product of operators may not contain any reference to the spin, in which case they can be factored out, the traces in the numerator and denominator cancel and we are left with the same result as if the trace had been only taken over the physical states.

If the product of states does contain any reference to the spin then the vacuum state in the numerator is annihilated. For large λ the leading contribution to the numerator comes from the physical states ($e^{-\beta\lambda}$) and in the denominator from the vacuum state ($e^{-\beta 0} = 1$). Thus by multiplying

by $e^{\beta\lambda}$ and taking the limit $\lambda \to \infty$ we obtain[1]

$$\lim_{\lambda \to \infty} e^{\beta\lambda} \langle V_1(\tau_1) \cdots V_m(\tau_m) \rangle_0^{\lambda} = \mathrm{Tr}_{\substack{\text{phys} \\ \text{states}}} \{ e^{-\beta \mathcal{H}^1_0} V_1(\tau_1) \cdots V_m(\tau_m) \}. \tag{2.47}$$

To obtain agreement with the average taken over physical states only we need to divide by the partition function $Z_1 = \mathrm{Tr}_{\text{phys states}} \{ e^{-\beta \mathcal{H}^1_0} \}$. Following Keiter (1968) we represent this projection operation as

$$P_1 \equiv \frac{1}{Z_1} \lim_{\lambda \to \infty} e^{\beta\lambda} \tag{2.48}$$

to be applied to any average that contains reference to a spin at site 1.

Iso-spin ($s \neq \frac{1}{2}$) : Many spins.

For a multi-spin system we need to generalize the projection operation P_1 derived in the last section. The basis vectors for a system containing m spins can be written as product states $|n\rangle_1 \; |n\rangle_2 \cdots |n\rangle_m$ where $|n\rangle_i = |n_{-s} \; n_{-s+1} \cdots n_s\rangle_i$ is a basis for the spin operators referring to site i. The zero-order spin Hamiltonian for this system we assume to be of the form

$$\mathcal{H}_0 = \sum_{i=1}^{m} \mathcal{H}_0{}^i \tag{2.49}$$

where $\mathcal{H}_0{}^i$ is the zero-order Hamiltonian for the i^{th} site.

The only physical states in the m-ion system are those that are products of m single ion physical states. (i.e. states $\prod_{i=1}^{m} |n\rangle_i$ where each $|n\rangle_i = |0,0 \cdots n_k = 1, 0 \cdots 0\rangle$ $k = -S, \cdots +S$). To enable the use of Wick's theorem we require a projection operator to remove the contribution of unphysical states to a trace. Consider the evaluation of $\langle Q(\tau) \rangle_0$ where $Q(\tau)$ contains real spin operators operating on μ ($0 \leqslant \mu \leqslant m$)

[1] Because λN_1 commutes with all intermediate operators then only one-particle intermediate states are possible also.

spin sites. We add to the zero-order Hamiltonian $\mathcal{H}_0$ a term λN where N is the *total* number operator for the m site system

$$N = \sum_{i=1}^{m} N_i$$

$$N_i = \sum_{\ell=-s}^{+s} a_{i\ell}^{\dagger} a_{i\ell} \ . \tag{2.50}$$

Whether $Q(\tau)$ contains real spin operators, ($\mu > 0$), or no references to spin ($\mu = 0$), we have $[Q,N] = 0$ and hence

$$Q^{\lambda}(\tau) = e^{(\mathcal{H}_0+\lambda N)\tau} Q\, e^{-(\mathcal{H}_0+\lambda N)\tau} = e^{\mathcal{H}_0\tau} Q e^{-\mathcal{H}_0\tau} \equiv Q(\tau) \ .$$

Considering the average with respect to this new Hamiltonian

$$\langle Q(\tau)\rangle_0^{\lambda} = \frac{\mathrm{Tr}_{\text{all states}}\{e^{-\beta(\mathcal{H}_0+\lambda N)} Q^{\lambda}(\tau)\}}{\mathrm{Tr}_{\text{all states}}\{e^{-\beta(\mathcal{H}_0+\lambda N)}\}} \tag{2.51}$$

then the only alteration is to weight each term in the traces by $e^{-\beta\lambda n}$ where n is the eigenvalue of N for the state. If $Q(\tau)$ contains no spin operators ($\mu=0$) then $Q(\tau)$ can be factored from the numerator trace which then cancels the denominator as for the single spin situation. If $Q(\tau)$ does contain real spin operators ($\mu>0$) then the trace in the numerator can be split into a product of two traces; one which contains $Q(\tau)$ with the trace over the states that $Q(\tau)$ acts upon, and another over the states upon which it does not act. Without loss of generality we can regard $Q(\tau)$ as acting on the first μ^{th} sites and the numerator becomes

$$\mathrm{Tr}_{\text{all states}}\{e^{-\beta(\mathcal{H}_0+\lambda N)} Q(\tau)\} = \tag{2.52}$$

$$\sum_{n} {}_1\langle n|{}_2\langle n|\cdots{}_{\mu}\langle n|\, e^{-\beta(\mathcal{H}_0+\lambda \sum_{i=1}^{\mu} N_i)} Q(\tau)\, |n\rangle_{\mu}\cdots|n\rangle_1$$

$$\sum_{n} {}_{\mu+1}\langle n|\cdots{}_m\langle n|\, e^{-\beta(\mathcal{H}_0+\lambda \sum_{i=\mu+1}^{m} N_i)}\, |n\rangle_m\cdots|n\rangle_{\mu+1} \ .$$

The action of $Q(\tau)$ on any state in the first trace that contains a vacuum state (i.e. $n_i = |00\cdots\rangle_i$ $1 \leqslant i \leqslant \mu$) results in a vanishing

contribution. The leading contribution to this trace comes from the physical states and is weighted by a factor $e^{-\beta\lambda\mu}$ while contributions from unphysical states are weighted by $e^{-\beta\lambda n}$ with $n>\mu$.

The denominator is also able to be split into the product of two traces; the second of which cancels the second part of the numerator trace. The leading contribution to the denominator is weighted by unity and arises from the vacuum state. If we multiply the trace by a factor $e^{\beta\lambda\mu}$ and allow λ to tend to infinity then the only contribution to the numerator is that from the physical states while the denominator tends to unity. To obtain agreement with the trace taken over only physical states it is necessary to divide by $\prod_{i=1}^{\mu} Z_i$ where

$$Z_i = \mathrm{Tr}_{\mathrm{phys}\ i} \langle n | e^{-\beta \mathcal{H}_0{}^i} | n \rangle_i \tag{2.53}$$

is the partition function for a system containing a single spin at site i.

We can express then the projection operation necessary to correct a trace which contains spin operators acting on μ sites by

$$P \equiv \frac{1}{\left(\prod_{i=1}^{\mu} Z_i\right)} \lim_{\lambda \to \infty} e^{\beta\lambda\mu} \quad . \tag{2.54}$$

2.2.3 Linked Cluster Theorem

The reason we transformed our spin operators to fermion operators was to enable the use of Wick's theorem. However as a result of this we shall see in this section that we no longer have the availability of a L.C.T. enabling the unlinked diagrams of the numerator to cancel the denominator. For example if we were considering the diagram expansion of (2.7) subject to the interaction (2.3), then we obtain the diagrams of figure 2.5. In these diagrams each loop is labelled by its site label and can be regarded as representing drone, quasi-spin or iso-spin loops.

It is necessary to apply the various projection operations of the

Figure 2.5

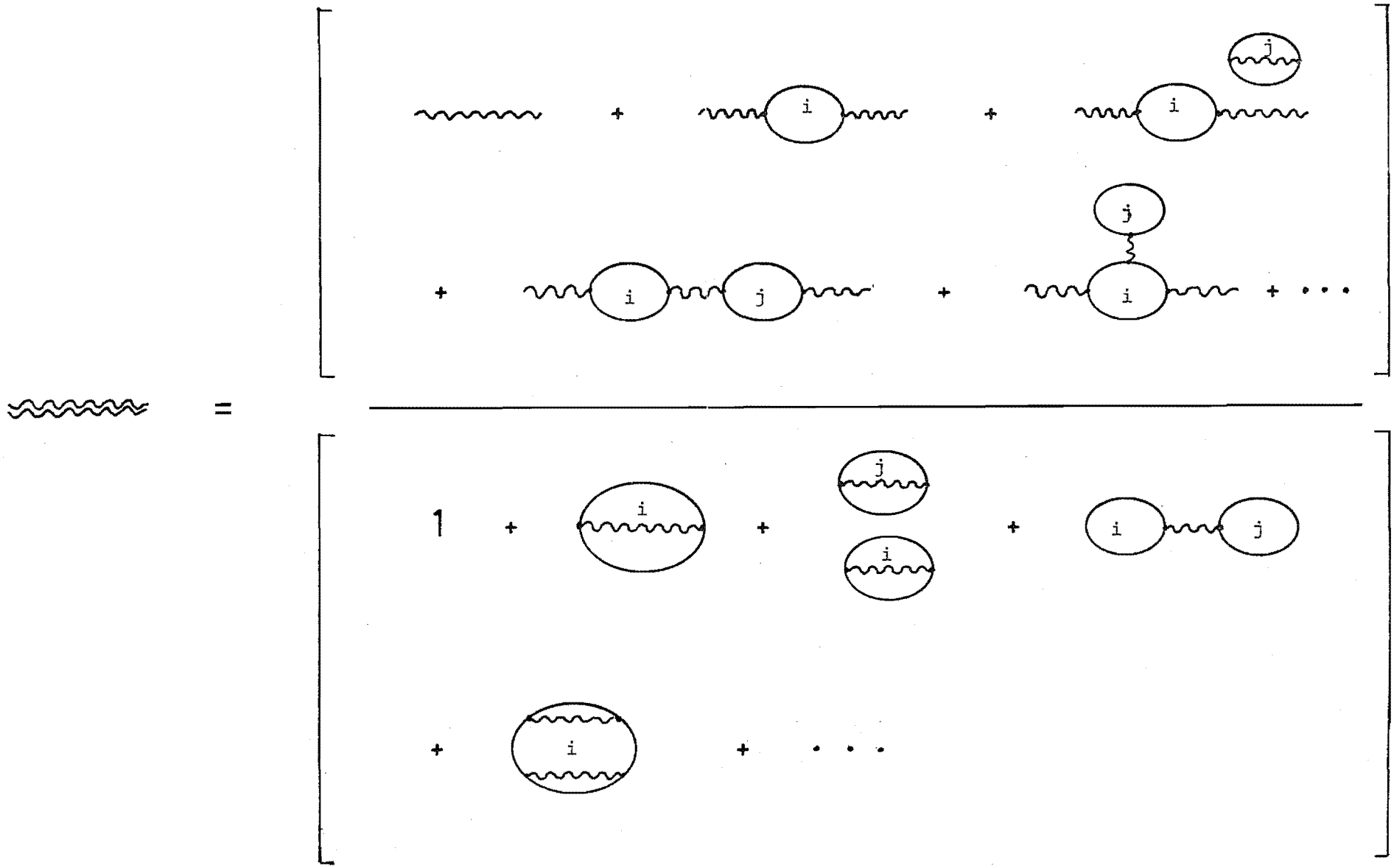

last section to both the numerator and the denominator individually. Let us identify C and D (as in figure 2.6) as connected and disconnected

Figure 2.6

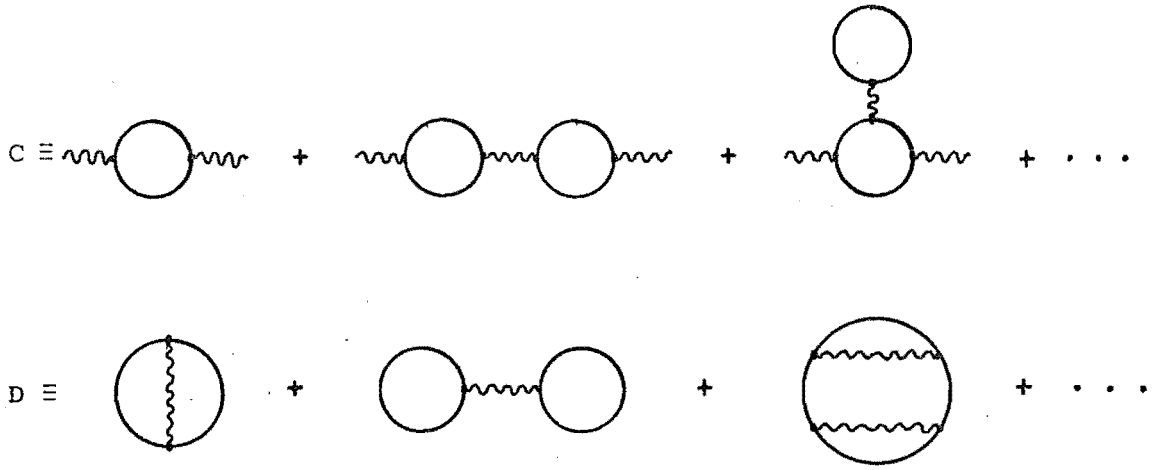

diagrams respectively and consider P to represent the action (2.30) for drones, (2.38) for quasi-spin and (2.54) for iso-spin.

In §2.1.4 the L.C.T. resulted from the ability to factor the numerator into two distinct parts (figure 2.2) involving connected and disconnected diagrams respectively. However for our case we have

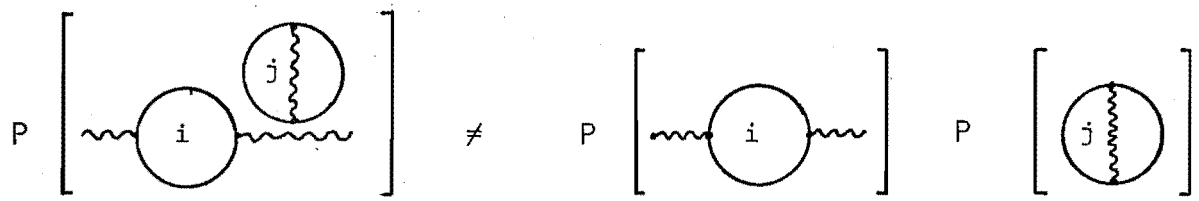

if i = j. (2.57)

For drones and quasi-spin this results because P on the L.H.S. means to multiply the $s = \frac{1}{2}$ diagram by $K_s(2)$ if $i = j$, $((K_s(1))^2$ if $i \neq j$), while those on the R.H.S. are to be multiplied by $(K_s(1))^2$. Because in general[1] $K_s(2) \neq (K_s(1))^2$ this factorization fails to occur and hence with it the L.C.T. fails also. For the iso-spin case it is found that for each closed fermion loop the diagram contributes a factor $f_D(\varepsilon_n + \lambda)$ and this results in a zero contribution upon the action of P if it contains more than one

[1] Note that for $s = \frac{1}{2}$ case all $K_s(\ell) = 1$ and hence the factorization and L.C.T. are recovered.

closed loop with the same site label. Thus for i = j the L.H.S. of (2.57) vanishes while the R.H.S. does not, again resulting in a loss of factorization and hence the L.C.T.

Keiter (1968) expressed this as

$$\mathcal{D} = \mathcal{D}^0 + \frac{P(C) + P(CD)}{1 + P(D)} \tag{2.58}$$

where the zero-order diagram $\mathcal{D}^0$ factors out bacause it is unaffected by the action of P.

In many problems, such as the evaluation of the absorption and Raman spectrum in chapters 3 and 5, this lack of a L.C.T. is no problem because the denominator is a constant that gives only trivial changes; however in other problems such as the spin-phonon coupled modes dispersion relation (§2.2.6) it is important to take account of this lack of a L.C.T. If we are dealing with a weakly coupled spin-phonon system for example, then we are able to expand $[1 + P(D)]^{-1}$ using the binomial theorem giving a result

$$\mathcal{D} = \mathcal{D}^0 + P(C) + [P(CD) - P(C)\cdot P(D)] + \cdots\cdots \quad . \tag{2.59}$$

Because $P(CD)$ and $P(C)\cdot P(D)$ are at least fourth order in the interaction (i.e. $\sim V^4$) then we can regard $\mathcal{D} \simeq \mathcal{D}^0 + P(C)$ to be correct to second order. However if we go to higher order then it is necessary to include higher expansions of (2.59).

Yolin (1965) in his evaluation of the dispersion relation for spin coupled modes did <u>not</u> realize this and as a result was criticized by Schultz and Kwok (1972) for his assuming a L.C.T. The first disconnected diagram to appear in the expansion (2.59) is

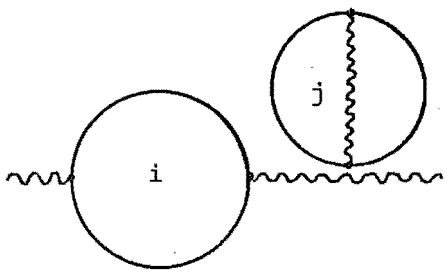

As described in §2.2.2 the $s = \frac{1}{2}$ projection procedure which was employed by Yolin involves the multiplication of the diagrams by a factor Y^n. Thus although the fourth order contributions to $P(CD) - P(C)\cdot P(D)$ cancel for $i \neq j$, (both have factor Y^2), the previous diagram is multiplied by a factor $Y - Y^2$ for $i = j$. This correction does not affect Yolin's calculation of the lifetime, (as it contributes no imaginary part), and hence his result agrees with that of other workers, (e.g. Toombs and Sheard 1973, Fidler and Tucker 1970), who used $s = \frac{1}{2}$ drones with the attendant L.C.T. This diagram would however result in a fourth-order shift contribution.

2.2.4 Dyson's Equation

Just as the projection operations affected the form of the L.C.T., they also affect the form of Dyson's equation. The availability for Dyson's equation for $\mathcal{D}$ for example

$$\mathcal{D} = \mathcal{D}^0 + \mathcal{D}^0 \, \Pi \, \mathcal{D} \tag{2.60}$$

depends on the ability to express a diagram such as

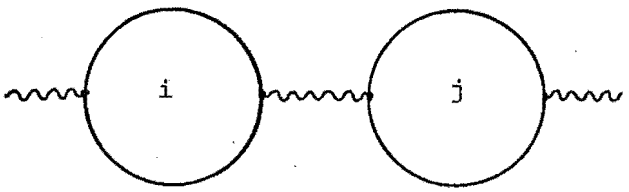

as the product of three factors

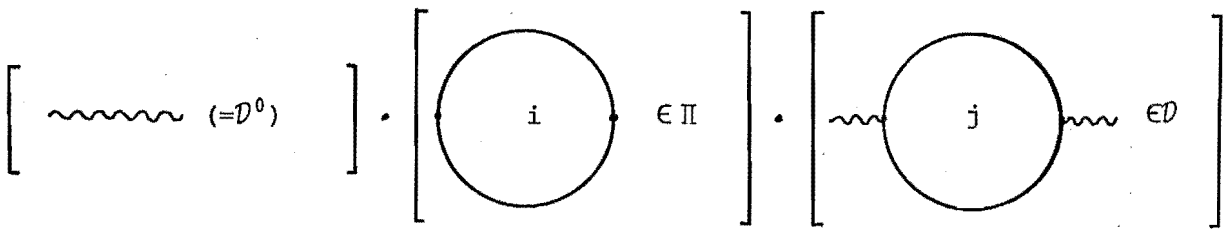

However again the action of P on such a diagram means that this is <u>not</u> possible unless $i \neq j$. If however we take as a self-energy

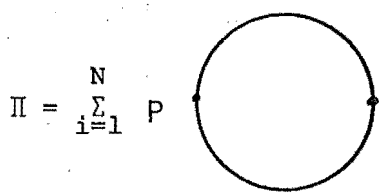

and use (2.60) recursively, we generate the expansion

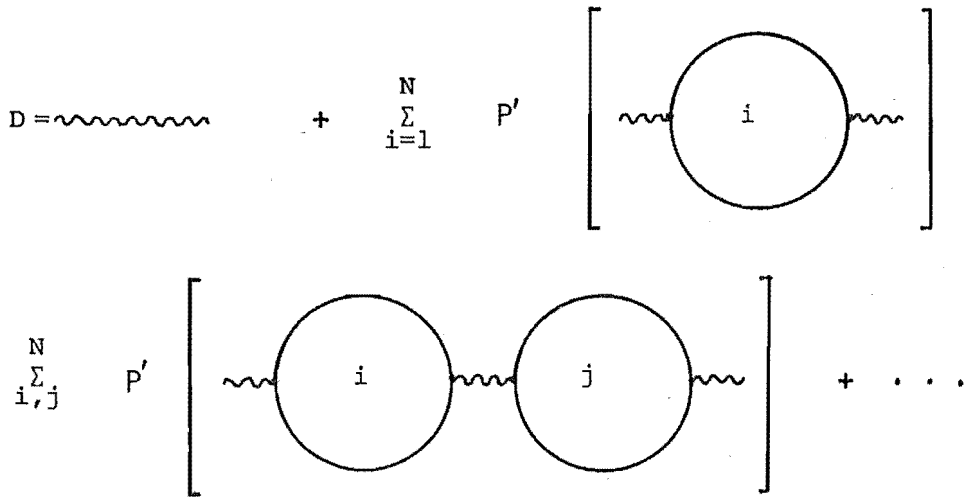

where P' acts as if every loop corresponds to a different site. It is clear that this generates the correct second-order diagrams, and also the correct fourth-order diagrams for $i \neq j$, etc., but gives an incorrect fourth-order contribution for $i = j$. If however an extra contribution is included in Π

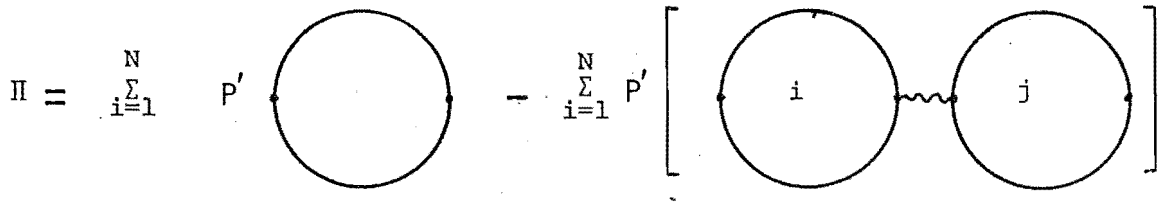

then the resulting fourth-order diagrams are correct but not the higher-order diagrams. Proceeding in this manner we can correct Π to any given order. Other fourth-order contributions to Π include

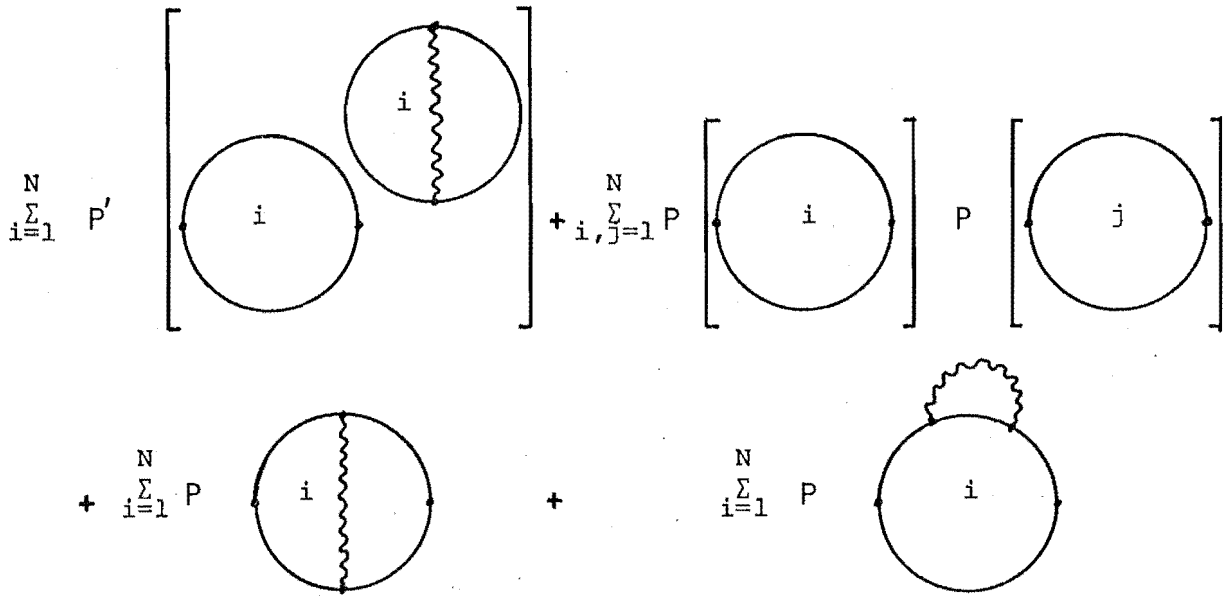

2.2.5 Iso-spin GF limiting procedure?

The works of Hernández and Walker (1972) and Stedman (1971a) would suggest (implicitly) that the operation (2.54) can be applied to the one-particle iso-spin G.F., (defined by equations (2.4) and (2.10) but with $a^{\dagger}$, a now referring to iso-spin operators), $G_{\mu\mu}(i\omega_n)$.[1] This has the diagram expansion

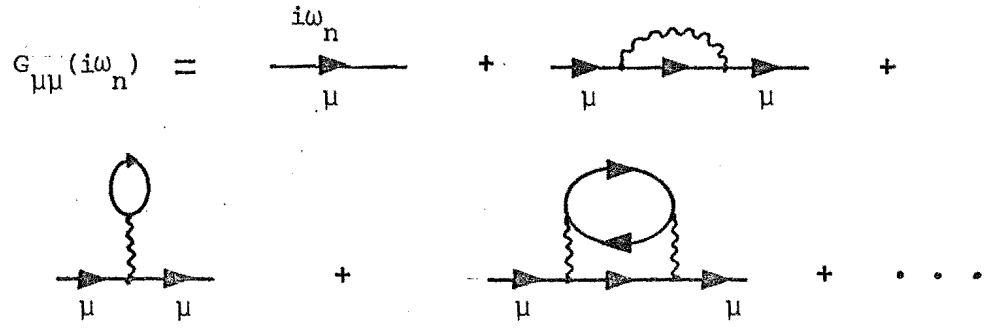

but applying P (2.54) to the leading diagram gives

$$P\left(\frac{1}{i\omega_n - \varepsilon_\mu - \lambda}\right) = \frac{1}{Z}\lim_{\lambda\to\infty}\frac{e^{\beta\lambda}}{i\omega_n - \varepsilon_\mu - \lambda} = \infty$$

which diverges. The results because we no longer have the situation, [V,N] = 0, because the V's no longer correspond to physical observables. However, this is not a difficulty in practical situations because in such calculations one ultimately calculates traces over physical quantities and though P applied to part of a diagram may result in divergences it will not when applied to the diagram as a whole. For example in the above case $P(G_{\mu\mu}(i\omega_n))$ diverges but it is only part of the diagram 3.13, (figure 4 and 5 of Hernández and Walker 1972), which corresponds to the physically observable absorption spectrum, and when P is applied to this diagram the result converges.

2.2.6 Spin-Phonon Coupled Modes (s = 1).

For the s = ½ case the three mappings considered are approximately equal in convenience with drones having a slight edge as a result of the

[1] They consider only one site so we have dropped site labels.

availability of the L.C.T. To evaluate their comparative usefulness for higher spin values we shall employ each to obtain the dispersion relation for spin-phonon coupled modes in a system containing spin one ions. We shall choose a Hamiltonian for the description of the interaction between the spins and phonons, $\mathcal{H}_{sp}$, such that phonons can induce transitions between any two of the three spin levels. Our Hamiltonian is chosen to be

$$\mathcal{H} = \mathcal{H}_s + \mathcal{H}_p + \mathcal{H}_{sp}$$

where

$$\begin{aligned} \mathcal{H}_s &= \sum_j \omega_0 \, S_j^z \\ \mathcal{H}_p &= \sum_{\underline{k}} \omega_{\underline{k}} \, b_{\underline{k}}^\dagger b_{\underline{k}} \\ \mathcal{H}_{sp} &= N^{-\frac{1}{2}} \sum_{\underline{k}j} B_{\underline{k}} \exp(i\underline{k}\cdot\underline{r}_j)\phi_{\underline{k}} \left[S_j^x + \xi(S_j^+ S_j^+ + S_j^- S_j^-)\right] \end{aligned} \tag{2.61}$$

where we have used the method described by Toombs and Sheard (1973) to transform the phonon operators such that only the p = 1 branch is coupled to the spins. This results in a coupling coefficient[1]

$$B_{\underline{k}} = \tfrac{1}{2} \epsilon \, (\omega_0 \omega_{\underline{k}})^{\frac{1}{2}}$$

where ϵ denotes the strength of the coupling. The $S^+S^+ + S^-S^-$ combination in (2.61) couples the highest and lowest spin levels of the triplet and because it can be expressed as a combination of S^x and S^y operators the iso-spin P operation (2.54) is applicable.

The coupled modes dispersion relation is to be found by considering the poles of the phonon G.F. (2.7). (e.g. for s = ½ case see Yolin (1965), Jacobsen and Stevens (1963) and Tucker (1972)). We shall now develop a diagram expansion and find the poles of (2.7) for each of the three mappings.

Drones

Using the notation of (2.24) we define G.F.'s

[1] The factor ½ in this expression for $B_{\underline{k}}$ corrects the typographical error in McKenzie and Stedman (1976) where it is given as ⅓.

$$\Delta_{j\mu,j'\mu'}(\tau) = -\langle T_\tau\{(e_{j\mu}(\tau) + e^\dagger_{j\mu}(\tau))(e_{j'\mu'}(0) + e^\dagger_{j'\mu'}(0))\}\rangle$$

$$A_{j\mu,j'\mu'}(\tau) = -\langle T_\tau\{d_{j\mu}(\tau)\, d^\dagger_{j'\mu'}(0)\}\rangle \qquad (2.62)$$

whose corresponding zero-order G.F.'s have Fourier coefficients that are diagonal μ,μ' and j,j'. (Because of the form of (2.61) they are also independent of these).

$$\Delta^0(i\omega_n) = 2/i\omega_n$$

$$A^0(i\omega_n) = \frac{1}{i\omega_n - \omega_0} \qquad (2.63)$$

Representing the propagators $\mathcal{D}_k$, Δ^0 and A^0 by wavy, broken and solid lines respectively we obtain the second-order diagrams of figure 2.7.

Figure 2.7

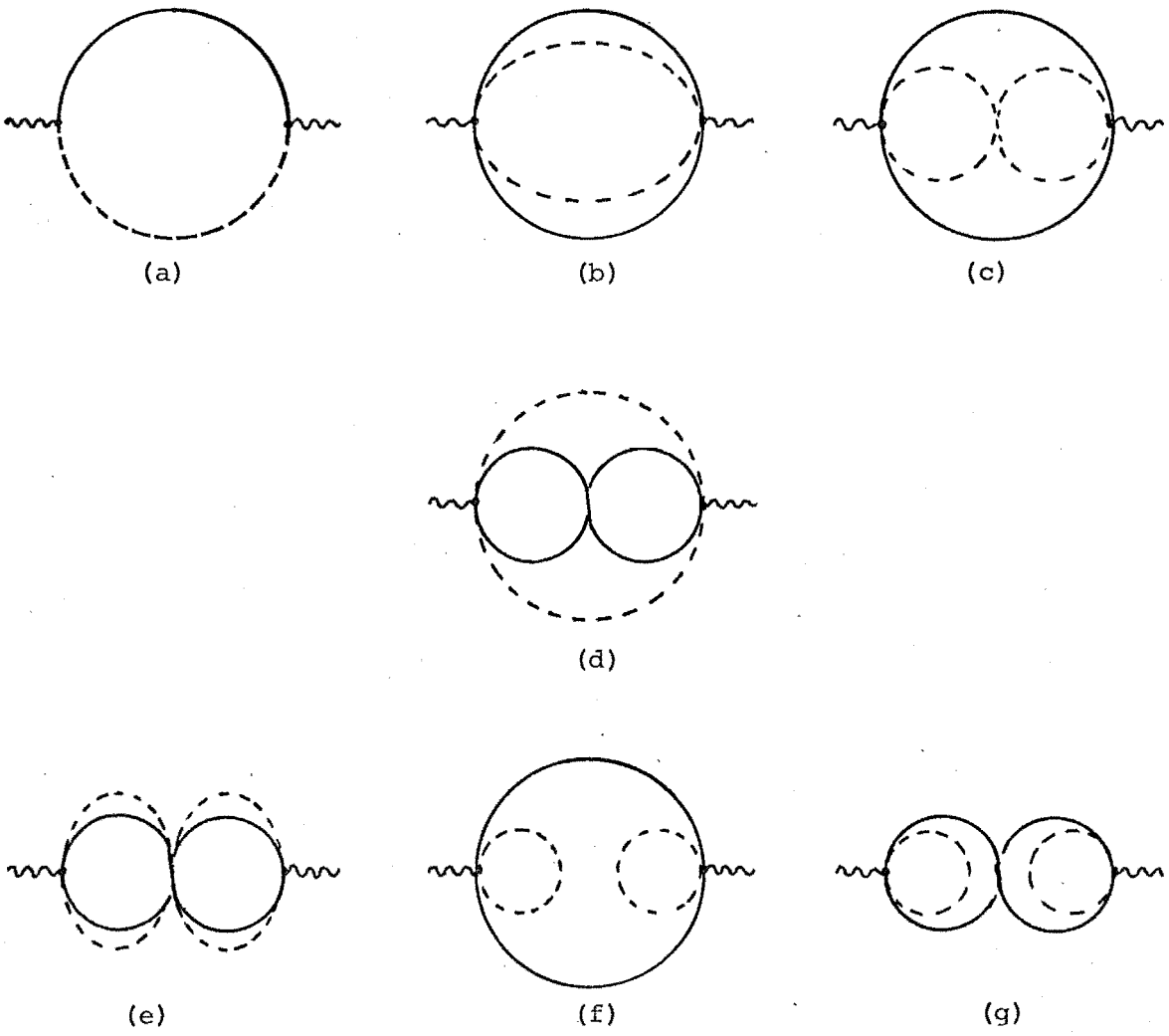

The twisting of the propagators in figure 2.7 c-e,g indicates which contractions have been performed and hence the number of free spin labels present and the correct $K_s(p)$ factors that result. Using the relation (2.16), (second-order term), and the <u>first</u> term of $\mathcal{H}_{sp}$, (2.61) we obtain an expression in the expansion of (2.7)

$$-\frac{1}{2!}\int_0^\beta d\tau_1 d\tau_2 \cdot \frac{1}{N}\sum_{j,j'}\sum_{q,q'}\sum_{\mu\mu'} B_q B_{q'} \exp i\{\underline{q}\cdot\underline{r}_j + \underline{q}'\cdot\underline{r}_{j'}\}$$

$$\langle T_\tau \{ \phi_k(\tau)\ \phi_{k'}(0)\ \phi_q(\tau_1)\ \phi_{q'}(\tau_2)$$

a

b

c

$$[d^\dagger_{j\mu}(\tau_1) - d_{j\mu}(\tau_1)][d^\dagger_{j'\mu'}(\tau_2) - d_{j'\mu'}(\tau_2)]$$

$$[e_{j\mu}(\tau_1) + e^\dagger_{j\mu}(\tau_1)][e_{j'\mu'}(\tau_2) + e^\dagger_{j'\mu'}(\tau_2)]\}\rangle_0$$

where contraction a gives an unlinked diagram and both b,c contribute to diagram 2.7a. Similarly if the <u>second</u> term of $\mathcal{H}_{sp}$ (2.61) is used one obtains an expression with the possible contractions

$$\phi_k(\tau)\quad \phi_{k'}(0)\ \phi_q(\tau_1)\ \phi_{q'}(\tau_2)$$

a

b

c

$$d^\dagger_{j\mu_1} d^\dagger_{j\mu_2}(\tau_1)\ d_{j'\mu_1'} d_{j'\mu_2'}(\tau_2) + d_{j\mu_1} d_{j\mu_2}(\tau_1)\ d^\dagger_{j'\mu_1'} d^\dagger_{j'\mu_2'}(\tau_2)$$

A C

B D

$$[e_{j\mu_1} + e^{\dagger}_{j\mu_1}(\tau_1)][e_{j\mu_2} + e^{\dagger}_{j\mu_2}(\tau_1)][e_{j'\mu'_1} + e^{\dagger}_{j'\mu'_1}(\tau_2)][e_{j'\mu'_2} + e^{\dagger}_{j'\mu'_2}(\tau_2)]$$

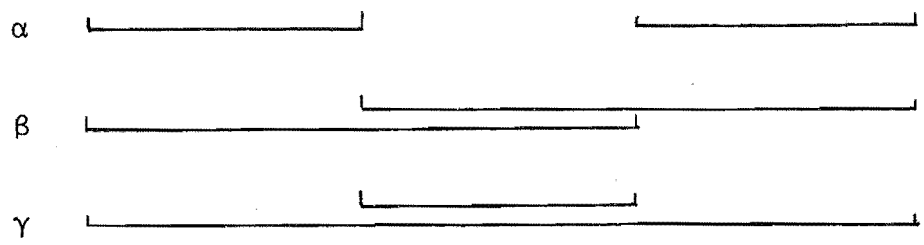

If we use the diagram convention

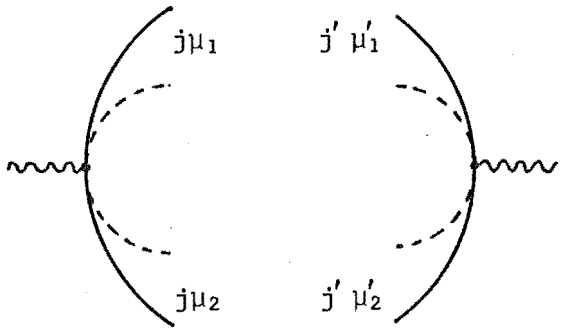

then one obtains the following correspondances between the contractions and diagrams.

diagram 2.7f ≡ contractions $(b+c)\cdot(A+C)\cdot\alpha$

" 2.7g ≡ " $(b+c)\cdot(B+D)\cdot\alpha$

" 2.7b ≡ " $(b+c)\cdot(A+C)\cdot\beta$

" 2.7d ≡ " $(b+c)\cdot(B+D)\cdot\beta$

" 2.7c ≡ " $(b+c)\cdot(A+C)\cdot\gamma$

" 2.7e ≡ " $(b+c)\cdot(B+D)\cdot\gamma$

Diagrams 2.7f and 2.7g involve a closed dotted loop that results in a factor

$$\beta^{-1} \sum_{i\omega_n} \Delta^0(i\omega_n) = \beta^{-1} \sum_{i\omega_n} \cdot \frac{2}{i\omega_n}$$

which vanishes because $i\omega_n = (2n + 1)\pi/\beta$. This leaves the contributions from diagrams 2.7a - e and table 2.4 summarizes the resulting Kronecker delta functions and signs that result from the various contractions.

TABLE 2.4

Contraction	Kronecker delta's	Sign
A + C	$\delta_{jj'}\ \delta_{\mu_1\mu_1'}\ \delta_{\mu_2\mu_2'}$	-1
B + D	$\delta_{jj'}\ \delta_{\mu_1\mu_2'}\ \delta_{\mu_2\mu_1'}$	+1
β	$\delta_{jj'}\ \delta_{\mu_1\mu_1'}\ \delta_{\mu_2\mu_2'}$	-1
γ	$\delta_{jj'}\ \delta_{\mu_1\mu_2'}\ \delta_{\mu_2\mu_1'}$	+1

From table 2.4 we can easily find the resulting number of free μ labels, (p), and hence the correct $K_1(p)$ factor and sign for each of the diagrams 2.7 a - e, which is summarized in table 2.5.

TABLE 2.5

Diagram	p	factor
2.7a	1	$K_1(1)$
2.7b	2	$-K_1(2)$
2.7c	1	$K_1(1)$
2.7d	1	$K_1(1)$
2.7e	2	$-K_1(2)$

From (2.32) and (2.29) we have the result

$$K_1(p) = \frac{2^p (e^{\beta\omega_0} + 1)(e^{-\beta\omega_0} + 1)}{(e^{\beta\omega_0} + 1 + e^{-\beta\omega_0})} \qquad (2.64)$$

and evaluating the self-energy diagram contributions for $s = \frac{1}{2}$ we obtain

diagram	contribution to self-energy $\Pi_k(i\omega_n)$
2.7a	$\frac{1}{2}\frac{\varepsilon^2\,\omega_0^2\,\omega_k}{(i\omega_n)^2-\omega_0^2}\cdot\frac{e^{\beta\omega_0}-e^{-\beta\omega_0}}{(e^{\beta\omega_0}+1)(e^{-\beta\omega_0}+1)}$
2.7b - e	$\frac{\xi^2\,\varepsilon^2\,\omega_0^2\,\omega_k}{(i\omega_n)^2-4\omega_0^2}\cdot\frac{e^{-\beta\omega_0}-1}{e^{-\beta\omega_0}+1}$.

(2.65)

Combining (2.65), (2.64) and table 2.5 we obtain a total contribution (second-order) to the self-energy

$$\Pi_k(i\omega_n)=\frac{\varepsilon^2\,\omega_0^2\,\omega_k^2\,(e^{\beta\omega_0}-e^{-\beta\omega_0})}{(e^{\beta\omega_0}+1+e^{-\beta\omega_0}}\left[\frac{1}{(i\omega_n)^2-\omega_0^2}+\frac{4\xi^2}{(i\omega_n)^2-4\omega_0^2}\right] \tag{2.66}$$

Quasi-spin

Using the notation of (2.25) we define G.F.'s

$$\Lambda_{j\mu,j'\mu'}(\tau)=-\langle T_\tau\{f_{j\mu}(\tau)\,f^\dagger_{j'\mu'}(0)\}\rangle$$
$$B_{j\mu,j'\mu'}(\tau)=-\langle T_\tau\{g_{j\mu}(\tau)\,g^\dagger_{j'\mu'}(0)\}\rangle \tag{2.67}$$

whose corresponding zero-order G.F.'s have Fourier coefficients that are diagonal in, and independent of, μ,μ' and j,j' and using (2.61) have the form

$$\Lambda^0(i\omega_n)=B^0(i\omega_n)=[i\omega_n-(\omega_0/2)]^{-1}. \tag{2.68}$$

Developing a diagram expansion we obtain the second-order diagrams as in figure 2.7 a - e, (diagrams 2.7 f - g are no longer possible), except that the solid and dotted lines now represent the propagators B^0 and Λ^0 respectively. The p and $K_s(p)$ factors are summarized in table 2.6.

TABLE 2.6

Diagram	p	factor
2.7a	1	$-K_1(1)$
2.7b	2	$-K_1(2)$
2.7c	1	$K_1(1)$
2.7d	1	$K_1(1)$
2.7e	2	$-K_1(2)$

The spin ½ diagram contributions to the self-energy $\Pi_k(i\omega_n)$ are (define $x = \beta\omega_0/2$)

diagram — contribution to self-energy $\Pi_k(i\omega_n)$

$$\text{2.7a} \qquad -\frac{1}{2}\frac{\varepsilon^2\,\omega_0^2\,\omega_k}{(i\omega_n)^2-\omega_0^2}\qquad\frac{e^x-e^{-x}}{(e^{-x}+1)(e^x+1)}$$

$$\text{2.7b - e} \qquad -\frac{\xi^2\cdot\varepsilon^2\,\omega_0^2\,\omega_k}{(i\omega_n)^2-4\omega_0^2}\qquad\frac{e^x-e^{-x}}{(e^x+1)^2\,(e^{-x}+1)^2} \tag{2.69}$$

while (2.39) and (2.36) give the relationship

$$K_1(p) = \frac{2^p(e^x+1)^2(e^{-x}+1)^2-4(e^x+1)(e^{-x}+1)}{(e^{\beta\omega_0}+1+e^{-\beta\omega_0})}\ . \tag{2.70}$$

Combining (2.70), (2.69) and table 2.6 we obtain a second-order contribution to the self-energy $\Pi_k(i\omega_n)$ that is identical to the drones result (2.66).

Iso-spin

We define a G.F. by

$$F_{j\mu,j'\mu'}(\tau) = -\langle T_\tau\{a_{j\mu}(\tau)\ a^\dagger_{j'\mu'}(0)\}\rangle \tag{2.72}$$

whose corresponding Fourier coefficients are diagonal in j and μ labels

$$F^0_\mu(i\omega_n) = \frac{1}{i\omega_n-\mu\omega_0}\qquad \mu = 0,\pm 1\ . \tag{2.73}$$

When the iso-spin projection operation is employed (2.54) then an energy λ is added to each energy level and $\mu\omega_0 \rightarrow \mu\omega_0 + \lambda$ in (2.73). Representing the level propagators F_1^0, F_0^0 and F_{-1}^0 by lines above, on and below the level of the phonon propagator respectively then we obtain the second-order diagrams of figure 2.8 Where each diagram represents two diagrams,

Figure 2.8

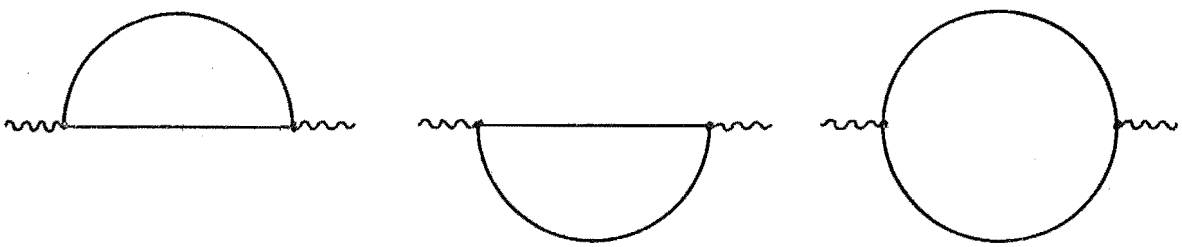

(a) (b) (c)

one for the sense of the level propagators arrows being clockwise and another having an anticlockwise sense. Evaluating the contributions from these diagrams we obtain the results summarized in table 2.7.

TABLE 2.7

Diagram(s)	Contribution to self-energy $\Pi_k(i\omega_n)$ (before P (2.54) is applied).
2.7a + 2.7b	$\dfrac{\epsilon^2 \omega_0^2 \omega_k}{(i\omega_n)^2 - \omega_0^2}$ U (λ)
2.7c	$\dfrac{4\xi^2 \epsilon^2 \omega_0^2 \omega_k}{(i\omega_n)^2 - 4\omega_0^2}$ U(λ)

where $U(\lambda) = [\exp\beta(-\omega_0 - \lambda) + 1]^{-1} - [\exp\beta(\omega_0 - \lambda) + 1]^{-1}$ contains all the λ dependence of the contributions. Upon applying (2.54) to this we obtain

$$P[U(\lambda)] = \frac{1}{e^{\beta\omega_0} + 1 + e^{-\beta\omega_0}} \lim_{\lambda\to\infty} e^{\beta\lambda}\, U(\lambda)$$

$$= \frac{e^{\beta\omega_0} - e^{-\beta\omega_0}}{e^{\beta\omega_0} + 1 + e^{-\beta\omega_0}} \qquad (2.74)$$

Again combining (2.74) and table 2.7 we obtain the self-energy contribution (2.66). After we have completed the evaluation of the dispersion relation we shall explain why the iso-spin method is the most convenient.

Dispersion Relation

The self-energy contribution (2.66) is to be substituted in (cf (2.19), (2.21))

$$\mathcal{D}_{\underline{k}}(i\omega_n) = \frac{1}{[\mathcal{D}^0_{\underline{k}}(i\omega_n)]^{-1} - \Pi_{\underline{k}}(i\omega_n)} \qquad (2.75)$$

and the analytic continuation $\mathcal{D}_{\underline{k}}(i\omega_n) \to \mathcal{D}_{\underline{k}}(\omega)$ performed by substituting ω for $i\omega_n$ in (2.75) and (2.66). The poles of the analytically continued function are to be determined by finding those values of ω for which the denominator vanishes. Such values satisfy the cubic equation

$$(\omega^2 - \omega_k^2)(\omega^2 - \omega_0^2)(\omega^2 - 4\omega_0^2) - \frac{\varepsilon^2\,\omega_0^2\,\omega_k (e^{\beta\omega_0} - e^{-\beta\omega_0})}{(e^{\beta\omega_0} + 1 + e^{-\beta\omega_0})}$$

$$[(\omega^2 - 4\omega_0^2) + 4\xi^2(\omega^2 - \omega_0^2)] = 0. \qquad (2.76)$$

Upon making the substitutions $y = (\omega/\omega_0)^2$ and $x = (\omega_k/\omega_0)^2$ this can be rewritten in the dimensionless form

$$(y - x)(y - 4)(y - 1) - \varepsilon^2 x\, Q(\omega_0)[(y - 4) + 4\xi^2(y - 1)] = 0 \qquad (2.77)$$

where $$Q(\omega_0) = \frac{e^{\beta\omega_0} - e^{-\beta\omega_0}}{e^{\beta\omega_0} + 1 + e^{-\beta\omega_0}}.$$

Following Abramowitz and Stegun (1965) we rewrite this in the form $y^3 + a_2y^2 + a_1y + a_0 = 0$ with coefficients $a_2 = -5 - x$, $a_1 = 4 + 5x - \varepsilon^2 Q(x)x(1 + 4\xi^2)$ and $a_0 = -4x + 4\varepsilon^2 Q(\omega_0)\, x\, (1 + \xi^2)$. Defining two parameters

$$q = \frac{1}{3} a_1 - \frac{1}{9} a_2^2$$

$$r = \frac{1}{6}(a_1 a_2 - 3a_0) - \frac{1}{27} a_2^3$$

then if the combination $\Theta = -(q^3 + r^2)$ is positive the cubic equation has three distinct real roots. If we define the two parameters

$$s = (r^2 + \Theta)^{1/6}$$

$$t = \frac{1}{3} \tan^{-1} (\Theta / r)$$

then the roots are

$$y_1 = 2s \cos t - \frac{1}{3} a_2$$

$$y_2 = -s \cos t - \frac{1}{3} a_2 + \sqrt{3}\, s \sin t$$

$$y_3 = -s \cos t - \frac{1}{3} a_2 - \sqrt{3}\, s \sin t.$$

Using these relations a computor generated plot of the dispersion relation is given in figure 2.9 with the parameters chosen such that

(1) $\xi = 1$

(2) $Q(\omega_0) = 1$,

for two values of the coupling coefficient ε^2.

Far from the regions of the crossings the curves tend to the unperturbed dispersion relations $\omega = \omega_k$, $\omega = \omega_0$ and $\omega = 2\omega_0$ and the deviation from these in the region of the crossing increases with increasing values of ε^2. In the regions far from the crossings the modes act like either pure spins or pure phonons while close to these regions they are to be regarded as neither pure spins or pure phonons but an inseparable coupling of them both.

The lifetime of these coupled modes is to be found by obtaining the imaginary part of the self-energy upon taking the analytic continuation (Toombs and Sheard 1973)

$$\Pi_k(i\omega_n) \rightarrow \Pi_k(\omega + i0^+).$$

From (2.66) we find that to second-order this gives

Figure 2.9

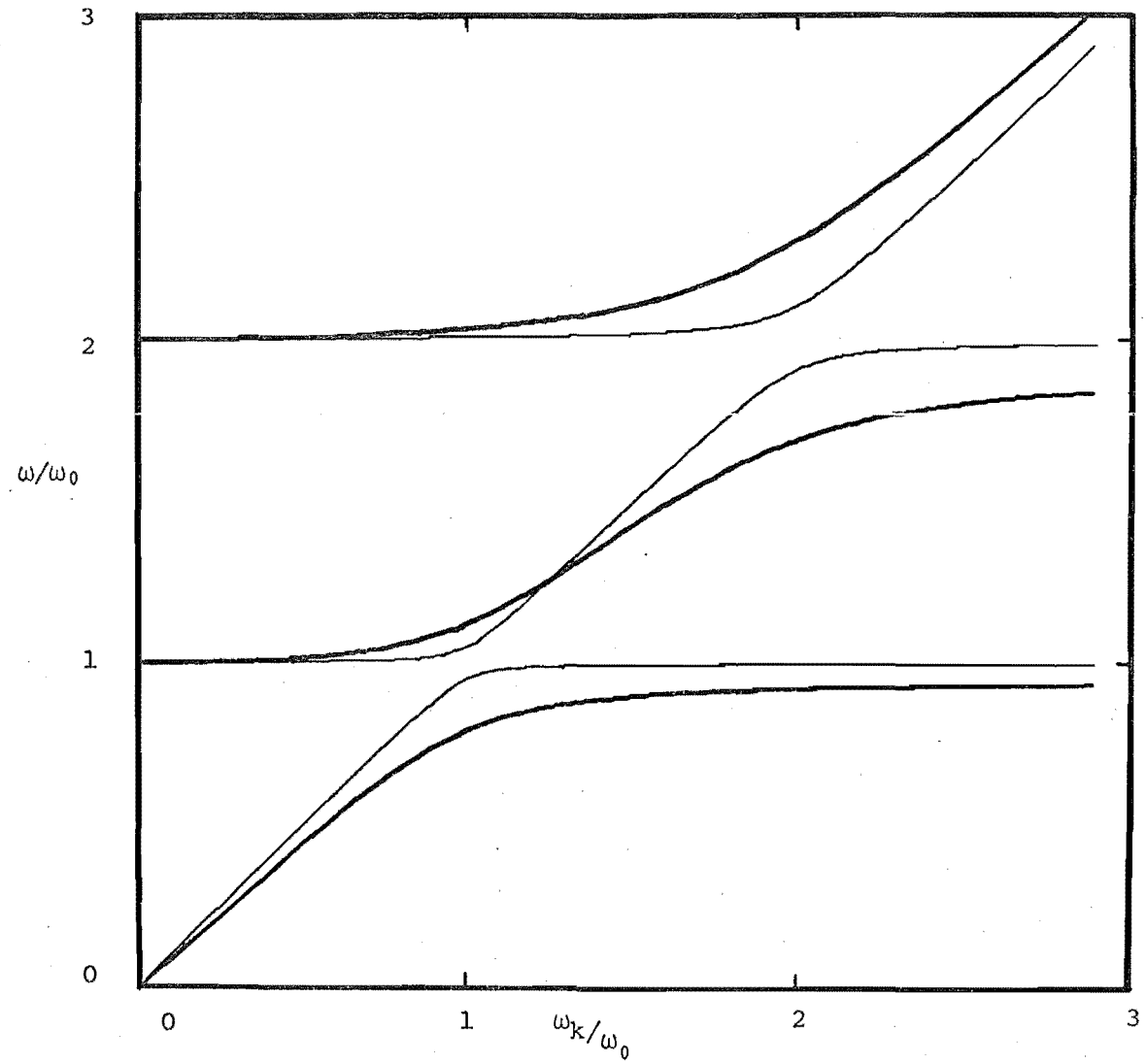
3
2
1
0
ω/ω_0
0
1
2
3
ω_k/ω_0
$\varepsilon^2 = 0.01$
$\varepsilon^2 = 0.1$

$$\text{lifetime}(\omega) = -\Pi\,\varepsilon^2\,\omega_0^2\,\omega_k\,Q(\omega_0)\Big\{\frac{\delta(\omega-\omega_0)}{\omega+\omega_0}+\frac{\delta(\omega+\omega_0)}{\omega-\omega_0}$$

$$+\,4\xi^2\,\frac{\delta(\omega-2\omega_0)}{\omega+2\omega_0}\qquad+\,4\xi^2\,\frac{\delta(\omega+2\omega_0)}{\omega-2\omega_0}\Big\} \tag{2.79}$$

indicating that the coupled-modes are not damped, (i.e. have infinite lifetime), to this order except at $\omega = \pm\omega_0$ and $\pm 2\omega_0$ which only occurs far from the coupled modes region.

2.2.7 Comparison of techniques

Having used the three spin mappings; drones, quasi-spin and iso-spin in a model calculation we find that the relative convenience of the iso-spin mapping makes it the obvious choice for work at higher spin values. This convenience comes mainly from the observation that the evaluation of diagram 2.8c for iso-spin involves only *one* contour integration while the evaluation of diagrams 2.7b - e for drones and quasi-spin each involve *three* nested integrations.

For general S the iso-spin approach would yield S(2S + 1) diagrams each requiring the evaluation of one integration compared with the drone and quasi-spin techniques which would result in only 2S diagrams but the number of free integration variables ranges from one for the first diagram to 4S-1 for the last diagram. Added to this advantage, the iso-spin method avoids the necessity of differentiating diagrams, (and the K factors), that the drone and quasi-spin diagrams 2.7b - e require.

If the interaction Hamiltonian (2.61) was taken to be linear in spin, (cf ξ=0), then the above complications to drones and quasi-spin would be no longer applicable and all three methods would be comparable; however such a choice of interaction is highly unrealistic as it restricts the system to transitions between adjacent levels.

Another advantage of the iso-spin mapping is the relative simplicity of the projection operation P (2.54). Also the diagrams can easily be given a physical interpretation in terms of phonons, (or photons), inducing transitions between levels. This will become more apparent

in the following chapters on absorption and Raman spectra.

We conclude then that although the drones, quasi-spin and iso-spin mappings are comparable for $s = \frac{1}{2}$ and interaction Hamiltonians linear in spin operators, the first two methods quickly become intractable with increasing spin and realistic choices of Hamiltonian, and the iso-spin technique renders it the most attractive method.

CHAPTER 3 : SINGLE ION ABSORPTION SPECTRUM

In this chapter we shall develop a thermal Green's function formulation that yields the absorption spectrum of a crystal containing many impurity ions. From this analysis we will show how to extract the absorption spectrum for a single ion and will provide the background for chapter 4 where the spectrum of ion pairs is discussed.

The optical absorption as a function of frequency ω_0 is given by the well known expression (Stedman 1971, Nishikawa and Barrie 1963, Kubo 1957)

$$\sigma(\omega_0) \sim \omega_0 \int_{-\infty}^{\infty} dt\{e^{-i\omega_0 t} - e^{i\omega_0 t}\}\langle M(t)M\rangle \qquad (3.1)$$

where the average is taken over the grand canonical ensemble and M is the dipole moment operator.

3.1 Description of the System:

The system we shall consider consists of a crystal containing impurity paramagnetic ions. The energy levels of these ions will be described using the iso-spin mapping discussed at length in the previous chapter,

$$\mathcal{H}_{imp} = \sum_{jm} \varepsilon_m a^{\dagger}_{jm} a_{jm} \qquad (3.2)$$

where again j is a site label and ε_m is the energy of level m which is taken to be site independent. The projection operation (2.54) involves adding an energy λ to each level written as

$$\varepsilon_m \rightarrow \lambda_m = \varepsilon_m + \lambda. \qquad (3.3)$$

Following Stedman (1972a) we represent the dipole moment operator by the expansion

$$M = \sum_{jmn} M_{mn} a^{\dagger}_{jm} a_{jn} . \qquad (3.4)$$

The action of the creation operator $a^{\dagger}_{jm}$ on the vacuum state creates an ionic level m at site j while a_{jm} annihilates this level. (Of course the vacuum state has no physical significance as was explained in §2.2.2). Each term of (3.4) corresponds to a transition from some impurity level

(n) to another (m) at some site (j) with matrix element $M_{mn} = \langle m|M|n\rangle$ which is taken to be site independent. In appendix 3A we show that the absorption spectrum is related to the thermal G.F.

$$G(i\omega_n) = \sum_{jj'} \sum_{abcd} M_{ab} M_{cd} \int_0^\beta d\tau e^{i\omega_n \tau} \langle T_\tau \{a_{ja}^\dagger(\tau)\, a_{jb}(\tau)\, a_{j'c}^\dagger(0)\, a_{j'd}(0)\}\rangle \tag{3.5}$$

where $i\omega_n = i2n\pi/\beta$, $n = 0, \pm 1, \pm 2, \cdots$

by the relationship

$$\sigma(\omega_0) \sim \frac{\omega_0}{2\pi i} \{G(\omega_0 + i0^+) - G(\omega_0 - i0^+)\} \tag{3.6}$$

This involves the discontinuity across the real axis of the function obtained by analytically continuing $i\omega_n$ to the whole complex plane. The absorption spectrum is to be found by developing a diagram expansion of the G.F. (3.5), analytically continuing it and using expression (3.6). However before we indicate the diagram expansion let us complete the description of the system.

We are interested in the effect of the phonons of the crystal on the absorption spectrum. The phonon Hamiltonian in the absence of interactions is

$$\mathcal{H}_{\text{phonon}} = \sum_k \omega_k b_k^\dagger b_k \tag{3.7}$$

and the interaction between the phonons and impurity levels is given by

$$\mathcal{H}^{\text{int}} = \sum_k \sum_{mn} \sum_j V_{mn}^{jk} a_{jm}^\dagger a_{jm} \phi_k \tag{3.8}$$

where $V_{mn}^{jk} = V_{mn} (\frac{\omega_k}{V})^{1/2} e^{i\underline{k}\cdot\underline{r}}$, with V the volume of the crystal, as given by Barrie and Rystephanick (1966). Each term in the interaction Hamiltonian (3.8) can be considered as a transition from level n to level m of the impurity at site j with either the creation or annihilation of a phonon with wave vector $\underline{k}$. This form of the interaction, like that for the s=1 spin coupled modes, enables transitions to occur between any two levels, the transition probability amplitude being given by the matrix element V_{mn}^{jk}.

3.2 Diagram Expansion

Using the approach outlined in chapter 2 we develop a diagram expansion of the G.F. (3.5) in frequency space. Figure 3.1 gives the leading second and fourth-order diagrams that contribute to the numerator and denominator, where solid, wiggly and dotted lines indicate level, phonon and photon propagators respectively. Although the photon propagators do not explicitly appear in expansion (3.6), they have been included in the diagrams of figure 3.1 to; (i) indicate the level sums (over a,b,c and d) in (3.5) (c.f. diagram rule c) and to (ii) give a clearer physical picture of the role of the photon in the absorption process.

To find and evaluate all diagrams of order 2n + 2 (i.e. containing n phonon propagators) we enumerate all topologically distinct diagrams and evaluate each according to the following rules:

(a) Assign a relevant parameter, (e.g. level and site label), and a frequency to each propagator, along with an arrow denoting its sense,[1] such that frequency is 'conserved' at each node and a net $i\omega_n$ travels through the diagram.

(b) Make the following replacements:

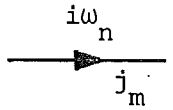

$$\rightarrow \quad F^0_{jm}(i\omega_n) = \frac{1}{i\omega_n - \lambda_m}$$

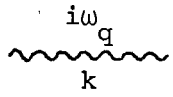

$$\rightarrow \quad \mathcal{D}^0_k(i\omega_q) = \frac{1}{i\omega_q - \omega_k} - \frac{1}{i\omega_q + \omega_k}$$

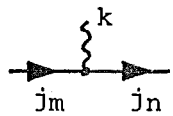

$$\rightarrow \quad V^{jk}_{mn}$$

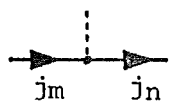

$$\rightarrow \quad M_{mn}$$

[1] For a level propagator, but not a phonon propagator, the sense of the frequency 'flow' is relevant to considerations of distinctness.

Figure 3.1

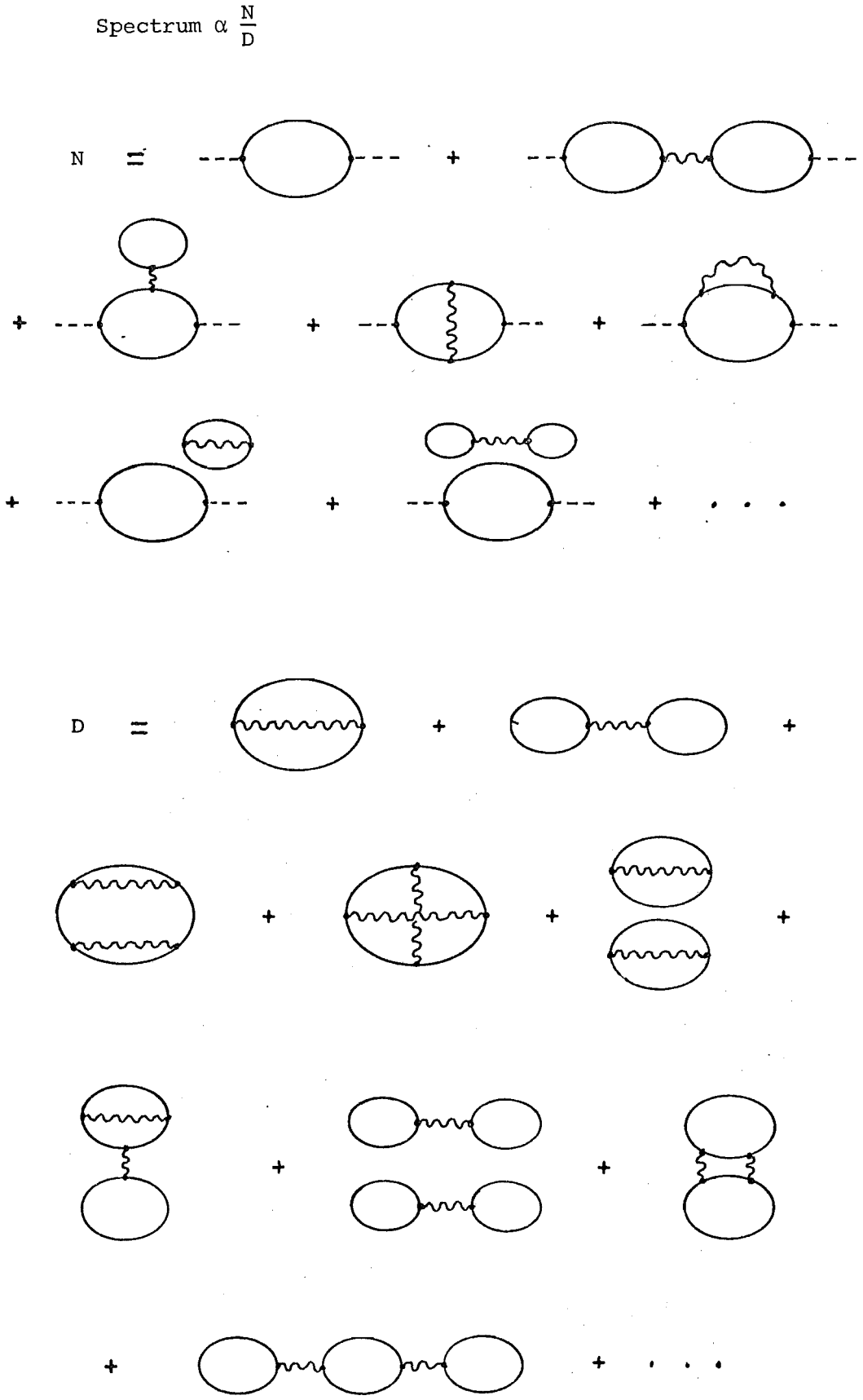

(c) Sum over all intermediate frequencies, wavevector sites and levels.

(d) Multiply the diagram by a factor $\beta^{-(n+1)}(-1)^F$ where F is the number of closed fermion loops.

(e) Whenever a particle line either closes on itself, or is joined by the same interaction line, insert a convergence factor $e^{i\omega_n 0^+}$.

The form of the interaction (3.8) and the dipole moment expansion (3.4) is such that all level propagators forming a closed loop must have the same site label, this being used to label the loop. Figure 3.1 then contains diagrams that contain one, two or more closed fermion loops, each loop being labelled by a site label. As expounded in the previous chapter the isospin representation introduces 'unphysical' states whose effect must be projected out of each diagram contributing to D and N.

3.3 Second-order Diagram.

Consider the contribution from the second-order diagram of figure 3.1 redrawn in figure 3.2.

Figure 3.2

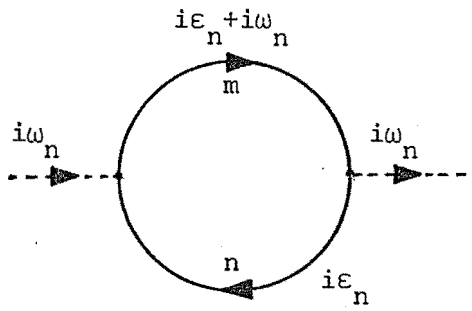

This gives upon applying the previously defined rules:

$$= -\sum_{mn} |M_{mn}|^2 \beta^{-1} \sum_{i\varepsilon_n} F_n^0(i\varepsilon_n)\, F_m^0(i\varepsilon_n + i\omega_n)$$

$$= -\sum_{mn} |M_{mn}|^2 \beta^{-1} \sum_{i\varepsilon_n} \frac{1}{i\varepsilon_n - \lambda_n} \cdot \frac{1}{i\varepsilon_n + i\omega_n - \lambda_m} \qquad (3.9)$$

The sum over frequencies $i\varepsilon_n = i(2n+1)\pi/\beta$ $n=0, \pm1, \pm2, \ldots$ involved in this expression can be replaced by a contour integral. (Fetter and Walecka p248 (1971), Schrieffer p196 (1964)).

$$(3.9) = \sum_{mn} |M_{mn}|^2 \oint_C \frac{dz}{2\pi i} f_D(z) \frac{1}{z - \lambda_n} \cdot \frac{1}{z + i\omega_n - \lambda_m} \qquad (3.10)$$

where the contour C is around the simple poles of the Fermi-Dirac function $f_D(z) = (e^{\beta z} + 1)^{-1}$ which occurs at $z = i(2n + 1)\pi/\beta$ with residues $-\beta$ (see figure 3.3).

Figure 3.3

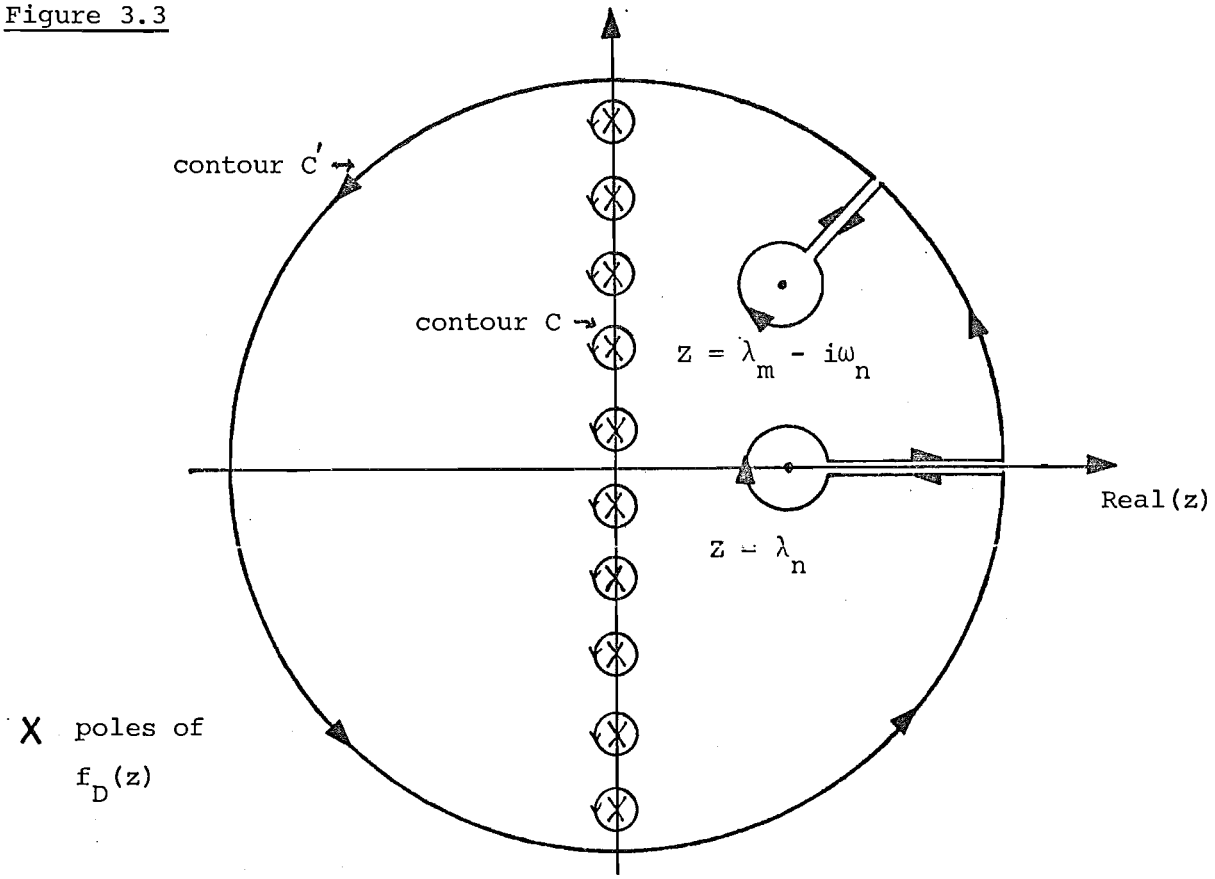

Using the properties of contour integrals, contour C can be deformed into contour C' without affecting the value of the integral. As the outer circle spreads radially out to infinity the contribution from this part of the contour can be shown to vanish and the contribution from the straight sections cancel leaving only the contributions from the two simple poles at $z = \lambda_m - i\omega_n$ and $z = \lambda_n$. Then from the residue theorem (Churchill 1960) this can be evaluated to give

$$(3.9) = - \sum_{mn} |M_{mn}|^2 \left[\frac{f_D(\lambda_n)}{i\omega_n + \lambda_n - \lambda_m} + \frac{f_D(\lambda_m - i\omega_n)}{-i\omega_n + \lambda_m - \lambda_n} \right] \qquad (3.11)$$

This result must now be analytically continued to the whole complex plane. The prescription given by Baym and Mermin (1961) (Chapter 2.1.1) involves the replacement of $i\omega_n$ by z, after all factors such as $e^{\beta i\omega_n}$ have been

reduced to ±1. In (3.11) there is a factor

$$f_D(\lambda_m - i\omega_n) = [e^{\beta(\lambda_m - i\omega_n)} + 1]^{-1} = [e^{\beta\lambda_m} e^{-\beta i\omega_n} + 1]^{-1} \qquad (3.12)$$

which using (3.5) can be written in the form $f_D(\lambda_m)$. This results in the analytically continued contribution

$$G(z) = - \sum_{mn} |M_{mn}|^2 [f_D(\lambda_n) - f_D(\lambda_m)] \cdot \frac{1}{z + \omega_{nm}} \qquad (3.13)$$

where $\omega_{nm} = \lambda_n - \lambda_m = \varepsilon_n - \varepsilon_m$.

Using this in (3.6) we obtain the contribution of the diagram of figure 3.2 to the spectrum

$$\sigma(\omega_0) = \omega_0 \sum_{mn} |M_{mn}|^2 [f_D(\lambda_n) - f_D(\lambda_m)] \, \delta(\omega_0 + \omega_{nm}) \qquad (3.14)$$

where we have used the well known result (Heitler 1954 p69)

$$\lim_{\varepsilon \to 0^+} \frac{1}{x \pm i\varepsilon} = \frac{P}{x} \mp i\pi\delta(x) \qquad (3.15)$$

where P denotes the principal value part.

Applying the isospin mapping (2.54) to (3.14) involves a factor

$$\frac{1}{Z} \lim_{\lambda \to \infty} e^{\beta\lambda} \left[\frac{1}{e^{\beta(\lambda + \varepsilon_n)} + 1} - \frac{1}{e^{\beta(\lambda + \varepsilon_m)} + 1} \right] \qquad (3.16)$$

$$= (e^{-\beta\varepsilon_n} - e^{-\beta\varepsilon_m}) / \sum_i e^{-\beta\varepsilon_i} \equiv \rho_n - \rho_m$$

where $\rho_i = \dfrac{e^{-\beta\varepsilon_i}}{\Sigma_j e^{-\beta\varepsilon_j}}$ is the population factor of level i. This gives, then, the contribution to the spectrum

$$\sigma(\omega_0) = \omega_0 \sum_{mn} |M_{mn}|^2 \, (\rho_n - \rho_m) \delta(\omega_0 + \omega_{mn}) \qquad (3.17)$$

which consists of a delta function peak at $\omega_0 = \omega_{mn}$.

This contribution is consistent with the interpretation that the spectrum arises from two types of contributions: an absorption term with a weighting of ρ_n where the ion in level n absorbs a photon and suffers a transition to a level m, minus an emission term with a weighting ρ_m where the ion in level m emits a photon and suffers a transition to a level n.

(see figure 3.4)

Figure 3.4

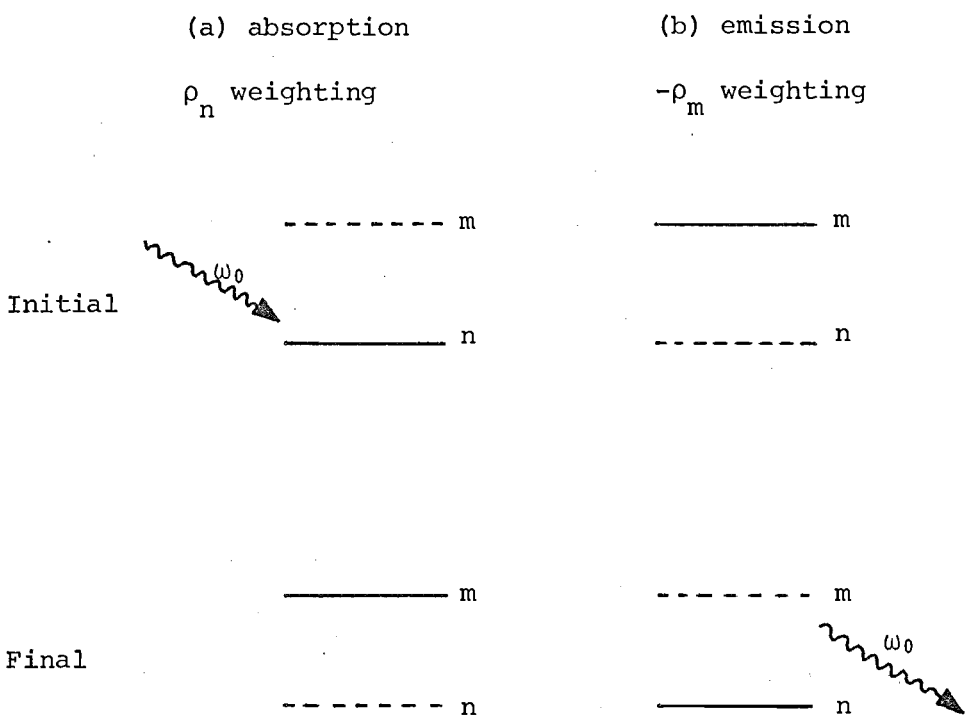

Each diagram of figure 3.1 can be similarly evaluated giving a spectral contribution.

3.4 Many Ion Spectrum

A closer study of the evaluation of the diagrams reveals that if a diagram contains two or more (say n) loops with the same site label, then instead of a factor of the form (3.16), then factors of the form

$$\frac{1}{Z} \lim_{\lambda \to \infty} e^{\beta\lambda} f_D(\lambda_{i_1}) f_D(\lambda_{i_2}) \cdots\cdots f_D(\lambda_{i_n}) \qquad (3.18)$$

appear which vanish identically for $n \geqslant 2$. Hence only diagrams containing at most one loop with any site label can contribute to the spectrum.

Thus if there was only one impurity ion in the crystal, the diagrams that contribute to the spectrum can be written as in figure 3.5.

Figure 3.5

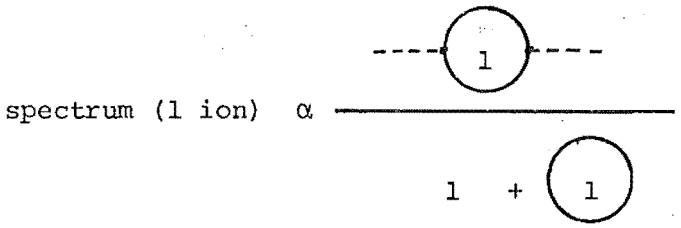

(3.19)

where by 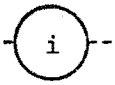 ,  is meant all connected, disconnected diagrams respectively containing only one loop referring to site i. (e.g. figure 3.6).

Figure 3.6

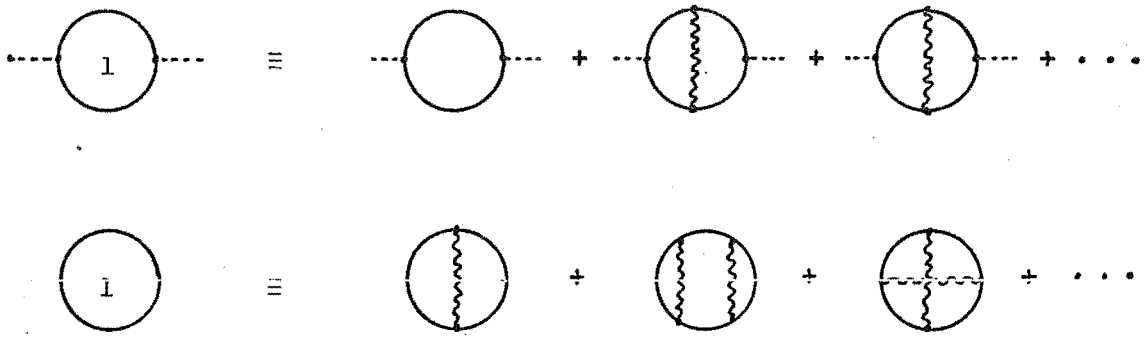

(Note that the contribution from 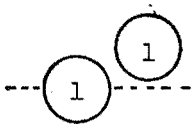 has vanished because it involves two loops with the same site labelling). Similarly for two impurity ions we obtain a contribution

Figure 3.7

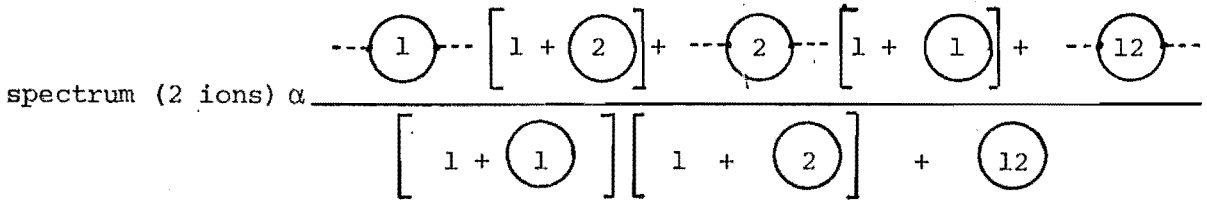

where 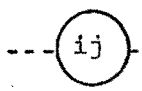 and  contain both a site i loop connected by phonons to a site j loop. (e.g. figure 3.8).

Figure 3.8

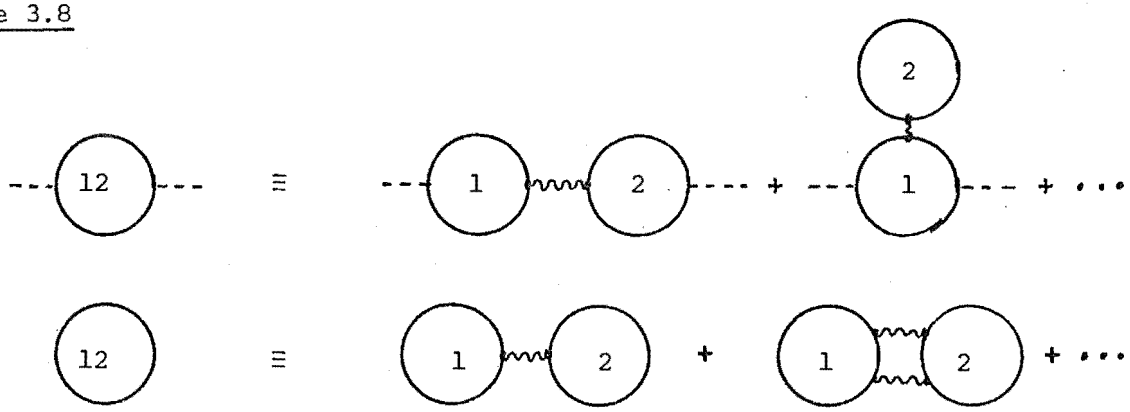

A consideration of the diagrams contributing to 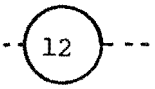 and  show that they contain one or more phonons that 'connect' site 1 to site 2. We shall see in the following chapter on pair spectra that such a contribution depends on the distance $R = |\underline{r}_1 - \underline{r}_2|$ between the ions approximately as R^{-3} at large[1] R. If the impurity ions are far apart in the crystal then the contributions from these terms are small and the spectrum can be written approximately as

Figure 3.9

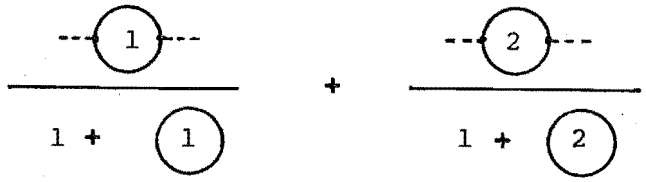

which is twice that of the one ion contribution. This analysis can be extended to an arbitrary number N of impurity ions; the contribution being N times that of the one ion spectrum if all diagrams involving one or more phonons connecting two or more ions are neglected. This means that the N ion spectrum can be obtained approximately by considering only the one-ion spectra; the intensity of the spectrum being proportional to the number of impurity ions present.

This approximation, (which previous authors have used but not analysed), is sufficient for low concentrations, C, of impurity ions in the host crystal because the probability of two ions being close together (e.g. nearest neighbours) is of the order C^2 (Johnstone (1975)) (Similarly

[1] By large we mean compared to the wavelength of the phonon involved.

the probability of triples is approximately C^3, etc.) However as the concentration of impurity ions is increased, the probability of the occurrence of (nearest neighbour) pairs increases and the above approximation becomes untenable. In chapter 4 we shall investigate the contributions arising from the  type diagrams and show that they correspond to and give the pair spectra, namely the extra spectral lines that appear as satellites to the main lines as the impurity concentration C is increased.

3.5 Single Ion Spectra

The single ion absorption spectrum has been described using diagram techniques by a number of workers, including Stedman (1970a,b, 1971a,b, 1972 a,b, 1973, 1976a, 1977) Hernández and Walker (1972), Nishikawa and Barrie (1963) and Barrie and Rystephanick (1966). In the rest of this chapter we shall present a new approach to this problem in an attempt to provide a description of the general spectrum, and particularly to line shapes, that is as complete as possible.

In the expression (3.19) for the single ion spectrum, the denominator is independent of the frequency $i\omega_n$ and hence (via (3.6)) can only give a multiplicative intensity contribution. As our interest lies more in relative line shape variations rather than say the variation of intensity with temperature we shall only consider the contribution of the numerator in (3.6). Contribution (3.17) arose from the second order diagram of figure 3.2 which contains no phonon propagators. We shall show that the effect of 'dressing' the level propagators with phonons is to broaden this delta function, to shift the position of the peak and to introduce phonon sidebands to the spectrum.

To obtain the above mentioned shift and broadening of the delta function, the contribution from an infinite number of diagrams needs to be summed. This is because any single diagram is found to give only delta functions and hence any finite sum of these diagrams will also give only delta functions. Fortunately however we have a method by which the

contribution of an infinite number of diagrams may be summed by evaluating only a finite number of diagrams. This is achieved using the Dyson equation presented in chapter 2. Denoting[1] $F_{mm'}(i\omega_n)$ as a double solid line, it has the diagram expansion given in figure 3.10.

Figure 3.10

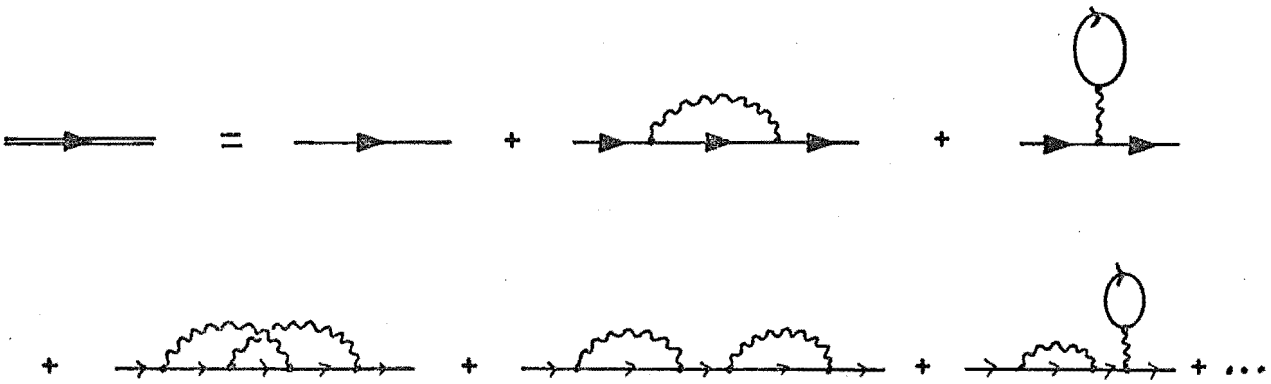

which can be written in the Dyson equation form as in figure 3.11a where the self energy function is defined by figure 3.11b.

Figure 3.11

(a)

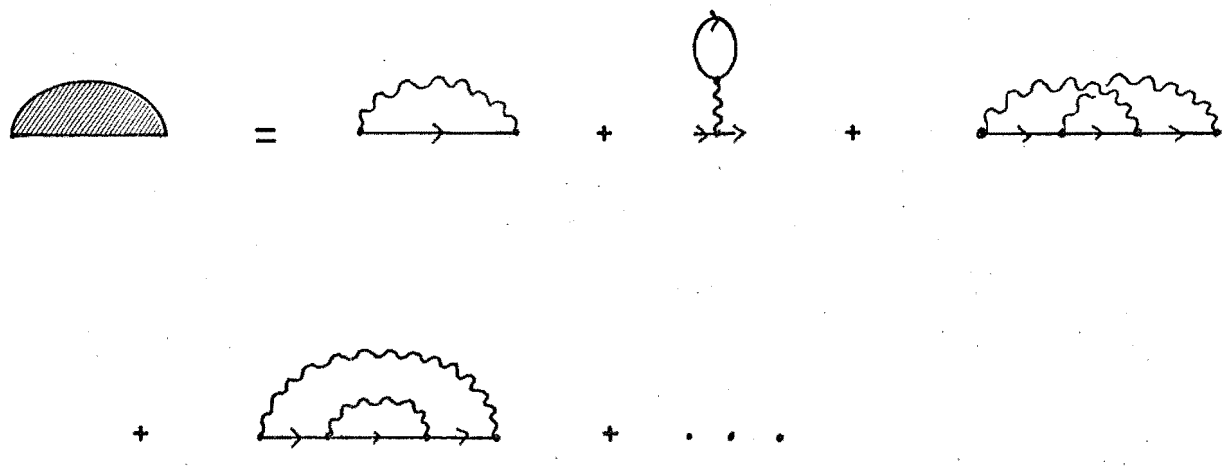

(b)

[1] As we are now considering only one ion we have dropped the site index.

The self energy only contains diagrams that cannot be split into two parts by severing a level propagator. The second contribution to the self energy contains a closed level propagator loop and hence as our basic diagram for the spectrum already contains one such loop, any diagram containing this will vanish. This means we must disregard its contribution to the self energy. Equation (3.22) can be written in terms of a matrix equation.

$$F(i\omega_n) = F^0(i\omega_n) + F^0(i\omega_n)\,\Sigma(i\omega_n)\,F(i\omega_n) \tag{3.24}$$

where the elements of the matrices are given by

$$[F(i\omega_n)]_{m,m'} = F_{mm'}(i\omega_n) \equiv$$

$$[F^0(i\omega_n)]_{m,m'} = \delta_{mm'}\,F^0_m(i\omega_n) \equiv \tag{3.25}$$

$$[\Sigma(i\omega_n)]_{m,m'} = \Sigma_{mm'}(i\omega_n) \equiv$$

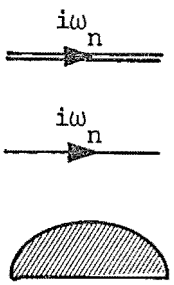

Equation (3.24) can be manipulated to obtain the inverse of $F(i\omega_n)$

$$F^{-1}(i\omega_n) = (F^0(i\omega_n))^{-1} - \Sigma(i\omega_n) \tag{3.26}$$

Because $F^0(i\omega_n)$ is a diagonal matrix then its inverse is also diagonal and its matrix elements are those of $F^{-1}(i\omega_n)$ are easily obtained. However this still leaves the problem of inverting the $F^{-1}(i\omega_n)$ matrix to obtain the required matrix elements of $F(i\omega_n)$. This problem is not easy to treat analytically in full generality and the usual approximation made is to assume that $\Sigma(i\omega_n)$ and hence $F(i\omega_n)$ is diagonal. This gives the solution

$$F_{mm}(i\omega_n) = \frac{1}{(F^0_m(i\omega_n))^{-1} - \Sigma_{mm}(i\omega_n)} \tag{3.27}$$

which we shall investigate shortly. Stedman (1976) has investigated the possibility of allowing non-zero off-diagonal $F_{mm'}(i\omega_n)$, but with states m,m' being degenerate (e.g. they may arise from the degenerate time-reversed conjugate states of a Kramers ion) where he showed that these

"interference diagrams" gave small shifts to the spectral lines.

In the following sections of this chapter we shall, for simplicity and to enable us to obtain analytic results, assume that the matrix $\Sigma(i\omega_n)$ is diagonal. It is possible to correct for some types of diagrams, such as that of figure 3.12a, which are disregarded by this approximation.

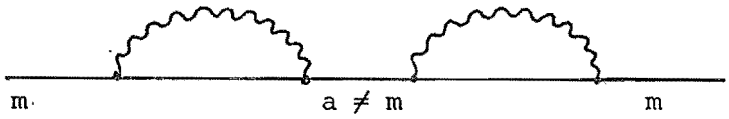

(a)

(b)

This is achieved by considering the diagram of figure 3.12b as contributing to the self energy $\Sigma_{mm}(i\omega_n)$ even though it is not a proper self energy in the sense that it can be split into two parts by severing propagator a. The effect of this approach is to considerably reduce the number of diagram contributions being neglected by the diagonal $\Sigma(i\omega_n)$ approximation.

3.5.1 Additive Diagram Contributions

Let us study the contribution from the diagram of figure 3.13

Figure 3.13

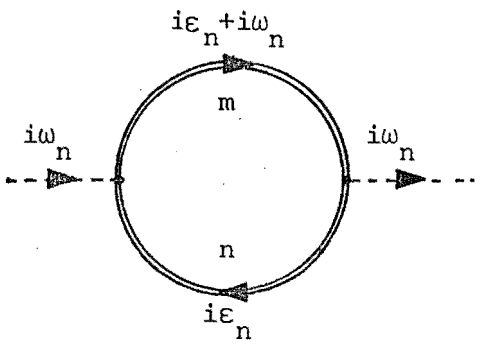

which is the equivalent diagram to that of figure 3.2 but with the zero-order level propagators replaced with dressed diagonal level propagators. This gives a contribution to (3.5)

$$- \sum_{mn} |M_{mn}|^2 \beta^{-1} \sum_{i\varepsilon} F_n(i\varepsilon_n) \, F_m(i\varepsilon_n + i\omega_n) \quad . \tag{3.28}$$

Again this can be converted to a contour integral about the poles of the Fermi-Dirac function.

$$(3.28) = \sum_{mn} |M_{mn}|^2 \oint_C \frac{dz}{2\pi i} f_D(z) \, F_n(z) \, F_m(z + i\omega_n) \tag{3.29}$$

Using (3.27) we obtain

$$F_m(z) = \frac{1}{z - \lambda_m - \Sigma_{mm}(z)} \tag{3.30}$$

and using the property that the self-energy function $\Sigma_{mm}(z)$ is regular everywhere in the complex plane except on the real axis where it has the property

$$\Sigma_{mn}(x + i0^+) = \Sigma^*_{mn}(x - i0^+) \quad x\varepsilon R \tag{3.31}$$

then similarly $F_m(z)$ is regular everywhere except on the real axis where it obeys

$$\frac{1}{2\pi i} [F_m(x + i0^+) - F_m(x - i0^+)] = \frac{\Gamma_m(x)/\pi}{[x - \lambda_m - \Delta_m(x)]^2 + \Gamma_m^2(x)}$$

$$\equiv L_m(x) \tag{3.32}$$

where

$$\Sigma_{mm}(x \pm i0^+) = \Delta_m(x) \pm i\Gamma_m(x) \quad . \tag{3.33}$$

Because the G.F.'s in (3.29) do not have simple poles but rather cuts along the lines $\mathrm{Im}(z) = 0, -i\omega_n$ then instead of deforming contour C into C' as in figure 3.3, it is deformed to C'' as in figure 3.14

Figure 3.14

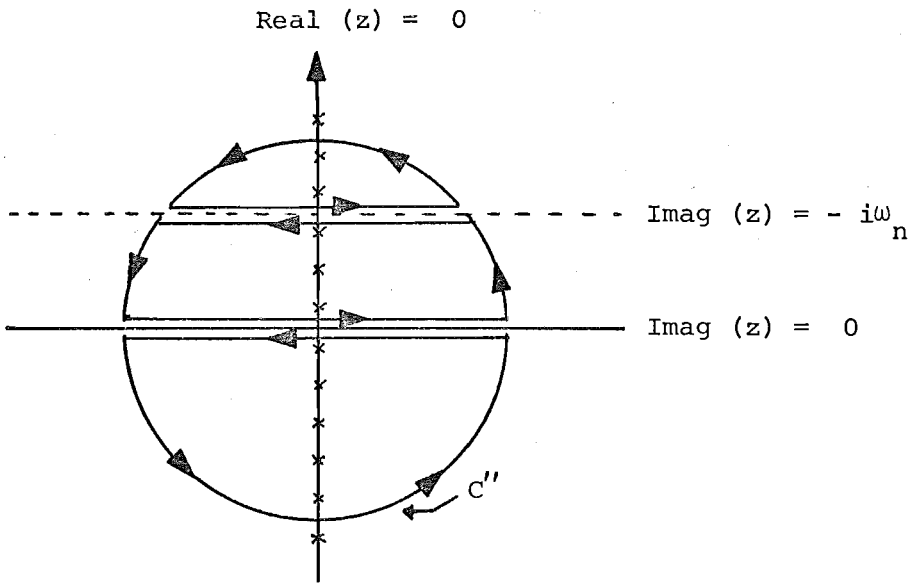

Again as the radius increases to infinity the contribution from the circular parts vanishes leaving only the contributions from the lines just above and below the cut lines giving

$$(3.28) = \sum_{mn} |M_{mn}|^2 \int_{-\infty}^{\infty} \frac{dx}{2\pi i} \{[F_n(x + i0^+) - F_n(x - i0^+)] F_m(x + i\omega_n)$$

$$+ F_n(x - i\omega_n) [F_m(x + i0^+) - F_m(x - i0^+)]\} \qquad (3.34)$$

where we have used the property of $f_D(x)$ given in (3.12).

Using (3.22) this can be rewritten as

$$(3.28) = \sum_{mn} |M_{mn}|^2 \int_{-\infty}^{\infty} dx\, f_D(x) \{L_n(x)\, F_m(x + i\omega_n)$$

$$+ F_n(x - i\omega_n)\, L_m(x) \}. \qquad (3.35)$$

To find the contribution to the spectrum we perform the procedure of (3.6) and obtain

$$\sigma(\omega_0) = \omega_0 \sum_{mn} |M_{mn}|^2 \int_{-\infty}^{\infty} dx[f_D(x) - f_D(x + \omega_0)]\, L_n(x) L_m(x + \omega_0) \qquad (3.36)$$

Because of the complex form of the integrand in this expression it is not possible to obtain an exact analytical result.

In chapter 8 we study this integral numerically for a model system and show that it gives approximately a lorentzian peak slightly shifted from

$\omega_0 = \omega_{mn}$ corresponding to the no-phonon-line (N.P.L.) peak and background phonon sidebands. We shall now present a method to obtain an approximate analytical expression for the N.P.L. peak.

The approximations that we need to make (which we shall refer to as the lorentzian or sharply peaked approximation) are

(i) the functions $\Delta_i(x)$, $\Gamma_i(x)$ of (3.33) are slowly varying

and

(ii) the function $L_n(x)$ is sharply peaked at the solution of the transcendental equation $x = \lambda_n + \Delta_n(x)$ which we denote $\bar{\lambda}_n$.[1]

These approximations allow us to replace the x dependence of the selected parts of the integrand by $\bar{\lambda}_n$; namely the Fermi-Dirac factors and all the Δ and Γ functions. This results in the convolution expression

$$\sigma(\omega_0) = \omega_0 \sum_{mn} |M_{mn}|^2 [f_D(\bar{\lambda}_n) - f_D(\bar{\lambda}_n + \omega_0)] \int_{-\infty}^{\infty} dx \quad \frac{\gamma_n/\pi}{(x - \delta_n)^2 + \gamma_n^2} \quad \frac{\gamma_m/\pi}{(x + \omega_0 - \delta_m)^2 + \gamma_m^2} \qquad (3.37)$$

where $\gamma_n \equiv \Gamma_n(\bar{\lambda}_n)$, $\gamma_m \equiv \Gamma_m(\bar{\lambda}_n + \omega_0)$, $\delta_n \equiv \lambda_n + \Delta_n(\bar{\lambda}_n) = \bar{\lambda}_n$

and $\delta_m \equiv \lambda_m + \Delta_m(\bar{\lambda}_n + \omega_0)$.

The convolution of two lorentzians is given in appendix 3B with the result

$$\sigma(\omega_0) = \omega_0 \sum_{mn} |M_{mn}|^2 [f_D(\bar{\lambda}_n) - f_D(\bar{\lambda}_n + \omega_0)] \frac{(\gamma_n + \gamma_m)/\pi}{(\omega_0 - \delta_m + \delta_n)^2 + (\gamma_n + \gamma_m)^2} \qquad (3.38)$$

which is a lorentzian centred on $\omega_0 = \delta_m - \delta_n$ with width $\gamma_n + \gamma_m$. The lorentzian is peaked at $\omega_0 - \lambda_m - \Delta_m(\bar{\lambda}_n + \omega_0) + \bar{\lambda}_n = 0$ which occurs at the solution of the transcendental equation $x - \lambda_m - \Delta_m(x) = 0$ which we write as $x = \bar{\lambda}_m$. Hence close to the peak of the N.P.L. we can replace γ_m by $\Gamma_m(\bar{\lambda}_m)$ and δ_m by $\bar{\lambda}_m$ and also $f_D(\bar{\lambda}_n + \omega_0)$ by $f_D(\bar{\lambda}_m)$. Writing $\bar{\lambda}_i$ as $\lambda + \bar{\epsilon}_i$ it is found that the only λ dependences appear in the Fermi-Dirac

[1] This is the L_∞ approximation of Stedman's (1972a) self-consistent series

$$\begin{aligned} x &= \lambda_n && L_0 \\ x &= \lambda_n + \Delta_n(\lambda_n) && L_1 \\ &\vdots && \vdots \end{aligned}$$

factors which give, upon the action of (2.54), a factor $\bar{\rho}_n - \bar{\rho}_m$ where

$$\bar{\rho}_i = e^{-\beta\bar{\epsilon}_i} / \sum_j e^{-\beta\epsilon_j}$$

The N.P.L. spectrum can be written as

$$\sigma(\omega_0) = \omega_0 \sum_{mn} |M_{mn}|^2 (\bar{\rho}_n - \bar{\rho}_m) \frac{(\gamma_n + \gamma_m)/\pi}{(\omega_0 - \bar{\omega}_{nm})^2 + (\gamma_n + \gamma_m)^2} . \quad (3.39)$$

Compared with (3.17) the delta functions have been broadened into lorentzians and shifted slightly from the basic ω_{mn} positions. If, rather than the diagram of figure 3.13, we had considered the contribution of the diagram where only propagators m,n respectively were replaced with full propagators and the remaining propagator remained a zero-order propagator, then the degree of braodening and shift would only be that contributed by the full propagator. These diagram contributions to the spectrum then allow, within the approximations made, the standard Wigner-Weisskopf interpretation to be made. That is each level can be regarded as being shifted from its zero-order position ϵ_i by an amount $\Delta_i(\bar{\lambda}_i)(\epsilon_i \rightarrow \epsilon_i + \Delta_i(\bar{\lambda}_i))$ and a width $\Gamma_i(\bar{\lambda}_i)$ associated with it such that the spectrum can be regarded as a series of lorentzians. Each of these results from a possible transition $n \rightarrow m$ and is peaked on the difference $(\bar{\epsilon}_n - \bar{\epsilon}_m)$ of its new energy levels. Its width is given by the sum of the relevant widths $(\Gamma_m(\bar{\lambda}_m) + \Gamma_n(\bar{\lambda}_n))$. Because of this algebraic additive nature of the width and shift these diagrams have been given the designation 'additive diagrams'.

3.5.2 Non-additive Diagrams

The lowest order diagrams that contribute to the single ion absorption spectrum not accounted for in figure 3.13 are those exhibited in figure 3.15.

Figure 3.15

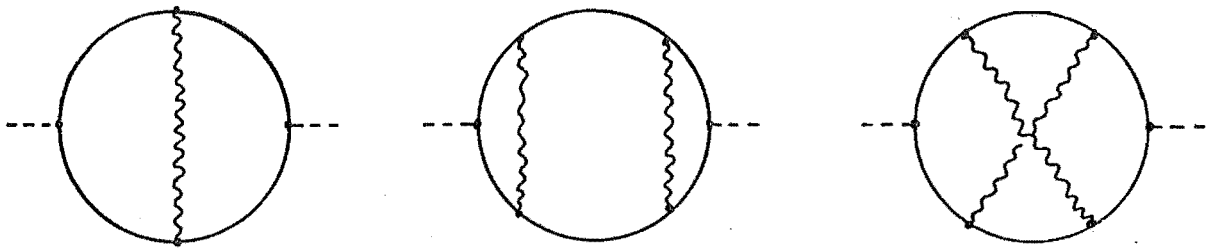

Each of the diagrams contains one or more phonon propagators connecting the upper and lower level propagators. Stedman (1971) has presented an approximate method of evaluating each of these diagrams contribution to the shift and width of the N.P.L.

We present a method whereby all these diagrams can be combined in a general expression for the absorption spectrum. This method is not able to produce a simple analytical expression for the shift and width of any spectral feature but does contain the full lineshape of the spectral feature.

Using Dyson's equation we are able to sum an infinite number of diagrams, as is required to obtain finite shifts and widths; the lowest order diagrams are given in figure 3.16.

Figure 3.16

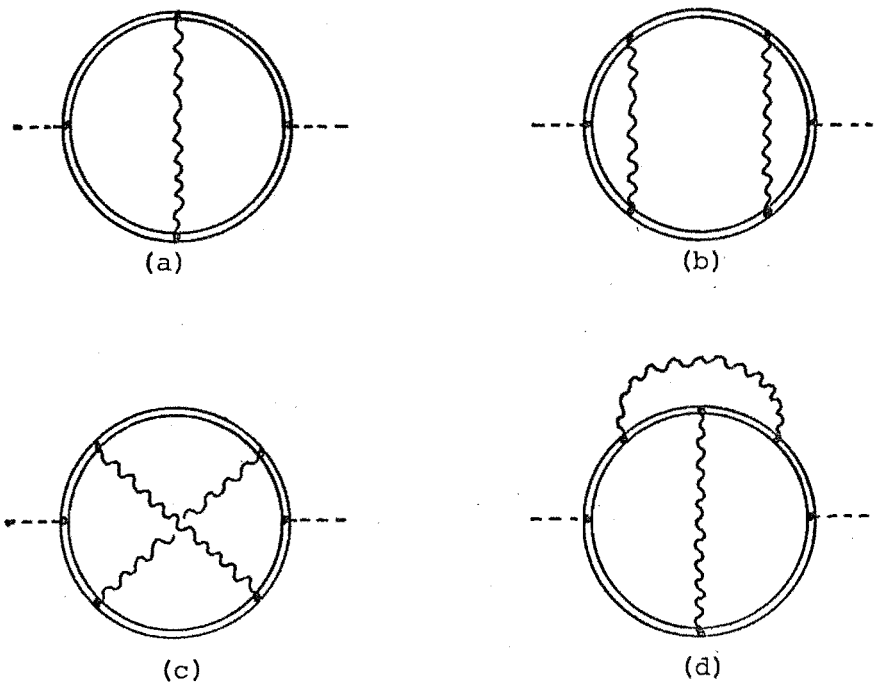

Diagram 3.16a gives a contribution

$$G(i\omega_n) = \sum_{abcd} \sum_{k} M_{ab} V^{k}_{bc} M_{cd} V^{-k}_{da} \beta^{-1} \sum_{i\omega_{n'}} e^{i\omega_{n'} 0^+} F_a(i\omega_{n'})$$

$$F_b(i\omega_n + i\omega_{n'}) \beta \sum_{i\omega_{n''}} e^{i\omega_{n''} 0^+} F_c(i\omega_{n''} + i\omega_n) F_d(i\omega_{n''}) \left\{ \frac{1}{i\omega_{n''} - i\omega_{n'} - \omega_k} \right.$$

$$\left. - \frac{1}{i\omega_{n''} - i\omega_{n'} + \omega_k} \right\} \qquad (3.40)$$

Converting the sums over $i\omega_{n'}$ and $i\omega_{n''}$ to contour integrals about the poles of the Fermi-Dirac function we obtain a spectral contribution[1].

$$\sigma(\omega_0) = \omega_0 \sum_{abcd} \sum_{k} \binom{n_k}{n_k+1} M_{ab} V^{k}_{bc} M_{cd} V^{-k}_{da} \int_{-\infty}^{\infty} dx [f_D(x) - f_D(x + \omega_0)]$$

$$\{L_a(x) A_d(x \pm \omega_k) + A_a(x) L_d(x \pm \omega_k)\} \qquad (3.41)$$

$$\{L_b(x + \omega_0) A_c(x + \omega_0 \pm \omega_k) + A_b(x + \omega_0) L_c(x + \omega_0 \pm \omega_k)\}$$

where $n_k = f_B(\omega_k)$

$$A_i(x) = \frac{x - \lambda_i - \Delta_i(x)}{[x - \lambda_i - \Delta_i(x)]^2 + \Gamma_i^2(x)}$$

The integrand of (3.41) contains four terms each of which is the product of two L_i functions and two A_i functions.

If we evaluate the contribution of diagram 3.15a, (the analogous diagram containing bare propagators), we obtain an expression similar to (3.41) but with the substitutions

$$\delta(x - \lambda_i) \quad \text{for} \quad L_i(x)$$
$$\text{and} \quad \frac{1}{x - \lambda_i} \quad \text{for} \quad A_i(x). \qquad (3.42)$$

[1] In (3.41) (and in subsequent equations) this represents the sum of two contributions: one with the factor n_k and the upper signs and another with the $(n_k + 1)$ factor and the lower signs.

The resulting integral is easily evaluated giving two delta functions peaked on N.P.L. positions (i.e. $\delta(\omega_0 - \omega_{ba})$ and $\delta(\omega_0 - \omega_{cd})$), and two delta function peaks shifted from N.P.L. positions by phonon frequencies, (i.e. $\delta(\omega_0 \pm \omega_k - \omega_{ca})$ and $\delta(\omega_0 \pm \omega_k - \omega_{db})$), which are interpreted as contributing to the one-phonon sidebands. The four delta function contributions are related to the four possible ways in which diagram 3.15a can be cut by a line running from below the diagram to above it. Those lines that cut two level propagators give N.P.L. type delta functions, (i.e. dotted lines (1) and (2) in figure 3.17), while those that also cut one phonon propagator result in sideband type delta functions (i.e. lines (3) and (4) in figure 3.17).

Figure 3.17

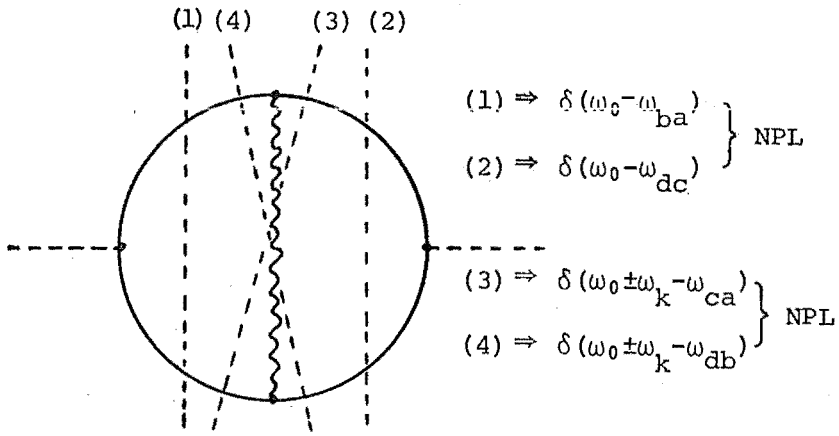

If we make the sharply peaked approximation in (3.41) we obtain convolutions of products of L_i and A_i functions which can be evaluated by the methods of appendix 3B. These convolutions result in approximately lorentzian contributions, (they contain <u>small</u> admixtures of antisymmetric A_i contributions), shifted slightly from the delta function contributions of diagram 3.15a. The identification (3.42) allows us to decide whether a particular contribution generally contributes to the N.P.L., the one-phonon sideband or some higher order phonon sideband. Similarly to the identification of figure 3.17, these correspond to vertical lines that cut two <u>full</u> or <u>dressed</u> level propagators and zero, one or more phonon propagators respectively. We use this identification to advantage in the

next section to obtain general expressions for their spectra.

3.5.3 General Expressions for Spectrum

By using the method explained in the previous section we can quickly decide whether a particular diagram contributes to the N.P.L., the one-phonon sideband or m-phonon sideband. This enables us to give a general expression for the N.P.L. that contains every contribution from the diagrams of figure 3.16, namely

$$\text{N.P.L. } \sigma(\omega_0) = \omega_0 \sum_{mn} \int_{-\infty}^{\infty} dx [f_D(x) - f_D(x+\omega_0)]\, L_n(x) L_m(x+\omega_0) \left| P_{mn}(x, x+\omega_0) \right|^2 \qquad (3.43)$$

where

$$P_{mn}(x,y) = M_{mn} + \sum_{ab} \sum_{k} \binom{n_k}{n_k+1} V^k_{ma} M_{ma} V_{bn} A_a(y \pm \omega_k) A_b(x \pm \omega_k)$$

$$+ \sum_{abcd} \sum_{k\ell} \binom{n_k}{n_k+1} \binom{n_\ell}{n_\ell+1} V^k_{ma} V^\ell_{ab} M_{bc} V^\ell_{cd} V^k_{dn} A_a(x \pm \omega_k) A_b(x \pm \omega_\ell)$$

$$A_c(y \pm \omega_k \pm \omega_\ell) A_d(y \pm \omega_k) + \cdots \qquad (3.44)$$

The first contribution to (3.44) is that which arose from diagram 3.13 given in (3.36); the second term appears as a cross term with the first in (3.41), (arising from diagram 3.16b), and the third term would arise from diagram 3.16b and so on to higher order in the coupling coefficient V^k_{ab}.

Expressions (3.43) and (3.44) can be given the diagram interpretation in figure 3.18; each diagram in expansion 3.18b gives a contribution to (3.44).

Figure 3.18

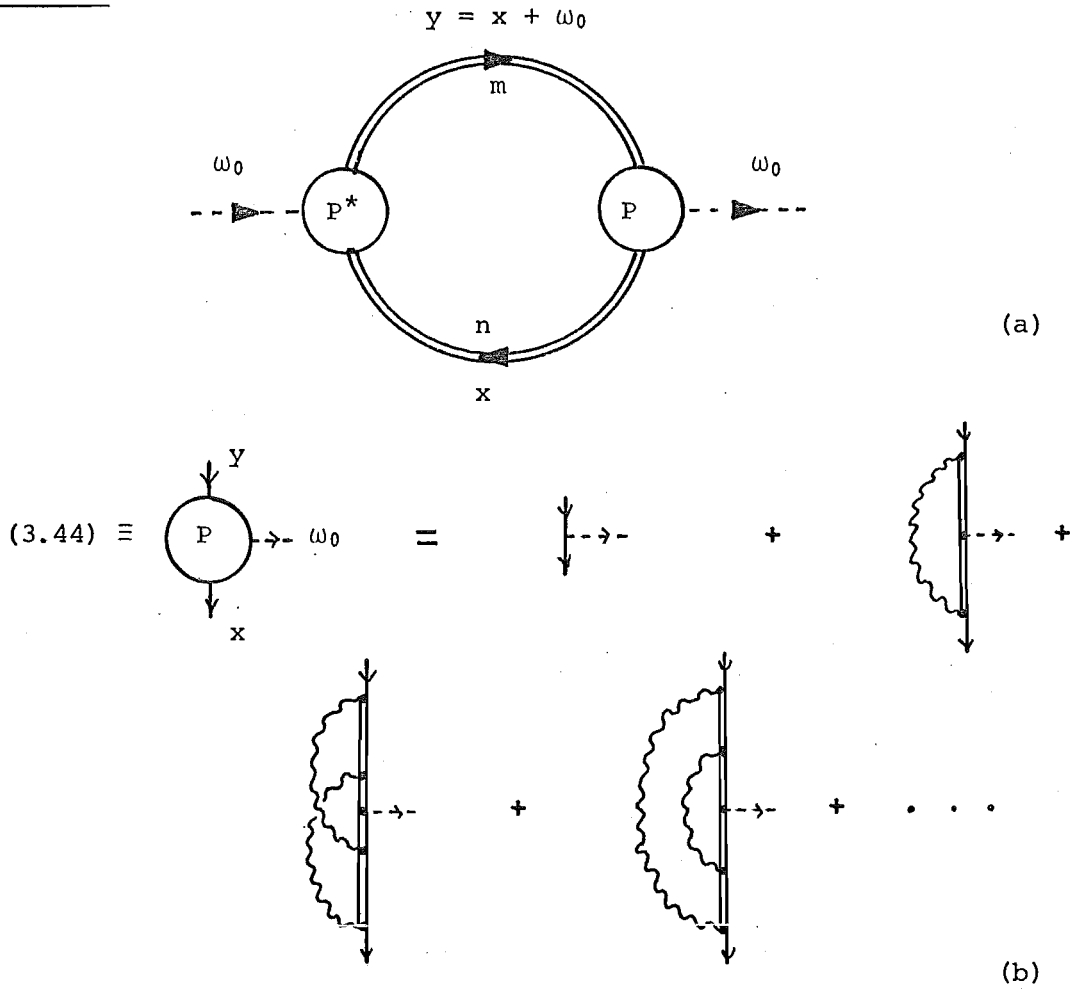

Similarly it is possible to sum over all contributions from figure 3.16 to the one-phonon sideband giving the general expression

$$^{1P}\sigma(\omega_0) = \omega_0 \sum_{mn} \sum_{k} \binom{n_k}{n_k+1} \int_{-\infty}^{\infty} dx \, [f_D(x) - f_D(x+\omega_0)] \, L_n(x)$$

$$L_m(x + \omega_0 \pm \omega_k) \, |Q_{mn}(x, \pm \omega_k, \omega_0)|^2 \qquad (3.45)$$

with the diagram equivalent and definition of given in figure 3.19.

Figure 3.19

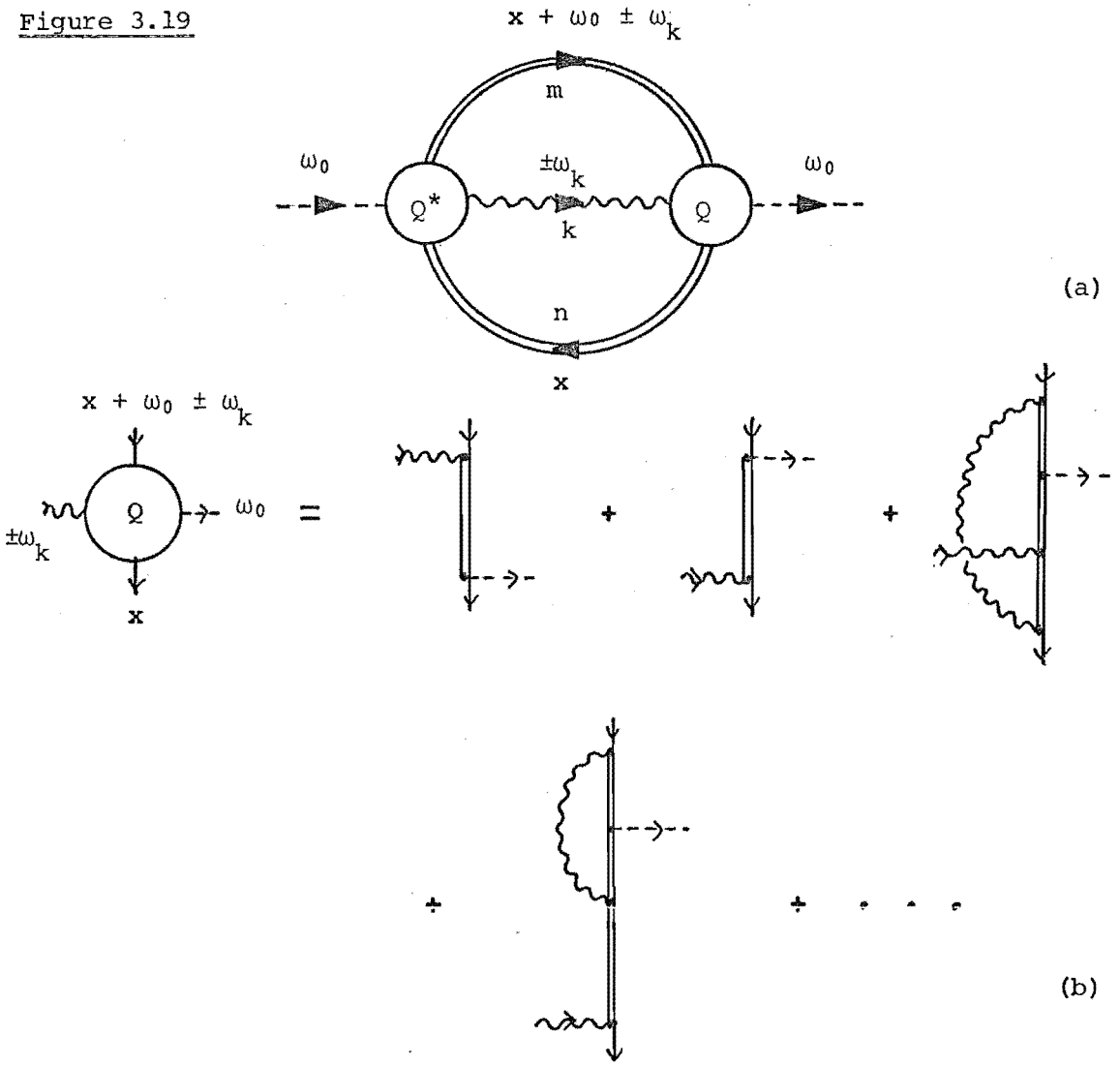

Similarly the general contribution to the two-phonon sideband is obtained from the diagram of 3.20

Figure 3.20

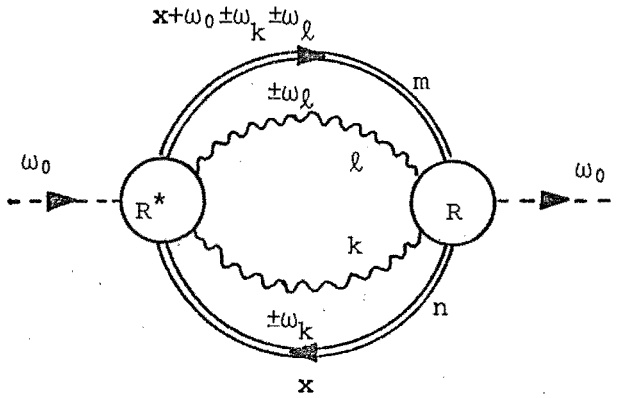

This approach can be extended to give a general expression for the m-phonon sideband spectrum if required.

It is possible to evaluate the convolutions in (3.43) and (3.45) if we make the sharply peaked approximation and also neglect the x dependence of the vertex functions P_{mn} and Q_{mn}. This gives an expression for the N.P.L. spectra

$$\sigma^{N.P.L.}(\omega_o) \simeq \omega_0 \sum_{mn} (\bar{\rho}_m - \bar{\rho}_n) \left|P_{mn}(\bar{\lambda}_n,\bar{\lambda}_m)\right|^2 \frac{(\gamma_m + \gamma_n)/\pi}{(\omega_o - \delta_m + \delta_n)^2 + (\gamma_m + \gamma_n)^2} \quad (3.46)$$

and for the one-phonon sideband spectra

$$\sigma^{1P}(\omega_0) \simeq \omega_0 \sum_{mn} \sum_{k} \left\{ \binom{n_k}{n_k+1} \bar{\rho}_n - \binom{n_k+1}{n_k} \bar{\rho}_m \right\} \left|Q_{mn}(\bar{\lambda}_n, \pm\omega_k, \omega_0)\right|^2 \frac{(\gamma_m + \gamma_n)/\pi}{(\omega_0 - \delta_m + \delta_n \pm \omega_k)^2 + (\gamma_m + \gamma_n)^2} \quad (3.47)$$

Expression (3.47) still contains a phonon sum involving the density of states for the crystal and results in a broad sideband to the N.P.L. at $\omega_o = \delta_n - \delta_m$ that reflects this dependence. For example any sharp peaks in the density of states can result in a corresponding sharp peak in the sideband spectrum.

The convolution could in principle be performed (albeit rather tediously) by retaining the x dependence of the vertex functions and using the methods of appendix 3B. In chapter 8 we evaluate some of these expressions numerically to test the accuracy of the results obtained from these approximations.

If rather than the actual lineshapes, we are more interested in the shift and width of the N.P.L., we might expect from (3.46) that we need only investigate the parameters $\delta_n - \delta_m$ and $\gamma_m + \gamma_n$ respectively. However Stedman (1971) has shown that significant contribution to the shift and width of the N.P.L. arise from the contributions we interpret as contributing to the sidebands. In our formalism we interpret this as

arising because the sideband contributions from (3.45) extend into the region of the N.P.L. spectrum. The one-phonon sideband contribution is limited because the phonon density of states vanishes as $\pm\omega_k$ tends to zero. However significant contributions from the two-phonon sideband are possible because ω_k, ω_ℓ may correspond to a peak in the density of states but $\pm(\omega_k - \omega_\ell)$ vanishes. Equation (3.47) then gives a contribution near the N.P.L. position hence affecting its shift and width. Stedman termed these non-additive contributions because they did not satisfy the additive Wigner-Weisskopf interpretation discussed in §3.5.1.

In the next section we evaluate the major additive shift and width contributions and their temperature dependence at low temperatures.

3.6 Shift and Width Functions

The second and fourth order diagrams that contribute to the self energy function are those of figure 3.21

Figure 3.21

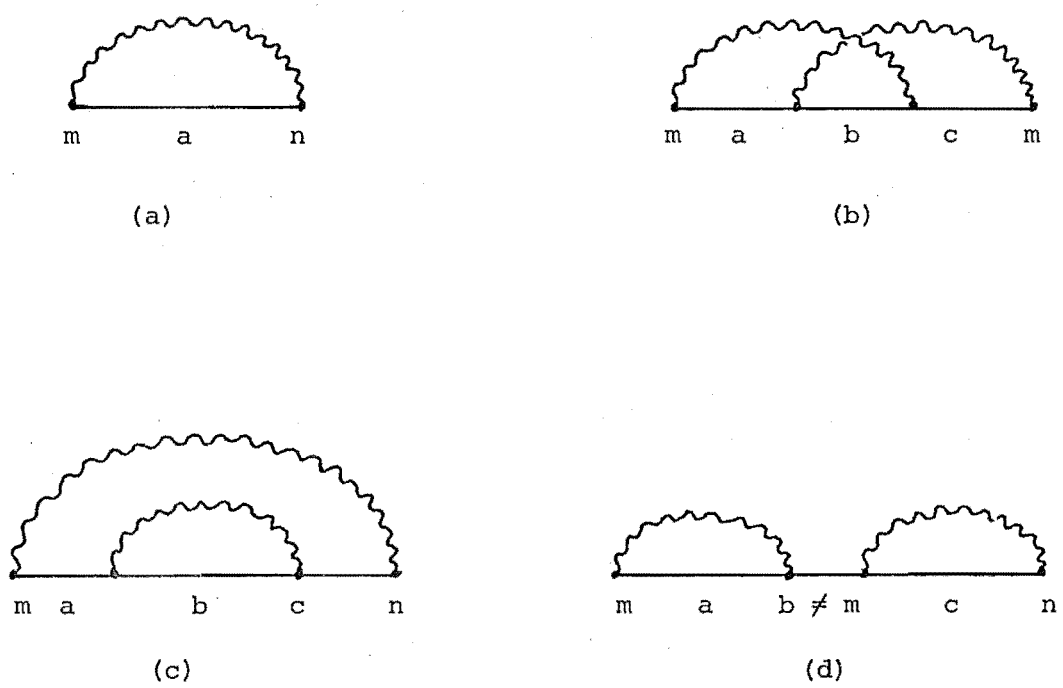

Evaluating the contribution from diagram 3.21a gives

$$
\begin{aligned}
{}^{a}\Sigma_m(i\omega_n) &= \beta^{-1} \sum_{i\omega_{n'}} \sum_{ak} F_a^0(i\omega_{n'})\, e^{i\omega_{n'}0^+}\, \mathcal{D}_k^0(i\omega_{n'} - i\omega_n)\, V_{ma}^k\, V_{am}^{-k} \\
&= -\oint_C \frac{dz}{2\pi i} f_D(z)\, e^{z0^+} \sum_{ak} |V_{ma}^k|^2\, F_a(z) \left\{ \frac{1}{z - i\omega_n - \omega_k} - \frac{1}{z - i\omega_n + \omega_k} \right\} \\
&= \sum_k \binom{n_k}{n_k+1} \sum_a \frac{|V_{ma}^k|^2}{i\omega_n \pm \omega_k - \lambda_a}
\end{aligned}
\tag{3.48}
$$

Using (3.33) and (3.15) this gives contributions to the shift and width functions

$$
\begin{aligned}
{}^{a}\Delta_m(\lambda_m) &= \mathcal{P} \sum_k \binom{n_k}{n_k+1} \sum_a \frac{|V_{ma}^k|^2}{\omega_{ma} \pm \omega_k} \\
{}^{a}\Gamma_m(\lambda_m) &= -\pi \sum_k \binom{n_k}{n_k+1} \sum_a |V_{ma}^k|^2\, \delta(\omega_{ma} \pm \omega_k)
\end{aligned}
\tag{3.49}
$$

Assuming a Debye model with acoustic phonons we can write these as

$$
\begin{aligned}
{}^{a}\Delta_m(\lambda_m) &= \sum_a |V_{ma}|^2\, \mathcal{P} \int_{-\omega_D}^{+\omega_D} d\omega\, \frac{f_B(\omega)\omega^3}{\omega_{ma} + \omega} \\
{}^{a}\Gamma_m(\lambda_m) &= -\pi \sum_a |V_{ma}|^2 \int_{-\omega_D}^{\omega_D} d\omega\, \omega^3 f_B(\omega)\, \delta(\omega_{ma} + \omega)
\end{aligned}
\tag{3.50}
$$

where we have used (3.8). In the low temperature limit these give temperature dependences T^4, T^3 if $\omega_D \ll |\omega_{ma}|$, $\omega_D \gg |\omega_{ma}|$ respectively for shifts and $\exp(-\varepsilon_{am}/k_BT)$ if $|\varepsilon_{am}| \sim kT$ or T dependences if $|\varepsilon_{am}| \ll kT$ for widths.

Similarly we obtain contributions from diagrams 3.21 b-d to self energy

$$
{}^{b}\Sigma_m(i\omega_n) = \sum_{k\ell} \binom{n_k}{n_k+1} \binom{n_\ell}{n_\ell+1} \sum_{abc} \frac{V_{ma}^k\, V_{ab}^\ell\, V_{bc}^{-k}\, V_{cm}^{-\ell}}{(i\omega_n \pm \omega_k - \lambda_a)(i\omega_n \pm \omega_k \pm \omega_\ell - \lambda_b)(i\omega_n \pm \omega_\ell - \lambda_c)} \tag{3.51}
$$

$$
{}^{c}\Sigma_m(i\omega_n) = \sum_{k\ell} \binom{n_k}{n_k+1} \binom{n_\ell}{n_\ell+1} \sum_{abc} \frac{V_{ma}^k\, V_{ab}^\ell\, V_{bc}^{-\ell}\, V_{cm}^{-k}}{(i\omega_n \pm \omega_k - \lambda_a)(i\omega_n \pm \omega_k \pm \omega_\ell - \lambda_b)(i\omega_n \pm \omega_k - \lambda_c)} \tag{3.52}
$$

$$d_{\Sigma_m}(i\omega_n) = \sum_{k\ell} \binom{n_k}{n_k+1}\binom{n_\ell}{n_\ell+1} \sum_{abc}^{b\neq m} \frac{V^{k}_{ma} V^{-k}_{ab} V^{\ell}_{bc} V^{-\ell}_{cm}}{(i\omega_n \pm \omega_k - \lambda_a)(i\omega_n - \lambda_b)(i\omega_n \pm \omega_\ell - \lambda_c)} \tag{3.53}$$

Choosing the terms containing a difference of phonon frequencies to maximise shift and width contributions, we can express these as

$$^4\Delta_m(\lambda_m) = \sum_{k\ell}\sum_{b} \frac{n_k(n_k+1)}{\omega_{mb} + \omega_k - \omega_\ell} \left| \sum_a \frac{V^{k}_{am} V^{\ell}_{am}}{\omega_{ma} + \omega_k} + \frac{V^{\ell}_{ma} V^{k}_{ab}}{\omega_{ma} - \omega_\ell} \right|^2 \tag{3.54}$$

$$^4\Gamma_m(\lambda_m) = \sum_{k\ell}\sum_{b} n_k(n_k+1)\,\delta(\omega_{mb} + \omega_k - \omega_\ell) \left| \sum_a \frac{V^{k}_{ma} V^{\ell}_{ab}}{\omega_{ma} + \omega_k} + \frac{V^{\ell}_{ma} V^{k}_{ab}}{\omega_{ma} - \omega_\ell} \right|^2$$

These give T^8 and T^5 dependences for shifts and T^4 or T^5 dependence for widths in the limits $\omega_D << |\omega_{ij}|$ and $\omega_D >> |\omega_{ij}|$.

These various temperature dependences are readily observed by monitering shifts and widths of spectral lines with temperature. (e.g. Kushida (1969)).

In the following chapter we shall return to the analysis of the diagrams involving pairs of ions, justifying our claim that they give rise to satellites to the N.P.L. and are to be identified with the pair spectra.

CHAPTER 4: ABSORPTION PAIR SPECTRA

4.1 Introduction

In analysing the absorption spectrum from a crystal containing N identical paramagnetic impurity ions, the usual approximation is to regard the spectrum as being the sum of N identical contributions from a single ion (cf chapter 3). This assumption would predict that the only spectral dependence on N, (the impurity concentration), is an intensity proportional to N. Experimentally however, although most spectral features or lines obey this relation, at higher impurity concentrations lines appear that are more strongly dependent on concentration (e.g. involving quadratic, cubic and higher N or concentration dependences.) This is apparent in figure 4.1 which is reproduced from Johnstone (1975) where the integrated intensity of the spectral lines from the infrared absorption spectrum of $CdBr_2$ (Co) crystals are plotted against various powers of the impurity concentration.

These lines that have non-linear dependences arise from interactions between impurity ion pairs (quadratic dependence), triples (cubic) and clusters (N^n $n \geqslant 4$ dependences). The spectrum intensity from these clusters is strongly dependent on the distances between the ions and these dependences reflect the probability of obtaining pairs, triples and clusters of ions in close proximity in the host crystal.

Four distinct classes of interactions between ions have been identified and a clear account of these is given in the reviews of Baker (1971a) and Bloor and Copland (1972). They are also discussed in the papers of Baker (1971b) and Wolf (1964, 1971). The following is a quick review of the main features of these interactions.

4.1.1 Magnetic multipole interactions

The interaction between two ions magnetic moments can be expanded in a multipole expansion which rapidly converges if the distance between the ion (R), greatly exceeds the typical dimensions of the ion (r). The

Figure 4.1.

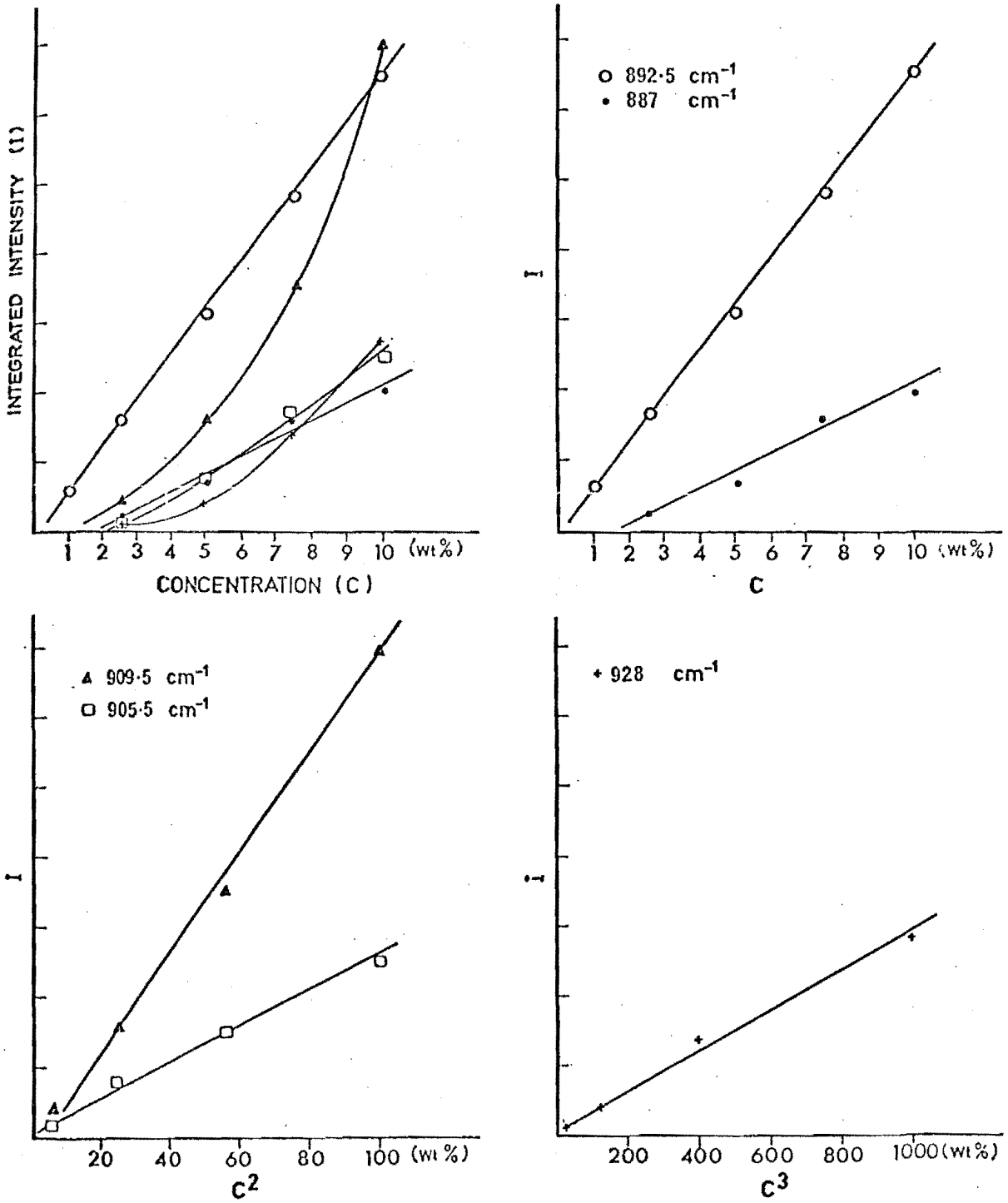

Integrated intensity of spectral lines from the infrared absorption spectrum of Cd Br_2(Co) crystals: reproduced from Johnstone (1975).

dipole-dipole interaction is the dominant contribution exceeding the dipole-octapole interaction by a factor of r^2/R^2 and hence is usually too small to be measured. The contribution from the dipole-dipole term is generally easily calculated and is composed of an isotropic part and an anisotropic, crystal structure dependent part.

4.1.2 Electric multipole interactions

This interaction arises from the *direct* part of the Coulomb interaction between the electrons whose wavefunctions are centred on different sites. If the sites $\underline{r}_i$, $\underline{r}_j$ are labelled i,j respectively and the electrons (1) and (2), then it has the form

$$\langle \psi_a(1)\psi_b(2) \left| \frac{e^2}{r_{12}} \right| \psi_a(1)\psi_b(2) \rangle \qquad (4.1)$$

where $R = r_{12} = |\underline{r}_1 - \underline{r}_2|$. Expanding the coulomb interaction about one centre in a multipole expansion (e.g. Wolf and Birgeneau 1968) results in a series expansion that is generally dominated by the dipole-dipole term. (But see comments by Wolf and Birgeneau (1968) on the importance of the higher-order terms.) Calculations of this interaction are complicated by both the polarization of the intervening medium (Baker and Mau 1967) and the screening of the 4f electrons by the diamagnetic 5s 5p shells.

4.1.3 Superexchange interaction

In most experimental situations it is found that an exchange interaction arising directly from the overlap of the wavefunctions of a pair of magnetic ions is rarely the interaction observed. Rather the *superexchange* mechanism, first suggested by Kramers (1934) more realistically accounts for the long range antiferromagnetic interactions. He suggested that the intermediate diamagnetic ligands between the magnetic ions provide a path by which the ions can couple. An approach for setting up models of superexchange has been developed by Newman and co-workers. (Bradbury and Newman 1968, 1971, Copland 1970, Stedman and Newman 1971.)

4.1.4 Exchange interaction

The *exchange* part of the Coulomb interaction arises from the indistinguishability of electrons expressed by the antisymmetry requirements and has the form (cf 4.1)

$$-\langle\psi'_a(1)\psi'_b(2)\left|\frac{e^2}{r_{12}}\right|\psi_b(1)\psi_a(2)\rangle \qquad (4.2)$$

Evaluation of these contributions is particularly simple for S state electrons or for ions whose orbital angular momentum is totally quenched (Van Vleck 1937) but is more complex for the general case of non-vanishing orbital angular momentum. (Van Vleck 1962, Elliot and Thorpe 1968.)

4.1.5 Virtual Phonon Exchange interaction

This interaction mechanism, first suggested by Sugihara (1959), arises through a modulation of the crystal field, felt by each ion upon the passage of a phonon through the lattice. The coupling can be described as an exchange of virtual phonons between the impurity ion sites, in a manner analagous to the way the coulomb force can be regarded as an exchange of photons (Barestetskii 1971) and the nuclear force as an exchange of mesons. (Bjorken and Drell 1964.)

Theoretical calculations on this are complicated by the complex phonon spectrum of real solids requiring many approximations to obtain analytical results. Orbach and Tachiki (1967) assumed in their analysis that acoustic phonons would be responsible for the coupling but Allen (1968) suggested for UO_2 that optical phonons would also give a significant contribution. Later analysis by Allen and Guggenheim (1971a,b) and Baker (1971b) has shown that generally the acoustic phonon coupling is one or two orders of magnitude smaller than the optical phonon coupling.

In this chapter we shall consider the diagrams of the previous chapter that pertain to the absorption *pair* spectra. These diagrams involve phonon propagators that 'connect' one ion to another and

hence correspond to the virtual phonon exchange interaction. The resulting pair lines are observed as satellites to the single ion spectral lines and the following analysis will yield the shifts of the pair lines from their *parent* single ion lines.

4.2 Pair Spectra Diagrams

In §3.4 we developed a diagram expansion for the multi-ion spectrum which resulted in diagrams containing phonon propagators that joined one ion level propagator loop to another (different ion because of the limiting procedure cf(3.18)) such loop. The lower order diagrams of this type are given in figure 3.8. In that chapter we claimed that such diagrams involved a strong dependence on the distance between the two ions and hence could be neglected for a sample containing low concentrations of impurity ions. In this chapter we wish to relax this restriction and calculate the spectrum from such diagrams.

Proceeding as for the single ion spectra and neglecting all diagrams containing triples and higher order clusters, and further neglecting pairs in the denominator, (we expect these still to be dominated by the single ion loops that they add to) the diagram contribution to the pair spectrum can be expressed as

$$\text{spectrum} \simeq \sum_{\substack{i,j \\ i\neq j}} \frac{P\left[\quad ij \quad\right]}{P\left[(1+\,i\,)\,(1+\,j\,)\right]} \tag{4.3}$$

This is exactly the contribution expected if we regard the total pair spectrum as the sum of the spectrum from the N(N-1)/2 possible pairs. Without loss of generality then we can regard our system as containing a single pair of impurity ions at positions $\underline{r}_1$ and $\underline{r}_2$. Just as for the single ion spectrum, the denominator of (4.3) is independent of the

frequency ω_0 and hence contributes only a multiplicative constant which we do not need to evaluate.

4.3 Product States and Matrix Representation

Although we could proceed to evaluate the spectrum from (4.3) it is advantageous to transform to a new basis. The basis we choose consists of the product states $|ab\rangle$ where $|a\rangle$, $|b\rangle$ are states for the single ions at $\underline{r_1}$ and $\underline{r_2}$ respectively. We redefine the operators a_{1a}, a_{2a} defined in (3.2)-(3.4) by the new two-particle operator

$$\psi_{ab} = a_{1a}\, a_{2b} \tag{4.4}$$

such that

$$\psi^{\dagger}_{ab}\, |vac\rangle = a^{\dagger}_{1a}\, a^{\dagger}_{2b}\, |vac\rangle = |ab\rangle, \tag{4.5}$$

Noting that only one level of each ion can be occupied at any time we have the identity

$$\sum_{a=\text{levels}} a^{\dagger}_{ia}\, a_{ia} = 1 \quad \text{for} \quad i = 1,2. \tag{4.6}$$

which enables us to transform (3.2), (3.4) and (3.8) to the forms (see appendix 4.A).

$$\mathcal{H}_{imp} = \sum_{mn} E_{mn}\, \psi^{\dagger}_{mn}\, \psi_{mn} \tag{4.7}$$

$$\begin{aligned} M &= \sum_{mn\ell} M^{1}_{mn}\, \psi^{\dagger}_{m\ell}\, \psi_{n\ell} + M^{2}_{mn}\, \psi^{\dagger}_{\ell m}\, \psi_{\ell n} \\ &= \sum_{mn\ell o} M_{mn\ell o}\, \psi^{\dagger}_{mn}\, \psi_{\ell o} \end{aligned} \tag{4.8}$$

$$\mathcal{H}_{int} = \sum_{mn\ell} \sum_{k} [V^{1k}_{mn}\, \psi^{\dagger}_{m\ell}\, \psi_{n\ell} + V^{2k}_{mn}\, \psi^{\dagger}_{\ell m}\, \psi_{\ell n}]\, \phi_k \tag{4.9}$$

where

$$E_{mn} = \lambda_m + \lambda_n \tag{4.10}$$

$$M_{mn\ell o} = M^{1}_{m\ell}\, \delta_{no} + M^{2}_{no}\, \delta_{m\ell}\,, \tag{4.11}$$

and M^{1}_{mn}, V^{1k}_{mn} represent the single ion coupling coefficients evaluated at ion 1.

If the single ion system contains m levels then we can label our m^2 product states by a label which runs from 1 to m^2. Ordering the states

by increasing energy, we can form the column vectors and m^2-tuples

$$\underset{\sim}{\psi} = \begin{pmatrix} \psi_1 \\ \psi_2 \\ . \\ . \\ . \\ \psi_{m^2} \end{pmatrix} \quad \text{and} \quad \underset{\sim}{\psi}^\dagger = (\psi_1^\dagger, \psi_2^\dagger, \ldots \psi_{m^2}^\dagger) \quad \text{respectively.}$$

This enables us to rewrite (4.7)-(4.9) as the matrix equations

$$\mathcal{H}_{imp} = \underset{\sim}{\psi}^\dagger \cdot \underline{\underline{E}} \cdot \underset{\sim}{\psi} \tag{4.12}$$

$$\mathcal{H}_{int} = \sum_k (\underset{\sim}{\psi}^\dagger \cdot \underline{\underline{V}}^{1k} \cdot \underset{\sim}{\psi} + \underset{\sim}{\psi}^\dagger \cdot \underline{\underline{V}}^{2k} \cdot \psi)\phi_k \tag{4.13}$$

$$M = \underset{\sim}{\psi}^\dagger \cdot \underline{\underline{M}} \cdot \underset{\sim}{\psi} \tag{4.14}$$

where the matrix elements of $\underline{\underline{E}}$, $\underline{\underline{V}}^{1k}$, $\underline{\underline{V}}^{2k}$ and $\underline{\underline{M}}$ are determined by comparison with (4.7)-(4.9).

$$\begin{aligned} E_{mn,pq} &= \delta_{mp}\, \delta_{nq}\, (E_m + E_n) \\ M_{mn,pq} &= M^1_{mp}\, \delta_{nq} + M^2_{nq}\, \delta_{mp} \\ V^k_{mn,pq} &= V^{1k}_{mp}\, \delta_{nq} + V^{2k}_{nq}\, \delta_{mp} \end{aligned} \tag{4.15}$$

We define a new pair propagator

$$F_{ij}\ (i\omega_n) = \int_0^\beta d\tau\ e^{i\omega_n \tau} \langle T_\tau \{\psi_i(\tau)\psi_j^\dagger(0)\}\rangle \tag{4.16}$$

whose zero-order form is

$$F^0_{ij}\ (i\omega_n) = \frac{\delta_{ij}\, \alpha_i}{i\omega_n - E_{ii}} \tag{4.17}$$

with

$$\alpha_i \equiv \frac{1 + e^{\beta E_{ii}}}{(1+e^{\beta E^1_{ii}})(1+e^{\beta E^2_{ii}})} \quad . \tag{4.18}$$

In these relations E_{ij} is the matrix element $[\underline{\underline{E}}]_{i,j}$ and is diagonal with matrix elements

$$\begin{aligned} E_{i,i} = E_{(ab),(ab)} &= \varepsilon_{ab} \\ &= \lambda_a + \lambda_b \\ &E^1_{i,i} + E^2_{i,i} \ . \end{aligned} \tag{4.19}$$

$E^1_{i,i}$, $E^2_{i,i}$ are defined by (4.19) and correspond to the energy levels of the first and second ion respectively. In the limit $\lambda \to \infty$ we have the relation $\alpha_i \to 1$.

4.4 Diagram Expansion

The propagators (4.16) $F_{ij}(i\omega_n)$ can be regarded as the matrix element $[F(i\omega_n)]_{i,j}$ of a matrix propagator defined by

$$F(i\omega_n) = \int_0^\beta d\tau\ e^{i\omega_n\tau} \langle T_\tau\{\underset{\sim}{\psi}(\tau) \otimes \underset{\sim}{\psi}^\dagger(0)\}\rangle \qquad (4.20)$$

where $\otimes$ denotes the *direct-product* of matrices. (Pease 1965.)

Defining

$$G(i\omega_n) = \int_0^\beta d\tau\ e^{i\omega_n\tau} \langle T_\tau\{M(\tau)\,M(0)\}\rangle \qquad (4.21)$$

the spectrum is given by the relation (3.6). Substituting (4.14) in (4.21) one obtains the diagram expansion given in figure 4.2. In figure 4.3 we have expanded diagram 4.2c in terms of the old single ion level propagators of chapter 3 to show the relation between these (heavy solid lines represent zero-order pair ion propagators, light solid lines represent zero-order single ion propagators). The diagrams of figure 4.2 can be summed to be rewritten in the form of figure 4.4. Dysons equation for the two ion level propagators is given in diagram form in figure 4.4(c) and algebraically is the matrix equation

$$F(i\omega_n) = F^0(i\omega_n) + F^0(i\omega_n)\ \Sigma(i\omega_n)\ F(i\omega_n) \qquad (4.22)$$

The contribution to $G(i\omega_n)$ is the sum of two parts; a contribution, (figure 4.4a), that is analogous to the additive diagrams of §3.5.1, and a contribution (figure 4.4b) analogous to the non-additive diagrams of §3.5.2. We shall make the approximation (mostly to enable analytical results to be obtained but also because they involve higher order diagrams) of neglecting the contribution of figure 4.4b and retaining

Figure 4.2.

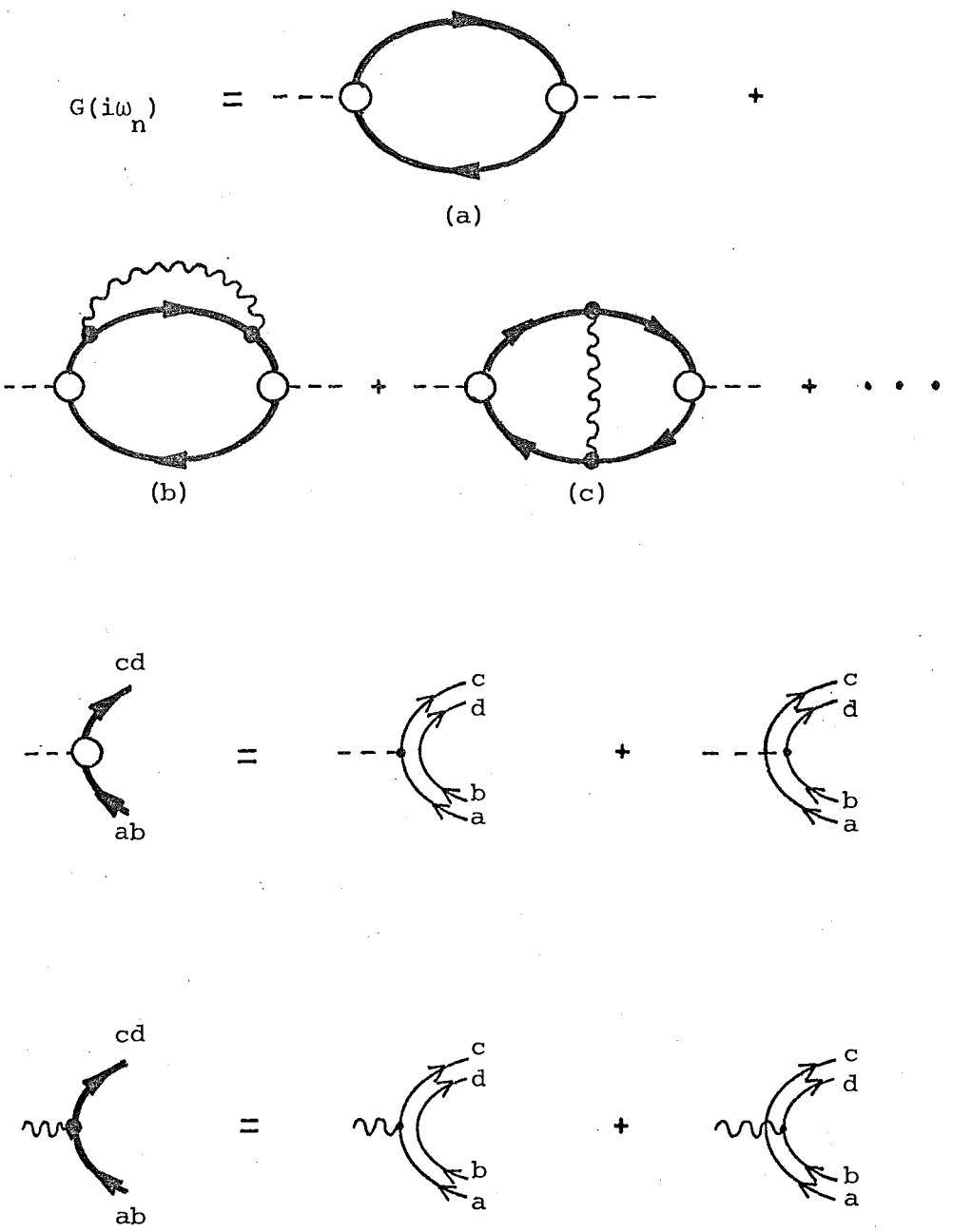

Figure 4.3.

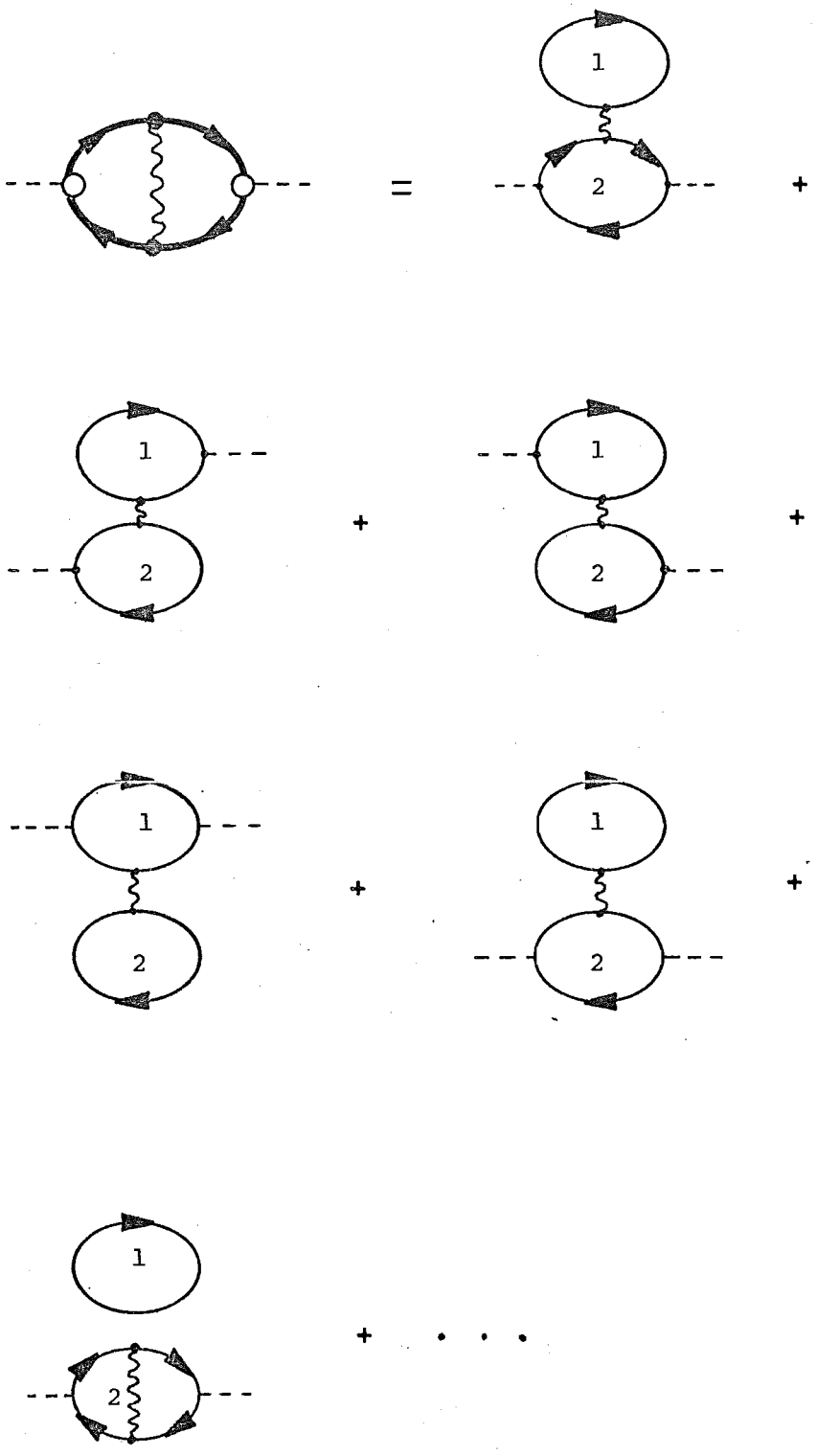

Figure 4.4.

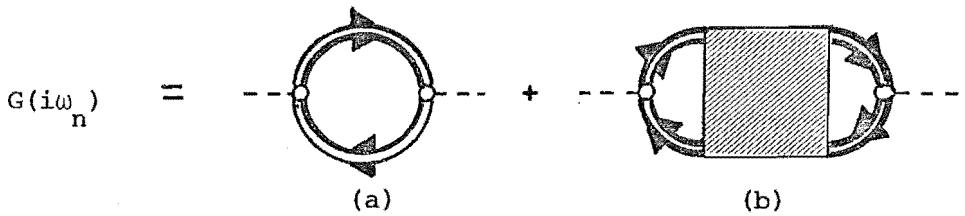

where

(c)

(d)

(e)

only the additive type diagrams of figure 4.4a. This contribution can be written in the form

$$G(i\omega_n) \sim \text{Trace}\,(\beta^{-1} \sum_{i\varepsilon} \underline{\underline{M}} \cdot F(i\varepsilon) \cdot \underline{\underline{M}} \cdot F(i\varepsilon + i\omega_n)) \qquad (4.23)$$

Evaluating this with zero-order propagators $F(i\varepsilon) \to F^0(i\varepsilon)$ gives us

$$\begin{aligned} G(i\omega_n) &= \sum_{ijk\ell} \beta^{-1} \sum_{i\varepsilon} M_{ij}\, F^0_{jk}(i\varepsilon)\, M_{k\ell}\, F^0_{\ell i}(i\varepsilon + i\omega_n) \\ &= \sum_{ij} \beta^{-1} \sum_{i\varepsilon} M_{ij}\, F^0_{jj}(i\varepsilon)\, M_{ji}\, F^0_{ii}(i\varepsilon + i\omega_n) \\ &= \sum_{ij} M_{ij}\, M_{ji}\, \alpha_j\, \alpha_i\, \beta^{-1} \sum_{i\varepsilon} (i\varepsilon - E_{jj})^{-1}\, (i\varepsilon + \omega_n - E_{ii})^{-1} \\ &= \sum_{ij} M_{ij}\, M_{ji}\, \alpha_j\, \alpha_i\, \frac{f_D(E_{jj}) - f_D(E_{ii})}{i\omega_n + E_{jj} - E_{ii}} \qquad (4.24) \end{aligned}$$

which gives upon substitution into (3.6)

$$\sigma(\omega_0) \sim \omega_0 \sum_{ij} M_{ij}\, M_{ji}\, \alpha_i\, \alpha_j\, (f_D(E_{jj}) - f_D(E_{ii})) \cdot \delta(\omega_0 + E_{jj} - E_{ii}) \qquad (4.25)$$

Rewriting this in terms of single level labels $i \equiv ab$ and $j = cd$ one obtains after applying limiting procedure (2.54) with $\mu = 2$

$$\sigma(\omega_0) \sim \omega_0 \sum_{ab\,cd} M_{abcd}\, M_{cd\,ab}\, (\rho_a\rho_b - \rho_c\rho_d)\, \delta(\omega_0 + \varepsilon_a + \varepsilon_b - \varepsilon_c - \varepsilon_d). \qquad (4.26)$$

Upon applying relation (4.11) to this expression we obtain

$$\begin{aligned} \sigma(\omega_0) \sim \omega_0 \{ &\sum_{ac} M^1_{ac}\, M^1_{ca}\, (\rho_a - \rho_c)\, \delta(\omega_0 + \omega_{ac}) \\ &+ \sum_{bd} M^2_{bd}\, M^2_{db} (\rho_b - \rho_d)\, \delta(\omega_0 + \omega_{bd}) \} \qquad (4.27) \end{aligned}$$

where we have used $\sum_n \rho_n = \sum_n \left(\frac{e^{-\beta\varepsilon_n}}{\sum_i e^{-\beta\varepsilon_i}} \right) = 1.$

The final expression (4.27) is identical to the sum of two zero-order, single-ion spectra (cf 3.17), one corresponding to site 1 and another to site 2. A study of figure 4.4 reveals that these contributions arise from the diagrams

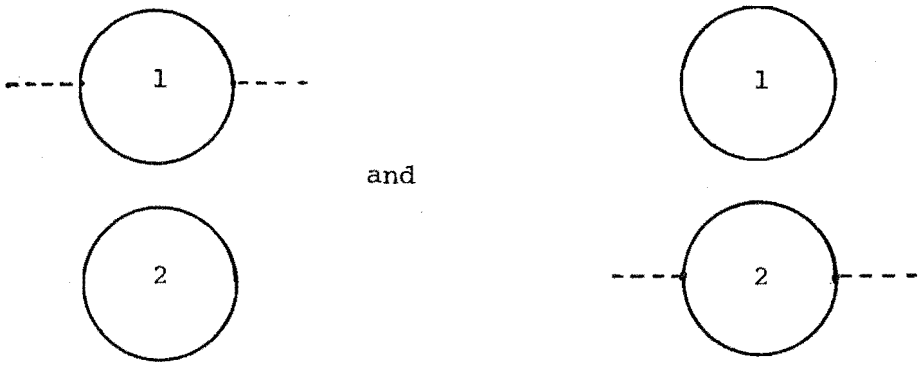

and hence are not related to the pair spectrum but rather are the contributions evaluated in chapter 3 for the single-ion spectrum. The pair spectrum diagrams must contain *at least* one phonon connecting (or joining) the two ions and any diagrams not of this form are to be neglected in the following analysis.

4.5 Two Level System

Before we go on to discuss the pair spectra of Kramers systems we shall apply the formalism to an idealized simple system - the two level system. The system consists of two impurity ions at $\underline{r}_1$, $\underline{r}_2$ respectively each with two levels $|a\rangle$, $|b\rangle$ and energies ε_a, ε_b respectively. The coupled two ion system then contains four levels: $|aa\rangle$ the ground state with energy $2\varepsilon_a$, $|ab\rangle$, $|ba\rangle$ degenerate with energy $\varepsilon_a + \varepsilon_b$, and the excited state $|bb\rangle$ with energy $2\varepsilon_b$. (cf figure 4.5.)

Figure 4.5.

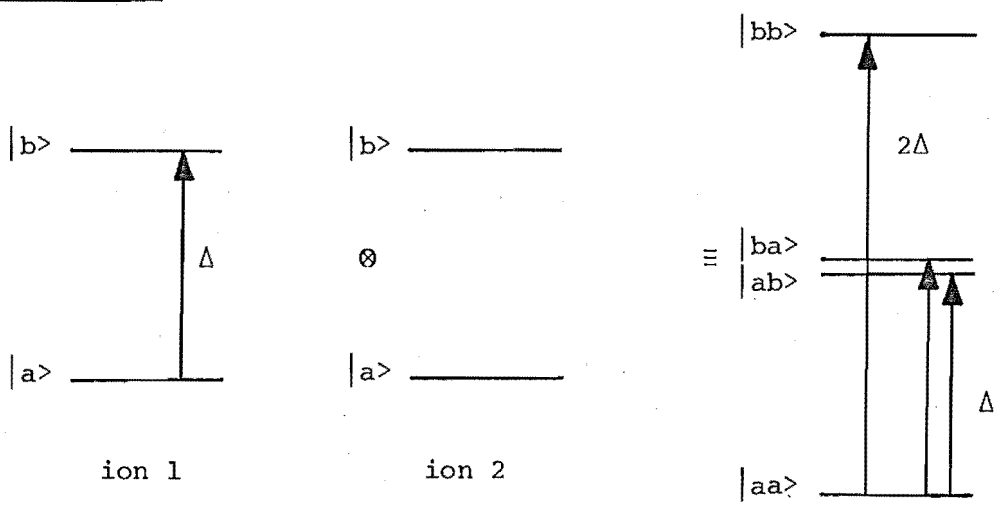

The zero-order spectrum from such a system (4.27) (at low temperatures when effectively only the ground state is occupied) consists of a peak at $\omega_0 = 2\Delta(\Delta = \omega_{ba})$ and two both at $\omega_0 = \Delta$ (cf transitions indicated on figure 4.5). We will concentrate our attention on the transitions from the ground state to the two degenerate states and find whether the virtual phonon exchange processes we are discussing can lift the degeneracy resulting in two distinct spectral lines close to $\omega_0 = \Delta$.

We form the vector $\underline{\psi}$ by the identification $\psi_1,\ldots,\psi_4$ with the product states ψ_{aa}, ψ_{ab}, ψ_{ba} and ψ_{bb} respectively. The self-energy matrix $\Sigma(i\omega_n)$ in Dyson's equation (4.22) is thus a square, rank four matrix. In the following sections we shall look for a possible splitting of the degenerate states under various approximations regarding this self-energy matrix.

4.5.1 Diagonal Self-Energy

The simplest approximation we can make is that the self-energy matrix is diagonal. This is the approximation we made for the single ion spectrum but as in that case we can minimise the effect of the approximation by extending the allowed structure of the self-energy diagrams (e.g. consider figure 3.12b).

Dyson's equation (4.22) can be rewritten in the more convenient form

$$F^{-1}(i\omega_n) = (F^0(i\omega_n))^{-1} - \Sigma(i\omega_n) \qquad (4.28)$$

Under the assumption of diagonal self-energy $\Sigma(i\omega_n)$ we see that because $F^0(i\omega_n)$ is diagonal (4.17) then $F^{-1}(i\omega_n)$ and hence $F(i\omega_n)$ is also diagonal and has the form

$$F_{ij}(i\omega_n) = \frac{\delta_{ij}\,\alpha_i}{i\omega_n - E_{ii} - \alpha_i\Sigma_{ii}(i\omega_n)} \qquad (4.29)$$

Using property (2.23) of the self-energy function we obtain the relationship

$$\frac{1}{2\pi i}\{F_{ij}(x+i0^+) - F_{ij}(x-i0^+)\} = \frac{\delta_{ij}\ \alpha_i\ \Gamma'_{ii}(x)/\pi}{[x - E_{ii} - \Delta'_{ii}(x)]^2 + \Gamma'^2_{ii}(x)}$$

$$\equiv L'_i(x) \qquad (4.30)$$

with $\Sigma_{ij}(x+i0^+) = \Delta_{ij}(x) + i\Gamma_{ij}(x)$

and $\Delta'_{ii}(x) = \alpha_i\ \Delta_{ii}(x)$, $\Gamma'_{ii}(x) = \alpha_i\ \Gamma'_{ii}(x)$.

Using these relations in (4.23) we obtain the spectrum

$$\sigma(\omega_0) \sim \omega_0 \sum_{ij} M_{ij}\ M_{ji}\ \alpha_i\ \alpha_j \int_{-\infty}^{\infty} dx (f_D(x) - f_D(x+\omega_0)) L'_i(x) L'_j(x+\omega_0) \qquad (4.31)$$

Upon applying the lorentzian approximation, the limiting procedure (2.54) and using single ion level notation we obtain

$$\sigma(\omega_0) \sim \omega_0 \sum_{abcd} M_{ab,cd}\ M_{cd,ab}\ (\bar{\rho}_a - \bar{\rho}_c)\ \frac{(\gamma_{ab}+\gamma_{cd})/\pi}{(\omega_0 + \delta_{ab} - \delta_{cd})^2 + (\gamma_{ab}+\gamma_{cd})^2} \qquad (4.32)$$

where $\gamma_{ab} = \Gamma'_{ab,ab}(\delta_{ab})$, $\delta_{ab} = \varepsilon_a + \varepsilon_b + \Delta'_{ab,ab}(\delta_{ab})$

and $\bar{\rho}_{ab} = \lim_{\lambda\to\infty} e^{2\beta\lambda}\ f_D(\delta_{ab}+2\lambda)/(\sum_n e^{-\beta\varepsilon_n})^2 \simeq \rho_a\ \rho_b$

Applying this to our two level system and picking out the transitions from the ground to the two degenerate states we obtain

$$\sigma(\omega_0) \sim \omega_0\ M_{ab}\ M_{ba}\{(\bar{\rho}_{aa} - \bar{\rho}_{ab})\ \frac{(\gamma_{aa}+\gamma_{ab})/\pi}{(\omega_0 + \delta_{aa} - \delta_{ab})^2 + (\gamma_{aa}+\gamma_{ab})^2}$$

$$+ (\bar{\rho}_{aa} - \bar{\rho}_{ba})\ \frac{(\gamma_{aa}+\gamma_{ba})/\pi}{(\omega_0 + \delta_{aa} - \delta_{ba})^2 + (\gamma_{aa}+\gamma_{ba})^2} \qquad (4.33)$$

which consists of lorentzians peaked at $\omega_0 = \delta_{ab} - \delta_{aa}$ and $\delta_{ba} - \delta_{aa}$ respectively. To observe any splitting then we require a non-vanishing difference between these two positions.

(i.e. $D = (\delta_{ab} - \delta_{aa}) - (\delta_{ba} - \delta_{aa}) = \delta_{ab} - \delta_{ba} \neq 0$). We have

$$D = (\varepsilon_a + \varepsilon_b + \Delta_{ab,ab}(\varepsilon_a + \varepsilon_b)) - (\varepsilon_b + \varepsilon_a + \Delta_{ba,ba}(\varepsilon_a + \varepsilon_b))$$

$$= \Delta_{ab,ab}(\varepsilon_{ab}) - \Delta_{ba,ba}(\varepsilon_{ab}) \qquad (4.34)$$

where $\varepsilon_{ab} \equiv \varepsilon_a + \varepsilon_b$. Thus a difference in the real part of the self

energy function diagonal matrix elements $\Sigma_{22}(i\omega_n)$ and $\Sigma_{33}(i\omega_n)$ is required to obtain a shift.

A study of these matrix elements however shows that they are identical. This is easily shown by the diagrams of figure 4.6 where the self-energy parts are each given in terms of their single ion propagators. It is clear that if ions 1 and 2 are interchanged then the diagrams are also interchanged (assuming identical ions) and hence the matrix elements are identical.

Figure 6.4.

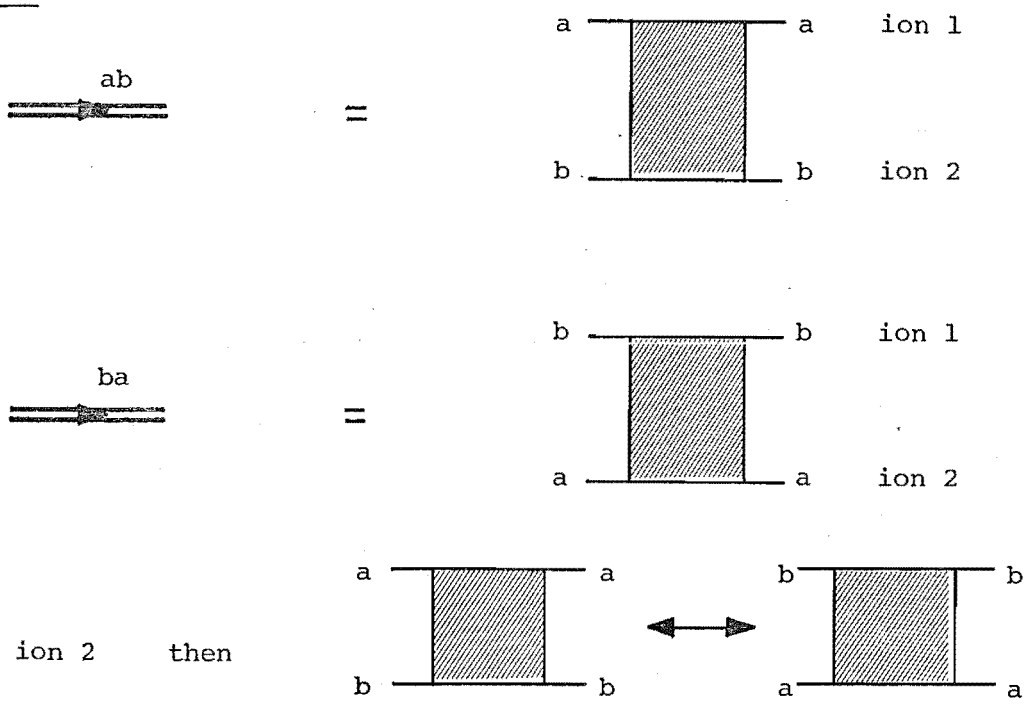

The assumption of diagonal self-energy then gives no splitting of the degenerate levels and hence no observable pair spectra. It should be noted however that this does not imply that there is no shift, only that both states shift by the same amount.

4.5.2 Block-Diagonal Self-Energy

The diagonal matrix elements considered in the previous section we label the direct (or Coulomb) interaction by analogy with the diagonal matrix elements of the Coulomb interaction (§4.1.2.) because

they have the structure (cf 4.1)

$$\Sigma_{22}(i\omega_n) = \langle\psi_a(1)\psi_b(2)|\ \Sigma(i\omega_n)\ |\psi_a(1)\psi_b(2)\rangle \qquad (4.35)$$

The off-diagonal matrix elements (such as $\Sigma_{23}(i\omega_n)$) are analogous to the exchange matrix elements (§4.1.3) having the structure (cf 4.2)

$$\Sigma_{23}(i\omega_n) = \langle\psi_a(1)\psi_b(2)|\ \Sigma(i\omega_n)\ |\psi_b(1)\psi_a(2)\rangle \qquad (4.36)$$

In this section we shall relax our assumption that $\Sigma(i\omega_n)$ is diagonal and only restrict it to block diagonal form, allowing non-zero matrix elements between degenerate states (e.g. between $|ab\rangle$ and $|ba\rangle$).

$\Sigma(i\omega_n)$ then takes the form

$$\Sigma(i\omega_n) = \begin{vmatrix} \Sigma_{11}(i\omega_n) & & & \\ & \Sigma_{22}(i\omega_n) & \Sigma_{23}(i\omega_n) & \\ & \Sigma_{32}(i\omega_n) & \Sigma_{33}(i\omega_n) & \\ & & & \Sigma_{44}(i\omega_n) \end{vmatrix} . \qquad (4.37)$$

The matrix elements Σ_{23} and Σ_{32} in terms of single ion propagators take the form given in figure 4.7.

Figure 4.7.

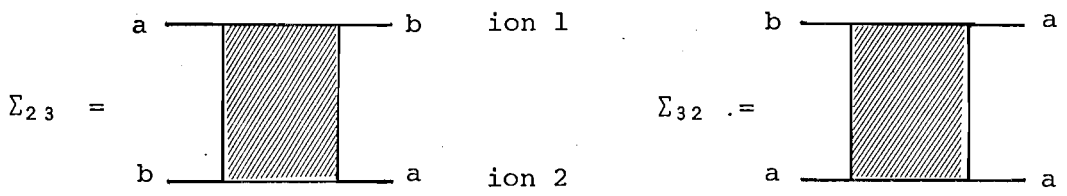

Again we see that interchanging ions 1 and 2 interchanges these matrix elements also and so they are identical.

4.5.3 Basis transformation

If we can find a basis transformation

$$\underline{\psi} \rightarrow \underline{\tilde{\psi}} = A \cdot \underline{\psi} \quad , \quad A^{\dagger} = A \qquad (4.38)$$

that preserves the form of Dyson's equation (4.22) and also diagonalizes the self-energy matrix then we can apply the results of §4.5.1.

Employing the transformation (4.38) we obtain the transformed results (see appendix 4B for derivations)

$$\grave{\psi}^{\dagger} = \underset{\sim}{\psi}^{\dagger} A^{\dagger} \tag{4.39}$$

$$\mathcal{H}_{imp} = \grave{\underset{\sim}{\psi}}^{\dagger} \cdot \grave{E} \cdot \grave{\underline{\psi}} \quad \text{where } \grave{E} = A\,E\,A^{\dagger} \tag{4.40}$$

$$\mathcal{H}_{int} = \sum_{k} (\grave{\underset{\sim}{\psi}}^{\dagger} \cdot \grave{V}^{1k} \cdot \grave{\underline{\psi}} + \grave{\underset{\sim}{\psi}}^{\dagger} \cdot \grave{V}^{2k} \cdot \grave{\underline{\psi}}) \phi_k \tag{4.41}$$

$$\text{when } \grave{V}^{ik} = A\,V^{ik}\,A^{\dagger} \quad i = 1,2.$$

$$\grave{F}(\tau) \equiv \langle T_{\tau}\{\grave{\psi}(\tau) \otimes \grave{\psi}^{\dagger}(0)\}\rangle = AF(\tau)A^{\dagger} \tag{4.42}$$

$$\grave{F}(i\omega_n) = \grave{F}^{0}(i\omega_n) + \grave{F}^{0}(i\omega_n)\grave{\Sigma}(i\omega_n)\grave{F}(i\omega_n) \tag{4.43}$$

$$\text{where } \grave{\Sigma}(i\omega_n) = A\Sigma(i\omega_n)A^{\dagger}.$$

These equations are identical to our unprimed equations enabling us to use all our previous analysis.

Choosing the specific form for A

$$A = \begin{vmatrix} 1 & & & \\ & \frac{1}{\sqrt{2}} & \frac{1}{\sqrt{2}} & \\ & \frac{1}{\sqrt{2}} & -\frac{1}{\sqrt{2}} & \\ & & & 1 \end{vmatrix} . \tag{4.44}$$

and hence $\grave{\psi}_1 = \psi_1$, $\grave{\psi}_2 = (\psi_2 + \psi_3)/\sqrt{2}$, $\grave{\psi}_3 = (\psi_2 - \psi_3)/\sqrt{2}$, $\grave{\psi}_4 = \psi_4$ we obtain the transformed matrices,

$$\grave{E} = E, \quad \grave{F}^{0}(i\omega_n) = F^{0}(i\omega_n) \text{ and}$$

$$\grave{V}^{1k} = \begin{vmatrix} V_{aa} & V_{ab} & -V_{ab} & 0 \\ V_{ba} & V_{aa}+V_{bb} & V_{aa}-V_{bb} & V_{ab} \\ -V_{ba} & V_{aa}-V_{bb} & V_{aa}+V_{bb} & V_{ab} \\ 0 & V_{ba} & V_{ba} & V_{bb} \end{vmatrix}^{1k}, \quad \grave{V}^{2k} = \begin{vmatrix} V_{aa} & V_{ab} & V_{ab} & 0 \\ V_{ba} & V_{aa}+V_{bb} & V_{bb}-V_{aa} & V_{ab} \\ V_{ba} & V_{bb}-V_{aa} & V_{aa}+V_{bb} & -V_{ab} \\ 0 & V_{ba} & -V_{ba} & V_{bb} \end{vmatrix}^{2k}$$

and

$$\grave{\Sigma}(i\omega_n) = \begin{vmatrix} \Sigma_{11} & & & \\ & \Sigma_{22}+\Sigma_{23} & & \\ & & \Sigma_{22}-\Sigma_{23} & \\ & & & \Sigma_{44} \end{vmatrix} (i\omega_n) \qquad (4.45)$$

where we have used the equalities $\Sigma_{22} = \Sigma_{33}$ and $\Sigma_{23} = \Sigma_{32}$.

We can now use the analysis of §4.5.1 and we obtain a splitting

$$\begin{aligned} \grave{D} &= \grave{\delta}_{ab} - \grave{\delta}_{ba} \\ &= \grave{\Delta}_{ab,ab}(\varepsilon_{ab}) - \grave{\Delta}_{ba,ba}(\varepsilon_{ab}) \end{aligned} \qquad (4.46)$$

which gives using the form of $\grave{\Sigma}(i\omega_n)$ (4.45)

$$\grave{D} = 2\grave{\Delta}_{ab,ba}(\varepsilon_{ab}). \qquad (4.47)$$

The resulting spectrum thus consists of two lorentzians with identical widths whose centres are $\grave{D}$ apart appearing as satellites to the single ion line at $\omega_0 = \Delta$.

4.5.4 Magnitude of splitting

The first order contribution to $\Delta_{ab,ba}(\varepsilon_{ab})$ and hence to $\grave{D}$ comes from the diagram of figure 4.8.

Figure 4.8.

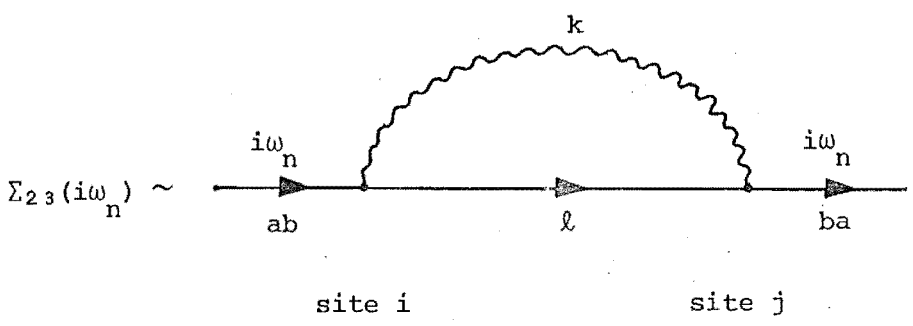

i,j indicate the site labels for the interaction centres.

The form of V^{1k} and V^{2k} restricts the possible values of i,j and the intermediate state ℓ to the cases

(a) $i = 1,\ j = 2$ and $\ell = bb$

or (4.48)

(b) $i = 2,\ j = 1$ and $\ell = aa$.

The contribution of each of these diagrams to $\Sigma_{23}(i\omega_n)$ and hence $\Delta_{23}(\varepsilon_{ab})$ is evaluated in appendix 4C giving

$$\Delta_{23}(\varepsilon_{ab}) = -\frac{V_{ab}V_{ba}}{c\,\pi^2\,R}\int_0^{k_D} dk\ \frac{k\,\sin(kR)\ \mathrm{den}(k)}{k^2 - k_0^2} \tag{4.49}$$

where $k_0 = \Delta/c$. This can be evaluated using the relevant density of states for the crystal resulting in approximately a R^{-3} dependence at large R.

In the following sections we shall generalize our formalism to deal with a larger number of levels.

4.6 Kramers System

Although the following analysis can be readily applied to a non-Kramers system we shall restrict our analysis to the specific case of a Kramers ion because it exhibits novel points of interest not correctly or fully analysed by previous workers (e.g. Baker (1971a), (1971b), Baker and Mau (1976)). A Kramers ion is one that contains an odd number of electrons. A theorem first proved by Kramers (1930) states that in the absence of a term in the Hamiltonian that breaks time reversal symmetry, the energy levels must appear in double degenerate pairs. The two degenerate states of the pair are time reversal conjugate states which we express by

$$|\bar{a}\rangle = T|a\rangle \tag{4.50}$$

where T is the time reversal operator.

We take our ionic level system to consist of conjugate pairs $a, \bar{a}; b, \bar{b}; \ldots$ with energies $\varepsilon_a = \varepsilon_{\bar{a}}$, $\varepsilon_b = \varepsilon_{\bar{b}}$ as is indicated in figure 4.9.

Figure 4.9.

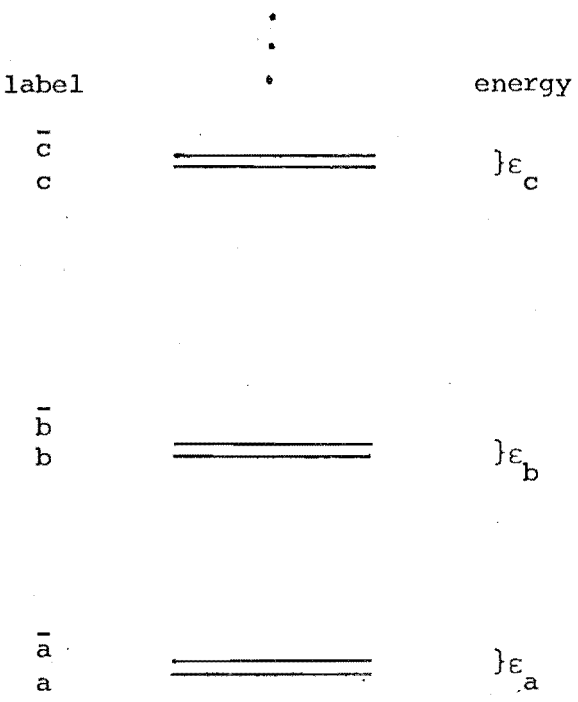

Figure 4.10.

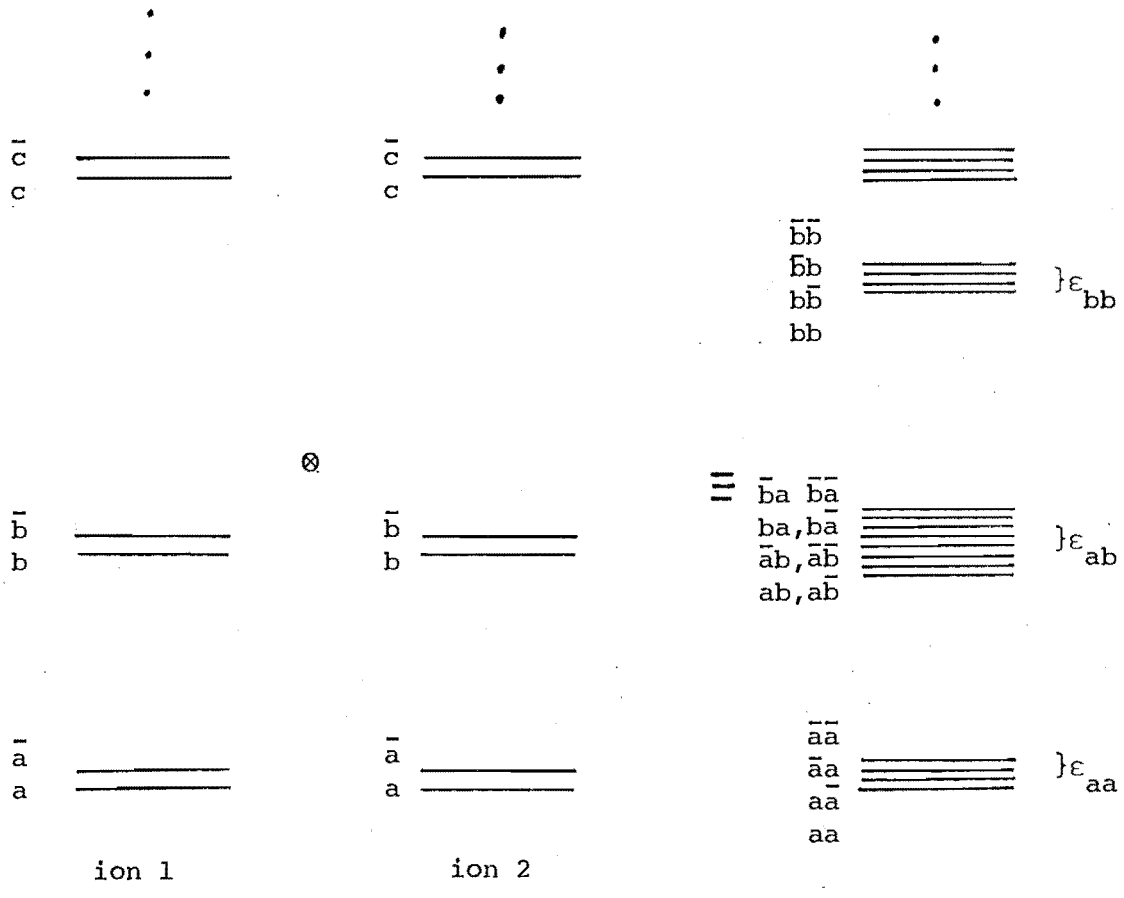

When the system consists of two such ions centred at $\underline{r}_1$ and $\underline{r}_2$ the product states $|ab\rangle$ (cf (4.5)) result in an energy level scheme indicated in figure 4.10.

It is clear that in this coupled system the ground state is 4-fold degenerate, the first excited state is 8-fold degenerate and higher states are also either 4 or 8-fold degenerate.

If we apply relation (4.27) to this system and consider absorption lines corresponding to transitions between the four ground state levels in the zero-order approximation (i.e. a,b,c,d in (4.27) take on the values a, $\bar{a}$ only) then all six possible transitions occur at $\omega_0 = 0$ which is identical to that from the single ion spectrum. In this chapter we wish to consider the contribution of higher order diagrams to investigate the possibility of obtaining a splitting between these four ground states which would split the single peak at $\omega_0 = 0$ into a number of separate peaks. Such peaks would then be observed as satellites to the single ion peak at $\omega_0 = 0$.

Consequences of time-reversal symmetry.

As a result of hermicity and the time reversal invariance of the interaction Hamiltonian (3.8) it is possible to obtain relationships between the coupling coefficients V^{ik}_{mn}. Without loss of generality we can consider the single ion Hamiltonian.

$$H^{int} = \sum_{mnk} a^{\dagger}_m a_n V^k_{mn} (b_k + b^{\dagger}_{-k}) \qquad (4.51)$$

(where again k represents wavevector $\underline{k}$ and polarization j with -k reversing the sign of $\underline{k}$).

Hermicity requirements give

$$(H^{int})^{\dagger} = \sum_{mnk} a_m a^{\dagger}_n (V^k_{mn})^* (b^{\dagger}_k + b_{-k})$$

$$= \sum_{mnk} a^{\dagger}_m a_n (V^{-k}_{nm})^* (b_k + b^{\dagger}_{-k})$$

$$= H^{int} = \sum_{mnk} a^{\dagger}_m a_n V^k_{mn} (b_k + b^{\dagger}_{-k})$$

and hence on comparing coefficients we obtain

$$V^{k}_{mn} = (V^{-k}_{nm})^{*} \tag{4.52}$$

Considering an operator 0 and its time reversal operator $\bar{0} = T\,0\,T^{-1}$ we have

$$0|a\rangle = \sum_{b} |b\rangle \langle b|0|a\rangle \tag{4.53}$$

and $\therefore$ $T0|a\rangle = \bar{0}\,T|a\rangle$

$$= \bar{0}|\bar{a}\rangle$$

$$= \sum_{b} |\bar{b}\rangle \langle b|0|a\rangle^{*} \tag{4.54}$$

$$= \sum_{b} |\bar{b}\rangle \langle \bar{b}|\bar{0}|\bar{a}\rangle$$

where the third step of (4.54) results because the action of T is antilinear and hence takes numbers to their complex conjugates. This then gives us the basic result of time reversal symmetry

$$\langle \bar{b}|\bar{0}|\bar{a}\rangle = \langle b|0|a\rangle^{*}$$

$$= \langle a|0^{\dagger}|b\rangle. \tag{4.55}$$

If we substitute the states $|a\rangle = |b\rangle = |mnk\rangle$ and observe that $|\bar{a}\rangle = |\bar{\bar{m}}\bar{\bar{n}} - k\rangle$ we have the relation

$$\langle mnk|V|mnk\rangle^{*} = |\bar{\bar{m}}\bar{\bar{n}} - k|V|\bar{\bar{m}}\bar{\bar{n}}k\rangle$$

$$\text{or} \quad (V^{k}_{mn})^{*} = V^{-k}_{\bar{\bar{m}}\bar{\bar{n}}} \tag{4.56}$$

Combining (4.52) and (4.56) then gives us the identity

$$V^{k}_{mn} = V^{k}_{\bar{\bar{n}}\bar{\bar{m}}} \tag{4.57}$$

Substituting the states m = a and n = $\bar{a}$ into (4.57) and using the result

$$T^{2}|a\rangle = T|\bar{a}\rangle = |\bar{\bar{a}}\rangle$$

$$= -|a\rangle \tag{4.58}$$

for an odd electron ion gives

$$V^{k}_{a\bar{a}} = V^{k}_{\bar{\bar{a}}\bar{a}} = -V^{k}_{a\bar{a}}$$

and hence

$$V^{k}_{a\bar{a}} = 0. \tag{4.59}$$

Similarly m = a, n = a gives the result

$$V^{k}_{aa} = V^{k}_{\bar{a}\bar{a}} \tag{4.60}$$

These relationships shall be exploited extensively in the remainder of this chapter to find equalities and cancellations among various matrix elements.

4.7 Self-Energy Diagonalization

We order the product states in the column vector $\underline{\psi}$ in order of increasing energy as indicated by figure 4.10, namely $\psi_1 = \psi_{aa}$, $\psi_2 = \psi_{a\bar{a}}$, $\psi_3 = \psi_{\bar{a}a}$, $\psi_4 = \psi_{\bar{a}\bar{a}}$, $\psi_5 = \psi_{ab}$, ... etc. We then make the approximation that the matrix $\Sigma(i\omega_n)$ of (4.22) is block diagonal as in §4.5.2 for the two-level system with the blocks extending over the degenerate manifolds (figure 4.11).

Figure 4.11.

$\Sigma(i\omega_n) =$

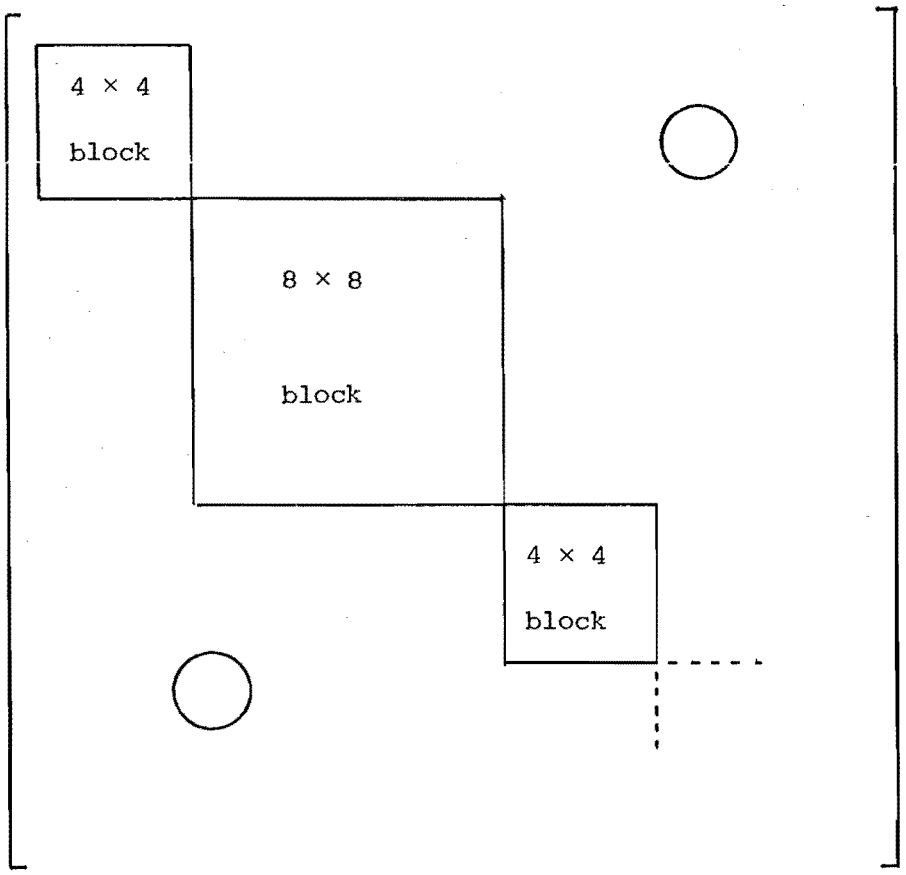

Again this approximation does not restrict us just to the ground state manifold, but still gives intermediate states from higher manifolds. Furthermore the effect of this approximation can also be reduced by extending the allowed structure of self-energy diagrams as was done for the single ion absorption spectrum (cf figure 3.12b).

Writing (4.22) in the form

$$F^{-1}(i\omega_n) = (F^0(i\omega_n))^{-1} - \Sigma(i\omega_n) \tag{4.61}$$

and noting that $F^0(i\omega_n)$ and hence $(F^0(i\omega_n))^{-1}$ is diagonal, (4.17), it is clear that a consequence of our block diagonal assumption is that $F^{-1}(i\omega_n)$ and hence $F(i\omega_n)$ is also block diagonal. This has uncoupled each manifold of degenerate product states and allows each manifold, and in particular the ground state manifold, to be regarded as an independent problem.

Concentrating our attention on the ground state manifold we shall investigate the possibility of symmetries resulting from the relationships (4.52), (4.56), (4.57), (4.59) and (4.60), and then introduce a basis transformation (cf (4.38)) in an attempt to diagonalize the self-energy and hence by using the methods of §4.5 obtain the resulting pair spectra splittings.

4.8 Self-Energy Matrix Symmetries

As a result of the relationships between the coupling coefficients that result from hermicity (4.52) and time-reversal symmetry (4.56) there exist relationships among the self-energy matrix elements. We wish to use these to find all possible cancellations and symmetries among matrix elements before exploiting any symmetries that result from the site symmetry group.

As a demonstration of the type of relationships that exist consider diagram 4.12a. This results in a contribution to the self-energy matrix element $\Sigma_{mm',nn'}(i\omega_n)$ of (see Appendix 4D)

$$\Sigma_{mm',nn'}(i\omega_n) \leftarrow \sum_{ab}\sum_{k\ell} \frac{n_k\, n_\ell\, V^{1k}_{ma}\, V^{1\ell}_{an}\, V^{2-k}_{m'b}\, V^{2-\ell}_{bn'}}{(i\omega_n - \varepsilon_{am'} + \omega_k)(i\omega_n - \varepsilon_{nm'} + \omega_k + \omega_\ell)(i\omega_n - \varepsilon_{nb} + \omega_\ell)} \tag{4.62}$$

If we apply relation (4.52) to each coupling coefficient we obtain an equality with the expression

Figure 4.12.

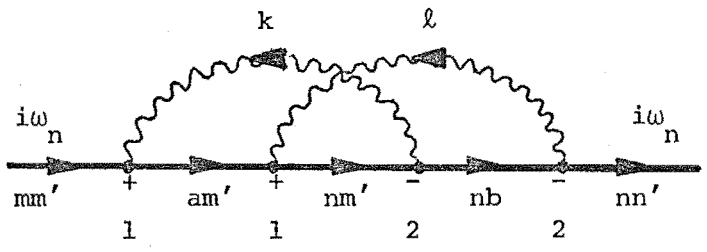

(a)

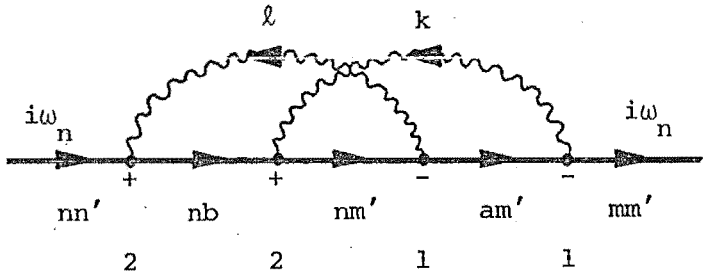

(b)

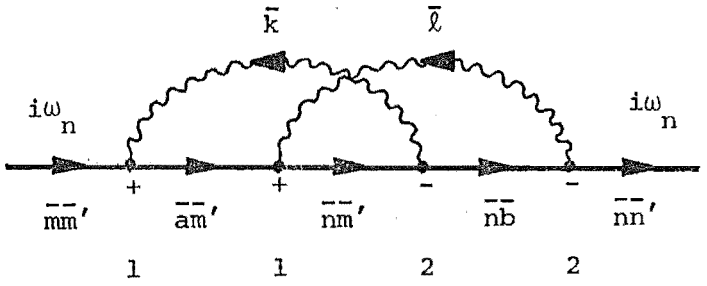

(c)

$$(4.62) = \sum_{ab}\sum_{k\ell} \frac{n_k\, n_\ell (V_{am}^{1-k})^* (V_{na}^{1-\ell})^* (V_{bm'}^{2k})^* (V_{n'b}^{2\ell})^*}{(i\omega_n - \varepsilon_{am'} + \omega_k)(i\omega_n - \varepsilon_{nm'} + \omega_k + \omega_\ell)(i\omega_n - \varepsilon_{nb} + \omega_\ell)} \qquad (4.63)$$

This is exactly the contribution to the self-energy matrix element $\Sigma_{nn',mm'}(i\omega_n)$ obtained from diagram 4.12b (appendix 4D) with the exception that each coupling coefficient is complex conjugated. Obtaining the contribution to the shift and width function matrix elements from these using (2.22), we then obtain the relationship for the contribution of these diagrams.

$$\Delta_{mm',nn'}(x) = \Delta^*_{nn',mm'}(x)$$

and

$$\Gamma_{mm',nn'}(x) = \Gamma^*_{mm',nn'}(x) \qquad (4.64)$$

It is simple to show that these relationships are obeyed for every diagram that contributes to these shift and width matrix elements and hence (4.64) is true for the total shift and width matrix elements.

Similarly applying equation (4.56) to each coupling coefficient of (4.62) we obtain an equality with

$$(4.62) = \sum_{ab}\sum_{k\ell} \frac{n_k\, n_\ell (V_{\bar{m}a}^{1-k}\, V_{\bar{a}n}^{1-\ell}\, V_{\bar{m}'b}^{2k}\, V_{\bar{b}n}^{2\ell})^*}{(i\omega_n - \varepsilon_{\bar{a}m'} + \omega_k)(i\omega_n - \varepsilon_{\bar{n}m'} + \omega_k + \omega_\ell)(i\omega_n - \varepsilon_{\bar{n}b} + \omega_\ell)} \qquad (4.65)$$

where the equality $\varepsilon_{ab} = \varepsilon_{\bar{a}\bar{b}}$ has also been used.

Contribution (4.59) is exactly the contribution to the self-energy matrix element $\Sigma_{\bar{m}\bar{m}',\bar{n}\bar{n}'}(i\omega_n)$ obtained from diagram 4.12c with the exception of the complex conjugation of the coupling coefficients. This relationship between the diagrams contributing to $\Sigma_{mm',nn'}(i\omega_n)$ and $\Sigma_{\bar{m}\bar{m}',\bar{n}\bar{n}'}(x)$ is also always able to be exhibited and results in the relationships.

$$\Delta_{mm',nn'}(x) = \Delta^*_{\bar{m}\bar{m}',\bar{n}\bar{n}'}(x)$$

and

$$\Gamma_{mm',nn'}(x) = \Gamma^*_{\bar{m}\bar{m}',\bar{n}\bar{n}'}(x). \qquad (4.66)$$

Applying equations (4.64) and (4.66) to the four by four matrix corresponding to the ground state manifold then gives

$$a \equiv M_{aa,aa} = M^*_{\bar{a}\bar{a},aa} = M_{\bar{a}\bar{a},\bar{a}\bar{a}} \tag{4.67}$$

$$b \equiv M_{\bar{a}a,\bar{a}a} = M^*_{\bar{a}a,\bar{a}\bar{a}} = M_{\bar{a}a,\bar{a}a} \tag{4.68}$$

$$c \equiv M_{aa,\bar{a}\bar{a}} = M^*_{\bar{a}\bar{a},aa} = -M^*_{\bar{a}\bar{a},\bar{a}a} = -M_{\bar{a}a,\bar{a}\bar{a}} \tag{4.69}$$

$$d \equiv M_{aa,\bar{a}a} = M^*_{\bar{a}a,aa} = -M^*_{\bar{a}a,a\bar{a}} = -M_{a\bar{a},\bar{a}\bar{a}} \tag{4.70}$$

$$e \equiv M_{aa,\bar{a}\bar{a}} = M^*_{\bar{a}\bar{a},aa} \tag{4.71}$$

$$f \equiv M_{a\bar{a},\bar{a}a} = M^*_{\bar{a}a,a\bar{a}} \tag{4.72}$$

where $M_{ab,cd}$ represents $\Delta_{ab,cd}(x)$ or $\Gamma_{ab,cd}(x)$.

The shift and width matrix elements then have the symmetry

$$\begin{vmatrix} a & c & d & e \\ c^* & b & f & -d \\ d^* & f^* & b & -c \\ e^* & -d^* & -c^* & a \end{vmatrix} \tag{4.73}$$

where a and b are real.

Furthermore, if the Kramers ions are equivalent then we have

$$\Sigma_{mm',nn'}(i\omega_n) = \Sigma_{m'm,n'n}(i\omega_n) \tag{4.74}$$

which results from exchanging the ion positions giving the equalities $c = d$ and $f = f^*$. The resulting matrix can now be block diagonalized by the matrix A of (4.38) to give a singlet and triplet structure.

$$\begin{vmatrix} a & \sqrt{2}c & 0 & e \\ \sqrt{2}c^* & b+f & 0 & -\sqrt{2}c \\ 0 & 0 & b-f & 0 \\ e^* & -\sqrt{2}c^* & 0 & a \end{vmatrix} \quad a,b,f \text{ real.} \tag{4.75}$$

For a particular system, to obtain the splittings of the pair spectra lines, we must evaluate the five independent shift matrix elements $\Delta(\varepsilon_{aa})$ and then diagonalize (4.75). The sum of the eigenvalues of matrix (4.75) is equal to the trace of this matrix and hence the "centre of gravity" of the split levels occurs at (a+b)/2. Hence the levels are split if any of the parameters a-b, c, e or f are non-zero.

The rest of this chapter will be devoted to evaluating the major contributions to these four parameters.

4.9 Matrix Element Contributions

We wish to evaluate the diagram contribution to the terms a-b, c, e and f that are likely to be the most significant. In doing this it is possible to obtain full or partial cancellations from different diagrams that result from the relationships (4.52)-(4.57) and care must be taken to account for these. When considering two diagrams of similar order we expect that the diagram that contains the fewest references to the excited state manifolds to give large contributions to the self-energy as the corresponding denominators are smaller.

4.9.1 Second Order Contributions

We might expect that the leading contributions to a-b, c, e and f come from the four second order diagrams of figure 4.13.

Figure 4.13.

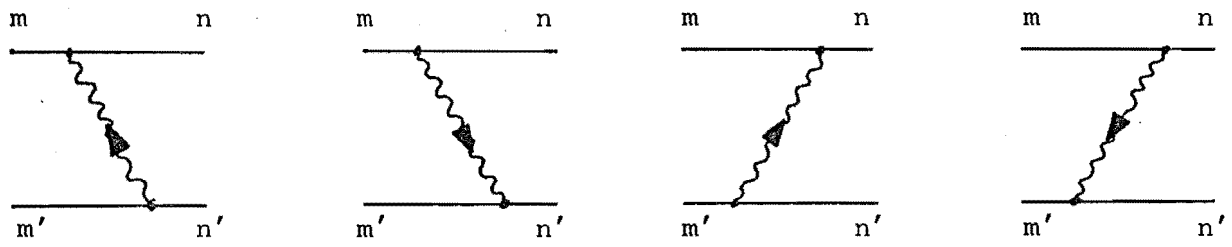

(note that unlike ordinary Feynman diagrams these are ordered and hence are not deformable) which give a contribution

$$\Sigma_{mm',nn'}(i\omega_n) = \sum_k V^{1k}_{mn} V^{2-k}_{m'n'} \left\{ \frac{n_k}{i\omega_n + \omega_k - \varepsilon_{nm'}} + \frac{n_k+1}{i\omega_n - \omega_k - \varepsilon_{mn'}} \right\}$$

$$+ \sum_k V^{1-k}_{mn} V^{2k}_{m'n'} \left\{ \frac{n_k}{i\omega_n + \omega_k - \varepsilon_{mn'}} + \frac{n_k + 1}{i\omega_n - \omega_k - \varepsilon_{nm'}} \right\} \qquad (4.76)$$

However for the contributions to c and e we have $m' = a$ and $n' = \bar{a}$ and hence (4.76) contains a factor $V_{a\bar{a}}^{2\pm k}$ which vanishes by (4.59). Similarly the contribution to f has $m' = \bar{a}$, $n' = a$ and hence contains the vanishing factor $V_{\bar{a}a}^{k}$. Hence there is no second order contribution to c, e or f. Although contribution (4.76) does give a non-vanishing contribution to a ($m = n = m' = n' = a$) and to b ($m = n = a$, $m' = n' = \bar{a}$) there is no contribution to a-b at this order because (4.76) gives identical contributions to a and b when we use the relation (4.60), namely:

$$a = b = \Sigma_{aa,aa}(\varepsilon_{aa}) = -\sum_k \frac{(V_{aa}^{1k} V_{aa}^{2-k} + V_{aa}^{1-k} V_{aa}^{2k})}{\omega_k}$$

$$= -2 \sum_k \frac{V_{aa}^{k} V_{aa}^{k}}{\omega_k} \cos(\underline{k}\cdot\underline{R}) \qquad (4.77)$$

4.9.2 Trivial Vertices

This result can be generalized to include all diagrams that include a trivial vertex, i.e. those that contain no intermediate states for ion 1 (figure 4.14a) or for ion 2 (figure 4.14b).

Figure 4.14

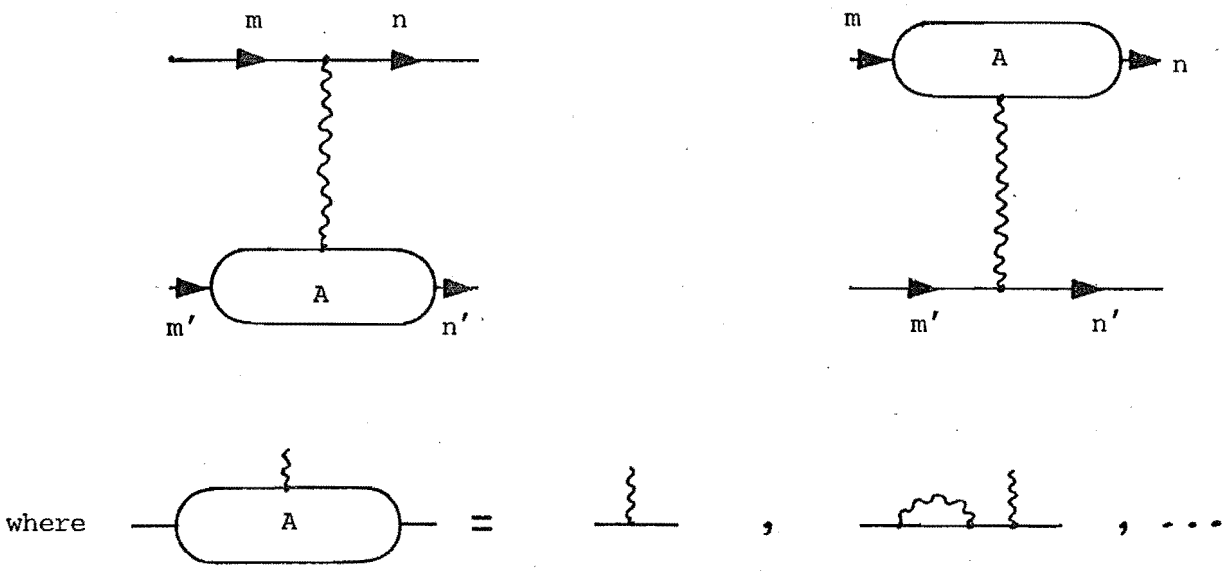

For contributions to c, e or f then (b)-type contributions (i.e. those that arise from diagrams of figure 4.14(b)) vanish as

before because they contain a vanishing $V_{a\bar{a}}^{2\pm k}$ factor. For (a)-type contributions (i.e. from diagram of figure 4.14(a)), then by; (i) using (4.57) on each phonon vertex referring to ion two and (ii) reversing the direction of phonons by regarding them as referring to phonons with time reversed labels ($k = \underline{k},j \rightarrow \bar{k} = -\underline{k},j$) and then (iii) rearranging (by a horizontal displacement of ion one vertex) so the new denominators are appropriate for the new topology, one obtains a contribution that cancels the original diagram. These operations are represented in figure 4.15 where $\bar{A}$ is to be obtained from A by (a) reflecting about the vertical, (b) each level propagator is to have its sense reversed and its label replaced by its time-reversed conjugate state and (c) each interval phonon propagator, sense reversed and its label replaced by its time reversed labels.

Figure 4.15

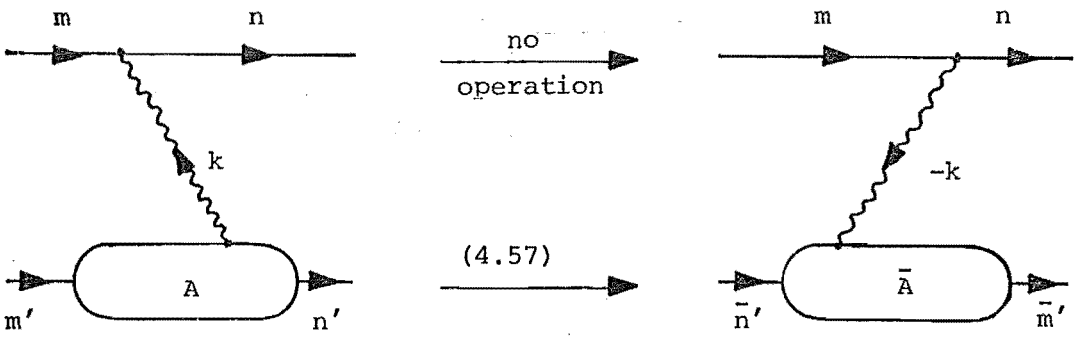

The cancellation relies explicitly on the eqalities $\varepsilon_a = \varepsilon_{\bar{a}}$, $\omega_k = \omega_{\bar{k}}$ which enable the repositioning of the upper vertex. In figure 4.16 we exhibit a specific example for a diagram that contributes to e.

Figure 4.16

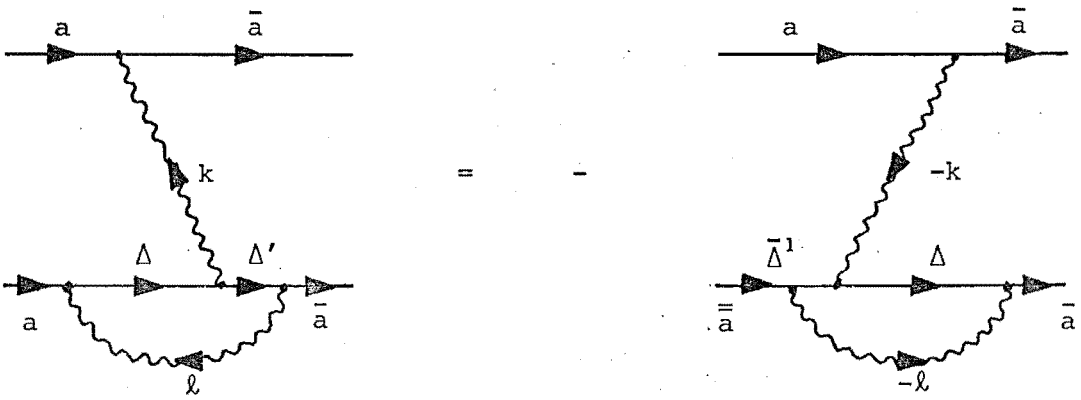

Figure 4.17.

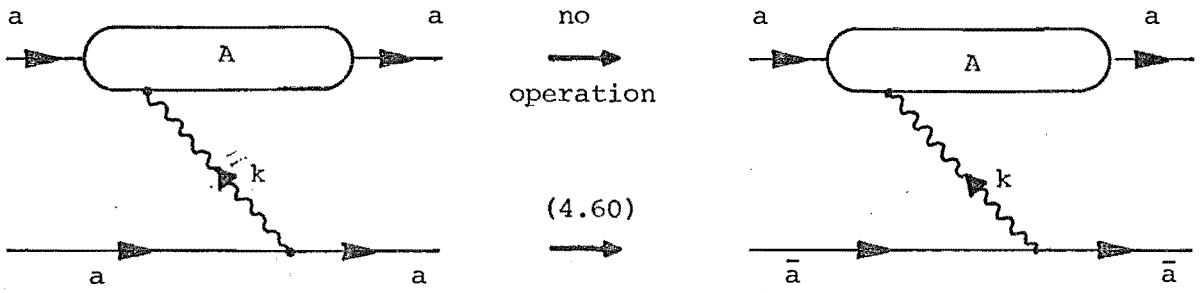

(a)

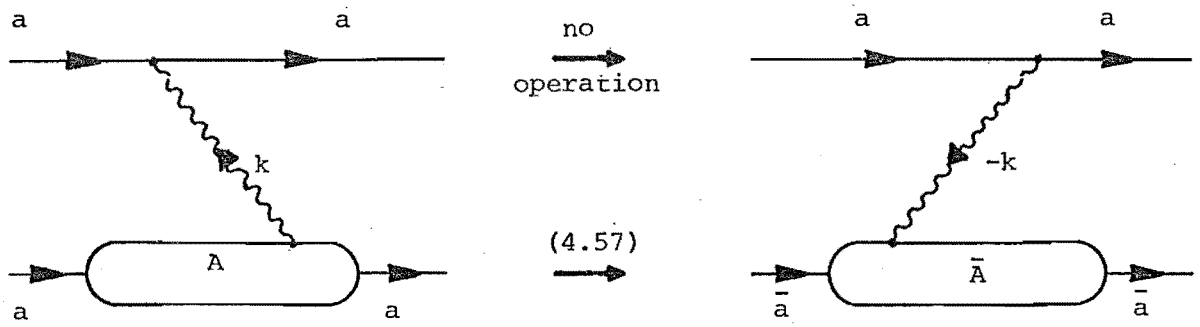

(b)

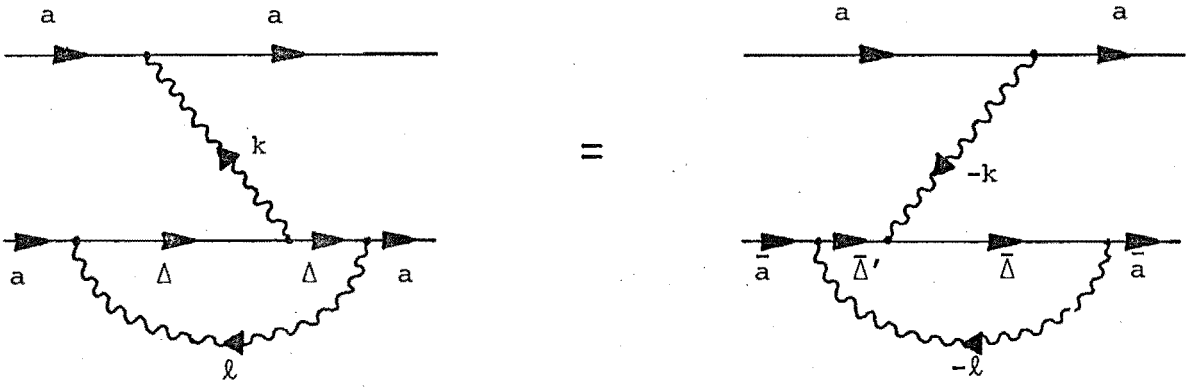

(c)

In a similar manner we can exhibit the equality of a and b (and hence the vanishing of a-b) for contributions that contain a trivial vertex. For (b)-type contributions the equality follows immediately from the equality (4.60) (see figure 4.17a) while for (a)-type contributions the transformation indicated in figure 4.17b and applied to a specific contribution in figure 4.17c exhibits the required equality. (This again uses the equalities $\varepsilon_a = \varepsilon_{\bar{a}}$, $\omega_k = \omega_{\bar{k}}$ to enable the trivial vertex to be repositioned.) Hence we see that diagrams containing trivial vertices give no contribution to c,e,f or a-b (though they do contribute to a+b of course and hence shift the 'centre of gravity' of the manifold). These results can be generalized to apply to quadratic and anharmonic effects also (McKenzie and Stedman 1978).

4.9.3 Fourth-Order Contributions

In this section we shall evaluate the contribution from all fourth-order diagrams taking account of all full or partial cancallations. Because we have shown that diagrams containing a trivial vertex give no contribution to a-b, c, e or f then the only contributions come from diagrams with the structure of those in figure 4.18.

Figure 4.18

We expect that diagrams containing fewer references to higher manifolds will give larger contributions to the matrix elements because they contain smaller denominators. This suggests that if $m = n$ (e.g. contributions to a,b or c) then the choice $\Delta = m$ will give the largest nonvanishing[1] contribution while if $m' = n'$ (e.g. contributions to a,b) then the choice $\Delta' = m'$ would be optimum. However the transformation of figure 4.19(a) shows the equality of a and b and figure 4.19(b) the cancellation that occurs among the diagrams contributing to c for the choice $\Delta = m(=a)$ while figure 4.19(c) shows the equality of a and b for diagrams with $\Delta' = m'$. To obtain non-vanishing contributions to a-b, c, e or f then we must not choose Δ and Δ' from the ground state manifold but rather from excited state manifolds with the expectation that the first excited state will result in larger contributions because of their smaller denominators.

The two diagrams of figure 4.18 represent the 12 diagrams of figure 4.20 each of which in turn represents four diagrams differing from each other by the choice of phonon direction.

Because the directions of the phonon propagators differ then strictly the corresponding $V_{m\Delta}^{l\pm k}$, etc will differ from diagram to diagram. However because each phonon travels between each ion, then the resulting position dependence is one of the four possibilities $e^{\pm i\underline{k}\cdot\underline{R}}\, e^{\pm i\underline{\ell}\cdot\underline{R}}$ ($\underline{R} = \underline{r}_1 - \underline{r}_2$). When we sum over k and ℓ we regard the only singular dependence in $\underline{k}$ and $\underline{\ell}$ to come from these factors and they all give the same result namely

$$\sum_{\substack{k\ell \\ \text{angular}}} e^{\pm i\underline{k}\cdot\underline{R}}\, e^{\pm i\underline{\ell}\cdot\underline{R}} = \int_{-1}^{+1} d\mu_k\, d\mu_\ell \int_0^{2\pi} d\phi_k\, d\phi_\ell\; e^{\pm ikR\mu_k}\, e^{\pm i\ell R\mu_\ell}$$

$$= 4(2\pi)^2 \frac{\sin kR}{kR} \frac{\sin \ell R}{\ell R} \qquad (4.78)$$

and hence are common to each diagram.

[1] The choice $\Delta = \bar{m}$ vanishes because it contains a vanishing factor $V_{m\bar{m}}^{k}$ as occurs if $m \neq n$ and we choose Δ from the ground manifold.

Figure 4.19.

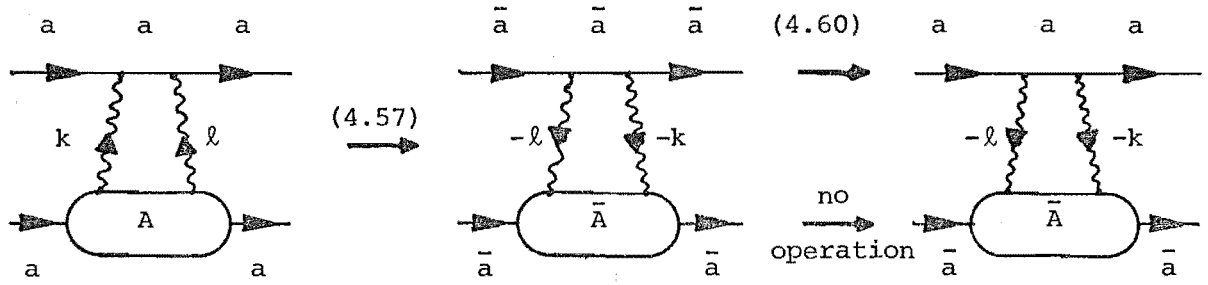

(a): equality of a and b

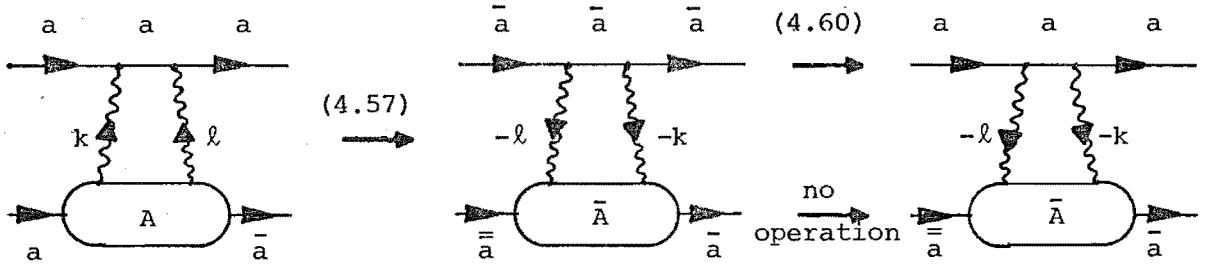

(b): cancelation of c

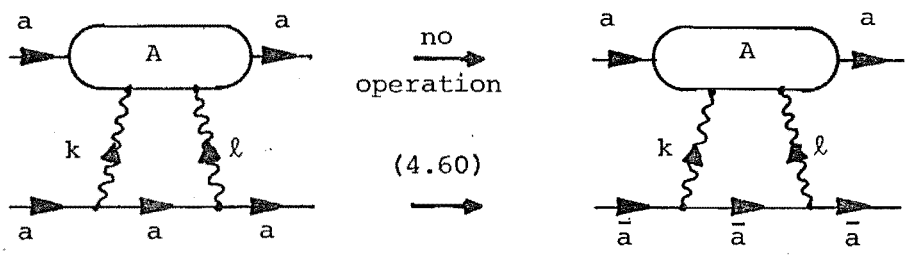

(c): equality of a and b

Figure 4.20

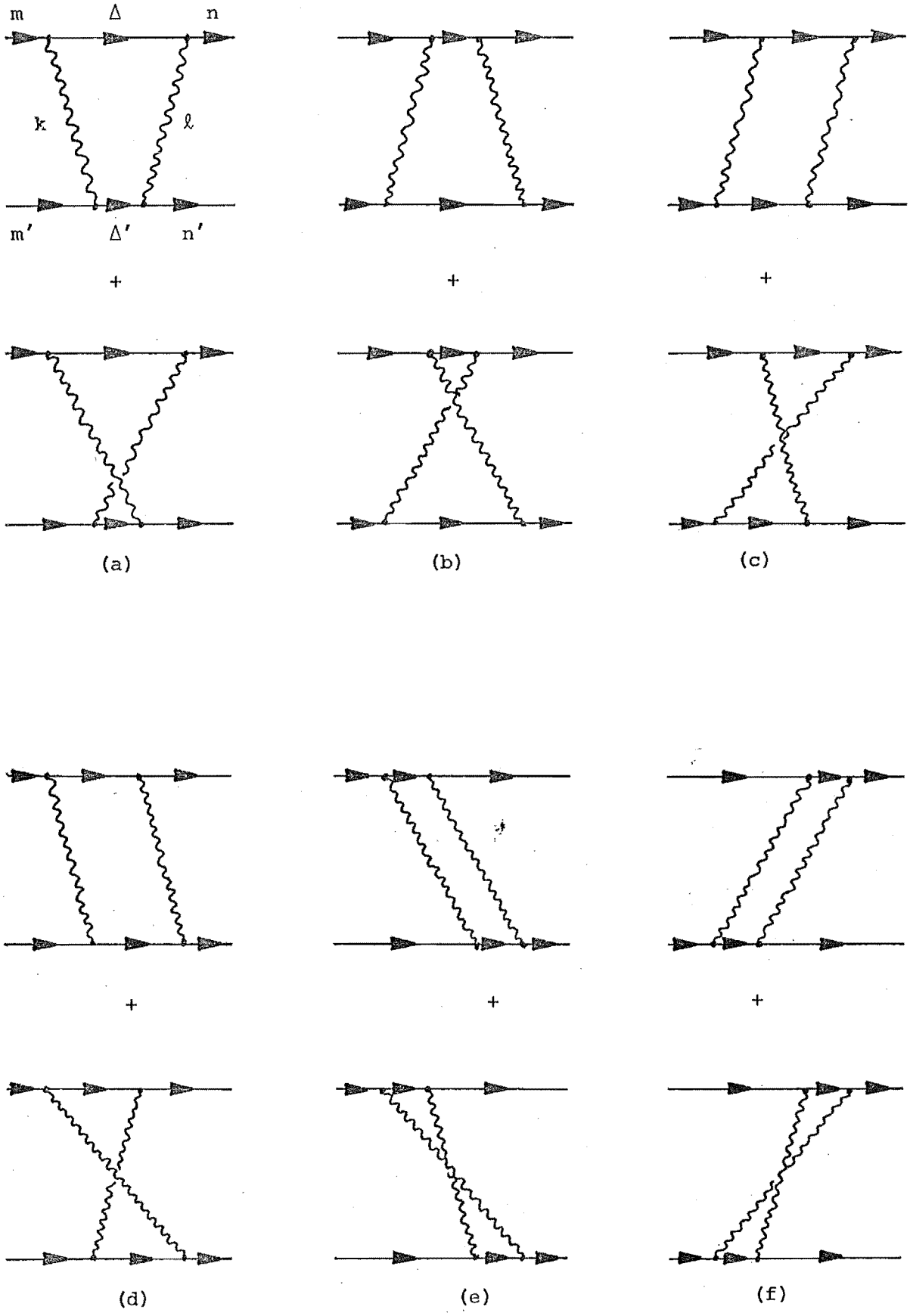

Furthermore the transformation of figure 4.21 gives partial cancellations between the upper and lower diagrams of each pair in figure 4.6a-f.

Figure 4.21

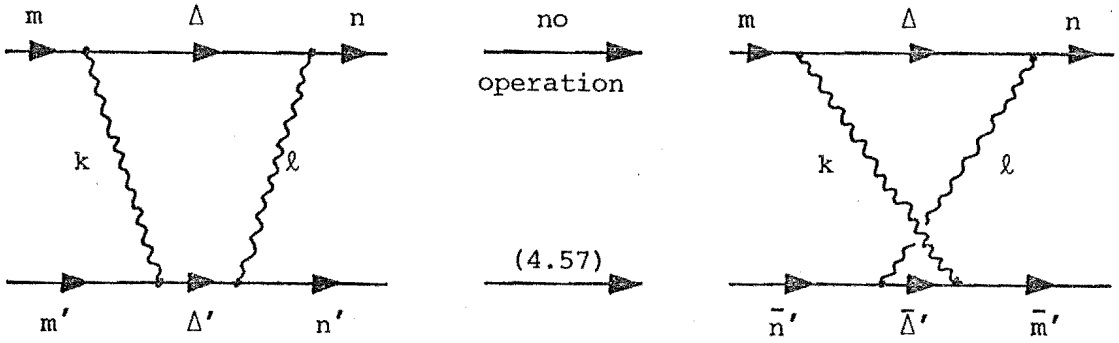

This also means the combination of V factors are the same for a diagram 4.20a-f when contributing to a-b (or c or e or f), and allows us to treat the V's and denominators separately.

The numerators for contributions to a-b, c, e and f are given in table 4.1 and are to be combined with the contributions from the diagrams of figure 4.20 enumerated in table 4.2.

The contribution of table 4.2 can be combined to give

$$\frac{4\, n_k^{\pm}\, n_\ell^{\pm}\, (\pm\omega_k)(\pm\omega_\ell)[\,(-\Delta-\Delta')(\pm 2\omega_k \pm 2\omega_\ell - \Delta - \Delta') + (\pm\omega_k \pm \omega_\ell)^2]}{(\pm\omega_k - \Delta)(\pm\omega_k - \Delta')(\pm\omega_\ell - \Delta)(\pm\omega_\ell - \Delta')(\pm\omega_k \pm \omega_\ell - \Delta - \Delta')(-\Delta-\Delta')(\pm\omega_k \pm \omega_\ell)} \cdot \tag{4.79}$$

If we have a system such that $\Delta, \Delta' \gg \omega_D$ then (4.79) reduces to

$$(4.73) \xrightarrow{\Delta,\Delta' \gg \omega_D} \frac{1}{\Delta'^2\Delta^2}\quad 4\, n_k^{\pm}\, n_\ell^{\pm}\, \frac{(\pm\omega_k)(\pm\omega_\ell)}{(\pm\omega_k \pm \omega_\ell)}. \tag{4.80}$$

For such a system the contributons to a-b, c, e and f then are all fourth-order in V ($\sim V^4$) and in Δ^{-1} and each contains an intergral over k and ℓ of the form (using Debye-model for acoustic phonons)

$$\frac{V^4 c^2}{\Delta'^2\Delta^2 R^2} \int_{-k_D}^{k_D} dk\; k^2\, \mathrm{den}(k)\, \sin(kR) f_B(ck) \int_{-k_D}^{k_D} d\ell\; \ell^2\, \mathrm{den}(\ell)\, \sin(\ell R) f_B(c\ell) \cdot \frac{1}{k+\ell}. \tag{4.81}$$

TABLE 4.1

$$\text{Numerator} = 4(2\pi)^2 \sum_{k\ell} \sum_{\Delta\Delta'} X \frac{\sin kR}{kR} \frac{\sin \ell R}{\ell R} \quad \text{where}$$

(no angular dependence)

Matrix element	X			
a - b	$V^k_{a\Delta}$	$V^\ell_{\Delta a}$	$V^k_{a\Delta'}$	$V^\ell_{\Delta' a}$
c	$V^k_{a\Delta}$	$V^\ell_{\Delta a}$	$V^k_{a\Delta'}$	$V^\ell_{\Delta'\bar{a}}$
e	$V^k_{a\Delta}$	$V^\ell_{\Delta\bar{a}}$	$V^k_{a\Delta'}$	$V^\ell_{\Delta'\bar{a}}$
f	$V^k_{a\Delta}$	$V^\ell_{\Delta\bar{a}}$	$V^k_{\bar{a}\Delta'}$	$V^\ell_{\Delta' a}$

TABLE 4.2

Diagram	Contribution(s)
4.20a	$\frac{n_k^{\pm} n_\ell^{\pm}}{(\pm\omega_k - \Delta)(\pm\omega_\ell - \Delta)} \left[\frac{1}{(-\Delta-\Delta')} - \frac{1}{\pm\omega_k \pm \omega_\ell - \Delta - \Delta'} \right]$
4.20b	$\frac{n_k^{\pm} n_\ell^{\pm}}{(\pm\omega_k - \Delta')(\pm\omega_\ell - \Delta')} \left[\frac{1}{(-\Delta-\Delta')} - \frac{1}{\pm\omega_k \pm \omega_\ell - \Delta - \Delta'} \right]$
4.20c	$\frac{n_k^{\pm} n_\ell^{\pm}}{(\pm\omega_\ell - \Delta)} \left[\frac{1}{(\pm\omega_k - \Delta')(-\Delta-\Delta')} - \frac{1}{(\pm\omega_\ell - \Delta')(\pm\omega_k \pm \omega_\ell - \Delta - \Delta')} \right]$
4.20d	$\frac{n_k^{\pm} n_\ell^{\pm}}{(\pm\omega_k - \Delta)} \left[\frac{1}{(-\Delta-\Delta')(\pm\omega_\ell - \Delta')} - \frac{1}{(\pm\omega_k \pm \omega_\ell - \Delta - \Delta')(\pm\omega_k - \Delta')} \right]$
4.20e	$\frac{n_k^{\pm} n_\ell^{\pm}}{(\pm\omega_k - \Delta)(\pm\omega_n \pm \omega_\ell)} \left[\frac{1}{\pm\omega_\ell - \Delta'} - \frac{1}{\pm\omega_k - \Delta'} \right]$
4.20f	$\frac{n_k^{\pm} n_\ell^{\pm}}{(\pm\omega_k \pm \omega_\ell)(\pm\omega_\ell - \Delta)} \left[\frac{1}{\pm\omega_k - \Delta'} - \frac{1}{\pm\omega_\ell - \Delta'} \right]$

where $n_k^{\pm} \equiv \begin{pmatrix} n_k \\ n_k + 1 \end{pmatrix}$ $\quad \Delta = \varepsilon_\Delta - \varepsilon_a$

$$\Delta' = \varepsilon_{\Delta'} - \varepsilon_a$$

and each contribution represents the sum of four terms.

Using the transformations $x = \beta ck$ and $y = \beta c\ell$ this can be written in the form,

$$= \frac{V^4 c^2}{\Delta'^2 \Delta^2 R^2} \cdot \frac{1}{(\beta c)^9} \int_{-\beta\omega_D}^{\beta\omega_D} dx\, x^4 \sin\left(\frac{Rx}{\beta c}\right) \frac{1}{e^x - 1} \int_{-\beta\omega_D}^{\beta\omega_D} dy\, y^4 \sin\left(\frac{Ry}{\beta c}\right)$$

$$\frac{1}{e^y - 1} \cdot \frac{1}{x+y} \cdot \qquad (4.82)$$

At low temperatures the integral has little temperature dependence and we find the splittings have a T^9 temperature dependence.

We conclude that for a Kramers system

(a) the four ground state manifold levels separate into a triplet and singlet system,

(b) the splittings are given by the eigenvalues of the matrix (4.69) and hence depend on (a-b), e, f and c with centre of gravity (a+b)/2,

(c) the second order diagrams do not contribute to splittings but can shift the levels "centre of gravity",

(d) any diagram containing a trivial vertex gives no contribution to splittings but can shift the levels "centre of gravity",

(e) the fourth-order diagram contribution to a-b, c, e, and f are of order V^4 and Δ^{-4} and at low temperature using a Debye density of states for acoustic phonons have a T^9 temperature dependence.

Result (e) above would be expected to affect the results of previous workers who have analysed Kramers ion pair interactions and assumed the interaction had a Δ^{-1} dependence. (e.g. Baker (1971b) and Anderson *et.al.* (1971) in their analysis of Ce - Ce pairs.) These workers may need to modify their analysis in the light of the present results.

As was our original aim we have presented a diagram technique that can conveniently and uniquely analyse the pair spectra of both Kramers

and non-Kramers ions, incorporating in a straightforward manner the multiple cancellations encountered.

CHAPTER 5 : RAMAN SPECTRUM : GENERAL

5.1 Introduction

A great increase in activity in Raman scattering and its related fields resulted from the introduction of extremely intense and narrow linewidth optical sources with the advent of the laser. The literature on this and related topics is vast and we shall content ourselves with mentioning the elementary reviews by Hayes (1975) and Moordian (1970), more technical reviews by Moordian (1972), Barker and Loudon (1972) and Franken and Ward (1963) and the books of Loudon (1973), Louisell (1973), Heitler (1954) and Cardona (1975).

In general a spectral line or feature is broadened by two essentially distinct processes. Homogeneous broadening is that which results from similar scattering centres, and includes, for example, natural or radiative broadening and phonon broadening. However in a sample containing many scattering centres, random variations throughout the sample can result in shifts in the position of the line and hence the resulting superposition of peaks is broader than any single peak. (See figure 5.1). This is termed inhomogeneous broadening and includes such effects as Doppler broadening in gases and strain broadening in crystals.

With the introduction of tunable laser sources and the development of new techniques it has been possible to suppress the inhomogeneous broadening, enabling a study of the homogeneous broadening mechanisms. (Szabo 1970, 1971 ; Riseberg 1972 ; Personov *et al* 1972 ; Delsart *et al* 1974 ; Kushida and Takushi 1975). In the light of these advances an analysis of the homogeneous broadening and shift of Raman spectral lines resulting from the interaction of phonons with impurity ions in crystals assumes greater significance. It is towards this problem that this chapter is directed.

It has not been uncommon in previous phenomenological theories of Raman spectral lineshapes to be content with adding small imaginary widths

Figure 5.1

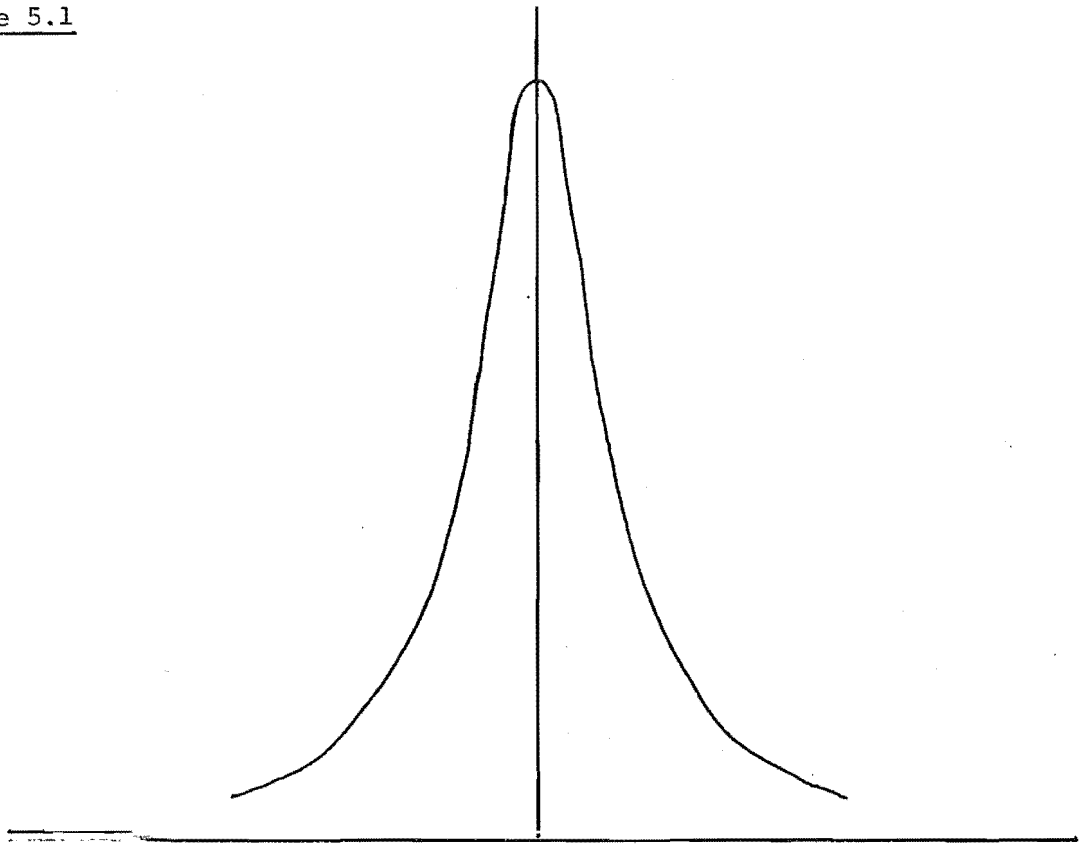

Homogenously broadened line

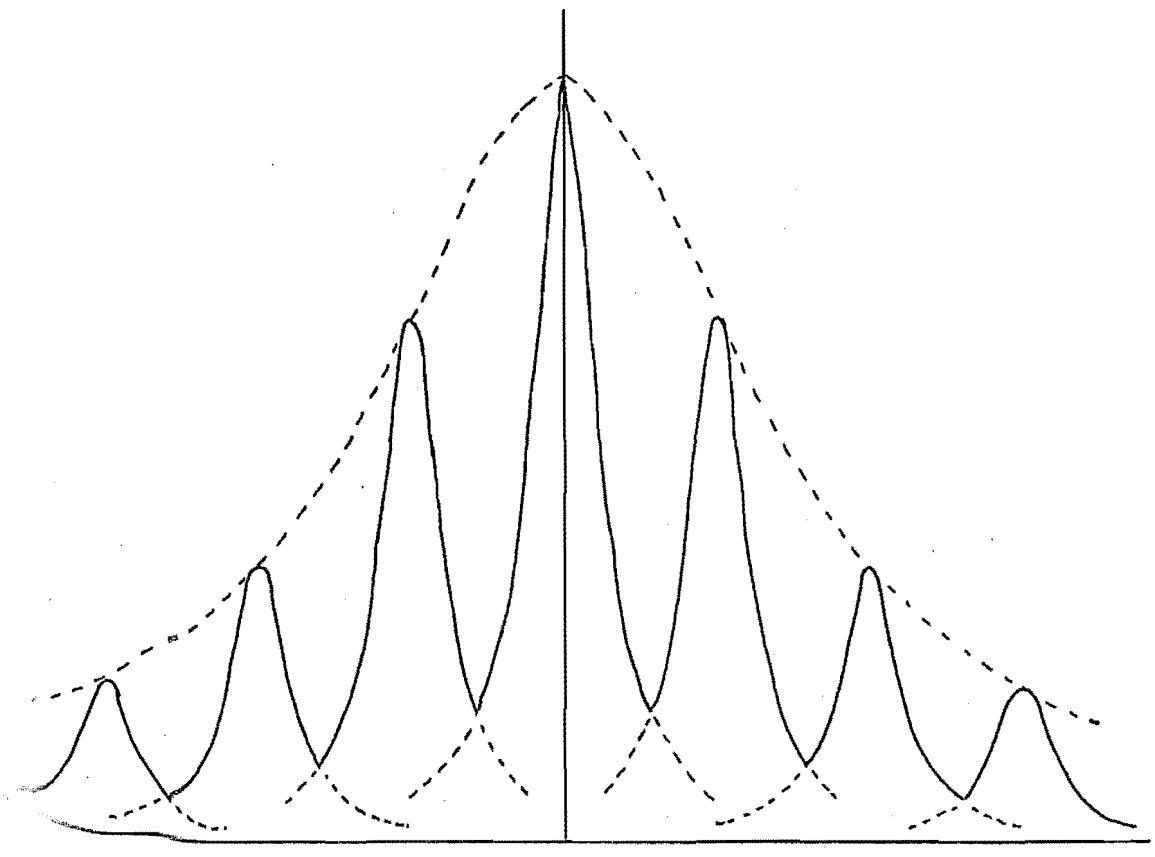

Inhomogeneously broadened line

to expressions to take into account homogeneous broadening (for example see review by Shorygin (1973)) and to make assumptions regarding additivity of linewidths, that we found were not justified for absorption in Chapter 3. In this chapter we present a quantum field theoretic description using thermal G.F. diagram techniques in which the broadening and shifts arise in a very natural way without the need of *ad.hoc.* introduction.

5.2 Scattering Geometry

A thermal G.F. theory of Raman scattering was presented by Kawabata (1970, 1971a,b) for steady state scattering from metals. This was extended to the time-dependent scattering regime by Kusunoki (1976) which he applied to resonance scattering from gas molecules. Cuden (1976) applied the theory to superconductivity. We shall present a theory that is a combination of both Kawabata's and Kusunoki's approach in an attempt to find the most natural description for our system of interest.

The scattering geometry we shall choose is that chosen by Kawabata and is shown schematically in figure 5.2. This limits the angles θ_0 and θ_s to the range

$$0^o \leqslant \theta_0, \theta_s \leqslant 90^o$$

and hence includes most situations of experimental interest such as the standard scattering geometry $\theta_s - \theta_0 = 90^o$. Although it does not include less common geometries such as transmission scattering, extension of the formalism to such situations is possible.

The incident radiation is generated in a region far from the crystal by some external current $\underline{J}^{ext}$. The radiation with frequency ω_0 then interacts with the impurities in the crystal which is taken to be in the lower half-plane. The scattered radiation is detected in the region V_D, again far away from the crystal, where a quantity proportional to the number of photons entering the region is evaluated. The regions V_E and V_D are taken to have dimensions much larger than that of the relevant radiation wavelengths.

Figure 5.2

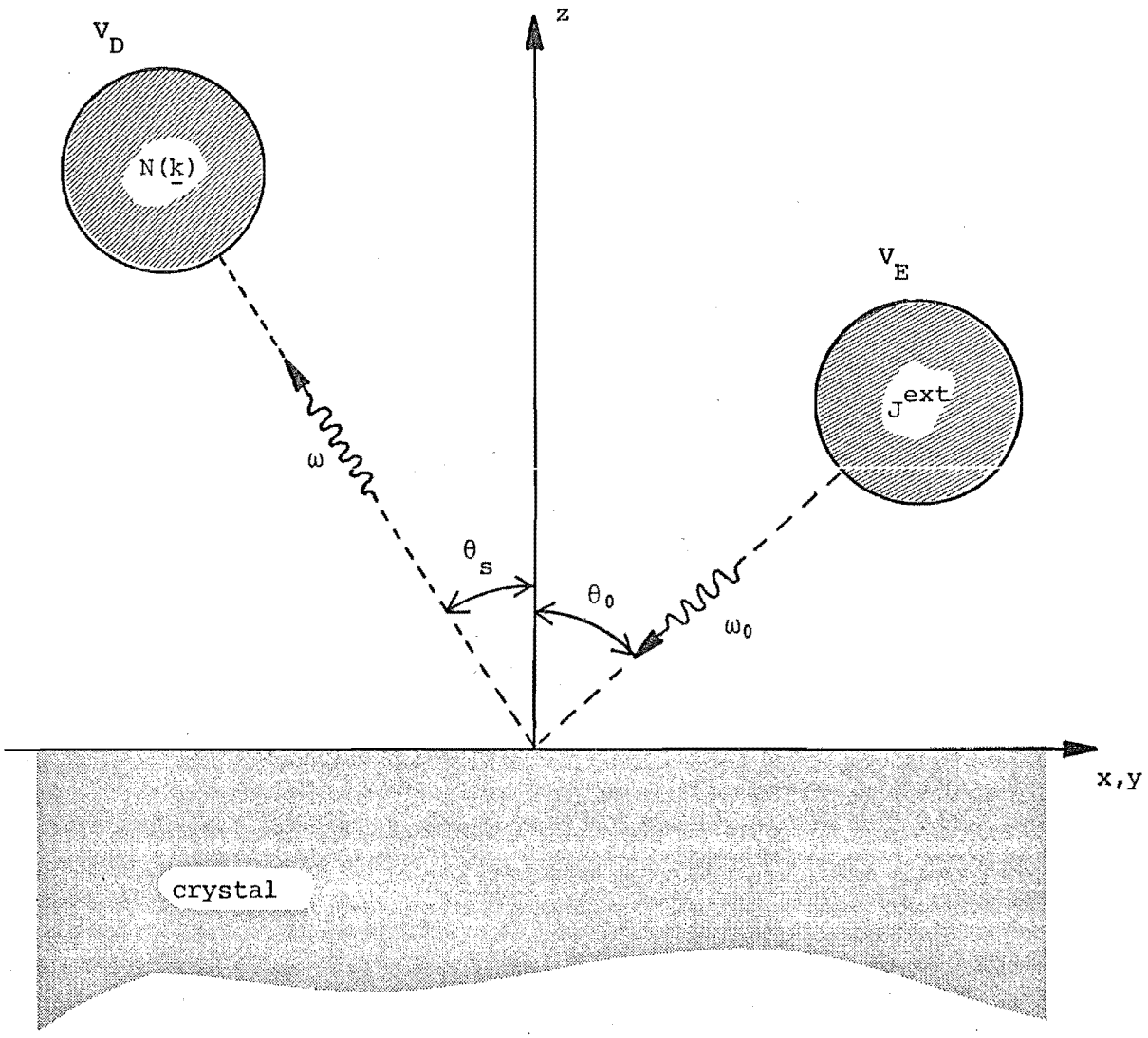

5.3 Quadratic Response Theory

If $\underline{A}(\underline{r})$ is the vector potential of the radiation field at position $\underline{r}$ we define the Fourier transform

$$\underline{A}(\underline{k}) \equiv \int_D d\underline{r}\, e^{-i\underline{k}\cdot\underline{r}}\, \underline{A}(\underline{r}) \qquad (k_z > 0) \tag{5.1}$$

where the integral is to be taken over the region V_D. The scattering process is to be regarded as the change in or response of $\underline{A}(\underline{k})$ to the external current $\underline{J}^{ext}(\underline{r})$.

The Hamiltonian that describes the interaction between the external current and the radiation field is[1] (Abrikosov *et.al.* 1963)

$$\mathcal{H}^{ext}(t) = -\int_E d\underline{r}\, \underline{A}(\underline{r}) \cdot \underline{J}^{ext}(\underline{r},t). \tag{5.2}$$

Kawabata (1971a) has shown that the linear response of $\underline{A}(\underline{k})$ to $\underline{J}^{ext}(\underline{r})$ vanishes because of the incoherent nature of the scattering and the random phase of $\underline{A}(\underline{k})$. A similar result was obtained by Schaich and Ashcroft (1971) in their work on photoemission. Following these results we use, rather than the standard linear response formalism, the higher-order quadratic response formalism. This was also developed by Kubo (1957[2], 1966) and is discussed in the works by Callen (1961) and Hameking and Wehrum (1975).

We define a quantity

$$N(\underline{k}) = (\underline{e}\cdot\underline{A}(\underline{k}))\cdot(\underline{e}\cdot\underline{A}^{\dagger}(\underline{k})) \tag{5.3}$$

related to the number of photons entering the collector with wavevector $\underline{k}$ and polarization $\underline{e}$. The quadratic response or change in this quantity resulting from $\underline{J}^{ext}(\underline{r})$ through (5.2) at time t is given by the expression

[1] We set the mass of the charge carriers and $\hbar$ to unity.

[2] Equation (2.29) in this reference is in error and has been corrected implicitly by a number of works such as equation (2.5) of Kawabata (1971a).

$$\langle \Delta N(\underline{k}) \rangle_t = - \int_{-\infty}^{t} dt_1' \int_{-\infty}^{t_1'} dt_2' \int_E d\underline{r}_1 \, d\underline{r}_2 \langle [[N(\underline{k}),$$

$$A_\alpha (\underline{r}, t_1' - t)], A_\beta (\underline{r}_2, t_2' - t)] \rangle J_\alpha^{ext}(\underline{r}_1, t_1') J_\beta^{ext}(r_2, t_2') \quad (5.4)$$

where $O(t) = e^{i\mathcal{H}t} O e^{-i\mathcal{H}t}$.

The external current is taken to have a rapid frequency variation, ω_0, and a slower variation to enable the description of scattering of laser pulses.

$$\underline{J}^{ext}(\underline{r}, t) = \underline{J}^{ext}(\underline{r}) \int_{-\infty}^{\infty} \frac{d\xi}{2\pi} S(\xi) e^{-i(\xi + \omega_0 + i\delta)t} + \text{c.c.} \quad (5.5)$$

where δ is an infinitesimal positive quantity. The slower time-dependence of the pulse is to be determined by the function $S(\xi)$ which from causality considerations must satisfy the property

$$S^*(\xi) = S(-\xi) \quad (5.6)$$

We consider here two possible forms of $S(\xi)$.

5.3.1 Laser Pulse

A specific form of the laser pulse shape considered by Kusunoki (1976) is that given by

$$S(\xi) = \frac{2i\Gamma_0 \sin[(T/2)(\xi - i\delta)]}{(\xi + i\Gamma_0)(\xi - i\delta)} \quad (5.7)$$

Evaluating (5.5) by means of a contour integral along the real axis and enclosing either the upper or lower half plane, the resulting pulse shape has the form

$$\underline{J}(\underline{r}, t) = \underline{J}(\underline{r}) e^{-i(\omega_0 + 2i\delta)t} \begin{cases} 0 & t \leqslant -\frac{T}{2} \\ [1 - e^{-\Gamma_0 (t + T/2)}] & -\frac{T}{2} \leqslant t \leqslant \frac{T}{2} \\ [1 - e^{-\Gamma_0 T}] \, e^{-\Gamma_0 (t - T/2)} & \frac{T}{2} \leqslant t \end{cases} \quad (5.8)$$

which is a pulse with exponential rise and fall times Γ_0^{-1} and lasting for a time T and is indicated in figure 5.3.

Figure 5.3

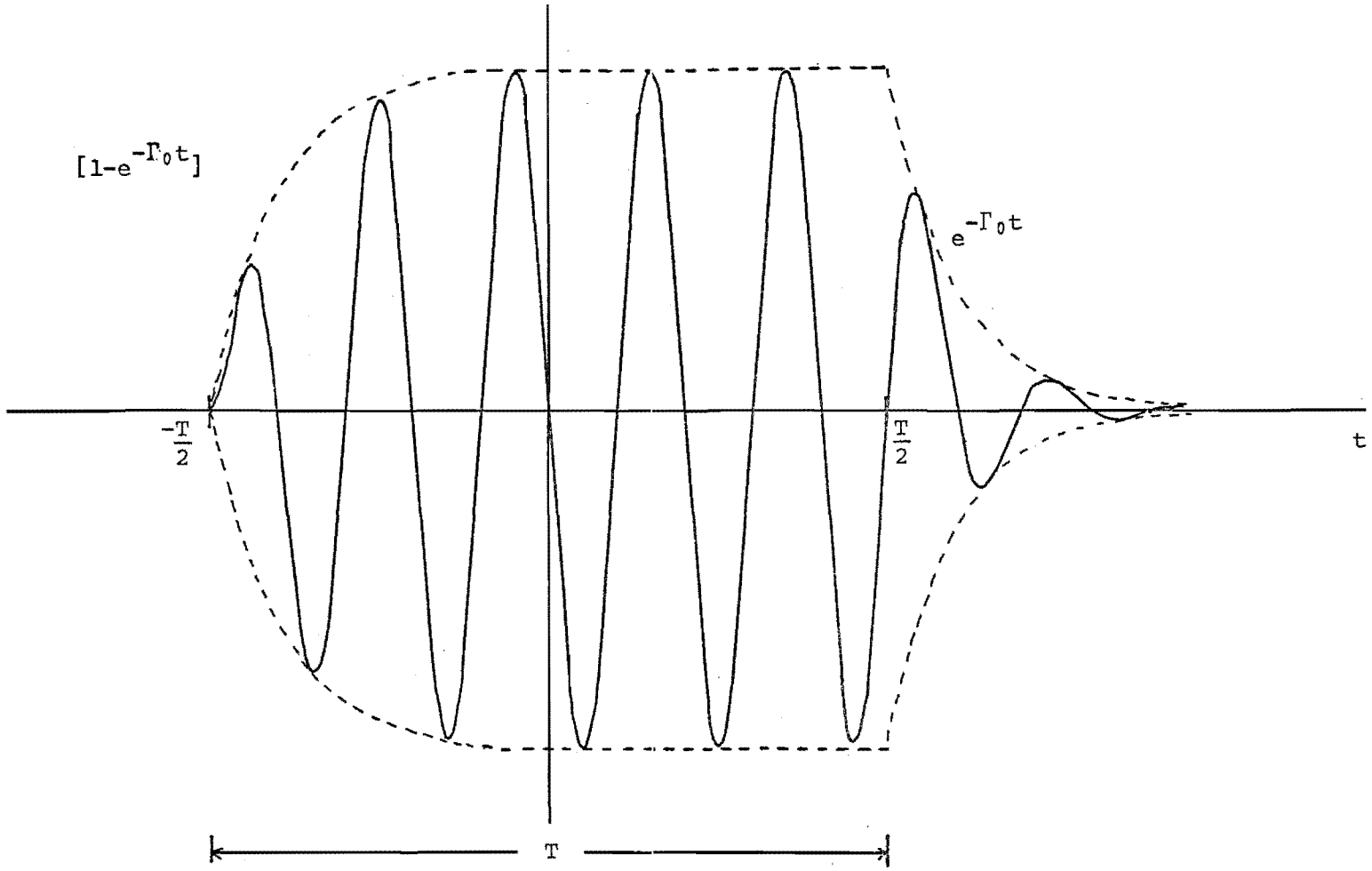

5.3.2 Steady State

Another important form that the function $S(\xi)$ can take is

$$S(\xi) = 2\pi\ \delta(\xi - i\delta) \tag{5.9}$$

which gives from (5.5) the time dependence

$$\underline{J}^{ext}(\underline{r},t) = \underline{J}^{ext}(\underline{r})\ e^{-i\omega_0 t} + c.c \tag{5.10}$$

This corresponds to the steady state case where the incident radiation is originating from a continuous wave (c.w.) laser rather than a pulsed (Q switched) laser.

The generality of the $S(\xi)$ function then allows us to not specify the shape of the laser pulse until we consider a specific situation.

Using (5.1) and (5.5) in (5.4) we obtain the expression

$$\langle \Delta N(\underline{k})\rangle_t = -\int_{-\infty}^{0} dt_1 \int_{-\infty}^{t_1} dt_2 \int_E d\underline{r}_1\, d\underline{r}_2 \int_D d\underline{r}_3\, d\underline{r}_4\, \exp\{i\underline{k}\cdot(\underline{r}_4 - \underline{r}_3)\}$$

$$e_\eta e_\zeta \langle [[A_\eta(\underline{r}_3)A_\zeta(\underline{r}_4),\ A_\alpha(\underline{r}_1, t_1 - t)],\ A_\beta(\underline{r}_2,\ t_2 - t)]\rangle$$

$$\int_{-\infty}^{\infty} \frac{d\xi_1}{2\pi} \int_{-\infty}^{\infty} \frac{d\xi_2}{2\pi}\ S(\xi_1 - \omega_0)S(\xi_2 + \omega_0)\exp\{-it(\xi_1 + \xi_2 + 2i\delta)\}$$

$$[J_\alpha(\underline{r}_1)J^*_\beta(\underline{r}_2)\exp\{-i(\xi_1 + i\delta)t_1 - i(\xi_2 + i\delta)t_2\}$$

$$+ J^*_\alpha(\underline{r}_1)\ J_\beta(\underline{r}_2)\exp\{-i(\xi_1 + i\delta)t_2 - i(\xi_2 + i\delta)t_1\}] \tag{5.11}$$

where we have used property (5.6), swapped ξ_1 and ξ_2 in various terms, made the transformations $t_1 = t_1' - t$ and $t_2 = t_2' - t$ and dropped two terms of order $\exp(\pm 2i\omega_0 t)$.

5.4 Thermal Greens' Function

Let us define a <u>two-time</u> thermal G.F.[1]

[1] This equation corrects a sign error in Kawabata's definition.

$$G^{II}_{\eta\zeta\alpha\beta}(\underline{r}_3,\underline{r}_4;\ \underline{r}_1,\underline{r}_2;\ i\omega_1,i\omega_2) = \int_0^\beta d\tau_1 d\tau_2\ e^{-i\omega_1\tau_1 - i\omega_2\tau_2}$$

$$<T_\tau\{A_\alpha(\chi_1)A_\beta(\chi_2)A_\eta(\underline{r}_3)A_\zeta(\underline{r}_4)\}> \qquad (5.12)$$

where $A(\underline{r},\tau) = e^{\mathcal{H}\tau}\ A(\underline{r})\ e^{-\mathcal{H}\tau}, \chi_i = \underline{r}_i,\tau_i$

and $i\omega_i = 2n_q\pi/\beta, n_q = 0, \pm1, \pm2, \cdots\cdots\ i = 1,2$.

Similarly a <u>three-time</u> thermal G.F. is defined

$$G^{III}_{\eta\zeta\alpha\beta}(\underline{r}_3,\underline{r}_4;\ \underline{r}_1,\underline{r}_2;\ i\omega_1,i\omega_2,i\omega_3) = \int_0^\beta d\tau_1\ d\tau_2\ d\tau_3$$

$$e^{-i\omega_1\tau_1 - i\omega_2\tau_2 + (i\omega_1 - i\omega_3)\tau_3}<T_\tau\{A_\alpha(\chi_1)A_\beta(\chi_2)A_\eta(\chi_3)A_\zeta(\underline{r}_4)\}> \qquad (5.13)$$

with $i\omega_i = 2n_q\pi/\beta \quad n_q = 0, \pm1, \pm2, \cdots\cdots\ i = 1,2,3.$

In appendix 5A it is proved that these two G.F. are related through the simple expression

$$G^{II}_{\eta\zeta\alpha\beta}(\underline{r}_3,\underline{r}_4;\ \underline{r}_1,\underline{r}_2;\ i\omega_1,i\omega_2) = \beta^{-1} \sum_{i\omega_3} G^{III}_{\eta\zeta\alpha\beta}(\underline{r}_3,\underline{r}_4;\ \underline{r}_1,\underline{r}_2;\ i\omega_1,i\omega_2,i\omega_3) \qquad (5.14)$$

and that $<\Delta N(\underline{k})>_t$ can be related to the G.F. G^{II}

$$<\Delta N(\underline{k})>_t = \int_E d\underline{r}_1\ d\underline{r}_2 \int_D d\underline{r}_3\ d\underline{r}_4\ \exp\{i\underline{k}\cdot(\underline{r}_4 - \underline{r}_3)\}\ e_\eta e_\zeta$$

$$\int_{-\infty}^{\infty} \frac{d\xi_1}{2\pi}\ \frac{d\xi_2}{2\pi}\ S(\xi_1 - \omega_0)S(\xi_2 + \omega_0)\ e^{-i(\xi_1+\xi_2+2i\delta)t}$$

$$G^{II}_{\eta\zeta\alpha\beta}(\underline{r}_3,\underline{r}_4;\ \underline{r}_1,\underline{r}_2;\ \xi_1 + i\delta,\ \xi_2 + i\delta)\ J^{ext}_\alpha(\underline{r}_1)\ \left(J^{ext}_\beta(\underline{r}_2)\right)^* \qquad (5.15)$$

where $G^{II}(\xi_1 + i\delta,\ \xi_2 + i\delta)$ [1] is the analytic continuation of $G^{II}(i\omega_1,i\omega_2)$ to the upper-half complex planes $(i\omega_1,i\omega_2 > 0)$.

[1]
Here and at other places where there will be no confusion we may drop the $\eta\zeta\alpha\beta$ and $\underline{r}_i$ labels on G^{II} ang G^{III}.

5.5 Diagram Expansion

The physical quantity $\langle \Delta N(\underline{k}) \rangle_t$ is related to the thermal G.F. G^{II} by expression (5.15). A diagram expansion of this G.F. is possible but such an approach does not explicitly exhibit the role of the exciting photon. If rather we use relationship (5.14) and hence generate a diagram expansion for the G.F. G^{III} we shall find that the role of the photons in any diagram becomes obvious by inspection. Before we proceed to generate this expansion however we are required to specify the Hamiltonian that describes the phonon system, the impurity ions system and their interaction with the external radiation and phonons. The form of this is essentially identical to that used for the absorption problem of Chapter 3 where the isospin mapping was used to describe the impurity ion energy levels. The zero-order isospin and phonon Hamiltonians are given by (3.2) and (3.7) respectively, while the interaction between them by Hamiltonian (3.8). The interaction with the radiation field takes the form

$$\mathcal{H}_{\text{imp-rad}} = \frac{-e}{m} \sum_j \sum_{mn} M^{\alpha}_{mn}(\underline{r}_j) a^{\dagger}_{mj} a_{nj} A_{\alpha}(\underline{r}_j) + \frac{e^2}{2m} \sum_j N(\underline{r}_j) A_{\beta}(\underline{r}_j) A_{\beta}(\underline{r}_j) \qquad (5.17)$$

where the dipole approximation has been used. (Louisell 1973 p270-72).

Using standard techniques we can expand the angular brackets in (5.13) which is represented by figure 5.4 where the solid lines represent the level propagators (2.72) and the dotted propagators photon G.F. defined by

$$E_{\alpha\alpha'}(\chi,\chi') = - \langle T_\tau \{ A_\alpha(\chi) A_{\alpha'}(\chi') \} \rangle \qquad (5.18)$$

and its Fourier component

$$E_{\alpha\alpha'}(\underline{r},\underline{r}', i\omega_n) = \int_0^\beta d\tau \, e^{i\omega_n \tau} E_{\alpha\alpha'}(\chi,\underline{r}') \qquad (5.19)$$

$$i\omega_n = 2\pi n/\beta \quad n=0, \pm 1, \pm 2, \ldots\ldots$$

The crosses in figure 5.4 represent the $N(\underline{r}_j)$ matrix elements of (5.17) while each intersection of two photons and a single level propagator

Figure 5.4

$$G^{III} = \frac{N}{D}$$

$$\chi_1 = \alpha\ \underline{r}_1\ \tau_1$$
$$\chi_2 = \beta\ \underline{r}_2\ \tau_2$$
$$\chi_3 = \eta\ \underline{r}_3\ \tau_3$$
$$\chi_4 = \zeta\ \underline{r}_4\ 0$$

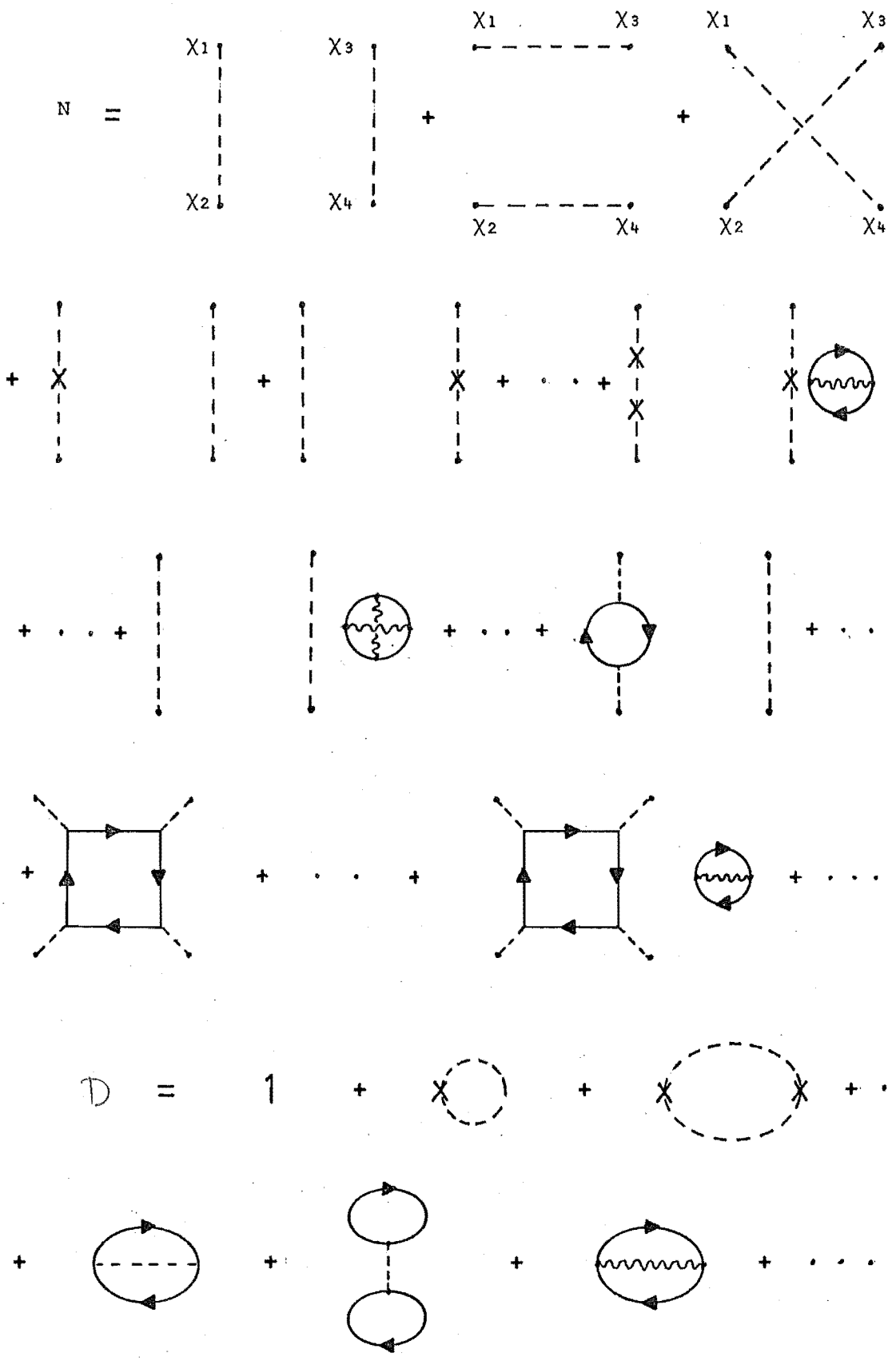

contains an $M^{\alpha}_{mn}(\underline{r}_j)$ matrix element.

The diagram expansion can be reexpressed as in figure 5.5. The form of this figure suggests a cancellation between the D factors on the numerator and denominator - the linked cluster theorem of Chapter 2. However just as for absorption, this property is destroyed by the necessity to apply the projection operation (2.54) to both the numerator and denominator independently. Again the form of the interaction (5.17) is such that closed level propagator loops in these diagrams must each have the same site label, which we use to label the loop, and any diagram that contains two loops with the same site label vanishes under the action (2.54). (e.g. diagrams of figure 5.6 if i=j). We want to investigate the effect of this for a crystal containing many impurity ions.

Figure 5.6

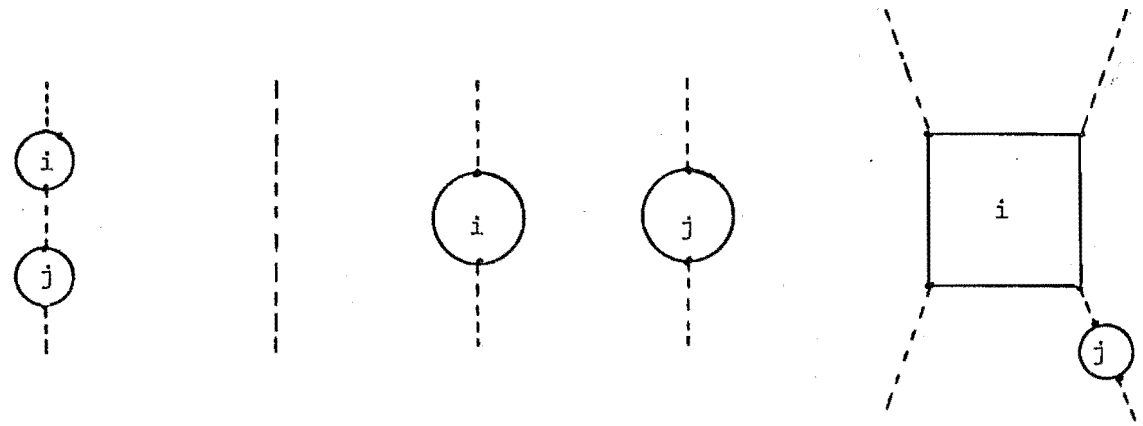

5.6 Single Ion Spectrum

We shall justify in this section the result, shown in §3.4 for the absorption spectrum, that the spectrum from N impurity ions can be approximated, for low concentrations, by N times that from a single ion.

The first step is to realize that only the fourth diagram in the numerator of figure 5.5 can contribute to the Raman spectrum. The other three diagrams correspond to one-photon processes such as absorption and emission.

Figure 5.5

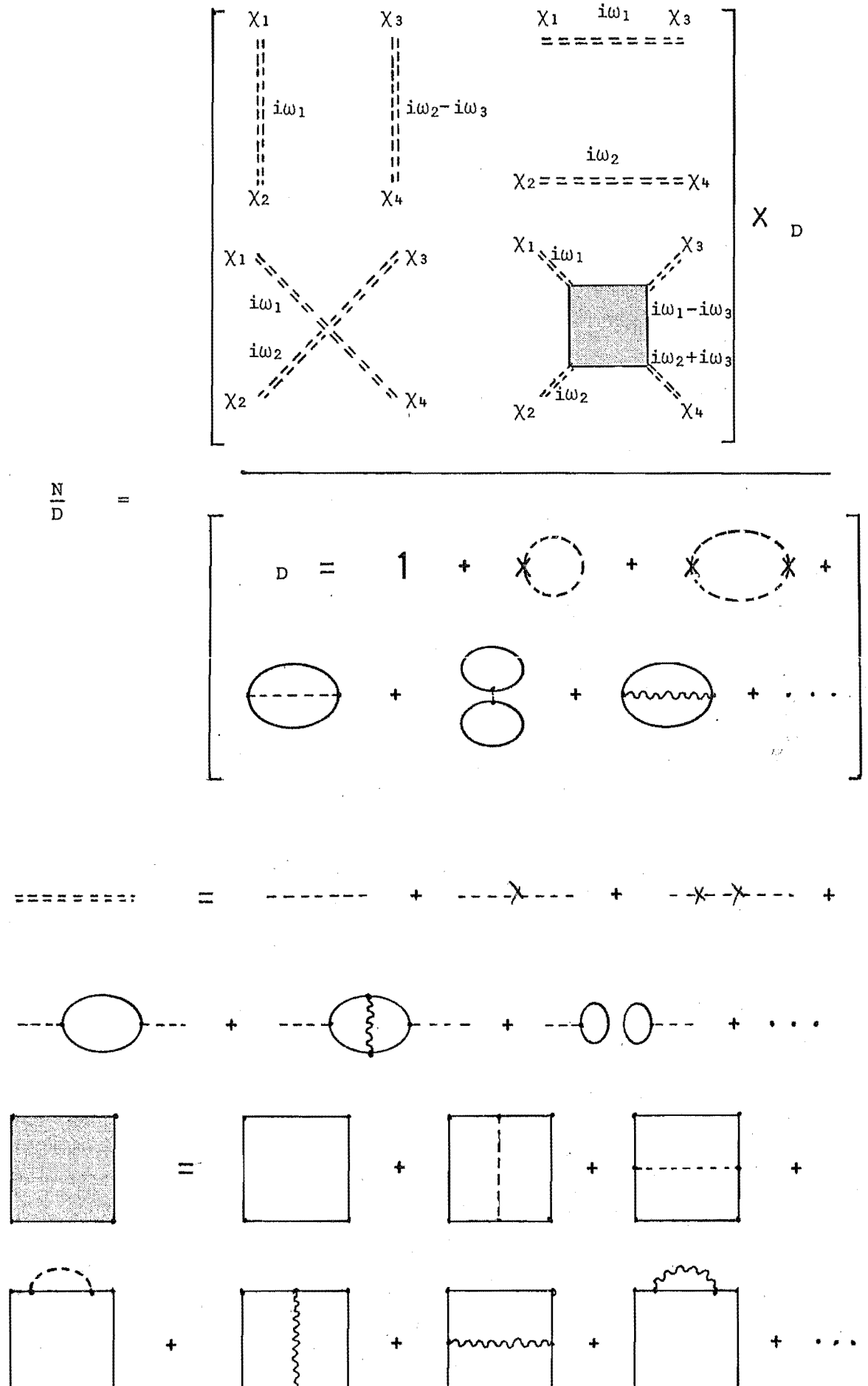

Keeping these diagrams only, and knowing that no two loops can have the same site label, we give in figure 5.7 the relevant diagrams to Raman scattering when the crystal contains one, two or three impurity ions. (The labels inside the squares and circles give the relevant site labels).

Because the factor $\{1 + (0)\}$ contains no level propagator loops it is unaffected by the limiting procedure and cancels from N and D for each case. In a similar manner to the absorption case, the diagrams

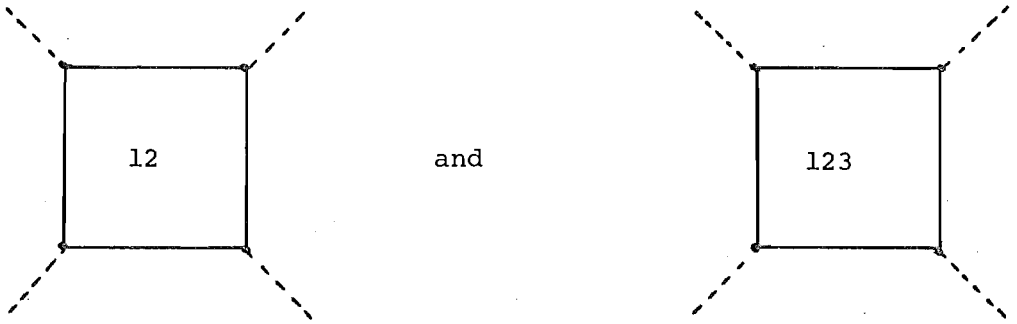

correspond to the Raman spectrum from pairs and triples respectively. Considering the remaining diagrams containing a square with only one label it will be noted that if the factors in the denominators of the forms (12) or (123) are ignored, then the contribution from the two and three ion cases is exactly the same as the sum of two and three single ion contributions respectively. As with the absorption case, this is a very reasonable approximation for samples containing low concentrations of impurity ions. Hence we can conclude that we need consider (a) diagrams containing only one level loop and (b) connected diagrams because the disconnected diagrams in the denominators result in only multiplicative intensity factors.

Within this normalization of the denominator we can express (5.13) for scattering from a single impurity ion at $\underline{r}$ as

$$G^{III}_{\eta\zeta\alpha\beta}(\underline{r}_3,\underline{r}_4;\ r_1,r_2;\ i\omega_1,i\omega_2,i\omega_3) = (e/m)^4 \sum_{\substack{abcd\\efgh}} M^{\alpha'}_{ab}\, M^{\beta'}_{cd}$$

$$M^{\eta'}_{ef}\, M^{\zeta'}_{gh}\ E_{\eta\eta'}(\underline{r}_3,r\ ;\ i\omega_1-i\omega_3)\ E_{\zeta\zeta'}(\underline{r}_4,r\ ;\ i\omega_2+i\omega_3) \qquad (5.20)$$

Figure 5.7

Spectrum (1 site) =

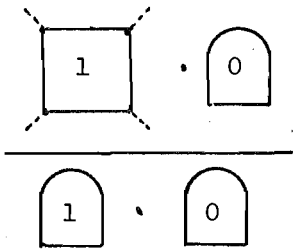

Spectrum (2 sites) =

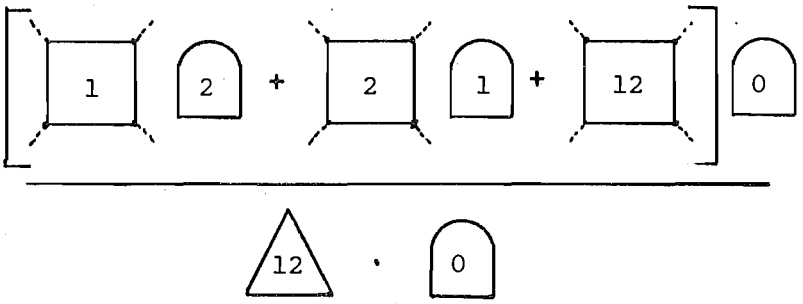

Spectrum (3 sites) =

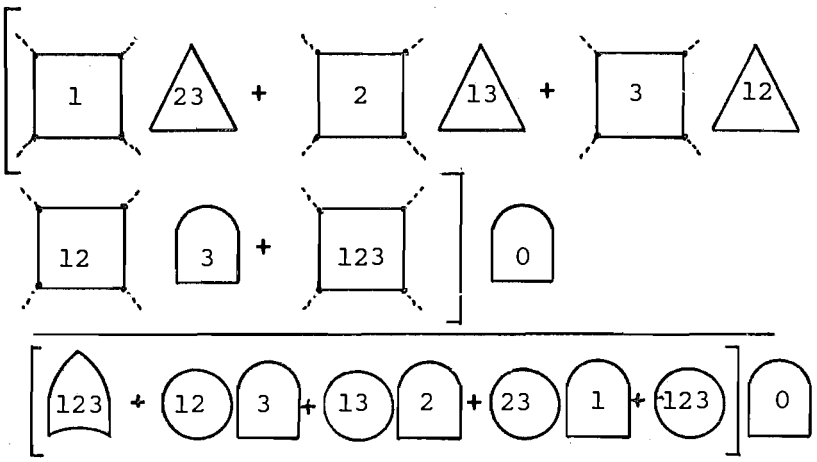

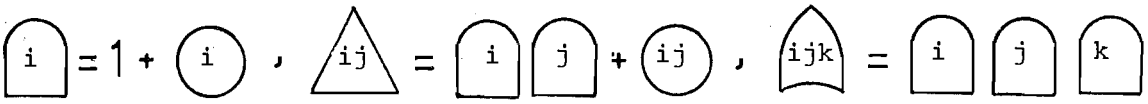

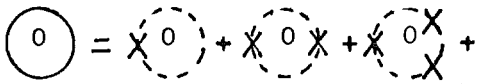

contain no level prop. loops.

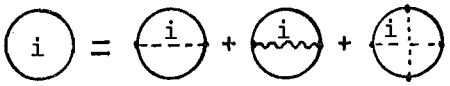

contain one level prop. loop.

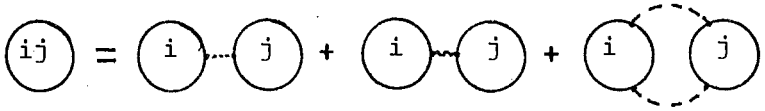

contain two level prop. loops.

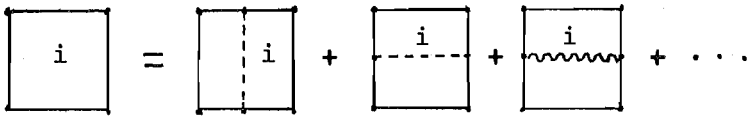

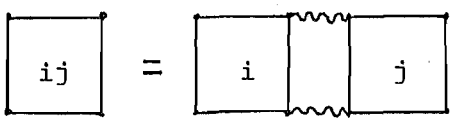

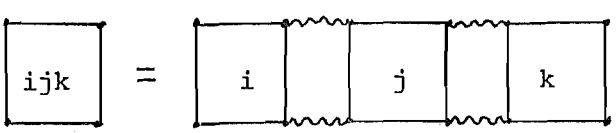

$$F^{III}_{ef,gh;ab,cd}(\underline{r};\, i\omega_1, i\omega_2, i\omega_3) E_{\alpha\alpha'}(\underline{r},\underline{r}_1;\, i\omega_1) E_{\beta\beta'}(\underline{r},\underline{r}_2;\, i\omega_2)$$

where $M^{\alpha'}_{ab} \equiv M^{\alpha'}_{ab}(\underline{r})$ etc., and we define

$$F^{III}_{ef,gh;ab,cd}(\underline{r}, i\omega_1, i\omega_2, i\omega_3) = \int_0^\beta d\tau_1' \, d\tau_2' \, d\tau_3' \, e^{-i\omega_1\tau_1' - i\omega_2\tau_2' + (i\omega_1 - i\omega_3)\tau_3'}$$

$$\langle T_\tau \{ a^\dagger_a \, a_b(\tau_1') \, a^\dagger_c \, a_d(\tau_2') \, a^\dagger_e \, a_f(\tau_3') \, a^\dagger_g \, a_h(0) \} \rangle \qquad (5.21)$$

where $a^\dagger_a \, a_b(\tau_1') \equiv a^\dagger_a(\tau_1') a_b(\tau_1')$, etc., and the diagrams arising in the expansion of (5.21) were restricted to a single loop.

5.7 Photon Propagators

To obtain $\langle \Delta N(\underline{k}) \rangle_t$, expression (5.20) for G^{III} is to be used in the relation (5.14) to obtain G^{II} which in turn is to be used in (5.15). In this section we shall study the sum over $i\omega_3$ involved in relation (5.14).

A study of the Lehmann representation of $G^{III}(i\omega_1, i\omega_2, i\omega_3)$ reveals that if $i\omega_3$ is analytically continued to the complex plane ($i\omega_3 \to \omega'$), then $G^{III}(i\omega_1, i\omega_2, \omega')$ is regular everywhere except on the four cut lines.

$$\mathrm{Im}(\omega') = i\Omega_n \equiv \begin{cases} 0 & n=1 \\ i\omega_1 & n=2 \\ -i\omega_2 & n=3 \\ i\omega_1 - i\omega_2 & n=4 \end{cases} \qquad (5.22)$$

If we evaluate the sum over $i\omega_3$ by converting to a contour integral around the poles of the Bose-Einstein function, then we have the added complication that in four places the poles of $f_B(\omega')$ and $G^{III}(i\omega_1, i\omega_2, \omega')$ coincide. The resolution of this complication is indicated in the work of Eliashberg (1962) on the transport equation for Fermi particles, giving the expression

$$G^{II}(i\omega_1, i\omega_2) = \int_C \frac{d\omega'}{2\pi i} f_B(\omega') \; G^{III}(i\omega_1, i\omega_2, \omega')$$

$$+ G^{III}(i\omega_1, i\omega_2, 0) + G^{III}(i\omega_1, i\omega_2, i\omega_1) + G^{III}(i\omega_1, i\omega_2, -i\omega_2)$$

$$+ G^{III}(i\omega_1, i\omega_2, i\omega_1 - i\omega_2) \qquad (5.23)$$

where the contour C is indicated in figure 5.8

Figure 5.8

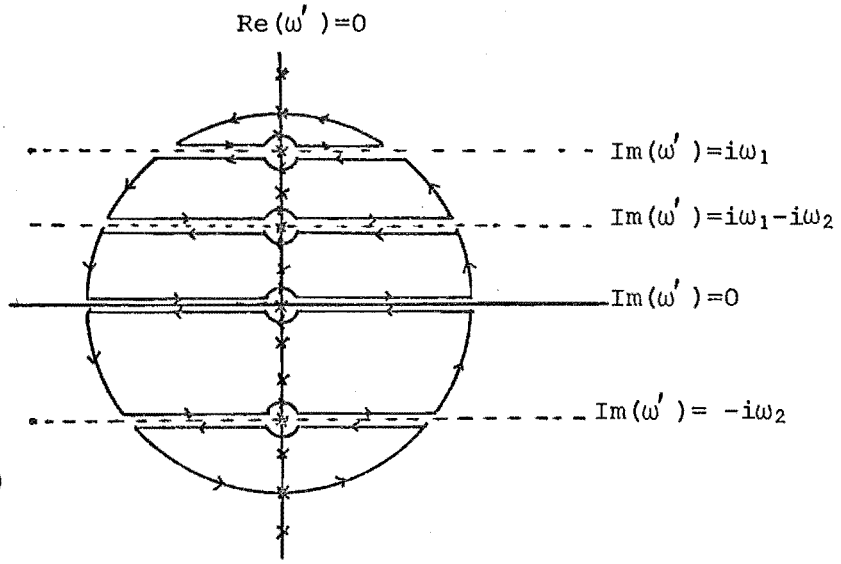

$\times$ = poles of $f_B(\omega')$

---- = cuts of G^{III}

——— = contour C

The contour over the large circle can be shown to vanish as before and the contour integrations about the four small circles exactly cancel the four extra terms in (5.23) leaving principal value integrals just above and below the four cut lines.

$$G^{II}(i\omega_1,i\omega_2) = P\int_{-\infty}^{\infty} d\omega' f_B(-\omega') \sum_{i\Omega_n} \cdot \frac{1}{2\pi i}$$
$$\{G^{III}(i\omega_1,i\omega_2,i\Omega_n + \omega' + i0^+) - G^{III}(i\omega_1,i\omega_2,i\Omega_n + \omega' - i0^+)\} \quad (5.24)$$

where $i\Omega_n$ takes the four values of (5.22).

We simplify these expressions by making the definitions

$$G^{II}_{\eta\zeta\alpha\beta}(\underline{k};\ \underline{r}_1,\underline{r}_2;\ i\omega_1,i\omega_2) = \int_D d\underline{r}_3\ d\underline{r}_4\ \exp\{i\underline{k}\cdot(\underline{r}_4 - \underline{r}_3)\}$$
$$G^{II}_{\eta\zeta\alpha\beta}(\underline{r}_3,\underline{r}_4;\ \underline{r}_1,\underline{r}_2;\ i\omega_1,\ i\omega_2)$$
$$\equiv \sum_{i\Omega_n} G'(i\Omega_n) \ . \quad (5.25)$$

where

$$G'(i\Omega_n) = -P\int_{-\infty}^{\infty} d\omega' f_B(-\omega') \frac{1}{2\pi i}\{G^{III}_{\eta\zeta\alpha\beta}(\underline{k};\underline{r}_1,\underline{r}_2;\ i\omega_1,\ i\omega_2,\ i\Omega_n + \omega' + i0^+)$$
$$- G^{III}_{\eta\zeta\alpha\beta}(\underline{k};\ \underline{r}_1,\underline{r}_2;\ i\omega_1,i\omega_2,i\Omega_n + \omega' - i0^+)\} \quad (5.26)$$

and

$$G^{III}_{\eta\zeta\alpha\beta}(\underline{k};\underline{r}_1,\underline{r}_2;\ i\omega_1,i\omega_2,i\omega_3) = (e/m)^4 \sum_{\substack{abcd\\efgh}} M^{\alpha'}_{ab}\ M^{\beta'}_{cd}\ M^{\eta'}_{ef}\ M^{\zeta'}_{gh}$$

$$E_{\eta\eta'}(\underline{k},\underline{r};\ i\omega_1 - i\omega_3)\ E_{\zeta\zeta'}(-\underline{k},\underline{r};\ i\omega_2+i\omega_3)\ F^{III}_{ef,gh;ab,cd}(\underline{r},i\omega_1,i\omega_2,i\omega_3)$$

$$E_{\alpha'\alpha}(\underline{r},\underline{r}_1;\ i\omega_1)\ E_{\beta'\beta}(\underline{r},\underline{r}_2;\ i\omega_2) \qquad (5.27)$$

where

$$E_{\alpha'\alpha}(\pm\underline{k},\underline{r};i\omega_n) \equiv \int_D d\underline{r}'\ e^{\mp i\underline{k}\cdot\underline{r}'}\ E_{\alpha'\alpha}(\underline{r}',\underline{r},\cdot i\omega_n) \qquad (5.28)$$

Inoue and Moriya (1970) give the solution of (5.28) upon analytic continuation for our scattering geometry and taking into account the dielectric constant of the medium and surface refraction

$$E_{\alpha'\alpha}(\underline{k},\underline{r};\ \xi) = \frac{8\pi k_z}{ck^2}\ \frac{\sin a(\pm\ \xi/c - k)}{(\pm\xi/c - k)}\ e^{iR(\pm\xi/c\ -k)}$$
$$\exp\{-i\underline{k}_{\|}\cdot\underline{r} + \gamma_s(\underline{k})z\}\ E_{\alpha'\alpha}(\underline{k}_{\|},ck)\quad \mathrm{Im}(\xi) \gtrless 0\ . \qquad (5.29)$$

and

$$E_{\alpha'\alpha}(-\underline{k},\underline{r},\xi) = -\frac{8\pi k_z}{ck^2}\ \frac{\sin a(\pm\ \xi/c + k)}{(\pm\xi/c + k)}\ e^{iR(\pm\ \xi/c + k)}$$
$$\exp\{i\underline{k}_{\|}\cdot\underline{r} + \gamma_s(-\underline{k})z\}\ E_{\alpha'\alpha}(-\underline{k}_{\|},\ -ck)\qquad \mathrm{Im}(\xi) \gtrless 0 \qquad (5.30)$$

where $\underline{R}$ is a vector to the centre of V_D (which is approximately parallel to $\underline{k}$) and the detector is taken to be a cube with sides of length 2a oriented with one side parallel to $\underline{k}$. $E_{\alpha'\alpha}(\underline{k}_{\|},\ ck)$ is given in dyadic form

$$E(\underline{q}_{\|},\ cq\ \mathrm{sgn}\ q_z) = q\ \mathrm{sgn}\ q_z[\gamma_s\ q_z(i\gamma_s q^2 - \gamma^2 q_z)^{-1}\underline{u}\,\underline{u}$$
$$+(iq_z-\gamma_s)^{-1}\underline{v}\,\underline{v}\ -iq_{\|}^2\ (i\gamma_s q^2 - \gamma^2 q_z)^{-1}\underline{z}\,\underline{z}\ +\ iq_z q_{\|}\ (i\gamma_s q^2 - \gamma^2 q_z)^{-1}\underline{u}\,\underline{z}$$
$$-\ \gamma_s q_{\|}\ (i\gamma_s\ q^2 - \gamma^2 q_z)^{-1}\underline{z}\,\underline{u}] \qquad (5.31)$$

where

$$q_{\parallel} = (q_x, q_y, 0)$$

$$\gamma_s(\underline{q}) = \{ - \varepsilon(cq \text{ sgn } q_z) q^2 + q^2 \}^{1/2} \quad \text{Re}(\gamma_s) > 0$$

$$\gamma_s = \gamma_s(\underline{q}) ; \; \gamma^2 = - \varepsilon(cq \text{ sgn } q_z) q^2$$

and $\underline{u}$, $\underline{v}$ and $\underline{z}$ are unit vectors in the Cartesian coordinate system in which $\underline{u}$ is taken parallel to $q_{\parallel}$ and $\underline{z}$ to the z axis. As we might expect then the photon G.F. is regular except on the line $\text{Im}(\omega') = 0$.

5.8 Identification of Terms

We will now consider each of the four terms contributing to (5.25) and show that only one of these actually contributes to the Raman spectrum.

5.8.1 Kawabata's Approach

One approach to this is that given by Kawabata (1971). If we expand (5.26) for $i\Omega_n = i\omega_1 (n=2)$ then one obtains

$$G'(i\omega_1) = - P \int_{-\infty}^{\infty} \frac{d\omega'}{2\pi i} f_B(-\omega') (e/m)^4 \sum_{\substack{abcd \\ efgh}} M^{\alpha'}_{ab} M^{\beta'}_{cd} M^{\eta'}_{ef} M^{\zeta'}_{gh}$$

$$E_{\zeta\zeta'}(-\underline{k},\underline{r}; i\omega_1 + i\omega_2 + \omega') \{ E_{\eta\eta'}(\underline{k},\underline{r}; - \omega' - i0^+) F^{III}_{ef,gh;ab,cd}(r, i\omega_1, i\omega_2, i\omega_1 + \omega' + i0^+)$$

$$- E_{\eta\eta'}(\underline{k},\underline{r}; - \omega' + i0^+) F^{III}_{ef,gh;ab,cd}(\underline{r}, i\omega_1, i\omega_2, i\omega_1 + \omega' - i0^+) \}$$

$$E_{\alpha\alpha'}(\underline{r},\underline{r}_1; i\omega_1) E_{\beta'\beta}(\underline{r},\underline{r}_2; i\omega_2) \qquad (5.32)$$

Kawabata then reasoned that when one took the limits $i\omega_i \to \xi_i + i\delta$, $i = 1,2$ (cf (5.15)) then the factor $E_{\zeta\zeta'}(-\underline{k},\underline{r}; i\omega_1 + i\omega_2 + \omega')$ becomes by (5.30) (and using $\xi_1 \simeq -\xi_2 \simeq \omega_0$).

$$E_{\zeta\zeta'}(-\underline{k},\underline{r};\ i\omega_1 + i\omega_2 + \omega') \simeq \frac{\sin a[(\xi_1+\xi_2+\omega')/c + k]}{(\xi_1+\xi_2+\omega')/c + k}$$

$$\simeq \frac{\sin[a(\omega'/c + k)]}{(\omega'/c + k)}$$

which is strongly peaked in the region $\omega' \simeq -ck$ because $a >> k^{-1}$. However in this region the factor $f_B(-\omega')$ becomes approximately $f_B(ck)$ which is extremely small at optical frequencies even at room temperature. Similar analysis for the $G'(i\omega_1)$ and $G'(i\omega_1 - i\omega_2)$ give small factors $f_B(ck)$ and $f_B(\omega_0 + ck)$ also, while for $G'(0)$ a much larger $f_B(ck - \omega_0)$ factor results. Kawabata's conclusion then, was that only the $G'(0)$ term would give a significant contribution to the Raman spectrum.

This approach relies on the assumption of a black-body radiation distribution (since the photon propagators are evaluated using a statistical partition function $e^{-\beta\mathcal{H}}$) and suggests only the contribution from $G'(0)$ is physically observable.

5.8.2 Present approach

This approach does not rely on the form of the Bose-Einstein function, but rather studies the position of the resulting spectral peaks from each contribution. In fact only the $G'(0)$ term is found to result in contributions that allow the standard Raman spectrum interpretation (i.e. $\omega = ck = \omega_0 + E_m - E_n$). The other three terms are found to allow alternative interpretations; the $G'(i\omega_1 - i\omega_2)$ corresponding to a two-photon absorption type process ($\omega + \omega_0 = E_m - E_n$) while both $G'(i\omega_1)$ and $G'(-i\omega_2)$ to a fourth-order absorption or emission process.

These two different approaches both agree however, that only the $G'(0)$ term of (5.25) is important for the Raman spectrum and it has the form

$$G'(0) = (e/m)^4 P\int_{-\infty}^{\infty} d\omega' \left(\frac{8\pi k_z}{k^2}\right)^2 E_{\eta\eta'}(\underline{k}_{\parallel}, ck)\, E_{\zeta\zeta'}(-\underline{k}_{\parallel}, -ck)$$

$$\frac{\sin a[(i\omega_1-\omega')/c - k]}{(i\omega_1-\omega')/c - k} \quad \frac{\sin a[(i\omega_2+\omega')/c + k]}{(i\omega_2+\omega')/c + k} \exp\{iR(i\omega_1+i\omega_2)/c\}$$

$$\sum_{\substack{abcd\\efgh}} M^{\alpha'}_{ab}\, M^{\beta'}_{cd}\, M^{\eta'}_{ef}\, M^{\zeta'}_{gh}\, F^{III}_{ef,gh;ab,cd}(\underline{r}; i\omega_1, i\omega_2, \omega')$$

$$E_{\alpha'\alpha}(\underline{r},\underline{r}_1;\, i\omega_1)\quad E_{\beta'\beta}(\underline{r},\underline{r}_2;\, i\omega_2)\ . \tag{5.33}$$

where we have defined

$$F^{III}_{ef,gh;ab,cd}(\underline{r}; i\omega_1, i\omega_2, \omega') = f_B(-\omega')\exp\{(\gamma_s(k)+\gamma_s^*(k))z\}$$

$$\frac{1}{2\pi i}\Big[F^{III}_{ef,gh;ab,cd}(\underline{r}, i\omega_1, i\omega_2, \omega' + i0^+)$$

$$-F^{III}_{ef,gh;ab,cd}(\underline{r}, i\omega_1, i\omega_2, \omega' - i0^+)\Big] \tag{5.34}$$

Upon carrying out the analytic continuation required in (5.14); $i\omega_1 \to \xi_1 + i\delta$ and $i\omega_2 \to \xi_2 + i\delta$ we obtain

$$G'(0) = (e/m)^4\left(\frac{8\pi k_z}{k^2}\right)^2 E_{\eta\eta'}(\underline{k}_{\parallel}, ck)\, E_{\zeta\zeta'}(-\underline{k}_{\parallel}, -ck)\, e^{i(R/c)(\xi_1+\xi_2)}$$

$$P\int_{-\infty}^{\infty} d\omega' \left(\frac{\pi a}{c}\right) U(\omega'-\omega_t) \sum_{\substack{abcd\\efgh}} M^{\alpha'}_{ab}\, M^{\beta'}_{cd}\, M^{\eta'}_{ef}\, M^{\zeta'}_{gh}$$

$$F^{III}_{ef,gh;ab,cd}(\underline{r}, \xi_1+i\delta,\ \xi_2+i\delta, \omega')\, E^R_{\alpha'\alpha}(\underline{r},\underline{r}_1, \xi_1+i\delta)\, E^R_{\beta'\beta}(\underline{r},\underline{r}_2, \xi_2+i\delta) \tag{5.35}$$

where we have used

$$E_{\alpha\alpha'}(\underline{r},\underline{r}', \xi) = E^R_{\alpha\alpha'}(\underline{r},\underline{r}', \xi) \qquad \mathrm{Im}(\xi) > 0 \tag{5.36}$$

$$= E^A_{\alpha\alpha'}(\underline{r},\underline{r}', \xi) \qquad \mathrm{Im}(\xi) < 0$$

the E^A, E^R being the advanced and retarded photon G.F. and have defined

$$U(\omega' - \omega_t) \equiv \frac{\sin(a/c)(\xi_1 - \omega' - \omega + i\delta)}{(\xi_1 - \omega' - \omega + i\delta)} \quad \frac{\sin(a/c)(\xi_2 + \omega' + \omega + i\delta)}{(\xi_2 + \omega' + \omega + i\delta)} \left(\frac{c}{\pi a}\right) \qquad (5.37)$$

where $\omega_t = \omega_0 - ck \equiv \omega_0 - \omega$.

5.9 Scattering Efficiency

We stated upon its definition that $N(\underline{k})$ was related to the number of photons inside the detector. In this section we make this statement more precise and obtain an expression for the scattering efficiency in terms of $\langle \Delta N(\underline{k}) \rangle_t$.

Using (5.34) in the chain of equations (5.35), (5.25) and (5.15) one obtains a quantity of the form

$$A_{\alpha'}^{inc}(\underline{r}, \xi_1) \equiv - \int_E d\underline{r}_1 E^R_{\alpha\alpha'}(\underline{r}, \underline{r}_1; \xi_1 + i\delta) J_\alpha^{ext}(\underline{r}_1) \qquad (5.38)$$

From Kubo's linear response theory (Kubo 1957) we find that the electromagnetic field generated at $\underline{r}$, t by the external current

$$J^{ext}(\underline{r}', t') = J^{ext}(\underline{r}') \int_{-\infty}^{\infty} \frac{d\xi}{2\pi} S(\xi - \omega_0) e^{-i(\xi + i\delta)t'} \qquad (5.39)$$

interacting via Hamiltonian (5.2) is

$$\langle A_{\alpha'}(\underline{r}, t) \rangle = \frac{i}{c} \int_{-\infty}^{t} dt' \int_E d\underline{r}' \langle [A_{\alpha'}(\underline{r}, t), A_\alpha(\underline{r}', t')] \rangle J_\alpha^{ext}(\underline{r}', t')$$

$$= - \int_{-\infty}^{\infty} \frac{d\xi}{2\pi} S(\xi - \omega_0) e^{-i(\xi + i\delta)t} \int_E d\underline{r}' E^R_{\alpha'\alpha}(\underline{r}, \underline{r}'; \xi_1 + i\delta) J_\alpha^{ext}(\underline{r}') \qquad (5.40)$$

Writing the incident radiation outside the sample as

$$\underline{A}^{inc}(\underline{r}, t) = \underline{e}_0 A_0 \int_{-\infty}^{\infty} \frac{d\xi}{2\pi} S(\xi - \omega_0) e^{i[\underline{k}_0 \cdot r - (\xi + i\delta)t]} \qquad (5.41)$$

where $\omega_0 = ck_0$ and $\underline{e}_0$ is a unit vector, then the vector potential at the ion position $\underline{r}$ is given by

$$A_{\alpha'}^{inc}(\underline{r},t) = \int_{-\infty}^{\infty} \frac{d\xi}{2\pi}\ S(\xi-\omega_0)e^{-i(\xi+i\delta)t}\ A_{\alpha'}^{inc}(\underline{r},\xi)$$

$$=A_0 \int_{-\infty}^{\infty} \frac{d\xi}{2\pi}\ S(\xi-\omega_0)(\underline{\underline{\Gamma}}(\xi+i\delta)\underline{e}_0)e^{i\underline{k}_{0\|}\cdot\underline{r}+\gamma_0 t}\ e^{-i(\xi+i\delta)(t-\frac{R_0}{c})} \tag{5.42}$$

where $\underline{\underline{\Gamma}}(\xi)$ is a tensor determined by the boundary conditions (i.e. the scattering geometry) tabulated by Kawabata (1971), R_0 is the distance from the ion to the centre of V_E, and

$$\gamma_0 = [-\varepsilon(\xi+i\delta)k_0^2 + k_{0\|}^2]^{1/2} \quad . \tag{5.43}$$

This gives us the relationship

$$\langle \dot{\Delta}N(\underline{k})\rangle_t = (e/m)^2 \left(\frac{8\pi k_z}{k^2}\right)^2 e_\eta\ E_{\eta\eta'}(\underline{k}_\|, ck)\ e_\zeta\ E_{\zeta\zeta'}(-\underline{k}_\|, -ck)$$

$$\int_{-\infty}^{\infty} \frac{d\xi_1}{2\pi}\ \frac{d\xi_2}{2\pi}\ S(\xi_1-\omega_0)S(\xi_2+\omega_0)e^{-i(\xi_1+\xi_2+2i\delta)[t-(R_0+R)/c]}\ \frac{\pi a}{c}$$

$$\int_{-\infty}^{\infty} d\omega'\ f_B(-\omega')\ U(\omega'-\omega_t)(\underline{\underline{\Gamma}}\cdot\underline{e}_0)_{\alpha'}\ (\underline{\Gamma}\cdot\underline{e}_0)^*_{\beta'}\ |A_0|^2$$

$$\sum_{\substack{abcd\\efgh}} M_{ab}^{\alpha'} M_{cd}^{\beta'} M_{ef}^{\eta'} M_{gh}^{\zeta'} \exp\{(\gamma_0+\gamma_0^*+\gamma_s(k)+\gamma_s^*(k))z\}$$

$$[F^{III}_{ef,gh;ab,cd}(\underline{r},\xi_1+i\delta,\xi_2+i\delta,\omega'+i0^+) - F^{III}_{ef,gh;ab,cd}(\underline{r},\xi_1+i\delta,\xi_2+i\delta,\omega'-i0^+)] \tag{5.44}$$

5.10 Scattering Cross Section

The number of incident photons per unit time interval is

$$\phi_0 = S\ \omega_0\ \cos\theta_0\ |A_0|^2\ /2\pi c \tag{5.45}$$

where $\cos\theta_0 = -(k_0)_z/k_0$ and S is the crystal surface area. The number of scattered photons belonging to a small region $d\underline{k}$ in $\underline{k}$ space which enter the volume V_D per unit time interval at time t is

$$\phi = k\langle \Delta N(\underline{k}) \rangle_t \, d\underline{k} \,/\, 2a(2\pi)^4 \tag{5.46}$$

Hence the scattering efficiency per unit frequency interval per unit solid angle is (using $d\underline{k} = (k^2/c)\, d\omega d\Omega$)

$$\frac{1}{\phi_0} \frac{\partial^2 \phi}{\partial \omega \partial \Omega} = \frac{2\pi c}{S\omega_0 \cos\theta_0 |A_0|^2} \cdot k^3 \frac{\langle \Delta N(\underline{k}) \rangle_t}{c2a(2\pi)^4} \tag{5.47}$$

which gives upon using (5.44)

$$\frac{1}{\phi_0} \frac{\partial^2 \phi}{\partial \omega \partial \Omega} = \frac{-4\omega \cos^2 \theta_s}{c^4 \omega_0 \cos\theta_0} (e/m)^4 \, e_\eta \, E_{\eta\eta'}(\underline{k}_{\parallel}, \omega)$$

$$e_\zeta E^*_{\zeta\zeta'}(-\underline{k}_{\parallel}, \omega) \exp\{(\gamma_0 + \gamma_0^* + \gamma_s + \gamma_s^*) z\} (\underline{\underline{\Gamma}} \cdot \underline{e}_0)_{\alpha'} (\underline{\underline{\Gamma}} \cdot \underline{e}_0)^*_{\beta'} T_{\alpha'\beta'\eta'\zeta'}(t) \tag{5.48}$$

where

$$\alpha'\beta'\eta'\zeta'(t) = \int_{-\infty}^{\infty} d\omega' \; U(\omega' - \omega_t) \; T_{\alpha'\beta'\eta'\zeta'}(t, \omega') \tag{5.49}$$

with

$$T_{\alpha'\beta'\eta'\zeta'}(t,\omega) = f_B(-\omega') \int_{-\infty}^{\infty} \frac{d\xi_1}{2\pi} \frac{d\xi_2}{2\pi} \; S(\xi_1 - \omega_0) S(\xi_2 + \omega_0)$$

$$e^{-i(\xi_1+\xi_2+2i\delta)[t - (R+R_0)/c]} \sum_{\substack{abcd \\ efgh}} M^{\alpha'}_{ab} M^{\beta'}_{cd} M^{\eta'}_{ef} M^{\zeta'}_{gh} \cdot \frac{1}{2\pi i}$$

$$[F^{III}_{ef,gh;ab,cd}(r, \xi_1 + i\delta, \xi_2 + i\delta, \omega' + i0^+) \tag{5.50}$$

$$- F^{III}_{ef,gh;ab,cd}(r, \xi_1 + i\delta, \xi_2 + i\delta, \omega' - i0^+)]$$

After having derived this expression for the scattering cross-section we shall concentrate our attention on obtaining the dependence of the function $T(t)$ for time dependent and steady state scattering (time-independent).

CHAPTER 6 : RAMAN SPECTRUM : STEADY STATE SCATTERING

In (5.9) we gave the form of $S(\xi)$ for the special case of a steady state source. Using this and the appropriate approximation

$$U(\omega' - \omega_t) \simeq \delta(\omega' - \omega_t) \tag{6.1}$$

which shall be justified in the next chapter, then we obtain the special case

$$T^{S.S.}_{\alpha\beta\eta\zeta}(0) = f_B(-\omega_t) \sum_{\substack{abcd \\ efgh}} M^{\alpha}_{ab} M^{\beta}_{cd} M^{\eta}_{ef} M^{\zeta}_{gh} \frac{1}{2\pi i}$$

$$\{F^{III}_{ef,gh;ab,cd}(\underline{r},\omega_0,-\omega_0,\omega_t+i0^+) - F^{III}_{ef,gh;ab,cd}(\underline{r},\omega_0,-\omega_0,\omega_t-i0^+)\} \tag{6.2}$$

In this chapter we shall expand F^{III} in terms of a diagram expansion and evaluate these and the corresponding spectrum using various approximation schemes.

6.1 Kramers - Heisenberg Formula

In this section we shall evaluate the lowest-order contribution to the steady state scattering and show that they give the well known Kramers-Heisenberg formula for the scattering cross-section. The lowest order diagram (those involving no phonon propagators) in the expansion of $F^{III}(i\omega_1,i\omega_2,i\omega_3)$ are given in figure 6.1. Upon evaluating the contribution of diagram 6.1a (see figure 6.2) we obtain a contribution

Figure 6.1

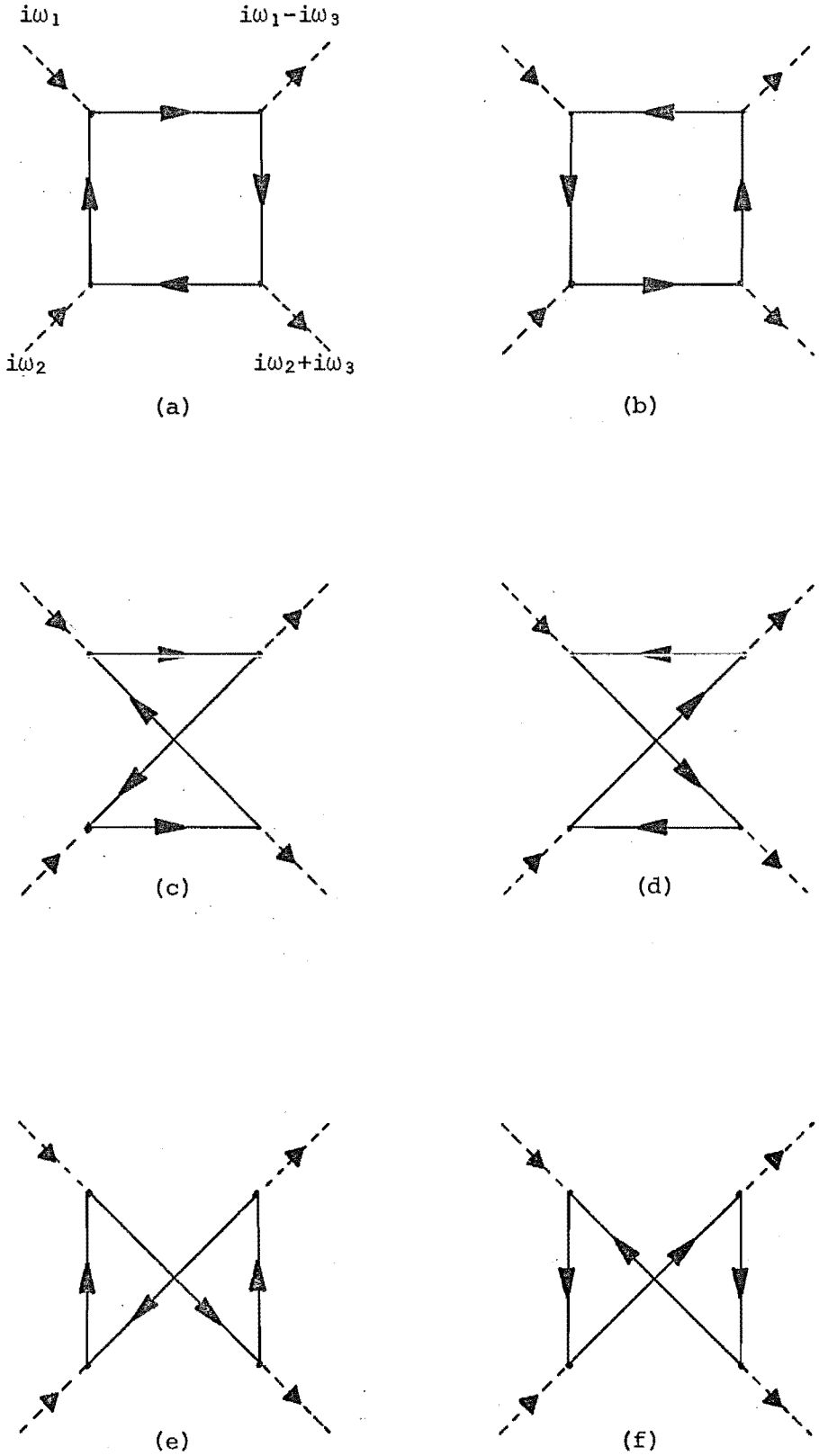

Figure 6.2

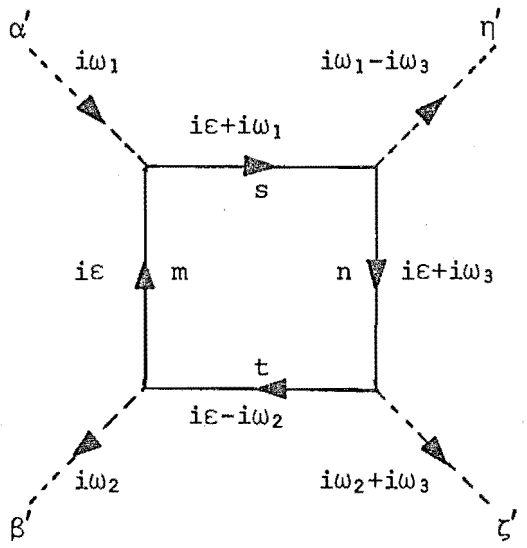

$$F^{III}(i\omega_1, i\omega_2, i\omega_3) = \sum_{mnab} M^{\alpha}_{ms} M^{\eta}_{sn} M^{\zeta}_{nt} M^{\beta}_{tm} \tag{6.3}$$

$$\beta^{-1} \sum_{i\varepsilon} F^0_m(i\varepsilon) \quad F^0_s(i\varepsilon + i\omega_1) \; F^0_n(i\varepsilon+i\omega_3) \; F^0_t(i\varepsilon+i\omega_2)$$

which can be evaluated by transforming the sum over $i\omega_3$ to a contour integral about the poles of the Fermi-Dirac function (see §3.3 for similar analysis for absorption diagram) to give

$$F^{III}(i\omega_1, i\omega_2, i\omega_3) = \sum_{mnst} M^{\alpha}_{ms} M^{\eta}_{sn} M^{\zeta}_{nt} M^{\beta}_{tm}$$

$$\left[\frac{1}{\omega_{mn} + i\omega_3}\left\{\frac{f_D(\lambda_m)}{\omega_{ms}+i\omega_1} \quad \frac{1}{\omega_{mt} - i\omega_2} - \frac{f_D(\lambda_n)}{\omega_{ns} + i\omega_1 - i\omega_3} \quad \frac{1}{\omega_{nt} - i\omega_2 - i\omega_3}\right\}\right.$$

$$\left. + \frac{1}{\omega_{st}-i\omega_1-i\omega_2}\left\{\frac{f_D(\lambda_s)}{\omega_{sm}-i\omega_1} \quad \frac{1}{\omega_{sn}-i\omega_1+i\omega_3} - \frac{f_D(\lambda_t)}{\omega_{tm}+i\omega_2} \quad \frac{1}{\omega_{tn}+i\omega_2+i\omega_3}\right\}\right] \tag{6.4}$$

Upon taking the discontinuity across the real axis $i\omega_3 \to \omega_t \pm i0^+$ and taking the limits $i\omega_1 \to \omega_0 + i\delta$, $i\omega_2 \to -\omega_0 + i\delta$ required in (6.2) we obtain a steady state contribution

$$T^{S.S.}_{\alpha\beta\eta\zeta}(0) = f_B(-\omega_0+\omega) \sum_{mn} (\rho_m - \rho_n)\,\delta(\omega_0-\omega+\omega_{mn}) \sum_s \frac{M^{\alpha}_{ms} M^{\eta}_{sn}}{\omega_{ms} + \omega_0} \sum_t \frac{M^{\zeta}_{nt} M^{\beta}_{tm}}{\omega_{mt} + \omega_0} \qquad (6.5)$$

where the limiting procedure (2.54) has been performed and we have used relation (3.15).

Diagram 6.2 gives a delta function contribution to the spectrum at $\omega = \omega_0 + \omega_{mn}$. Again, like the zero-order contribution to the absorption spectrum, it consists of the difference of two contributions. From the form of the delta function which gives the conservation of energy for the process it is clear that the initial and final states for these two different contributions are those represented schematically by figure 6.3

Figure 6.3

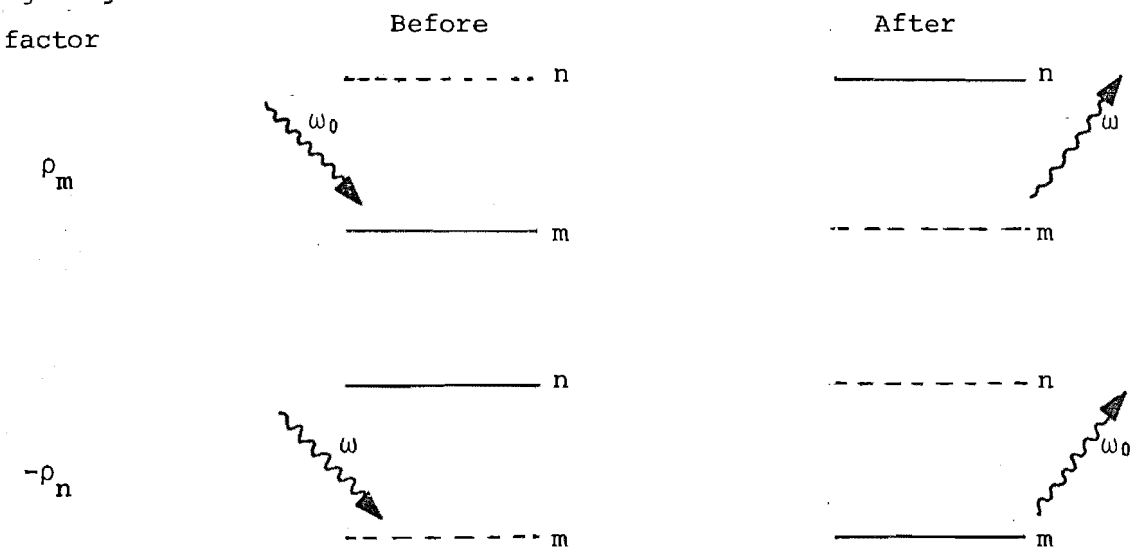

A similar calculation for the other five diagrams of figure 6.1 reveals that one obtains contributions from diagrams 6.1a - d but that diagram 6.1e and 6.1f give no contribution. It is possible to combine the contributions from 6.1a - d to give the relation

$$T^{S.S.}_{\alpha\beta\eta\zeta}(0) = f_B(-\omega_0+\omega) \sum_{mn} (\rho_m-\rho_n)\,\delta(\omega_0-\omega+\omega_{mn}) \qquad (6.6)$$

$$ {}^0P^{\alpha\eta}_{mn}(\omega_0+i\delta) \left[{}^0P^{\beta\zeta}_{mn}(\omega_0+i\delta) \right]^* $$

where

$$ {}^0P^{\alpha\eta}_{mn}(i\omega_1) = \sum_s \left[\frac{M^\alpha_{ms} M^\eta_{sn}}{\omega_{ms}+i\omega_1} + \frac{M^\eta_{ms} M^\alpha_{sn}}{\omega_{ms}-i\omega_1+\omega_t} \right] . \qquad (6.7)$$

This expression is identical to the well known Kramers-Heisenberg formula first obtained by Kramers and Heisenberg (1925) by an application of the correspondence principle to a classical formula. Since then it has been rederived by other methods (Born and Huang (1954), Kondilenko *et.al.* (1960), Low (1952), Gontier and Trahin (1971)) and has been used in various forms by many authors (Loudon (1964), Woodward (1967), Maradudin (1966), Trifonov and Poiker (1966)). The difficulty with this result is two-fold. Firstly it gives a lineshape with zero linewidth (delta function spike) and hence gives none of the expected lineshapes, and secondly it predicts an infinite scattering intensity when the incident frequency ω_0 matches an ion transition frequency ω_{sm} ((6.6) - (6.7)). Since the work of Weisskopf and Wigner (1930 a,b) the former of these has usually been approached by assigning an intrinsic width to each energy level and regarding the lineshape corresponding to a transition from one level to another as being a lorentzian whose width is the sum of the widths of the two levels involved. Attempts to remove the second singularity have been made by adding a finite imaginary part to the denominators of (6.7) corresponding to the width of the intermediate state. (Shorygin (1973), Krushinskii and Shorygin (1961), Morozov and Shorygin (1966)). The approach presented in this thesis deals with these questions quite naturally, resulting in finite linewidths (and approximately lorentzian lineshapes) and giving finite intensities on resonance.

6.2 Generalization of Kramers-Heisenberg Formula.

We now wish to study the generalization of the steady state spectrum

where we include the contribution of higher-order diagrams to the expansion of $F^{III}(i\omega_1, i\omega_2, i\omega_3)$. In figure 6.4 we give the diagram expansion of $F^{III}(i\omega_1, i\omega_2, i\omega_3)$ corresponding to figure 6.2, there being similar diagrams corresponding to figure 6.1b - d also. Upon evaluating diagram 6.4a we obtain a steady state contribution to the scattering cross-section,

$$T^{S.S.}_{\alpha\beta\eta\zeta}(0) = f_B(-\omega_0+\omega)\Big\{\sum_{m_1n_1}(\rho_{m_1}-\rho_{n_1})\,\delta(\omega_{m_1n_1}+\omega_0-\omega)$$
$$\sum_{m_2sn_2}\sum_{k}\frac{V^k_{m_1m_2}\,M^{\alpha}_{m_2s}\,M^{\eta}_{sn_2}\,V^k_{n_2n_1}\binom{n_k}{n_{k+1}}}{(\omega_{m_1m_2}\pm\omega_k)(\omega_{m_1s}+\omega_0\pm\omega_k)(\omega_{m_1n_2}+\omega_t\pm\omega_k)}\sum_{t}\frac{M^{\zeta}_{n_1t}\,M^{\beta}_{tm_1}}{(\omega_{m_1t}-i\omega_2)}$$
$$+\sum_{m_2n_2}(\rho_{m_2}-\rho_{n_2})\,\delta(\omega_{m_2n_2}+\omega_0-\omega)\sum_{s}\frac{M^{\alpha}_{m_2s}\,M^{\eta}_{sn_2}}{(\omega_{m_2s}+\omega_0)}$$
$$\sum_{n_1tm_1}\sum_{k}\frac{V^k_{n_2n_1}\,M^{\zeta}_{n_1t}\,M^{\beta}_{tm_1}\,V^k_{m_1m_2}\binom{n_{k+1}}{n_k}}{(\omega_{m_2m_1}+\omega_t\mp\omega_k)(\omega_{m_2t}+\omega_0\mp\omega_k)(\omega_{m_2m_1}\mp\omega_k)} \qquad (6.8)$$

By considering the energy flows on the photon propagators (cf figure 6.2) and the limiting values $i\omega_1 \to \omega_0 + i\delta$, $i\omega_2 \to -\omega_0 + i\delta$ and $i\omega_3 \to \omega_t \pm i0^+$ it is instructive, although it has neither physical or mathematical meaning or significance, to join and label the photon propagators as indicated in figure 6.5

Figure 6.5

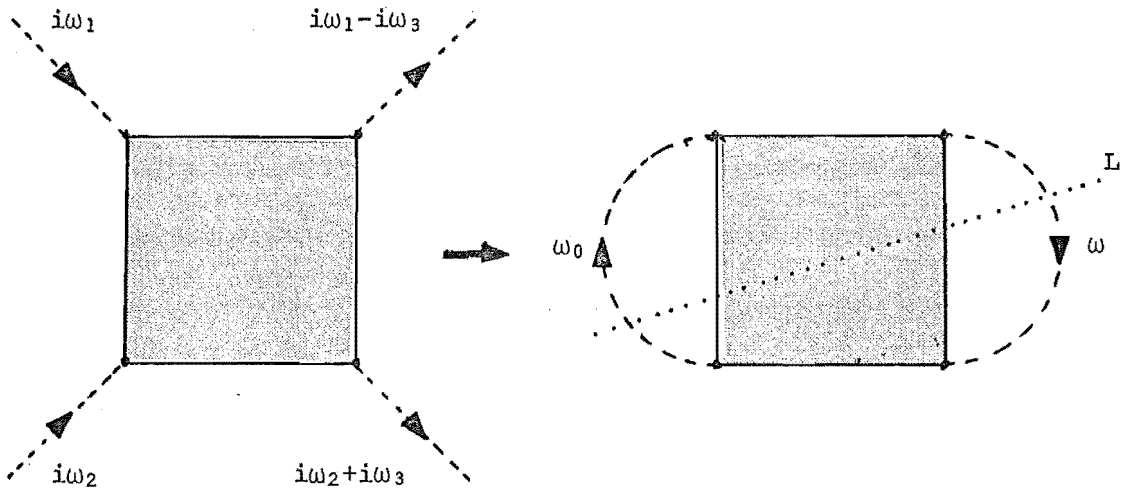

Then if any line is drawn from left to right across the resulting diagram (e.g. L), it results in a delta function containing the algebraic sum of all propagators that it crosses (only once) with signs taken positive or negative if the arrow on the propagator is moving up or down respectively

Figure 6.4

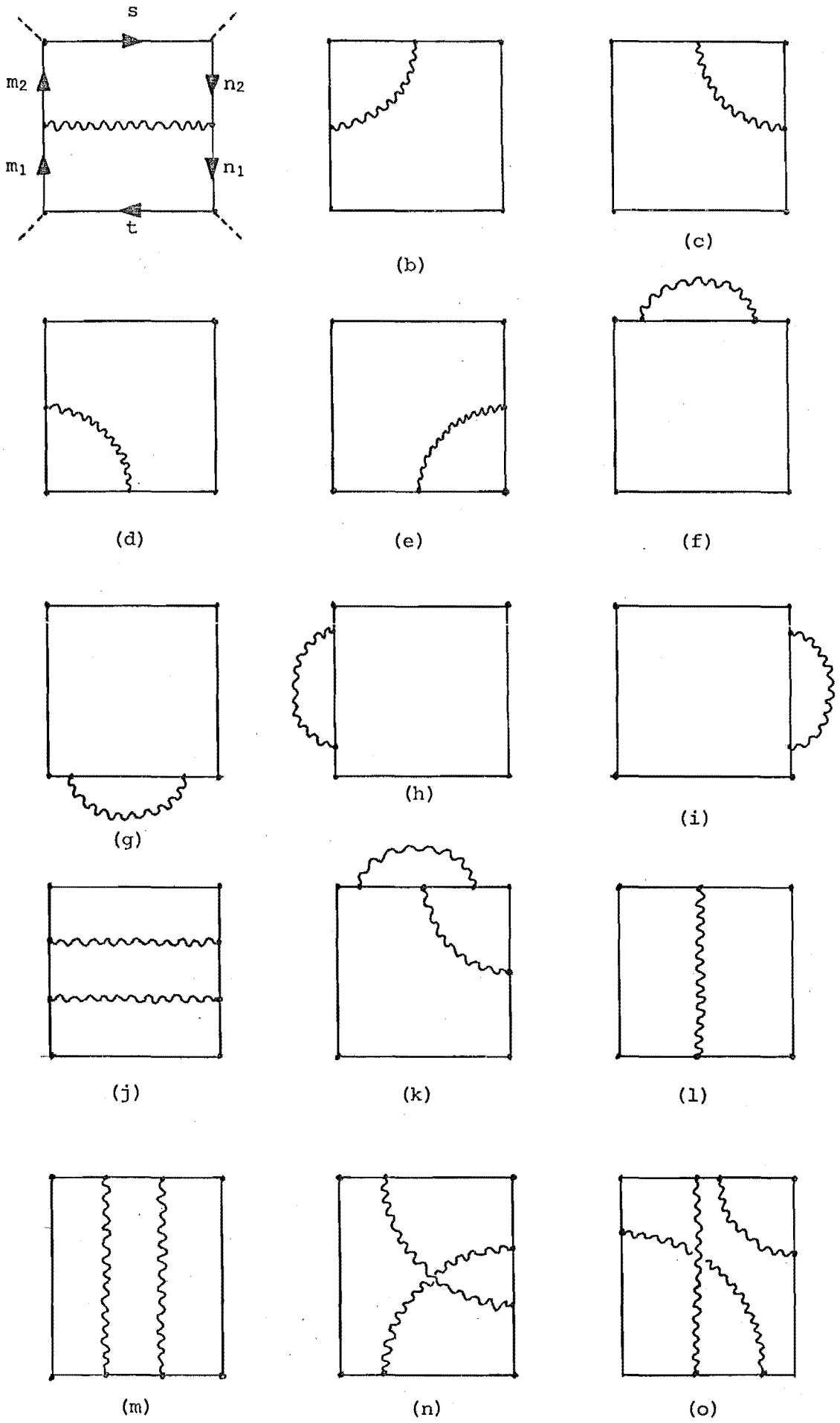

relative to the line. For example, redrawing figure 6.4a as in figure 6.6, we see that there are two possible lines that cut in this manner, L_1 and L_2, that contribute Raman-type delta functions, $\delta(\omega_{m_1 n_1}+\omega_0-\omega)$, $\delta(\omega_{m_2 n_2}+\omega_0-\omega)$ respectively. These correspond to the first and second terms of (6.8) respectively.

Figure 6.6

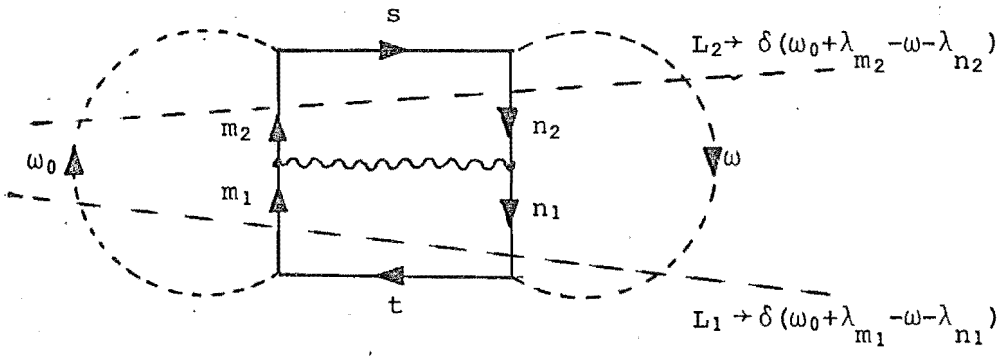

There are two other possible ways of cutting the diagram, each of which will cut the phonon propagator. As such, the resulting delta function will contain a phonon energy and as we will show later, these correspond to phonon Raman processes.

Closer study of the first term of (6.8) shows that it is very similar to expression (6.5) with the exception that the sum over s in (6.5) has become a more complex sum over s, n_2, m_2 and k in (6.8). The observation suggests that this contribution would arise if an extra term was included in (6.7) and it was then used in (6.6). Following this lead we evaluate each diagram of figure 6.4 and pick out those contributions that have Raman-type delta functions (i.e. those corresponding to cut lines across diagrams of the forms L_1 and L_2 of figure 6.6 that cut no phonon lines), then we find we can write these in the form of (6.6) except that we replace ${}^{0}P^{\alpha\eta}_{mn}(i\omega_1)$ of (6.7) by a more general ${}^{b}P^{\alpha\eta}_{mn}(i\omega_1)$ where

Figure 6.7

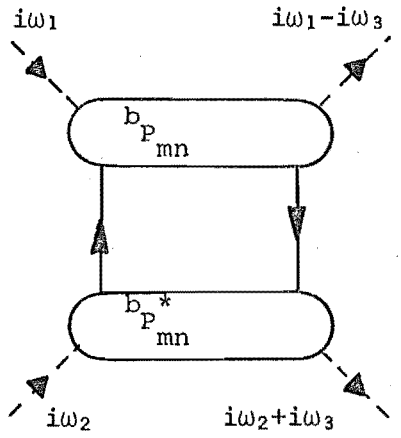

Raman spectrum α

where

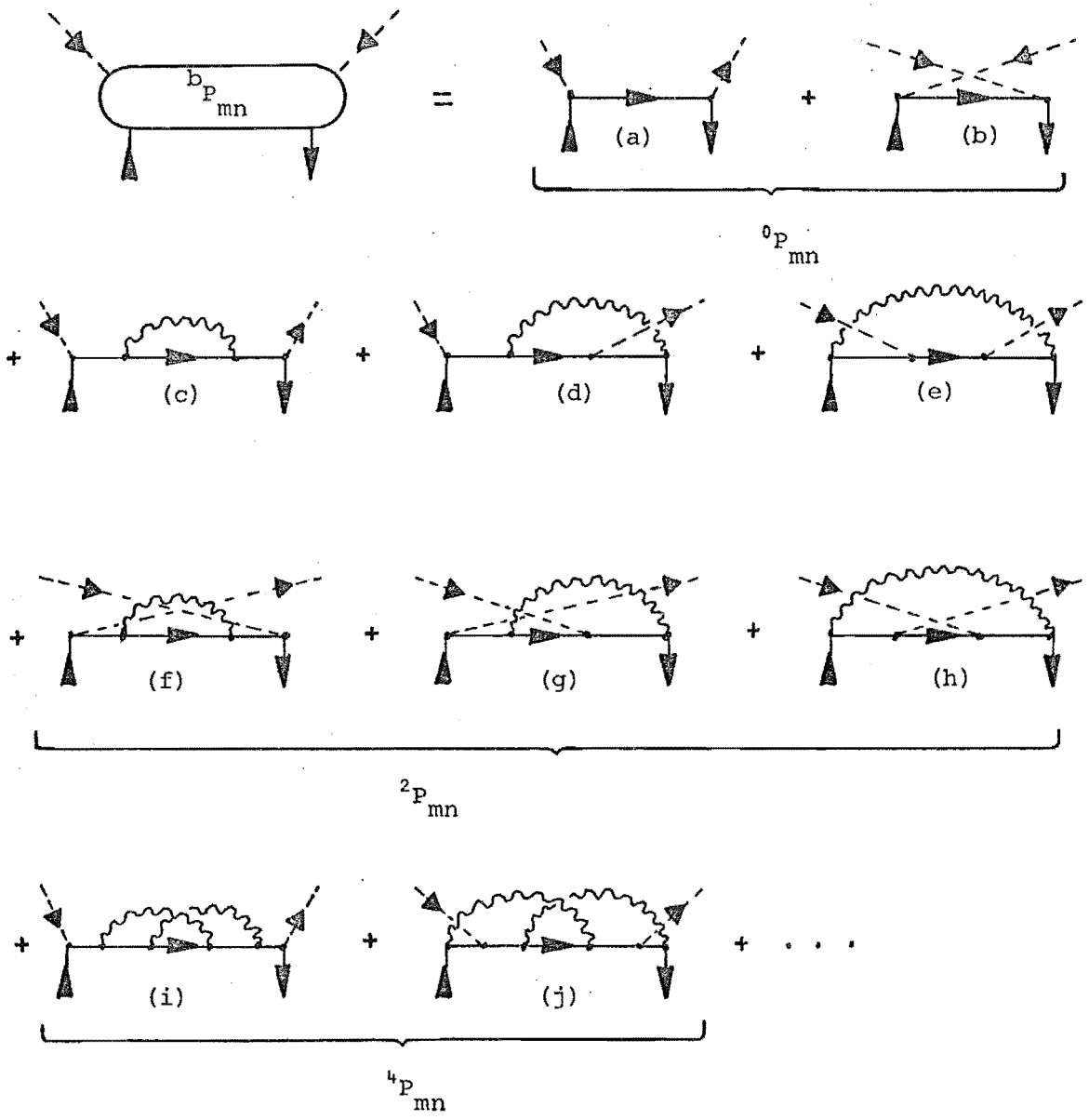

$$b_{P_{mn}}^{\alpha\eta}(i\omega_1) = {}^{0}P_{mn}^{\alpha\eta}(i\omega_1) + {}^{2}P_{mn}^{\alpha\eta}(i\omega_1) + {}^{4}P_{mn}^{\alpha\eta}(i\omega_1) + \cdots \qquad (6.9)$$

where for example

$$\begin{aligned} {}^{2}P_{mn}^{\alpha\eta}(i\omega_1) = \sum_{abc} \sum_{k} \binom{n_k}{n_{k+1}} \Bigg[& \frac{V_{ma}^{k} M_{ab}^{\alpha} M_{bc}^{\eta} V_{cn}^{k}}{(\omega_{ma} \pm \omega_k)(\omega_{mb} + i\omega_1 \pm \omega_k)(\omega_{mc} \pm \omega_k + \omega_t)} \\ & + \frac{V_{ma}^{k} M_{ab}^{\eta} M_{bc}^{\alpha} V_{cn}^{k}}{(\omega_{ma} \pm \omega_k)(\omega_{mb} - i\omega_1 + \omega_t \pm \omega_k)(\omega_{mc} + \omega_t \pm \omega_k)} \\ & + \frac{V_{ma}^{k} M_{ab}^{\alpha} V_{bc}^{k} M_{cn}^{\eta}}{(\omega_{ma} \pm \omega_k)(\omega_{mb} + i\omega_1 \pm \omega_k)(\omega_{mc} + i\omega_1)} + \cdots \Bigg] \end{aligned} \qquad (6.10)$$

In view of the form of this expression it is clear that the form of diagrams that contribute to the Raman spectrum are as indicated in figure 6.7. There is a unique correspondence to each diagram of ${}^{0}P_{mn}$, ${}^{2}P_{mn}$ and each term contributing to (6.7) and (6.10) respectively. Diagrams 6.7a - b (corresponding to ${}^{0}P_{mn}$) are often given for the Raman scattering process. By considering their corresponding terms (e.g. (6.7)) and using the result from perturbation theory that the denominators of (6.7) take the form of the difference of the energy of the intermediate and the initial state, one obtains the two processes indicated in figure 6.8 (cf figure 6.3).

Figure 6.8

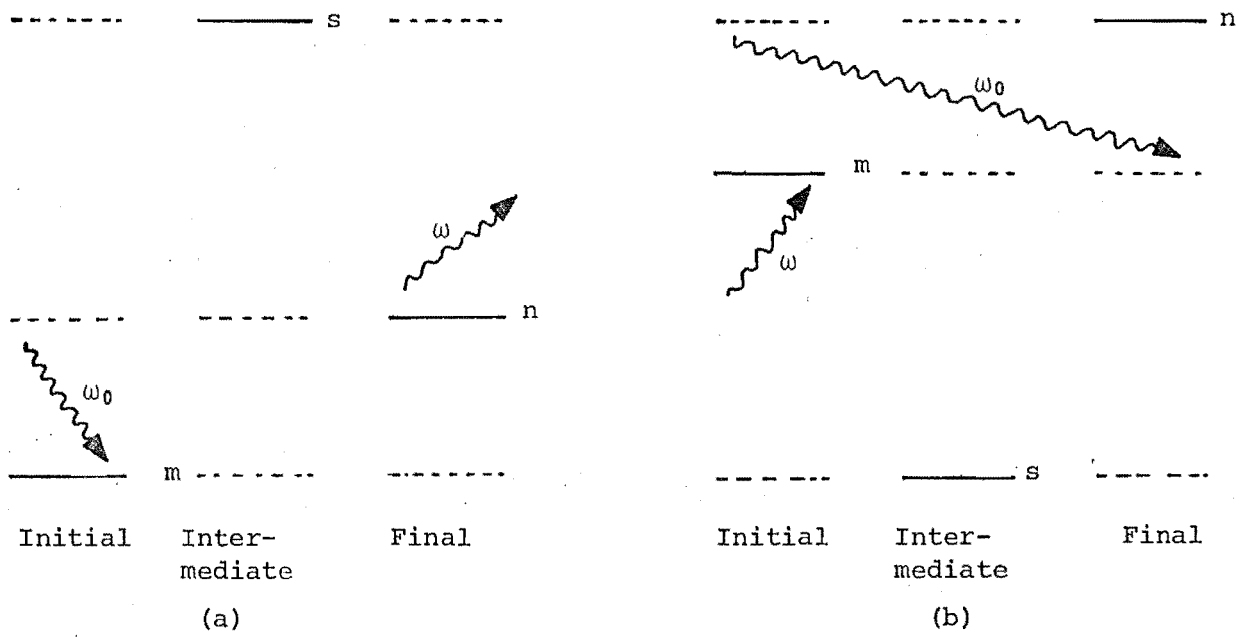

Figure 6.9

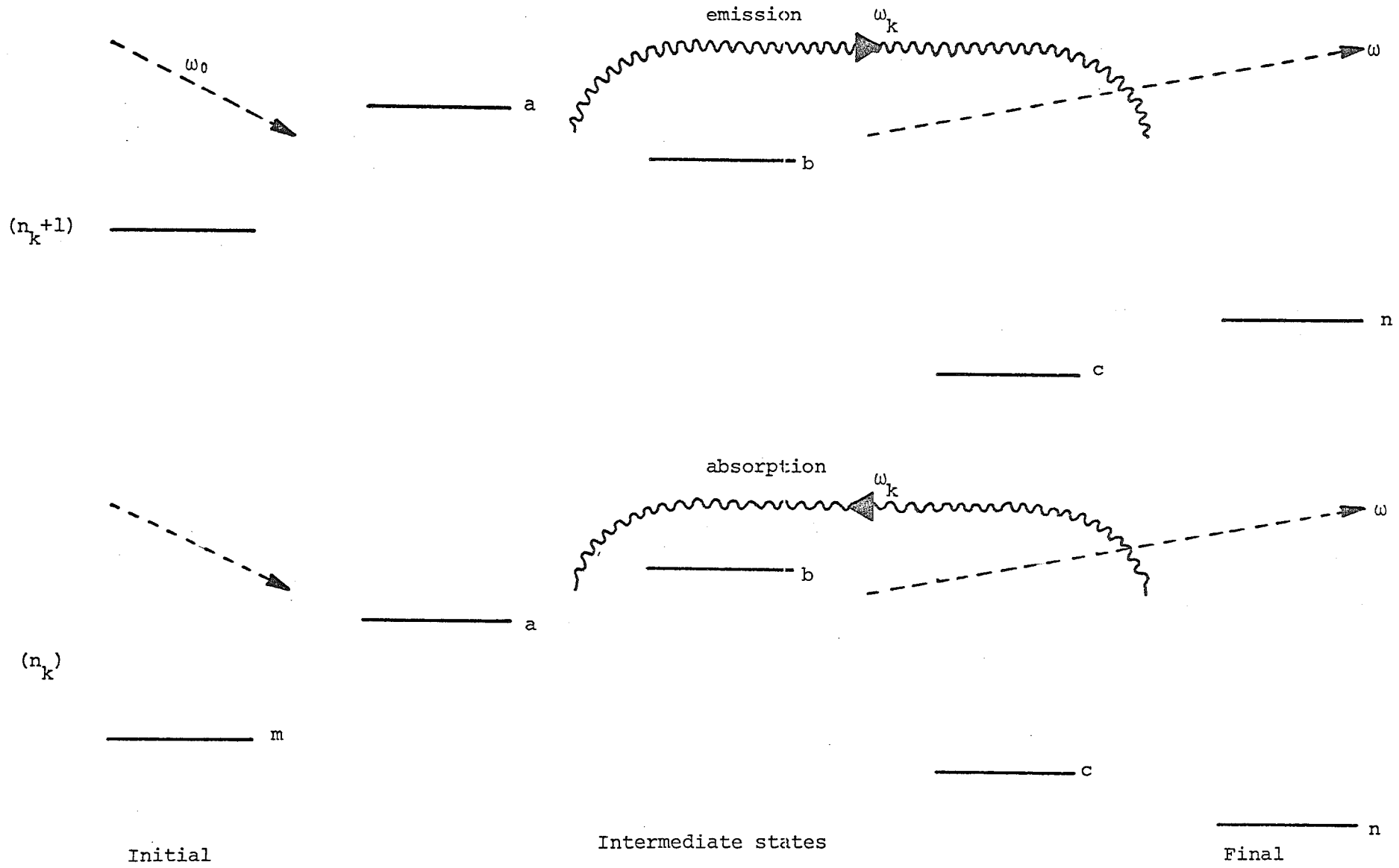
emission
ω_k
ω_0
a
b
(n_k+1)
n
c
absorption
ω_k
ω
b
a
(n_k)
m
c
n
Initial
Intermediate states
Final

In figure 6.8 a,b the intermediate state s(which is summed over) is a 'virtual' state and there is no requirement that say the transition m to s with absorption of a photon of energy ω_0, conserves energy. In a similar manner each diagram of figure 6.7 has a similar interpretation that can easily be found from a study of the diagram. This gives an understanding of the types of processes that are contributing to P_{mn}. For example diagram 6.7d has the two interpretations of figure 6.9 with weightings n_{k+1} and n_k.

Although any diagram that contributes a Raman-type delta function can be incorporated in this generalized Kramers-Heisenberg formula, only a finite number of diagrams can be evaluated. However, just as for the absorption spectrum, an infinite number of diagrams need to be summed over to give any finite width to the Raman spectral line. In the following section we shall use the Dyson equation to sum an infinite number of diagrams and hence obtain a finite linewidth.

6.3 General Lineshape

In §6.1 we evaluated the contribution of figure 6.2 to the Raman spectrum. Following the approach we took to the absorption problem, we shall now replace each level propagator by 'dressed' propagators (figure 6.10) and re-evaluate its contribution giving

Figure 6.10

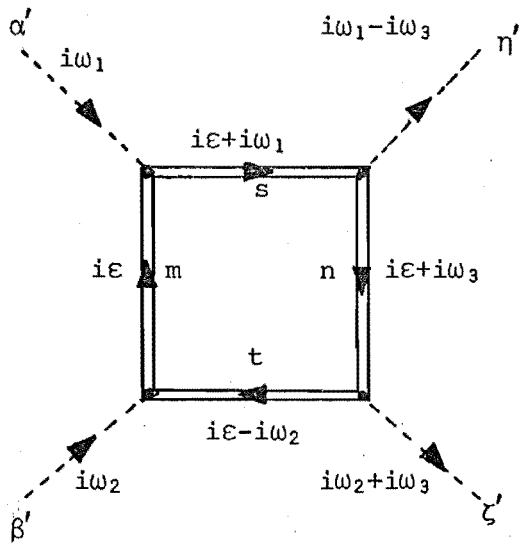

$$T^{S.S.}_{\alpha\beta\eta\zeta}(0) = f_B(-\omega_0+\omega) \sum_{mnst} M^{\alpha}_{ms} M^{\eta}_{sn} M^{\zeta}_{nt} M^{\beta}_{tm}$$

$$\int_{-\infty}^{\infty} dx[f_D(x) - f_D(x+\omega_t)]\ L_m(x)\ L_n(x+\omega_t)\ F_s(x+\omega_0+i\delta)\ F_t(x+\omega_0-i\delta) \tag{6.11}$$

We obtain a similar expression (3.37) for the absorption spectrum with the exception of the $F_s(x+\omega_0+i\delta)\ F_t(x+\omega_0+i\delta)$ factors. In the previous situation we used the sharply peaked nature of the lorentzian $L_m(x)$ at $x = \bar{\lambda}_m$ to remove the x dependences of the f_D, Γ_i and Δ_i functions. If we follow the same procedure and make the further approximation of replacing the x dependences of the F_s and F_t functions we obtain the result

$$T^{S.S.}_{\alpha\beta\eta\zeta}(0) = f_B(-\omega_0+\omega) \sum_{mn} (\bar{\rho}_m - \bar{\rho}_n) \frac{(\gamma_n+\gamma_m)/\pi}{(\omega_0-\omega+\delta_m-\delta_n)^2 + (\gamma_n+\gamma_m)^2}$$

$$\sum_s \frac{M^{\alpha}_{ms} M^{\eta}_{sn}}{\omega_0+\delta_m-\delta_s-i\gamma_s} \cdot \sum_t \frac{M^{\zeta}_{nt} M^{\beta}_{tm}}{\omega_0+\delta_m-\delta_t+i\gamma_t} \tag{6.12}$$

The similarities and differences between this and (6.5), the bare propagator case, are easy to see; the result has the same structure but the delta function has been broadened into a lorentzian. Imaginary parts corresponding to the widths of the intermediate states have appeared in the denominators and all energies appearing have been shifted (i.e. $\omega_m \to \delta_m = \omega_m + \Delta_m(\bar{\lambda}_m)$).

If we consider the four diagrams of figure 6.1a - d that resulted in the Kramers-Heisenberg expression and re-evaluate these with each 'bare' level propagator being replaced by its corresponding 'dressed' propagator (figure 6.11) we obtain

$$T^{S.S.}_{\alpha\beta\eta\zeta}(0) = f_B(-\omega_0+\omega) \int_{-\infty}^{\infty} dx[f_D(x) - f_D(x+\omega_t)]$$

$$\sum_{mn} L_m(x)\ L_n(x+\omega_t)\ {}^0P^{\alpha\eta}_{mn}(x,\omega_0+i\delta)\ [{}^0P^{\beta\zeta}_{mn}(x,\omega_0+i\delta)]^* \tag{6.13}$$

Figure 6.11

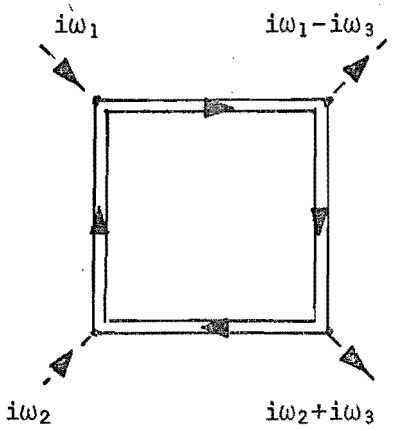

(a)

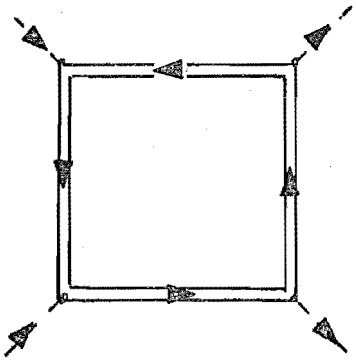

(b)

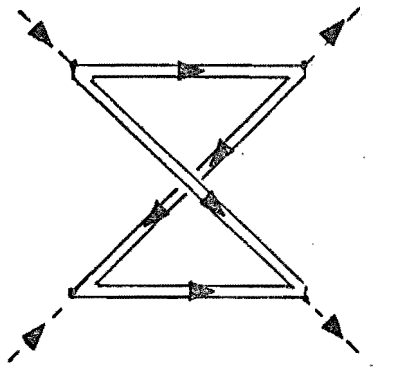

(c)

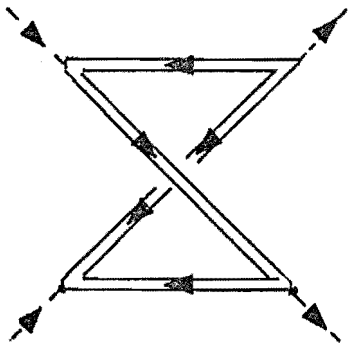

(d)

where

$$ {}^{0}P^{\alpha\eta}_{mn}(x,i\omega_1) = \sum_s \left[\frac{M^{\alpha}_{ms} M^{\eta}_{sn}}{x+i\omega_1-\lambda_s-\Sigma_s(x+i\omega_1)} + \frac{M^{\eta}_{ms} M^{\alpha}_{sn}}{x-i\omega_1+\omega_t-\lambda_s-\Sigma_s(x-i\omega_1+\omega_t)} \right] $$

(6.14)

Making the same approximations again we obtain

$$ T^{S.S.}_{\alpha\beta\eta\zeta}(0) = f_B(-\omega_0+\omega) \sum_{mn} (\bar{\rho}_m-\bar{\rho}_n) \frac{(\gamma_m+\gamma_n)/\pi}{(\omega_0-\omega+\delta_m-\delta_n)^2+(\gamma_n+\gamma_m)^2} $$

$$ {}^{0}P^{\alpha\eta}_{mn}(\bar{\lambda}_m, \omega_0+i\delta) \left[{}^{0}P^{\beta\zeta}_{mn}(\bar{\lambda}_m,\omega_0+i\delta) \right]^* \qquad (6.15) $$

which is a generalization of the Kramers-Heisenberg expression (6.7) but now with the expected lorentzian peak with a width the sum of level m,n widths and with imaginary contribution to the denominators corresponding to the width of the intermediate state. Another alteration of course is that each energy level has been shifted from its original position also ($\omega_m \to \delta_m$). If we allow each diagram of figure 6.4 to also be replaced by one with full rather than bare level propagators then it is possible to obtain a generalized form of (6.14), the only difference being a generalization of ${}^{0}P_{mn}(x,i\omega_1)$ to ${}^{f}P_{mn}(x,i\omega_1)$ which takes the form

$$ {}^{f}P^{\alpha\eta}_{mn}(x,i\omega_1) = {}^{0}P^{\alpha\eta}_{mn}(x,i\omega_1) + {}^{2}P^{\alpha\eta}_{mn}(x,i\omega_1) + \cdots\cdots \qquad (6.16) $$

where for example

$$ {}^{2}P^{\alpha\eta}_{mn}(x,i\omega_1) = \sum_{abc} \sum_k \binom{n_k}{n_{k+1}} \frac{V^k_{ma} M^{\alpha}_{ab} M^{\eta}_{bc} V^k_{cn}}{F_b^{-1}(x+i\omega_1\pm\omega_k)} + \frac{V^k_{ma} M^{\eta}_{ab} M^{\alpha}_{bc} V^k_{cn}}{F_b^{-1}(x-i\omega_1+\omega_t\pm\omega_k)} $$

$$ A_a(x\pm\omega_k)A_b(x+\omega_t\pm\omega_k) + \sum_{abc} \sum_k \binom{n_k}{n_{k+1}} \left[\frac{M^{\alpha}_{ma} V^k_{ab} M^{\eta}_{bc} V^k_{cn}}{F_a^{-1}(x+i\omega_1)F_b^{-1}(x+i\omega_1\pm\omega_k)} \right. $$

$$ \left. + \frac{M^{\eta}_{ma} V^k_{ab} M^{\alpha}_{bc} V^k_{cn}}{F_a^{-1}(x-i\omega_1+\omega_t) F_b^{-1}(x-i\omega_1+\omega_t\pm\omega_k)} \right] A_c(x+\omega_t\pm\omega_k) + \cdots \qquad (6.17) $$

This allows us to interpret these contributions to the cross-section as arising from diagrams 6.12 and 6.13. Note that there is no diagram contributing to ${}^{2}P_{mn}$ of the structure of diagram 6.7c as this is already included in diagram 6.13a and to include it again would result in multiple counting. If the approximation of replacing the x dependence of ${}^{f}P_{mn}(x,i\omega_1)$ is replaced by $x=\overline{\lambda}_m$ then we obtain a result identical to (6.15) but with ${}^{0}P_{mn}(x,i\omega_1)$ being replaced by ${}^{f}P_{mn}(x,i\omega_1)$.

Our analysis of the Raman N.P.L. has taken on a progression of complication and we summarize the major steps here. Firstly in §6.1 we evaluated the contribution of the six diagrams of figure 6.1 which contained bare level propagators. Two of these were found not to contribute to the Raman spectrum while the other four gave the standard Kramers-Heisenberg formula (equation (6.6)-(6.7)). In §6.2 we included all diagrams containing bare propagators (figure 6.4) which resulted in a generalized Kramers-Heisenberg formula (equations (6.9) - (6.10)) still giving a delta function lineshape. In §6.3 we repeated these two cases but replaced the bare level propagators by dressed level propagators. The result for the four diagrams (figure 6.11) was to broaden the delta function into a lorentzian lineshape and to give a modulus squared function $|{}^{0}P_{mn}|^2$ that stayed finite on resonance. (Equations (6.13) - (6.14)). Including all diagrams (figure 6.12) gave a generalized ${}^{f}P_{mn}$ function (equations (6.16) - (6.17)) and allowed the interpretation of figure 6.13.

6.4 One-Phonon Raman Scattering.

When we discussed the possible ways of cutting figure 6.6 we stated that there were cuts that resulted in delta functions containing phonon frequencies. In this section we shall discuss these types of contributions.

Upon evaluating contributions from diagrams where a line cuts one phonon propagator then it is possible to combine these into the expression

Figure 6.12

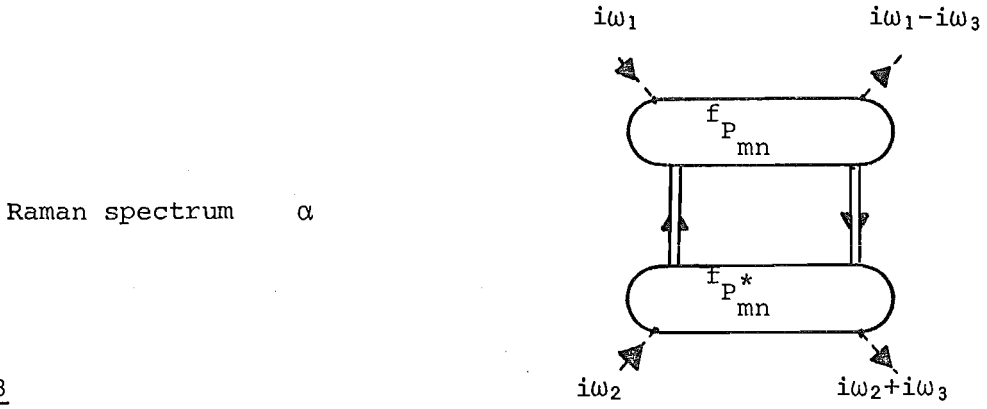

Figure 6.13

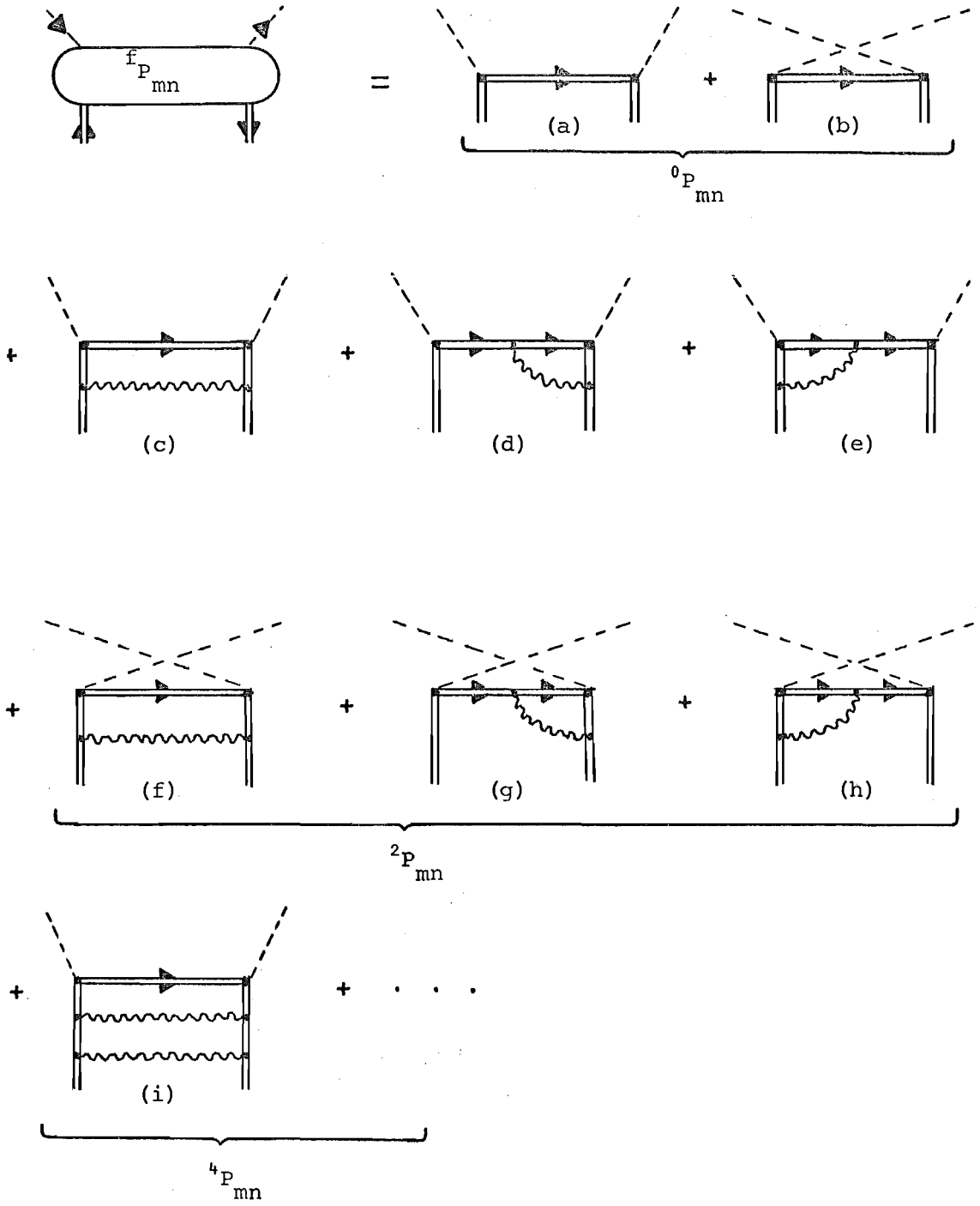

$$T^{S.S.}_{\alpha\beta\eta\zeta}(0) = f_B(-\omega_0+\omega) \sum_{mn} \sum_{k} \left\{ \rho_m \binom{n_k}{n_{k+1}} - \rho_n \binom{n_{k+1}}{n_k} \right\}$$

$$\delta(\omega_0-\omega\pm\omega_k+\omega_{mn}) \quad {}^{b}Q^{\alpha\eta}_{mnk}(\omega_0+i\delta, \pm\omega_k) \left[{}^{b}Q^{\beta\zeta}_{mnk}(\omega_0+i\delta,\pm\omega_k) \right]^* \tag{6.18}$$

with

$${}^{b}Q^{\alpha\eta}_{mnk}(i\omega_1,\pm\omega_k) = {}^{1}Q^{\alpha\eta}_{mnk}(i\omega_1,\pm\omega_k) + {}^{3}Q^{\alpha\eta}_{mnk}(i\omega_1,\pm\omega_k)+\cdots \tag{6.19}$$

where

$${}^{1}Q^{\alpha\eta}_{mnk}(i\omega_1,\pm\omega_k) = \sum_{ab} \left[\frac{M^{\alpha}_{ma} M^{\eta}_{ab} V^{k}_{bn}}{(\omega_{ma}+i\omega_1)(\omega_{mb}+\omega_t)} + \frac{M^{\eta}_{ma} M^{\alpha}_{ab} V^{k}_{bn}}{(\omega_{ma}-i\omega_1+\omega_t)(\omega_{mb}+\omega_t)} \right.$$

$$\left. + \frac{V^{k}_{ma} M^{\alpha}_{ab} M^{\eta}_{bn}}{(\omega_{ma}\pm\omega_k)(\omega_{mb}+i\omega_1\pm\omega_k)} + \frac{V^{k}_{ma} M^{\eta}_{ab} M^{\alpha}_{bn}}{(\omega_{ma}\pm\omega_k)(\omega_{mb}-i\omega_1+\omega_t\pm\omega_k)} + \frac{M^{\alpha}_{ma} V^{k}_{ab} M^{\eta}_{bn}}{(\omega_{ma}+i\omega_1)(\omega_{mb}+i\omega_1\pm\omega_k)} \right] \tag{6.20}$$

These can be regarded as arising as contributions from the diagrams of the form given in figure 6.14. This result can be generalized also by replacing each 'bare' level by a 'dressed' level propagator giving

$$T^{S.S.}_{\alpha\beta\eta\zeta}(0) = f_B(-\omega_0+\omega) \sum_{mn} \sum_{k} \binom{n_k}{n_{k+1}} \int_{-\infty}^{\infty} dx \left[f_D(x) - f_D(x+\omega_t) \right]$$

$$L_m(x) \; L_n(x+\omega_t\pm\omega_k) \; {}^{f}Q^{\alpha\eta}_{mnk}(x,\omega_0+i\delta,\pm\omega_k) \left[{}^{f}Q^{\beta\zeta}_{mnk}(x,\omega_0+i\delta,\pm\omega_k) \right]^* \tag{6.21}$$

where

$${}^{f}Q^{\alpha\eta}_{mn}(x,i\omega_1,\pm\omega_k) = \sum_{ab} \left[\frac{M^{\alpha}_{ma} M^{\eta}_{ab} V^{k}_{bn}}{F_a^{-1}(x+i\omega_1)} + \frac{M^{\eta}_{ma} M^{\alpha}_{ab} V^{k}_{bn}}{F_a^{-1}(x-i\omega_1+\omega_t)} \right] A_b(x+\omega_t)$$

$$+ \sum_{ab} \left[\frac{V^{k}_{ma} M^{\alpha}_{ab} M^{\eta}_{bn}}{F_b^{-1}(x+i\omega_1\pm\omega_k)} + \frac{V^{k}_{ma} M^{\eta}_{ab} M^{\alpha}_{bn}}{F_b^{-1}(x-i\omega_1+\omega_t\pm\omega_k)} \right] A_a(x\pm\omega_k) + \cdots \tag{6.22}$$

and having the corresponding diagram interpretation of figure 6.15. Again making the approximation that $L_m(x)$ is strongly peaked allows the

Figure 6.1

$\rho_m \; n_k \; \delta(\omega_{mn}+\omega_t+\omega_k) \quad \leftrightarrow$

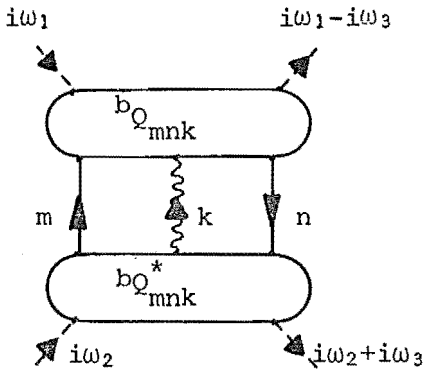

$\rho_m (n_k+1) \; \delta(\omega_{mn}+\omega_t-\omega_k) \leftrightarrow$

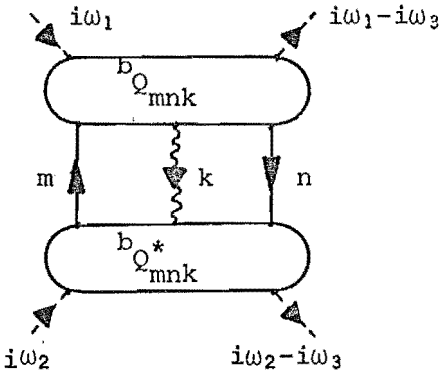

where

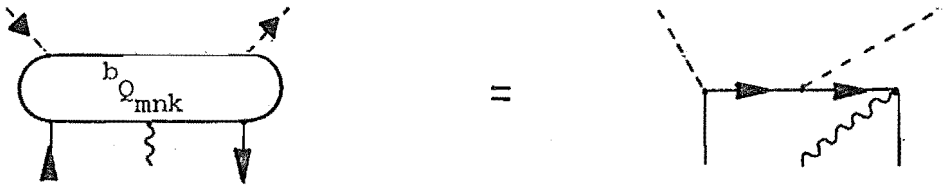

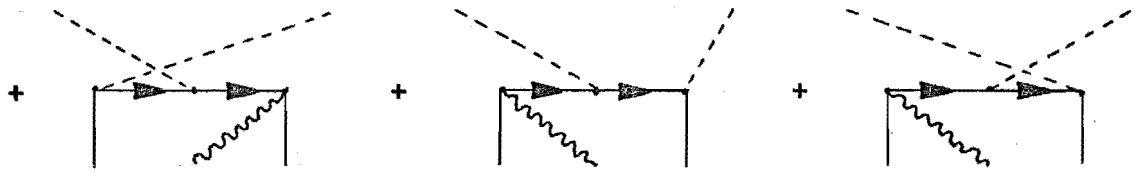

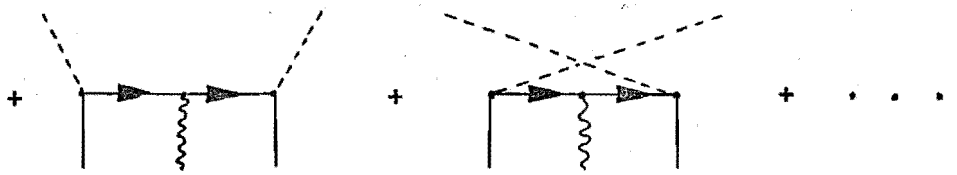

Figure 6.15

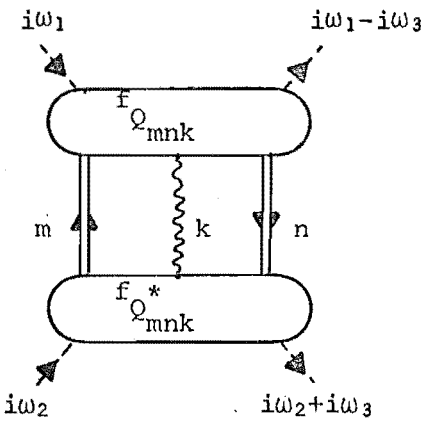

where

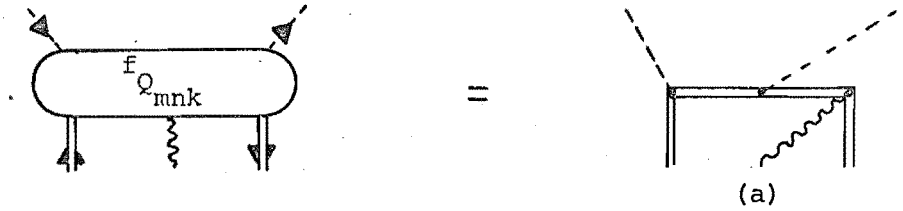

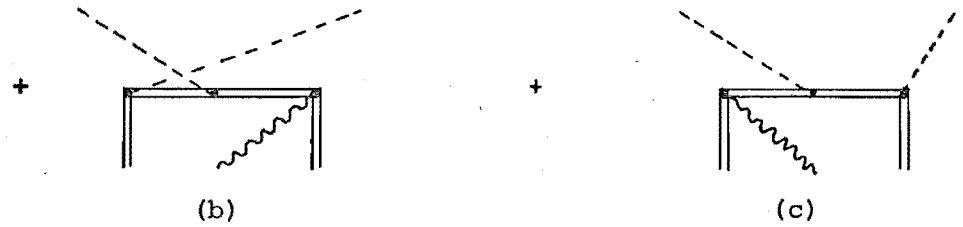

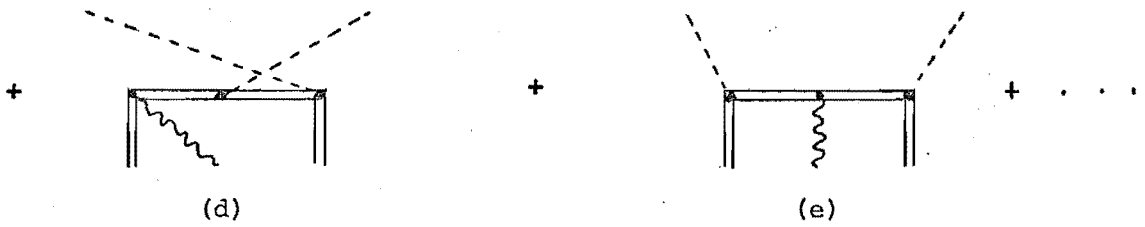

evaluation of (6.21)

$$T^{S.S.}_{\alpha\beta\eta\zeta}(0) = f_B(-\omega_0+\omega) \sum_{mn} \sum_{k} \left\{ \bar{\rho}_m \begin{pmatrix} n_k \\ n_{k+1} \end{pmatrix} - \bar{\rho}_n \begin{pmatrix} n_{k+1} \\ n_k \end{pmatrix} \right\}$$

$$\frac{(\gamma_m+\gamma_n)/\pi}{(\omega_0-\omega\pm\omega_k+\delta_m-\delta_n)^2 + (\gamma_m+\gamma_n)^2} \; f_{\underset{\sim}{Q}mnk}{}^{\alpha\eta}(\bar{\lambda}_m, \omega_0+i\delta, \pm\omega_k) \left[f_{\underset{\sim}{Q}mnk}{}^{\beta\zeta}(\bar{\lambda}_m, \omega_0+i\delta, \pm\omega_k) \right]^* \tag{6.23}$$

It is clear from the form of the delta function in (6.18) and the position of the lorentzian in (6.23) that these diagrams correspond to first-order Raman processes wherein the electronic system undergoes a transition and there is a phonon either emitted or absorbed in the process. The phonon Raman process that is usually described (e.g. Pinczuk and Burstein (1975)) is one in which a phonon is either created or destroyed and the electronic system stays in the same state. However Kane-Maguire and Konigstein (1973) have found evidence for the above type of process in thulium gallium garnets (TmGaG) and call it the 'vibro-electronic' effect.

For a system with translational invariance the usual phonon Raman process (i.e. m = n in (6.18), (6.21) and (6.23)) can be shown (Pinczuk and Burstein (1975)) to require that the phonon momentum $\underline{k}$ be approximately zero. However for the system we are considering the intermediate states are impurity ion levels that have no translational invariance like the host crystal ions; they are far apart and randomly distributed within the host lattice. Hence we are unable to assign any momentum labels to the level propagators and the above $\underline{k} \simeq 0$ restriction is relaxed.

The resulting phonon sideband spectrum is a broad peak on either side of the N.P.L. that reflects the phonon density of states. For example if the density of states contains a sharp peak this may be seen as a similar sharp peak in the Raman sideband spectrum.

The theory we have presented is also applicable to the analysis of host-ion scattering. In appendix 6B we show how momentum considerations can be included in our analysis and that we regain the usual result that the

sum over both photon and phonon wave-vectors vanish. For the one-phonon scattering situation this means that only $\underline{k} \simeq 0$ phonons are observed in the spectrum. The only restriction on the application of the theory to this situation results from our treating each site as being independent. This restricts us to situations where the coupling between the ions is small and can be neglected. For example consider Raman scattering in yttrium aluminium garnet (YAG) where each (cubic) unit cell contains 96 ions. The lowest excited states of the Aℓ and O are much higher in energy than those of the (paramagnetic) Y ions. Hence we expect the phonon Raman spectrum to be dominated by the Y-photon-phonon interactions. The Y ions are separated by considerably more than nearest-neighbour coordination distances and hence we expect the coupling between ions to be small and the present theory to be applicable.

6.5 Multi-Phonon Raman Scattering

It is possible to extend the analysis of the last section to m-phonon processes by an obvious extension of the diagram of figure 6.15. The relevant diagrams are those given in figure 6.16. Of course as m increases the contribution to the spectrum expected decreases because they are higher order in V^{k}_{mn} which we require to be small if our perturbation approach is to be valid.

The bare phonon propagators of figure 6.16 can be replaced by dressed phonon propagators by including anharmonic phonon decay processes. The phonon Dyson equation is presented in figure 6.17 and results in a propagator

$$\mathcal{D}_k(i\omega_{n'}) = \frac{1}{i\omega_{n'} - \omega_k - \Pi_k(i\omega_{n'})} \qquad (6.23)$$

where $\Pi_k(i\omega_{n'})$ is the phonon self-energy or polarization part which satisfies

$$\Pi_k(x \pm i0^+) = \Delta_k(x) \pm i\Gamma_k(x) \quad . \qquad (6.24)$$

Figure 6.16

n-phonon spectrum α

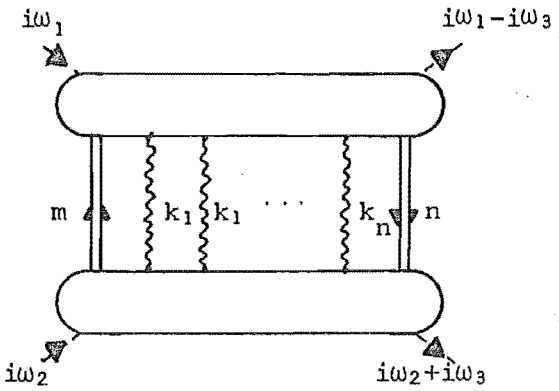

where

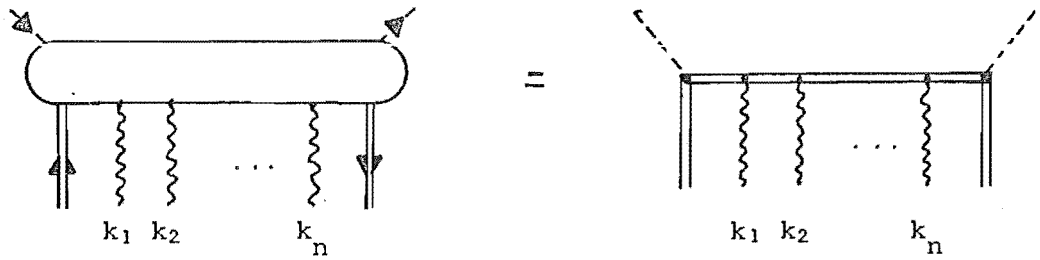

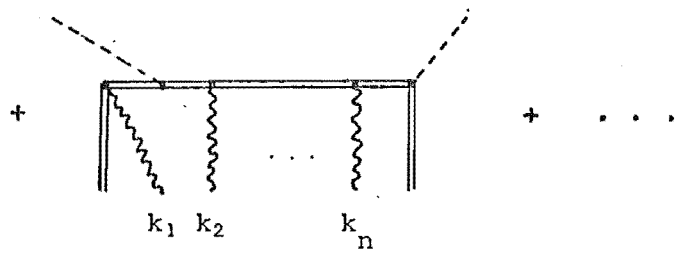

+ . . .

Figure 6.17

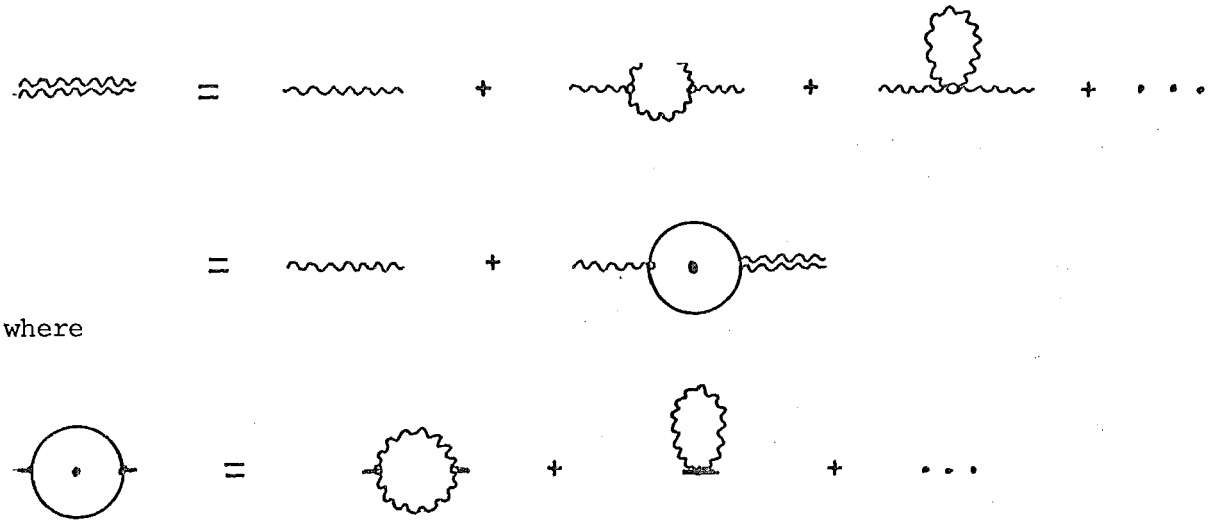

where

Evaluating the contribution from figure 6.16 with all bare phonon propagators replaced by dressed propagators we can study the effect of the phonon lifetime on the m-phonon Raman lineshape. In appendix 6A we evaluate the contribution from diagram 6.18 under the assumption of the sharply peaked approximation and neglecting x dependences of the vertex function Q_{mn}. This results in a lorentzian lineshape whose width is $\gamma_m+\gamma_n+\gamma_k(\gamma_k=\Gamma_k(\bar{\omega}_k))$ peaked at $\delta_n-\delta_m+\bar{\omega}_k$ $(\bar{\omega}_k=\omega_k+\Delta_k(\bar{\omega}_k))$.

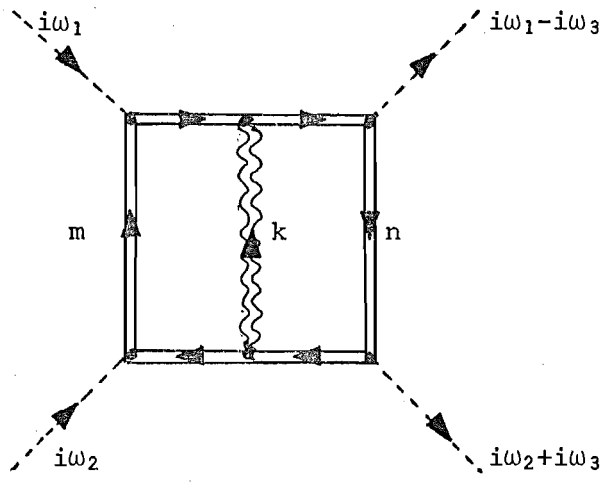

This result can be generalized to the m-phonon spectrum and under the same simple approximations results in a lorentzian lineshape with a width $\gamma_m+\gamma_n+\gamma_{k_1}+\gamma_{k_2}+\cdots+\gamma_{k_m}$. This corrects the assumption of Klein and

Colwell (1971) that the width of an m-phonon line only reflects the lifetimes of the phonons; rather we find ionic level lifetimes are also included in the total linewidth.

The approach used by Stedman (1971a) for estimating the contribution of the non-additive absorption diagrams (cf §3.5.4) can be employed to estimate the contribution of non-additive diagrams to the Raman spectrum. (By Raman non-additive diagrams we mean those diagrams not contained in figure 6.11). This method predicts identical contributions to the Raman N.P.L. from these diagrams as was found for the absorption N.P.L. (McKenzie and Stedman 1977). Within the present approach these contributions are to be regarded, just as for the absorption spectrum, as resulting from the extension of the m-phonon lineshapes into the region of the N.P.L.

CHAPTER 7. RAMAN SPECTRUM : TIME DEPENDENT SCATTERING

7.1 Introduction

When radiation is used to excite some substances (e.g. CaF_2) it is found that radiation can be emitted at distinctly different frequencies and the emitted radiation can persist for some time after the exciting radiation has terminated. (Jenkins and White 1957). This phenomena is called fluorescence (F.); the incident light excites the atomic or molecular system to real excited levels which then decay (after a time interval determined only by the laws of statistics) to lower levels.

This contrasts with Raman scattering (R.S.) where the incident radiation excites the system to a virtual intermediate level (not necessarily a higher level) before the transition to the final level. A real transition to an intermediate state is an energy conserving process and can be identified experimentally by a measurement of, (at least), the energy of the system in the intermediate state. A virtual transition to an intermediate state need not conserve energy (by an amount ΔE), and the intermediate state may be thought of as lasting a finite time τ given by the uncertainty relation $\tau\Delta E \sim \hbar$ (§ 7.3).

The concepts of F. and R.S. have clarified over a considerable period of time and we refer the reader to the review of Behringer (1974) for an extensive discussion of its history. These ideas are clearly defined in the far from resonance regime, but near or on resonance (i.e. where the incident frequency matches or closely matches the frequency difference between the initial and intermediate states), the distinction between resonance fluorescence (R.F.) and resonance Raman scattering (R.R.S.), as they are then called, is far from clear.

In the last few years a large number of theoretical and experimental papers dealing with these phenomena have appeared. Some of these deal with the question of whether it is possible and/or meaningful to distinguish between these two processes and if so, how this is to be

achieved experimentally. In the following section we shall give a brief review of what we regard as the most important of these, as a background for the rest of this chapter.

7.2 Literature Review

7.2.1 Steady State Scattering

This avalanche of papers began with the experimental work of Fouche and Chang (1972) who studied the intensity of the fundamental Stokes band of I_2 as a function of the incident laser frequency. They reasoned that because R.F. involved real intermediate states then if the pressure of foreign gas (N_2) mixed with the I_2 was increased, the increased number of collisions would remove more of the energy from the excited states before re-emission and hence 'quench' or reduce the R.F. intensity. R.R.S. involves 'virtual' levels and they suggested that it should not be quenched. They found that at certain values of the incident laser frequency the output could be quenched, while for other values it was not. They suggested the identification of R.F. and R.R.S. respectively for these regions.

Yu *et.al.* (1973) and Yu and Shen (1974,1975) studied the Raman spectrum of solid Cu_2O near resonance and observed shifts in a number of phonon peaks as a function of the incident photon energy. They interpreted this as resulting from phonon dispersion.

St.Peters *et.al.* (1973) repeated the experiment of Fouche and Chang but were unable to reproduce their results. They found that the region previously identified as R.R.S. is quenched at higher foreign gas pressures and hence they disagree with the R.R.S. identification.

The theoretical paper of Klein (1973) considered the results of Yu *et.al.* and argued that "resonance scattering is often equivalent to absorption into a resonant state followed by luminescence from that state". This interpretation however was challenged by Shen (1974) who used a density-matrix formalism to argue that "resonance Raman scattering and hot luminescence [i.e. resonance fluorescence] are two distinct physical

processes, although they are always simultaneously present and can interfere with each other". He argued that they would have distinct lineshapes which may be useful to distinguish them in steady state experiments. He suggested that a transient time-resolving experiment would be more appropriate for distinguishing these processes.

A very clear statement of the distinctions between the points of view presented by Klein and Shen was given in the work of Solin and Merkelo (1975). Their intuitive approach used Einstein A and B coefficients and supported the view of Klein that RRS and RF were equivalent. They suggested that Shen's interpretation resulted only from algebraic manipulations. They stated that "the claims that RRS ..... is essentially instantaneous and that this is the fundamental distinction between RRS and RS ..... is incorrect".

Aminov (1975) attempted to resolve these disagreements in part by claiming that the contribution given by Shen, interpreted as RRS, could be neglected relative to the RF contribution. He concluded "that as the exciting frequency ..... approaches resonance the total efficiency of Raman scattering ..... transforms to the efficiency of the [RF] in accordance with the point of view of Klein". However in appendix 7A we show that his proof that the contribution interpreted by Shen as RRS is much less than the RF contribution is false and that they could be expected to be similar in magnitude near resonance. This obviously invalidates his conclusions. However this paper was not greatly quoted by subsequent authors and hence seems to have had little influence on the course of the controversy.

Although subsequent authors have not commented on their ideas a novel approach was presented by Jacon and Van Labeke (1975) on the transition of the spectrum from RRS to RF. Their thesis was that if the intermediate state was discrete then the scattering was to be labelled RF, while for an intermediate state that was part of a continuum it was to be labelled RRS. Dealing with a simple model and starting with discrete intermediate

states (and hence RF), increasing the foreign gas pressure increases the linewidth of the intermediate states until they broaden to form a continuum thus completing the transition to RRS.

7.2.2 Time-Dependent Scattering

In 1974 a distinctly different experimental technique was introduced partly in an attempt to clarify these concepts. This was the idea, suggested by Shen, of a transient time-resolving experiment. The first of these was performed by Williams *et.al.* (1974) who studied the time dependence of the output from I_2 vapour upon excitation by rectangular (100 ns) laser pulses. Using a spectrometer of resolution less than 2 cm^{-1} they studied the emission triplet from the P(13) and R(15) transitions (Halldorsson and Menke (1970)) by means of photocounting techniques.

On exact resonance the output contained only one component with a long ($\simeq$ 300 ns) decay time. However further from resonance ($\simeq$ 1 GHz) they found the output consisted of two components : the previous long decay part and a contribution (whose relative magnitude increased with increasing distance from resonance) with a decay time of the order of the rise time of the pulse ($\simeq$ 3ns). They interpreted the on-resonance decay rate as reflecting the linewidth of the intermediate state. They expected the off-resonance lifetime (Δt) to be limited by the frequency difference ($\Delta\omega$) between the excited state and the incident laser frequency via the uncertainty principle (i.e. $\Delta t \simeq \frac{1}{\Delta\omega}$). Although the on-resonance case is consistent with their interpretation, the off-resonance curve consisted of both long and short components rather than just a short component as expected from their interpretation. They suggested however that this resulted because the absorption lineshape would be wide enough to allow both on and off resonance components to appear simultaneously.

Schwartz (1975) emphasised the importance of the uncertainty principle in discussing experiments of this type and in particular pointed out that any experiment designed to test the assumption of Williams *et.al.*, namely that the off-resonance time decay was determined by the amount of

off-resonance (i.e. $\Delta t \sim \frac{1}{\Delta\omega}$), was impossible.

O Berg *et.al.* (1974) presented a theory for the system studied by Williams *et.al.* where "all the ramifications of the uncertainty principle are built in automatically". They concluded that "there was no exponentially decaying component which depended on the frequency difference between the exciting pulse and the resonance".

Similar conclusions were presented in a paper by Friedman and Hochstrasser (1974) where the nature of the exciting pulse was also emphasised. They classified the decay at long times in the extreme limits as:

(a) RF if $\Gamma_p >> \Gamma_i$ (where $\Gamma_p \equiv$ rise time of laser pulse, $\Gamma_i \equiv$ width of intermediate state) with time dependence $e^{-\Gamma_i t}$

and (b) RRS if $\Gamma_i >> \Gamma_p$ with time dependence $e^{-\Gamma_p t}$.

Further papers which essentially agree with these two are the works of Mukamel and Jortner (1975), Metiu *et.al.* (1975) and Fulton (1974).

The work of Williams *et.al.* was extended by Rousseau *et.al.* (1975) where they repeated the experiment also allowing the I_2 gas pressure to vary. In the off-resonance regime they found that if they increased the gas pressure then the relative magnitude of the long lived component also increased. The interpretations given by Williams *et.al.* for their experiment were not consistent with this result and they presented a new interpretation. The short component that follows the laser pulse was interpreted as the Raman term while the long component they called the 'redistribution' term. They regarded the redistribution component as resulting from quasi-elastic collisions between I_2 gas molecules where the molecule remains in the same quantum state but suffers a phase change. These collisions broaden the intermediate state by an amount which increases with the number of collisions and hence with the gas pressure.

These conclusions were considered by Hackett (1976) who included other possible collision processes and concluded that "the existence of elastic collisional transfer processes [i.e. quasi-elastic collisions] cannot be

positively proved [from their data]."

Mukamel *et.al.* (1975, 1976) presented a powerful Louville space formalism in which they explicity account for the collision process. They claim that the experimental results of Rousseau *et.al.* "cannot be elucidated by a naive extension of the theory advanced for the 'isolated' molecule, simply modifying the molecular radiative-decay width by the addition of a pressure-dependent term". They claim their theory is consistent with these results.

Other time-dependent theories have been presented by Courtens and Szöke (1977), Huber (1970) and Kimble and Mandel (1975).

Much of the controversy has been academic; it is not so important to be able to label an experimental process RRS or RF but rather to be able to understand and/or predict the frequency/time dependence of the emitted radiation. An analysis of the Raman spectra time/frequency dependence that is valid upon excitation by a nearly or exactly resonant laser pulse would seem opportune. In the remainder of this chapter we shall calculate such dependences for scattering from impurity ions in a crystal using the formalism developed in chapter 5.

7.3 Time-Frequency Uncertainty Requirements

One of the basic principles of quantum mechanics is the uncertainty principle developed by Heisenberg (1927). (For comments on this principle see the papers by Aharonov and Bohn (1961,1964), Bohn and Bub (1966 a,b), Aharonov and Safko (1975) and Mayants *et.al.* (1976)).

$$\Delta t \, \Delta E \gtrsim \hbar \tag{7.1}$$

where Δt is the uncertainty in time and ΔE the uncertainty in the energy of the system during this period. This has important consequences for our time-dependent analysis. If we assume the time-resolved measurements are performed with a minimum time interval uncertainty

$$\Delta t = a/c \tag{7.2}$$

then there is a corresponding minimum frequency resolution given from (7.1) by

$$\Delta\omega = \Delta E/\hbar \sim (\Delta t)^{-1} = c/a \tag{7.3}$$

As stated by Kusunoki (1976) the parameter ω' in the expression for the Raman cross-section (5.49) corresponds physically to the energy actually transferred to the sample by the scattering process. From (7.3) we then obtain

$$|\omega' - \omega_t| \lesssim c/a \tag{7.4}$$

In figure 7.1 we plot $|S(\xi)|^2$ for the laser pulse shape we considered in § 5.3.1 (equation 5.7, figure 5.3) for particular values of the pulse length (T), and the rise time (Γ_0). This function is seen to be sharply peaked about $\xi = 0$ with a width at half maximum of the order of the minimum of Γ_0 and T^{-1}. This effectively limits the values of $|\xi_1 - \omega_0|$ and $|\xi_2 + \omega_0|$ in (5.49) to within these limits, namely

$$|\xi_1 - \omega_0|, \ |\xi_2 + \omega_0| \sim \min(\Gamma_0, T^{-1}) \tag{7.5}$$

As an extreme example of this consider the steady state analysis of chapter 6 where $\min(\Gamma_0, T^{-1}) = 0$ and we took $|\xi_1 - \omega_0|, \ |\xi_2 + \omega_0| = 0$.

In this analysis we shall assume the conditions

$$\omega_0 \sim \omega \gg c/a \gg \Gamma_0, \ T^{-1} \tag{7.6}$$

which are realised in actual experiments of this type. For example in the series of experiments conducted by Williams *et.al.* (1974) and Rousseau *et.al.* (1975,1976) (hereafter referred to as WR) they used a single mode 5145Å incident laser frequency, with rectangular pulses from a minimum of 20ns with a 3ns rise time. Assuming a detector with dimensions of the order of 1cm then the parameters in (7.6) take the values $\omega_0 \sim 10^{15}\ s^{-1}$, $a/c \sim 10^{10}\ s^{-1}$, $T^{-1} \sim 5 \times 10^{7}\ s$, $\Gamma_0 \sim 3 \times 10^{8}\ s^{-1}$ which easily satisfy (7.6). Combining the inequalities (7.4) - (7.6) gives

Figure 7.1

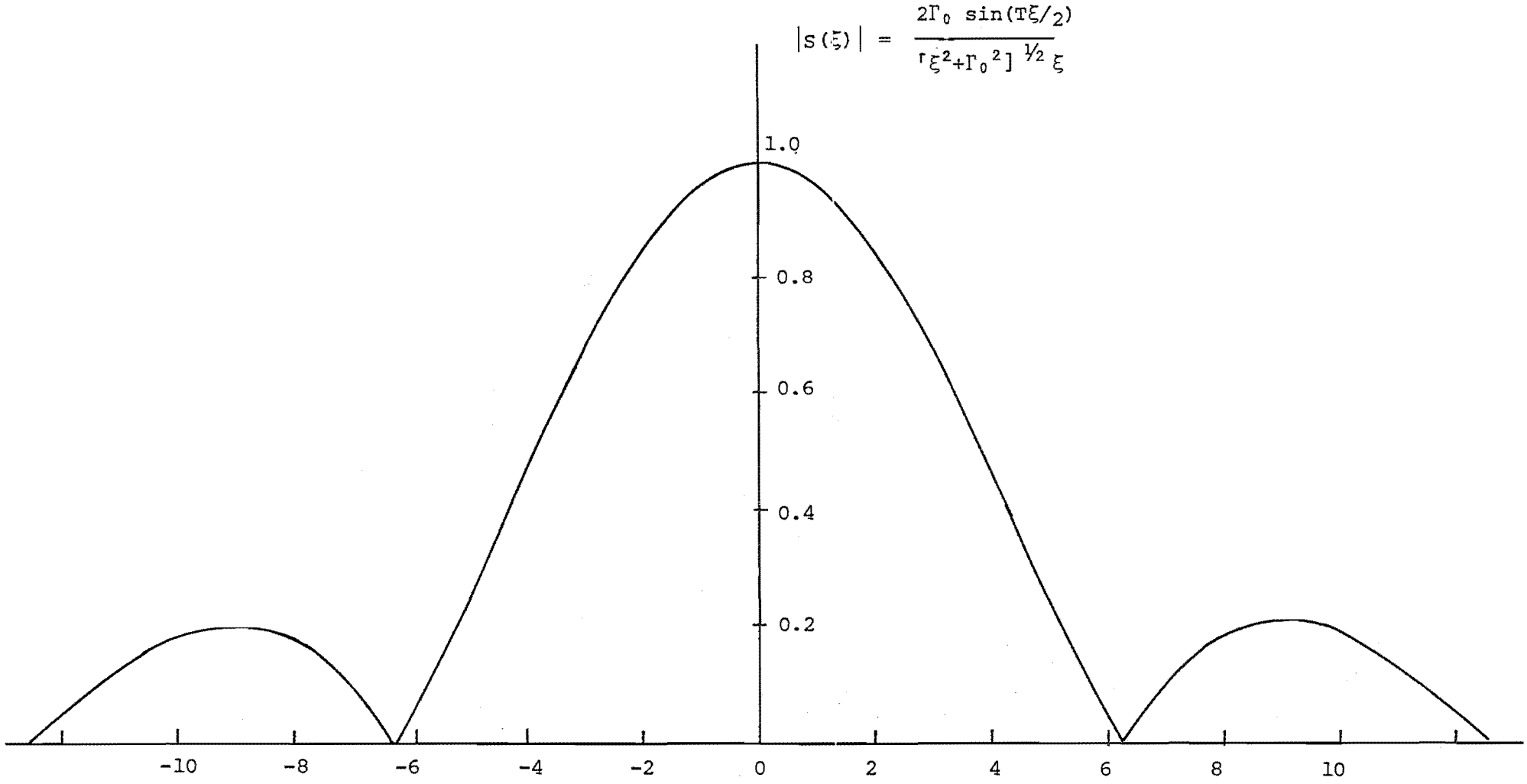

Plot of $|S(\xi)|$ with $\Gamma_0 = 100$, $T = 1$

$$|\omega' - \omega_t| \sim c/a >> \Gamma_0, T^{-1} \sim |\xi_1 - \omega_0|, |\xi_2 + \omega_0| \qquad (7.7)$$

which enables us to approximate $U(\omega' - \omega_t)$ defined in (5.37) by

$$U(\omega' - \omega_t) \simeq \left| \frac{\sin(a/c)(\omega' - \omega_t)}{\omega' - \omega_t} \right|^2 \frac{c}{\pi a} \qquad (7.8)$$

For steady state scattering the time resolution (7.2) can be allowed to become as large as one likes (enabling the frequency resolution to improve) which is equivalent to allowing (a/c) to become large. In this limit $U(\omega' - \omega_t)$ can be approximated by a delta function as in (6.1).

It will be found that evaluating the Raman cross section (5.50) results in approximately lorentzian functions of ω' with width Γ_s, of the order of the initial and final states of the transition. This gives two possible regimes. The first is the

(a) quasi-steady state scattering where the time resolution is taken to be long compared with Γ_s^{-1} enabling the delta function approximation (6.1) to be made, giving

$$T(t,\omega_0,\omega) \simeq T(t,\omega_t) \qquad (7.9)$$

The poor time resolution corresponds (cf 7.3) to a sharp frequency resolution $\Delta\omega << \Gamma_s$ enabling the structure of the Raman spectral line to be resolved, however only the long term time dependences are obtainable.

The other regime is

(b) transient scattering where the time resolution Δt is short compared with Γ_s^{-1} and the delta function approximation (6.1) is no longer valid. In this case we are required to evaluate the integral over ω' in (5.49). The good time resolution enables us to observe rapid changes in the temporal output but the corresponding poor frequency resolution $\Delta\omega \gtrsim \Gamma_s$ means that the output is the integrated intensity over a frequency region large compared with the spectral line.

The experiments of W.R. were performed in the transient scattering

regime. They chose their frequency resolution $\Delta\nu \lesssim 2cm^{-1}$ which results in an uncertainty in time $\Delta t \gtrsim 10^{-10}s$. This gave a time resolution enabling the observation of the rise and fall of the laser pulse (~ 3ns rise time) but the frequency resolution was not sufficient to resolve the spectral line (although it is small enough to be sure the output is arising only from the spectral line.)

7.4 Bare Time Dependence

In this section we shall calculate the time dependence of the transient Raman scattering spectrum for the diagrams in figure 6.1 which are zero-order in the phonon propagators. Evaluating their contribution to (5.49) gives the result

$$T_{\alpha\beta\eta\zeta}(t) = \int_{-\infty}^{\infty} d\omega' \, U(\omega' - \omega_t) f_B(-\omega') \sum_{mn} (\rho_m - \rho_n)$$

$$\delta(\omega' + \omega_{mn}) \; {}^0\Pi_{mn}^{\alpha\eta}(\omega, t) \left[{}^0\Pi_{mn}^{\beta\zeta}(\omega', t) \right]^* \qquad (7.10)$$

where

$${}^0\Pi_{mn}^{\alpha\eta}(t, \omega') = \int_{-\infty}^{\infty} \frac{d\xi}{2\pi} S(\xi - \omega_0) e^{-i\xi(t - \bar{R}/c)} \; {}^0P_{mn}^{\alpha\eta}(\xi + i\delta) \qquad (7.11)$$

with $\bar{R} \simeq R_0 + R$ and ${}^0P_{mn}^{\alpha\eta}(i\omega_1)$ is defined by (6.7). Using the delta function to remove the sum over ω' we obtain

$$T_{\alpha\beta\eta\zeta}(t) = \sum_{mn} (\rho_m - \rho_n) \; U(\omega_{nm} - \omega_t) f_B(-\omega_{nm}) \; {}^0\Pi_{mn}^{\alpha\eta}(\omega_{nm}, t) \left[{}^0\Pi_{mn}^{\beta\zeta}(\omega_{nm}, t) \right]^* \qquad (7.12)$$

Rather than a delta-function spectrum that we obtained in chapter 6 (cf 6.6) for the steady-state spectrum we find this has been broadened into the function $U(\omega_{nm} - \omega_t)$. From (7.8) we see that the width of this function is approximately c/a which, as we might expect, is the minimum frequency resolution (cf 7.3). The time dependence of (7.12) is contained wholly in the functions ${}^0\Pi(t, \omega_{nm})$ which are calculated in appendix 7B. In figure 7.3 we give the time dependence of this for scattering from a

model system with energy levels at 0,1 and 8 (cf figure 7.2) (arbitrary units) where

Figure 7.2

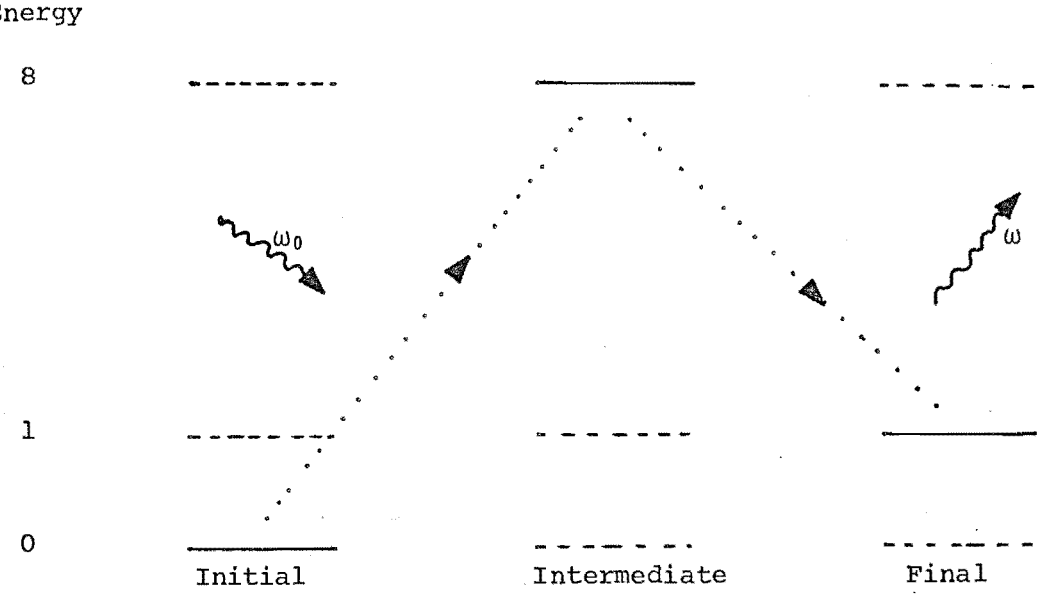

the system is initially in level 0 and goes via the intermediate state level 8 to the final level 1.

Figure 7.3 consists of a base page which indicates the form of the laser pulse ($\Gamma_0 = 6T$) while successive overlays give the time response as the incident laser frequency ω_0 approaches the resonant frequency between the initial and intermediate levels ($\omega_0 \to 8.0$).

As ω_0 approaches resonance the magnitude of the output increases as might be expected, however it now tends to a finite value in contrast with expression (6.7) for steady state scattering, which we found increased without limit. Although this infinity has disappeared, another pathological effect has now appeared because after the duration of the laser pulse, the output does not decay with time, but remains at a constant non-zero value. This is obviously not physical and we shall find in the next section that to obtain an output that decays to zero long after the pulse we must replace the 'bare' level propagators by 'dressed' level propagators as in figure 6.11.

The process of 'dressing' the level propagators can be interpreted

Figure 7.3

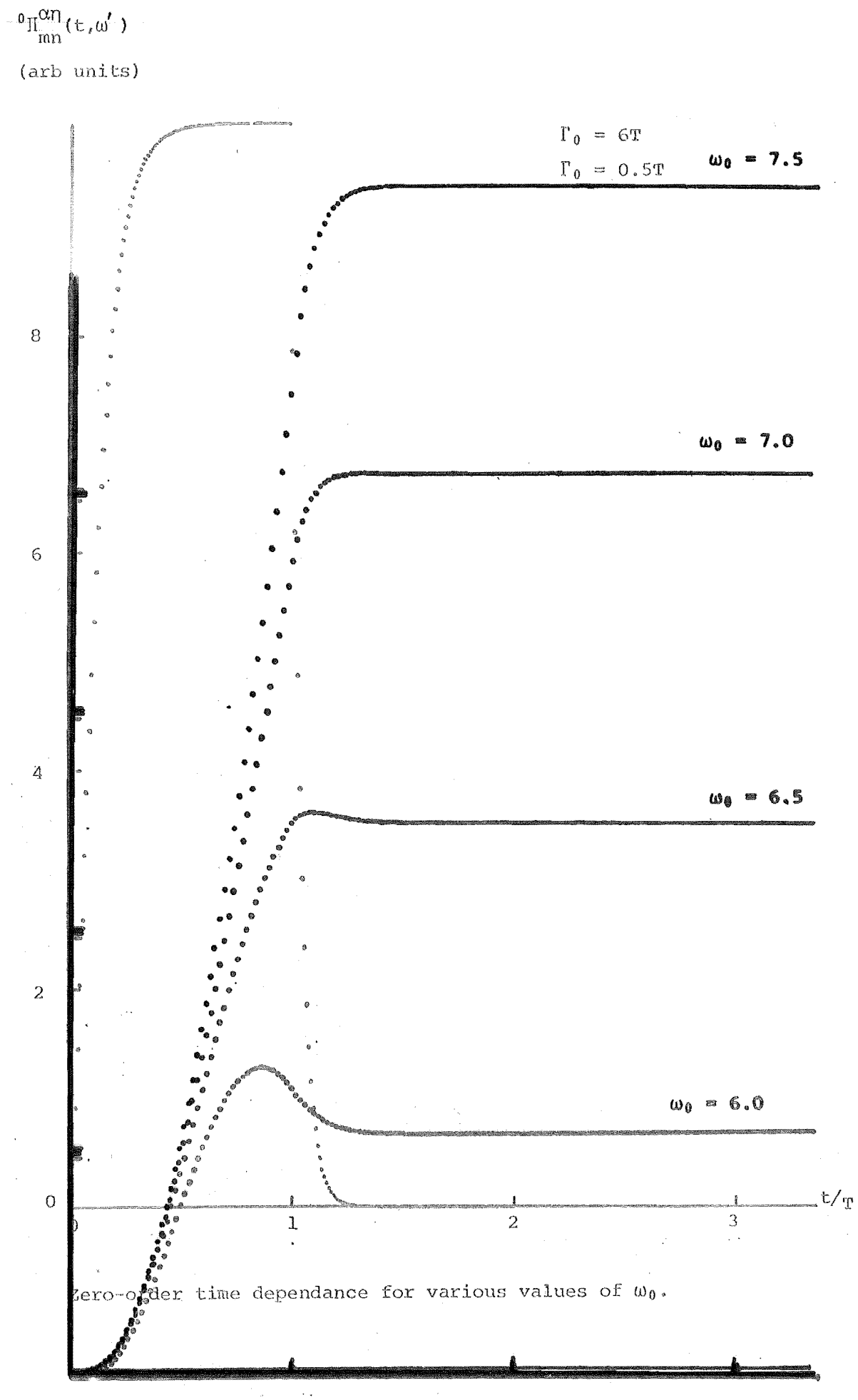

Zero-order time dependance for various values of ω_0.

physically as including processes by which the initial, final and intermediate states can decay and hence limit their lifetime. These are reflected in both the decay of the spectrum with time and the non-zero width of the Raman lineshape.

7.5 Dressed Time Dependence

Evaluating the contributions of the diagrams of figure 6.11 to $T(t,\omega')$ we obtain

$$T_{\alpha\beta\eta\zeta}(t,\omega') = f_B(-\omega'_B) \int_{-\infty}^{\infty} dx[f_D(x)-f_D(x+\omega')] \sum_{mn} L_m(x)$$

$$L_n(x+\omega') \; {}^0\Pi_{mn}^{\alpha\eta}(t,x,\omega') \left[{}^0\Pi_{mn}^{\beta\zeta}(t,x,\omega')\right]^* \qquad (7.13)$$

where the time dependent function is defined by

$${}^0\Pi_{mn}^{\alpha\eta}(t,x,\omega') = \int_{-\infty}^{\infty} \frac{d\xi}{2\pi} S(\xi) e^{-i(\xi+\omega_0)(t-\bar{R}/c)} \; {}^0P_{mn}(x,\xi+\omega_0+i\delta) \qquad (7.14)$$

with ${}^0P_{mn}^{\alpha\eta}(x,i\omega_1)$ defined by (6.14) but with ω_t replaced by ω'.

We again can use the lorentzian approximation to enable the integral over x to be performed resulting in the expression

$$T_{\alpha\beta\eta\zeta}(t,\omega') = f_B(-\omega')(\bar{\rho}_m-\bar{\rho}_n) \frac{(\gamma_m+\gamma_n)/\pi}{(\omega'+\delta_m-\delta_n)^2+(\gamma_m+\gamma_n)^2}$$

$${}^0\Pi_{mn}^{\alpha\eta}(t,\bar{\lambda}_m,\omega') \left[{}^0\Pi_{mn}^{\beta\zeta}(t,\bar{\lambda}_m,\omega')\right]^* \qquad (7.15)$$

7.5.1 Quasi-steady state scattering

To obtain the quasi-steady state scattering time dependence (7.9) we need only substitute $\omega' = \omega_t (=\omega_0-\omega)$ in (7.15). In this particular case we would be able to resolve the lorentzian lineshape because of the small frequency resolution. The time dependence is given by the function ${}^0\Pi_{mn}(t,\bar{\lambda}_m,\omega_t)$ which is evaluated in appendix 7B.

The time dependence is seen to be a sum of two parts which result from

Figure 7.4(b)

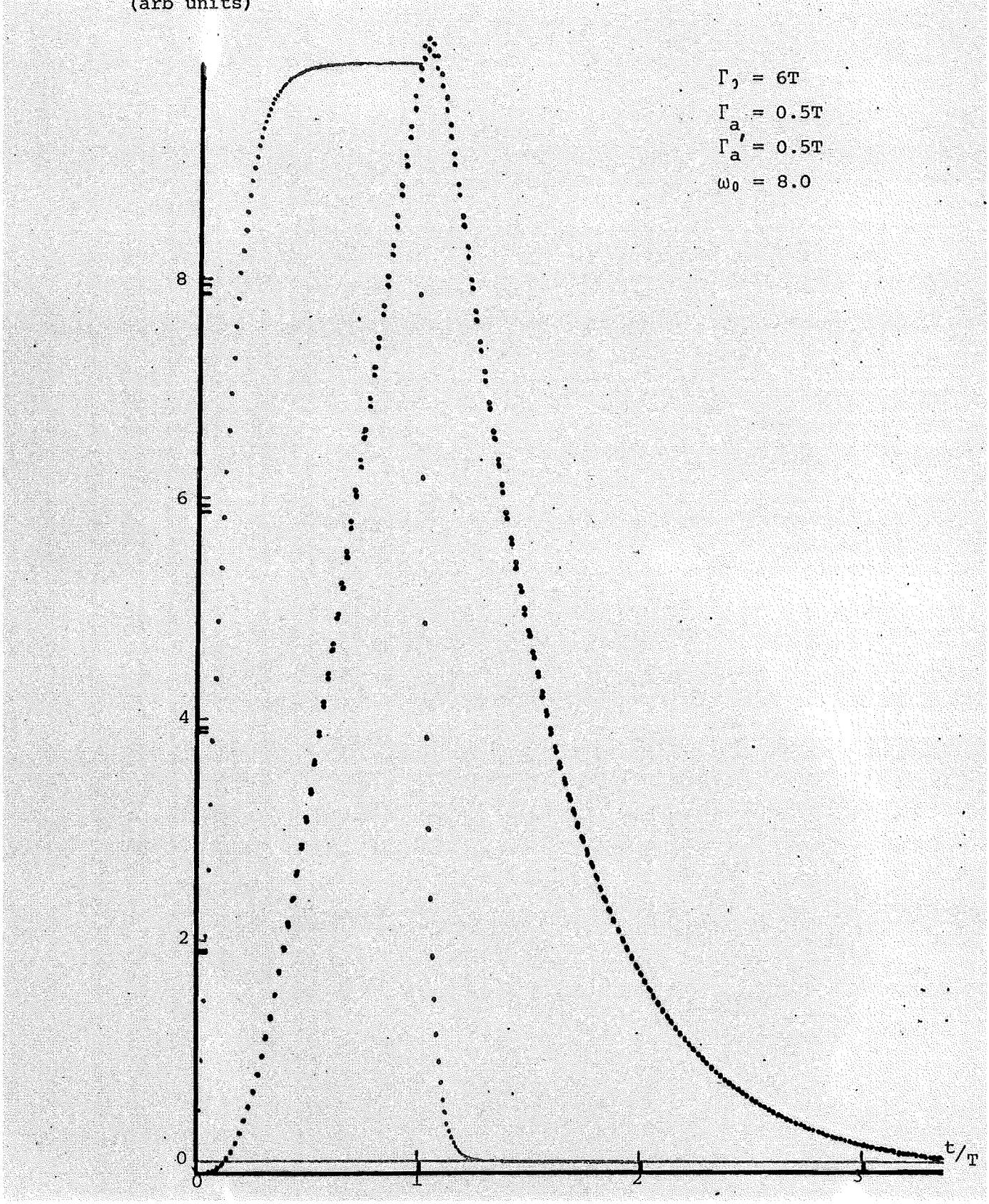

Comparison of time dependance when only first term in sum overs s is chosen (figure 7.46) relative to that when both are chosen (figure 7.4c).

the two contributions to ${}^0P_{mn}(\bar{\lambda}_m, i\omega_1)$ (cf (6.14)). Each of these contains a sum over (virtual) intermediate states (labelled a). Resonant scattering occurs when the incident laser frequency ω_0 closely matches the energy difference $\delta_a - \delta_m$ for some particular a, say a_r, in the sum over intermediate states. (If the intermediate levels are closely spaced then it is possible that a number of levels are close to resonance. We shall not consider this possibility but the following discussion could be generalized to include them simply by expressing the output as a sum of the contribution from each of these terms). Close to resonance the contribution to the sum over a will be dominated by this term and it is an excellent approximation to restrict our attention to this term. Furthermore the first part of this term will give a much larger contribution than the second part and it is a good approximation to only consider the contribution of this first term. For this reason Kusunoki (1976) only considers the contribution of diagram 6.11a in his analysis of resonant scattering from gas molecules. In figure 7.4 we have plotted the time-dependence for the model of § 7.2 (cf figure 7.2) near resonance (ω_0=8) comparing the contribution from the first part only (figure 7.4b) and that with both parts (figure 7.4c). For this system this approximation is clearly justified as the two plots are almost identical. Within the approximation the form of ${}^0\Pi^{\alpha\eta}_{mn}(t,\bar{\lambda}_m,\omega')$ is

$$
{}^0\Pi^{\alpha\eta}_{mn}(t,\bar{\lambda}_m,\omega') = \frac{M^{\alpha}_{ma}\, M^{\eta}_{an}}{(\Delta_a+i\gamma_a)(\Delta_a+i\gamma_a-i\Gamma_0)} \begin{cases} 0 & t<t_- \\ (\Delta_a+i\gamma a)\left[1-e^{-\Gamma_0(t-t_-)}\right] & \\ -i\Gamma_0\left[1-e^{-(\gamma_a-i\Delta_a)(t-t_-)}\right] & t_-<t<t_+ \\ (\Delta_a+i\gamma_a)\left[1-e^{-\Gamma_0 T}\right]e^{-\Gamma_0(t-t_+)} & \\ -i\Gamma_0\left[1-e^{-(\gamma_a-i\Delta_a)T}\right]e^{-(\gamma_a-i\Delta_a)(t-t_+)} & t>t_+ \end{cases}
$$

where $\Delta_a = \omega_0+\delta_m-\delta_a$ and $t_\pm = \bar{R}/c \pm T/2$.

Equation (7.16) which gives the quasi-steady state scattering ($\omega' \to \omega_t$) consists of two parts. One has the characteristic time rise and decay of the laser pulse (Γ^0), while the other has that of the width of the

intermediate state (γ_a). For any realistic system we have

$$\gamma_a << \Gamma_0 \tag{7.17}$$

so that the second term has a much slower rise and decay rate. The relative magnitudes of these two terms are given by the factors $(\Delta_a+i\gamma_a)$ and $i\Gamma_0$ respectively. On resonance ($\Delta_a=0$) we see from (7.17) that the term with time constant γ_a will dominate, while far from resonance ($\Delta_a \gtrsim \Gamma_0$) the term that follows the laser pulse will dominate. This feature is clearly seen in the time dependent data of Williams *et.al.* (1974) which we have reproduced in figure 7.5.

Their experiment was performed in the transient regime and because ${}^0\Pi_{mn}(t,\bar{\lambda}_m,\omega')$ (cf (7.16)) is independent of ω' the time and frequency dependences of (7.13) separate with (7.16) giving the time dependence of the whole spectrum.

7.5.2 Transient Scattering

To obtain the frequency dependence for the transient regime we combine (7.15) and (5.49) giving the convolution

$$\int_{-\infty}^{\infty} d\omega' \, U(\omega'-\omega_t) f_B(-\omega') \quad \frac{(\gamma_m+\gamma_n)/\pi}{(\omega'+\delta_m-\delta_n)^2+(\gamma_m+\gamma_n)^2} \tag{7.18}$$

The function $U(\omega'-\omega_t)$ has a width $\Delta\omega$, the minimum frequency resolution. If $\Delta\omega >> \gamma_m+\gamma_n$ then we can approximate the lorentzian in (7.18) by a delta function and the lineshape is given by the function $U(\delta_n-\delta_m-\omega_t)$. However for values of $\Delta\omega \sim \gamma_m+\gamma_n$ then (7.18) is approximately the integrated intensity over the spectral line which is the situation for Williams *et.al.* experiment.

The time dependence (7.16) exhibits an oscillatory type factor $\exp(i\Delta_a t)$ which we shall refer to as 'ringing'. The period of these oscillations is Δ_a^{-1} and hence depends on the amount of detuning from exact resonance. For the experimental situation of WR ($\Delta_a \simeq 2.2$ GHz) such oscillations would be expected to have a period 0.5 ns. As such

Figure 7.5 Experimental data of Williams *et.al.* (1974).

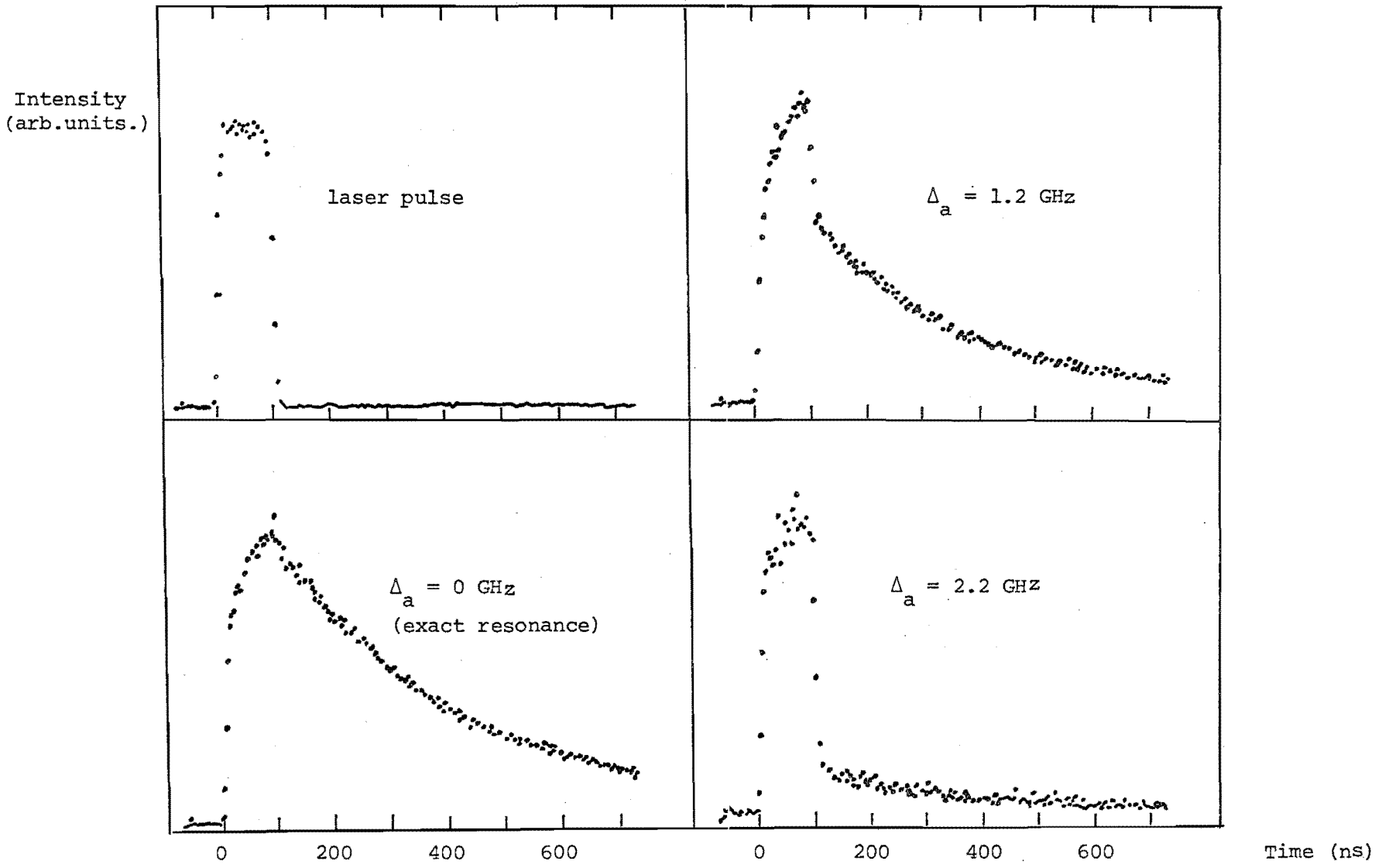

they are too rapid to be resolved by their apparatus and hence are not apparent in their time dependent plots (figure 7.5).

Closer to resonance the 'ringing' period increases and we might expect it to be more apparent. In figure 7.6 we have plotted the output (7.10) from the model system of figure 7.2 for values of $\Delta_a^{-1} \simeq \Gamma_a$. The ringing behaviour is clearly apparent in these plots and we might expect them to be observable experimentally. Restrictions on our ability to resolve such oscillations result from a number of effects that would tend to 'wash' them out. If the dimensions of the scattering region, Δs, is such that it contains more than a single scattering centre, the output from each will not be in phase. This restricts us to regions such that $\Delta s << c\Delta_a^{-1}$ if 'ringing' is to be observed. Another restriction is that any variations in the energy level differences and hence Δ_a between the various ions, be much smaller than Δ_a. Such variations could for example arise from changes in the crystal field environment due to strains in the crystal for solids or from Doppler shifts due to velocity variations in gases.

The 'ringing' effects are to be found in other time dependent theories of Raman scattering, (Huber 1970 O Berg *et.al.* 1974 , Friedman and Hochstrasser 1974 , Mukamel *et.al.* 1975, 1976 and Kimble and Mandel 1975 especially figures 1 - 4), however only two of these make any comments on the possible observation of these. O Berg *et.al.* claim that although the absorption resonance was Doppler broadened and thus would tend to "cause an incoherent superposition of the oscillatory decays and average them out", such oscillations can be seen in the experimental results of W.R. A study of figure 7.5 shows that such oscillations are not clearly resolved, (especially considering our earlier comments regarding their equipment resolution), but it could explain some of the scatter in the long decaying components. Mukamel and Jortner (1975) make the comment that for their system "the oscillatory interference contribution is smeared out due to averaging over Δ_a".

Optimum conditions for the observation of 'ringing' is a system where the scattering is from a single scattering centre (or at least a number

Figure 7.6

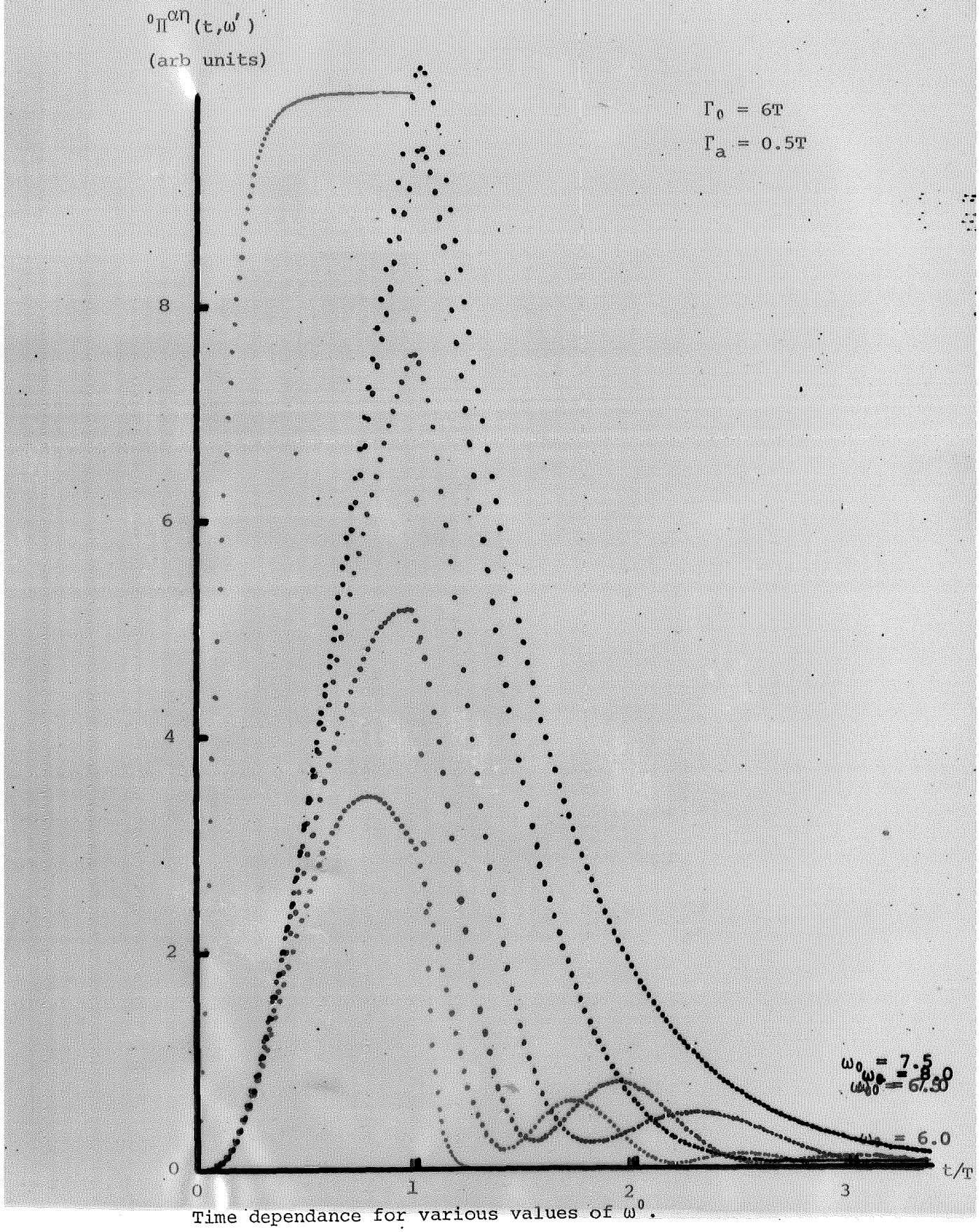

Time dependance for various values of ω^0.

of similar, localised ions), and is detected using a system with adequate time resolution to measure the oscillations with period Δ_a^{-1}. Because previous experiments did not realize these conditions they do not exhibit any clear evidence for this effect, but we expect a suitably designed experiment to observe 'ringing'.

7.6 Time Dependence of General Raman Spectrum

It is a simple matter to generalize the results of the previous section to include the contribution from all diagrams represented in figures 6.12 - 6.13. This is achieved by allowing ${}^0P^{\alpha\eta}_{mn}(x,\xi+\omega_0+i\delta)$ of (7.14) to be replaced by ${}^fP^{\alpha\eta}_{mn}(x,\xi+\omega_0+i\delta)$ defined in (6.16) - (6.17) giving the more general version of (7.15).

$$T_{\alpha\beta\eta\zeta}(t,\omega') = f_B(-\omega')(\bar{\rho}_m - \bar{\rho}_n) \quad \frac{(\gamma_m+\gamma_n)/\pi}{(\omega'+\delta_m-\delta_n)^2 + (\gamma_m+\gamma_n)^2}$$

$$f\Pi^{\alpha\eta}_{mn}(t,\bar{\lambda}_m,\omega') \left[f\Pi^{\beta\zeta}_{mn}(t,\bar{\lambda}_m,\omega') \right]^* \tag{7.19}$$

with

$$f\Pi^{\alpha\eta}_{mn}(t,\bar{\lambda}_m,\omega') = \int_{-\infty}^{\infty} \frac{d\omega'}{2\pi} S(\xi) e^{-i(\xi+\omega_0)(t-\bar{R}/c)} \; fP^{\alpha\eta}_{mn}(x,\xi+\omega_0+i\delta) \tag{7.20}$$

The integral over ξ in (7.20) is evaluated by converting to a contour that is closed either in the upper or lower half plane. Each term of $fP^{\alpha\eta}_{mn}(x,\xi+\omega_0+i\delta)$ contributes poles to the lower half plane only. This is equivalent to the causal property (cf Appendix 7B).

$$\frac{1}{\phi_0}\frac{\partial^2\phi}{\partial\omega\partial\Omega} = 0 \quad \text{for} \quad t < t_- = T/2 - \bar{R}/c. \tag{7.21}$$

Each pole is a distance γ_i from the real axis, where γ_i is the width of an intermediate level, and this results in yet another rising ($t_- < t < t_+$) and decaying ($t > t_+$) exponential component in the time dependence of $f\Pi(t,\bar{\lambda}_m,\omega')$. However only the lower order (in V^k_{ab}) terms of $P^{\alpha\eta}_{mn}$ are expected to result in large contributions and near resonance an even

smaller number of these will be dominant.

Kusunoki (1976) evaluated the contribution from the diagram of figure 7.7

Figure 7.7

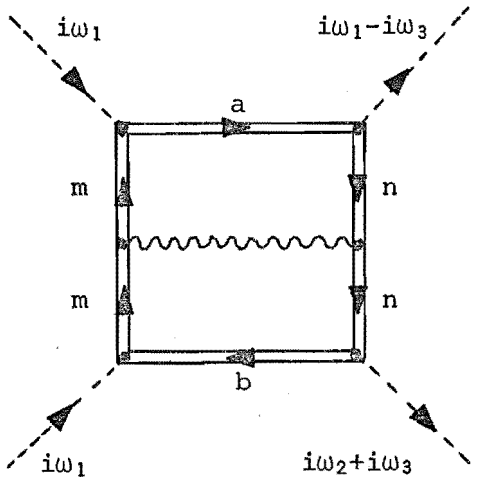

The contribution of this diagram is contained in the present formalism by the first term of ${}^{2}P_{mn}^{\alpha\eta}$ is (6.17) (cf diagram 6.13c) and is evaluated in appendix 7B.

7.7 Time-Dependence of One-Phonon Scattering Spectrum

Other diagrams evaluating by Kusunoki (1976) are those presented in figure 7.8

Figure 7.8

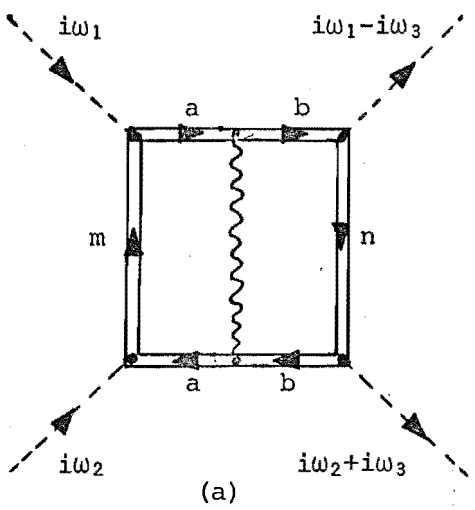

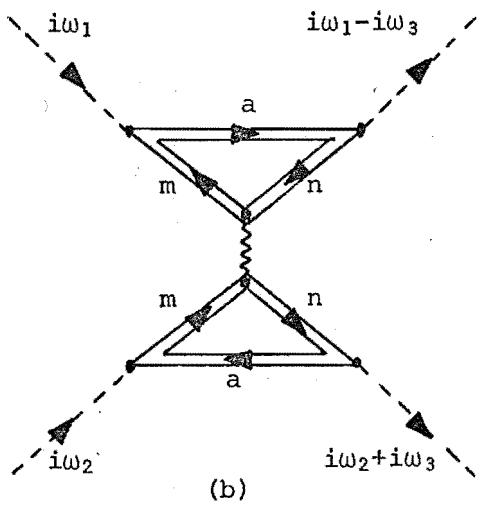

In §5.6 we argued that for the single ion spectrum only diagrams containing one closed level loop could give a non-vanishing contribution and hence there can be no contribution from diagram 7.8b. In the analysis of Kusunoki he limited himself to one scattering molecule and the Hamiltonian he chooses for the description of the molecular level system is completely equivalent to our (3.2). In his analysis he did not realize the consequences of this mapping and so erroneously included the diagram 7.8b. Another consequence of his not applying the limiting procedure (2.54) is that his level populations remain expressed in terms of Fermi-Dirac functions $f_D(\varepsilon_i)$ rather than Maxwell-Boltzman (ρ_i) factors as in (3.16).

In chapter 6 we associated diagram 7.8a, along with all diagrams of figure 6.15, with one-phonon Raman scattering. In this section we evaluate the time dependence of this spectrum.

Evaluating the contribution of these diagrams to (5.50) gives

$$T_{\alpha\beta\eta\zeta}(t,\omega') \simeq f_B(-\omega') \sum_{mn} \sum_{k} \left\{ \bar{\rho}_m \binom{n_k}{n_{k+1}} - \bar{\rho}_n \binom{n_{k+1}}{n_k} \right\}$$

$$\frac{(\gamma_m+\gamma_n)/\pi}{(\omega'+\delta_m-\delta_n\pm\omega_k)^2+(\gamma_m+\gamma_n)^2} \, {}^{f}\Theta^{\alpha\eta}_{mn}(t,\bar{\lambda}_m,\omega',\pm\omega_k) \left[{}^{f}\Theta^{\beta\zeta}_{mn}(t,\bar{\lambda}_m,\omega',\pm\omega_k) \right]^* \tag{7.22}$$

where

$${}^{f}\Theta^{\alpha\eta}_{mn}(t,x,\omega',\pm\omega_k) = \int_{-\infty}^{\infty} \frac{d\xi}{2\pi} S(\xi) e^{-i(\xi+\omega_0)(t-\bar{R}/c)} \, {}^{f}\Omega^{\alpha\eta}_{mn}(x,\xi+\omega_0+i\delta,\pm\omega_k) \tag{7.23}$$

where ${}^{f}\Omega^{\alpha\eta}_{mn}$ is defined by (6.22). The time dependence of the term that contains the diagram 7.8a evaluated by Kusunoki (cf diagram 6.15e) is evaluated in appendix 7C.

Equation (7.22) (with ω' replaced by ω_t) gives the quasi-steady state time dependence. To obtain the transient time dependence, (7.22) must be convolved with $U(\omega' - \omega_t)$ in (5.49) which will have the effect of broadening the lorentzian by an amount dependent on the minimum frequency resolution $\Delta\omega$.

With sufficient resolution it would be possible to measure the time dependence of the NPL and the one-phonon sideband separately. The expressions for these time dependences, (appendix 7B.4 and 7B.11), indicate that these would have different dependences. Although it is not possible to give a simple statement about the qualitative differences in general, on exact resonance the one-phonon sideband has a larger long-lived component, (relative to the short component), than the NPL. Indeed the relative magnitudes of the long and short components in the one-phonon sideband vary throughout the sideband. We hope that these predictions will encourage experiments to be conducted to study the relative time dependence of different parts of the Raman spectrum.

7.8 Diagram Interpretation

The formalism of Kusunoki (1976) and ours are very similar even though we consider scattering from impurity ions in solids and he deals with scattering from gas molecules. The close parallel arises because he deals with a single molecule whose levels he expresses in terms of fermion operators analogous to our $a^{\dagger}_{im}$, a_{im} operators, and also couples the fermion operators to a boson bath to represent the effect of molecular collisions, which is analogous to our ion-phonon interaction. This similarity allows us to make some comments on Kusunoki's work.

At low pressures Kusunoki (1976) identified the various diagrams contributing to the spectrum as Raman scattering (RS), collision induced redistribution scattering (CIRS), final state redistribution scattering (FRS) and final state transfer scattering (FTS) as indicated in figure 7.8. (The diagrams and intermediate states are restricted to those that contain the relevant resonance (cf 7.5.1)). Kusunoki interprets these in terms of the conventional terms discussed in § 7.1 claiming that RRS is equivalent to RS (figure 7.9a), RF is equivalent to CIRS (figure 7.9b) and that the resonant spectrum contains these contributions plus the interference between them represented by FRS (figure 7.9c) and FTS (figure 7.9d).

Figure 7.9

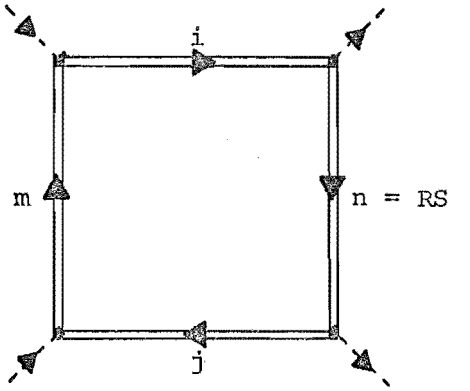

(a)

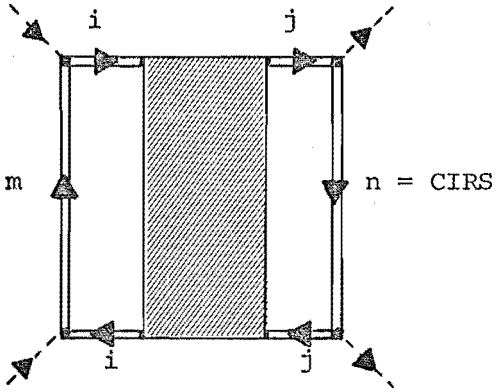

(b)

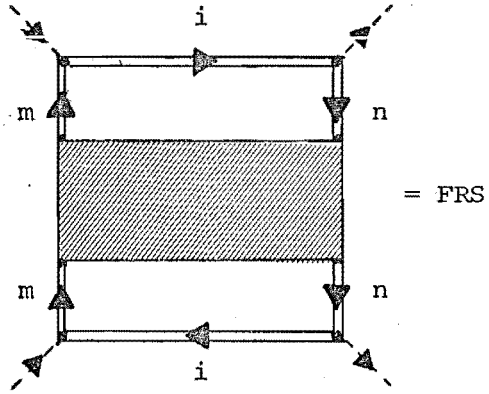

(c)

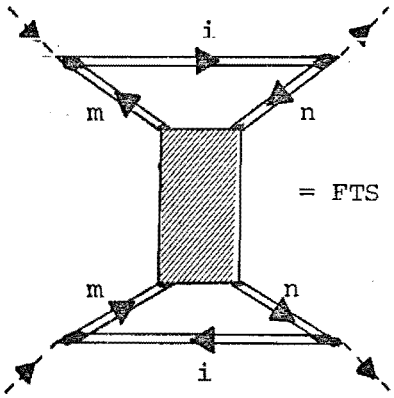

(d)

where

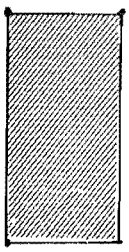

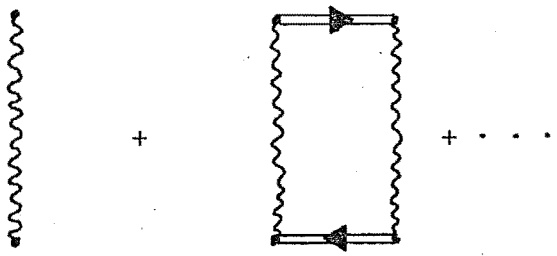

(e)

Although we are not concerned to offer yet another distinction between RRS and RF we are forced into concluding, as a result of our work, that Kusunoki's prescriptions are inadequate.

In § 7.7 we pointed out that as a consequence of the limiting procedure (3.54), diagram 7.9d, identified as FTS vanishes identically. This results because the diagram contains two fermion loops both referring to the same molecule. To obtain a non-vanishing contribution from such a diagram the loops must refer to two distinct molecules. In our formalism such contributions will be negligible for separated ions (cf chapter 4). Kusunoki includes only final state broadening in his diagrams (i.e. assumes $\Gamma_m = 0$); initial state broadening will also influence the spectrum and has been included in our analysis.

We suggest different diagram identifications for FRS and FTS. Defining FRS as the effect on the spectrum of quasi-elastic collisions off the final state, then diagrams such as figure 7.10a will contribute. Initial state collisions (figure 7.10b) and interference effects with initial (figure 7.10c) and intermediate (figure 7.10d,e) states will also give contributions to the resonance spectrum. All these contributions have been included in (7.20) derived in § 7.6. Also included in this expression are diagrams like figure 7.10f which we regard as contributing to FTS, defined as the effect of collisions which take the molecule from the final state n into a different level j. The Raman scattering spectrum includes all these terms and hence we do not support Kusunoki's prescription for distinguishing RRS and RF in terms of certain classes of these diagrams.

The diagrams identified by Kusunoki as CIRS, we have identified as one-, two- and multi-phonon Raman scattering (cf (7.22)). The fluorescence spectrum is peaked at $\omega = \delta_i - \delta_n$ where i is the resonant intermediate state, while the above contributions are peaked at $\omega=\omega_0+\delta_m-\delta_n \pm\omega_k \pm\omega_\ell \cdots\cdots$ (cf (7.22)) and hence on resonance ($\omega_0=\delta_i-\delta_m$) at $\omega=\delta_i-\delta_n\pm\omega_k\pm\omega_\ell\cdots\cdots$. These contributions are shifted by the phonon frequencies ($\pm\omega_k\pm\omega_\ell \cdots$) from the fluorescence spectrum and thus we do not agree with Kusunoki's interpretation that these diagrams are related to fluorescence.

Figure 7.10

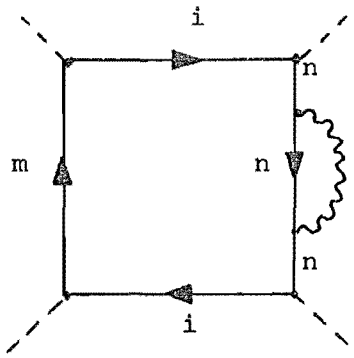

(a)

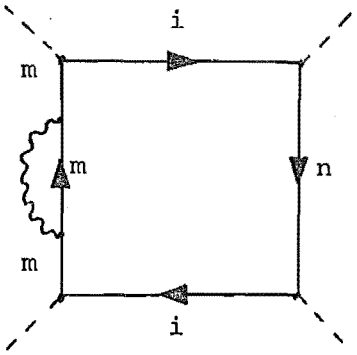

(b)

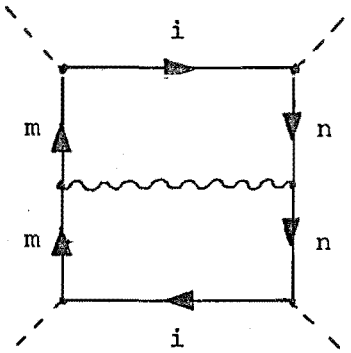

(c)

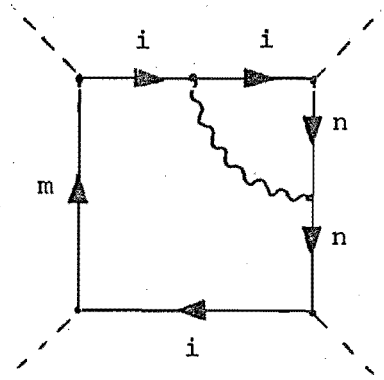

(d)

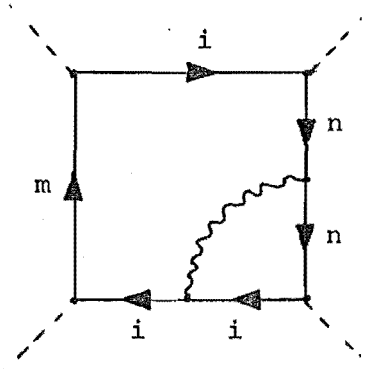

(e)

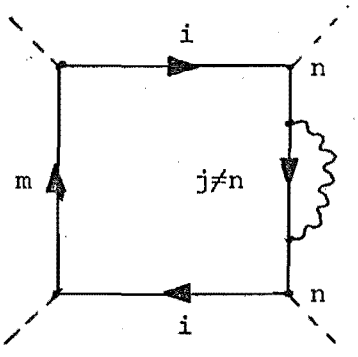

(f)

We conclude that the formalism we present involving the use of the P and Π (7.14) factors for a description of the time-dependence is an improvement on the approach employed by Kusunoki which involves evaluating the time-dependence of each diagram separately. His neglect of the initial state width (γ_m=0), and in places such as the calculation of the CIRS time-dependence the final state width (γ_n=0) also, will not be valid in some experimental situations. It would predict narrower line widths than the present work where these are included. By including only resonant diagrams his results are restricted in application to near resonance with a well separated level while the present work is also applicable to the far from resonance regime. Private correspondence (1977) has indicated that Kusunoki did not have a clear understanding of the physical significance of his diagrams. This resulted in his including the vanishing diagram 7.7b and presenting rather unphysical definitions of the FRS and FTS processes which this work has corrected.

CHAPTER 8 : NUMERICAL RESULTS

8.1 Introduction

As a result of the generality of the formalism we have presented, to obtain lineshapes the resulting expressions have usually contained complex convolutions (e.g. (3.43), (3.45), (5.14), (5.18). To evaluate these we have used various approximations such as the "sharply peaked" or "lorentzian" approximation discussed in §3.5.1. This approximation enabled us to obtain an analytic result for the convolution, usually resulting in lorentzian type lineshapes. Because of the complexity of the functions involved a justification of the approximation is difficult by analytical means. Hence in this chapter we wish to study a model three level system and obtain the various absorption and Raman lineshapes by performing the convolution numerically and compare the results obtained with those obtained using our various approximation schemes.

8.2 The Model

The model system consists of three energy levels labelled one to three with (dimensionless) energies $\varepsilon_1 = 0.0$, $\varepsilon_2 = 1.0$ and $\varepsilon_3 = 8.0$ (cf figure 8.1)

Figure 8.1

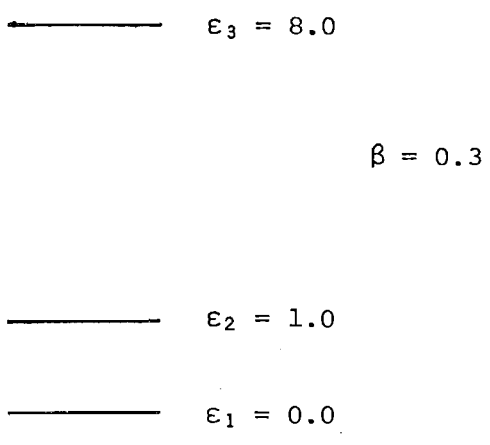

The temperature is chosen such that the parameter β takes on the value 0.3.

All level propagators are taken to be dressed but with only the second-order diagram of figure 8.2 contributing to the self-energy.

Figure 8.2

giving

$$\Sigma_m(i\omega_n) = \sum_{a=1}^{3} \sum_k \binom{n_k}{n_k+1} \frac{V^k_{ma} V^k_{am}}{i\omega_n - \varepsilon_a \pm \omega_k} \tag{8.1}$$

which upon analytic continuation and application of definition (3.32) results in shift and width functions

$$\Delta_m(x) = \sum_{a=1}^{3} \sum_k \binom{n_k}{n_k+1} V^k_{ma} V^k_{am} \frac{P}{x - \varepsilon_a \pm \omega_k} \tag{8.2}$$

$$\Gamma_m(x) = \pi \sum_{a=1}^{3} \sum_k \binom{n_k}{n_k+1} V^k_{ma} V^k_{am} \delta(x - \lambda_a \pm \omega_k) \tag{8.3}$$

where P denotes the principal value.

The sum over k in these and other expressions is evaluated by converting to an integral over phonon frequencies giving

$$\sum_k \binom{n_k}{n_k+1} (V^k)^2 \; g(\pm\omega_k) \rightarrow \int_{-\omega_D}^{+\omega_D} d\omega' \, \omega' \; D(\omega') f_B(\omega') g(\omega') \tag{8.4}$$

where $(V^k)^2$ represents two V^k_{ab} coefficients and we have used their $\omega_k^{1/2}$ dependence (cf 3.8). The function $D(\omega')$ gives the phonon density of states; because the pathological nature of the Debye density of states at the cutoff frequency ω_D causes numerical problems, a more realistic (cf Kittel 1971) density of states that approached zero more smoothly at ω_D was chosen:

$$D(\omega') = \begin{cases} \omega'^2 & |\omega'| < \frac{\omega_D}{2} \\ \frac{\omega_D^2 - \omega'^2}{3} & \frac{\omega_D}{2} < |\omega'| < \omega_D \\ 0 & |\omega'| > \omega_D \end{cases} \qquad (8.5)$$

The cutoff parameter ω_D was chosen to have the value 10.0. For simplicity the coefficients M_{ab} and V^k_{ab} were chosen independent of a and b with values

$$V_{ab} = (0.001)^{1/2} \quad \forall a,b = 1,2,3$$

$$M_{ab} = 1 \qquad \forall a,b = 1,2,3.$$

8.3 Program Details

The numerical calculations were evaluated by a program written in Burroughs extended algol and run on the University of Canterbury Burroughs 6700 computer. All integrations were performed using an adaptive Simpsons rule routine (McKeeman 1962, Lyness 1969) using a relative accuracy of 10^{-4}.

When the sum over k in (8.2) is converted to a principal value integral (8.4) then special methods are required because of the singularity at $\omega' = \varepsilon_a - x$. Three methods were investigated to evaluate these integrals.

(a) Heitlers Method:

This method is suggested by Heitler (1954) and is based on the relationship

$$\frac{P}{x} = \lim_{\varepsilon \to 0} \frac{x}{x^2+\varepsilon^2} \qquad (8.5)$$

This replaces the singular integrand by a non-singular (but sharply peaked) integrand and then the integral can be performed by means of normal methods and the limit $\varepsilon \to 0$ taken. This method however was found to be most unsatisfactory, requiring large process times for each integral and not giving very good accuracy.

(b) Symmetric Pairing Method:

This method takes advantage of the sign change at the singularity and the resulting partial cancellations from regions on either side of it to

give a rather complex finite difference formula. (Bareiss and Neuman 1965). Although this method was faster and more accurate than Heitler's method the following method was more suited to the program.

(c) Substracting out the Singularity:

The aim of this approach (Davis and Rabinowitz 1967) is to subtract out the singular part of the integrand giving two integrals; one which contains the singularity as can be performed analytically and the remaining integral is smoothly varying in the region of the old singularity enabling numerical integration to be performed easily. This method was used because it was found to be the fastest and give the most accurate results.

The lineshape expressions contain two or more nested integrations; to keep the required computation time to reasonable levels it was often necessary to evaluate the inner integrals at a number of points and then interpolate between these in evaluating the outer integrals. In such cases the program used a cubic spline routine which is demonstrated in figure 8.3 for the shift and width functions.

8.4 Absorption Lineshapes

8.4.1 No-Phonon Line

The largest contribution to the absorption spectrum comes from diagram 3.13 and is given by convolution (3.36).

Using our model we evaluated numerically the contribution from the term n=0, m=1 and obtained the points of figure 8.4. The dotted line is a least square fit to these numerical points with a lorentzian with three variable parameters;

$$\ell(x) = A \frac{B}{(x-C)^2 + B^2} \quad . \tag{8.6}$$

The best fit lorentzian has parameter values A=0.69, B=0.083, C=0.92. It can be seen that the lineshape is not exactly lorentzian but rises faster and falls slower than the best fit lorentzian. This non-lorentzian dependence appears to be mostly due to the appearance of the Fermi-Dirac

Figure 8.3 Plots of the x dependances of the shift and width functions.

The symbols Δ and 0 represent calculated points and the solid curve is a cubic spline fit to these.

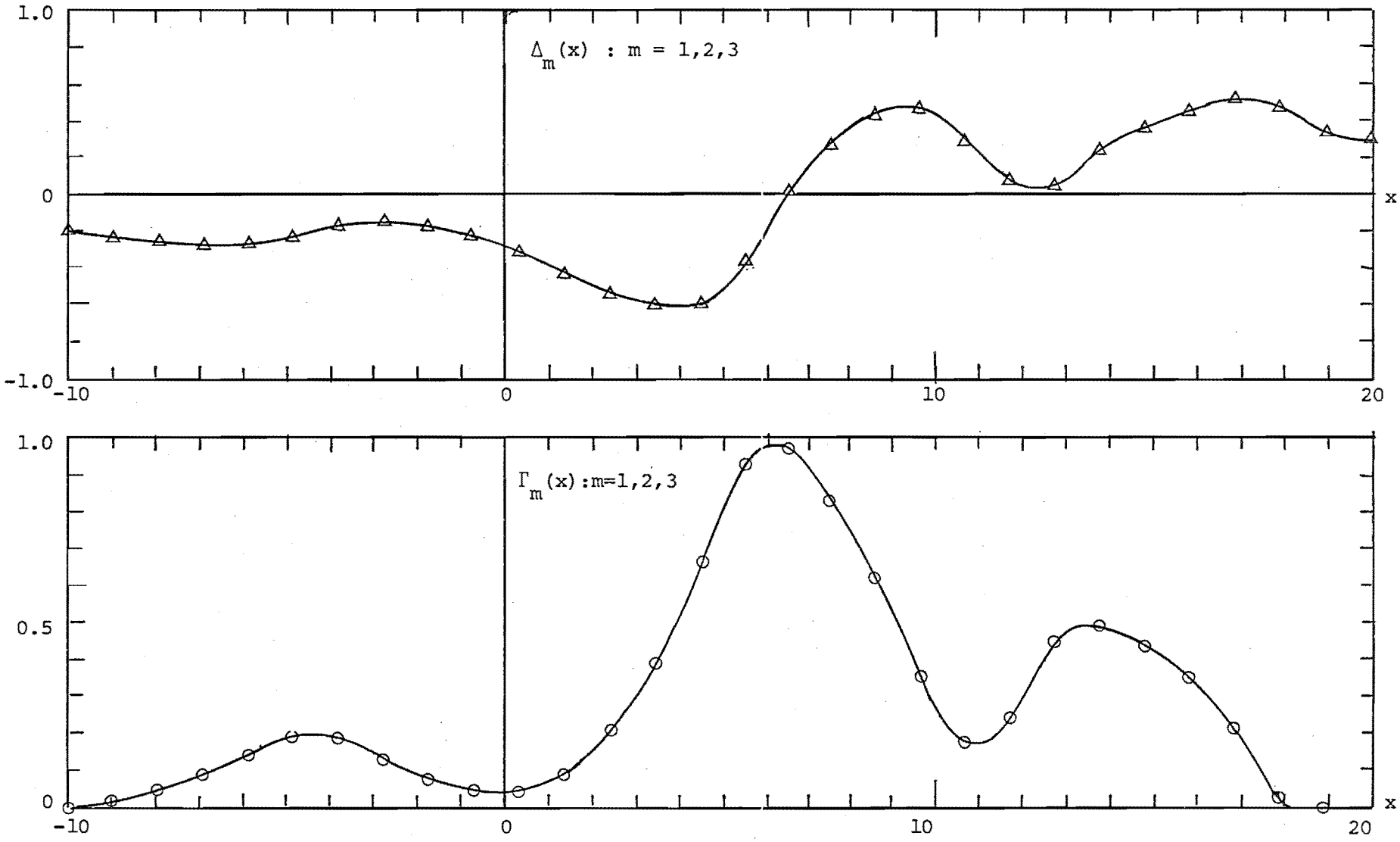

Figure 8.4

Absorption lineshape

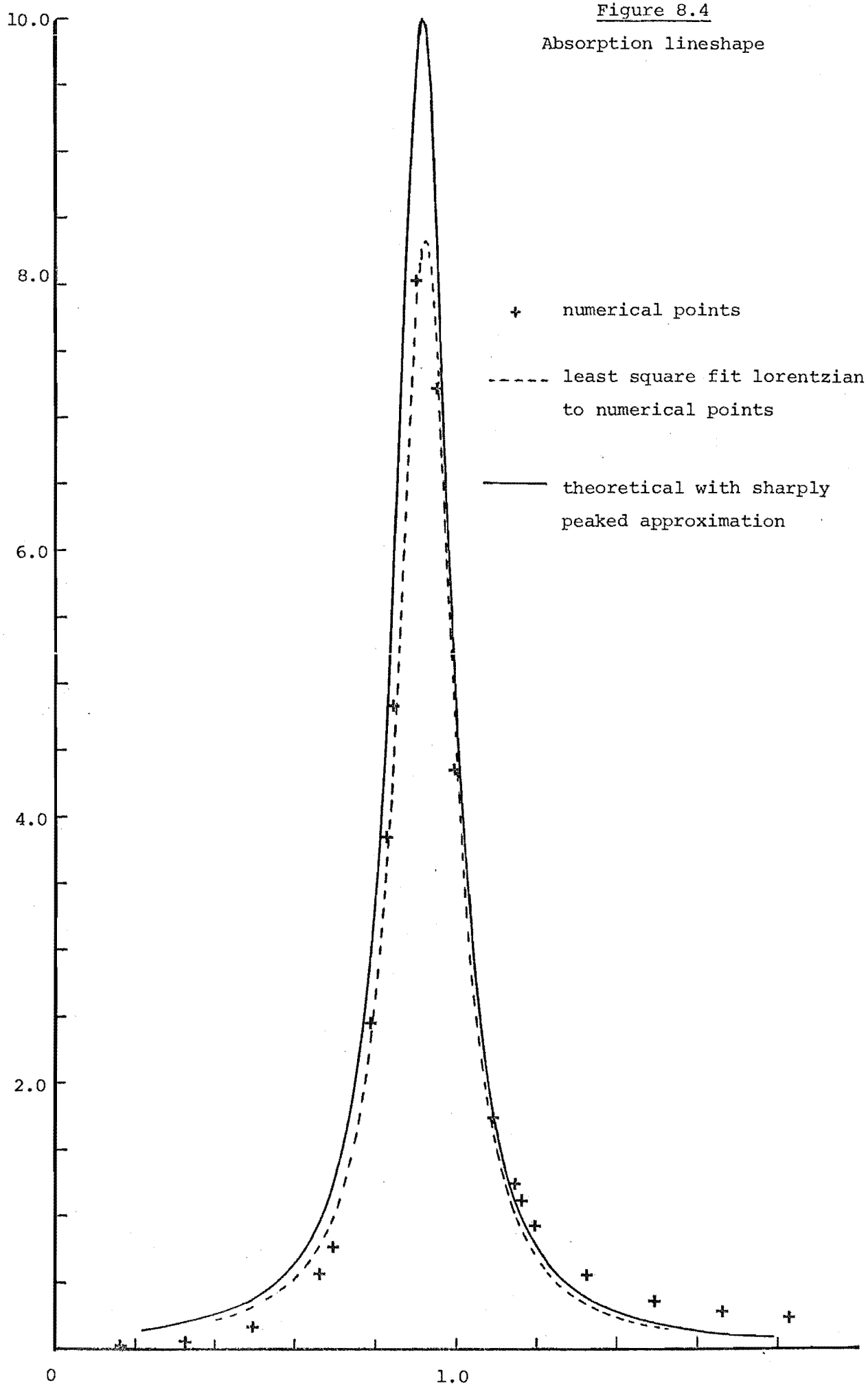

function in the integrand.

We wish to compare these numerical points with the analytical lineshape predicted by the sharply peaked approximation (3.38). Assuming the lorentzian $L_0(x)$ is peaked at the solution of $x=\Delta_0(x)$ defining $\bar{0}$ and similarly $\bar{1}$ being given by the solution of $x = 1 + \Delta_1(x)$ we obtain the following values by means of a graphical solution (figure 8.5)

$$\begin{aligned} \bar{0} &= -0.2678 \\ \bar{1} &= \ 0.6451 \end{aligned} \tag{8.7}$$

giving the parameters $\delta_0 = -0.2678$, $\delta_1 = 0.6451$ and $\gamma_0 = 0.03979$, $\gamma_1 = 0.04946$. This then results in a lorentzian peaked at $C = \delta_1-\delta_0 = 0.91$ with width $B = \gamma_0+\gamma_1 = 0.089$. Although this position C agrees well with the numerical points least square fit, the width B does not.

In an attempt to obtain better agreement between the numerical and analytic lineshapes an alternative method of obtaining the parameters $\delta_0,\delta_1,\gamma_0$ and γ_1 was investigated. The full functions $L_0(x)$ and $L_1(x)$ were calculated and these parameters were obtained from a least square fit of a lorentzian to each of these curves (figure 8.6). These gave the values $\delta_0 = -0.2678$, $\delta_1 = 0.6449$ which are essentially the same as the other approximation scheme but give $\gamma_0 = 0.3681$, $\gamma_1 = 0.0445$ which give a better estimate of the lineshape width $B = \gamma_0 + \gamma_1 = 0.081$. Using these parameters the analytical lorentzian is plotted on the same graph as the numerical points (figure 8.4 - solid curve). This is seen to be a reasonable approximation to the lineshape and justifies the use of the sharply peaked approximation to obtain the approximate position and width of the lineshape. However the full numerical calculation would be required for accurate lineshape determination.

We then investigated the effect of generalizing $P_{mn}(x,y)$ from M_{mn} to the first two terms of (3.44) (cf first two diagrams of figure 3.18b). Defining

$$^2P_{01}(x,\omega_0) = \sum_{ab=1}^{3} \sum_k \binom{n_k}{n_{k+1}} V^k_{0a} \, M_{ab} \, V^k_{b1} \, A_a(x+\omega_0\pm\omega_k) A_b(x\pm\omega_k) \tag{8.8}$$

Figure 8.5 Graphical solution of transcendental equations

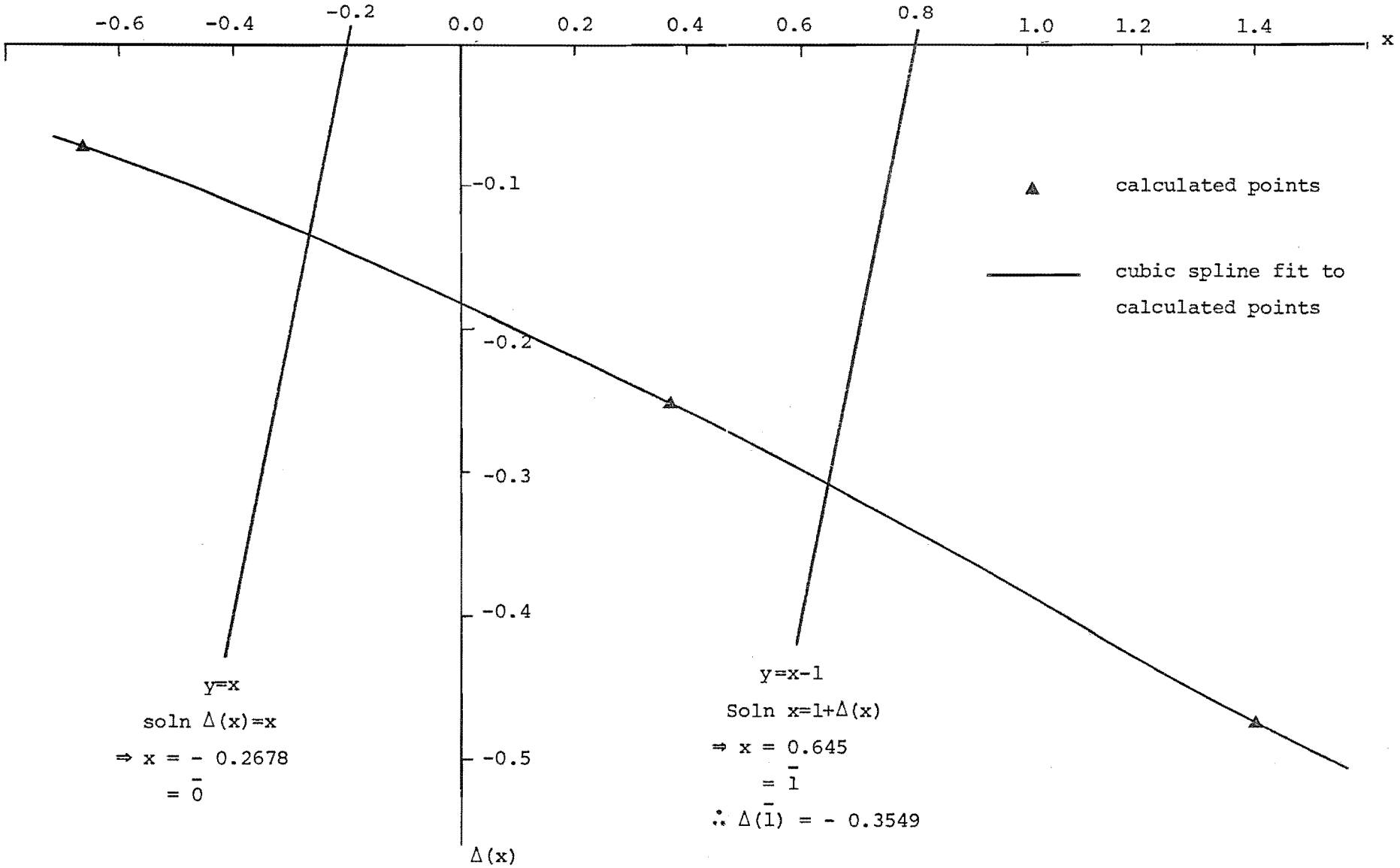

Figure 8.6

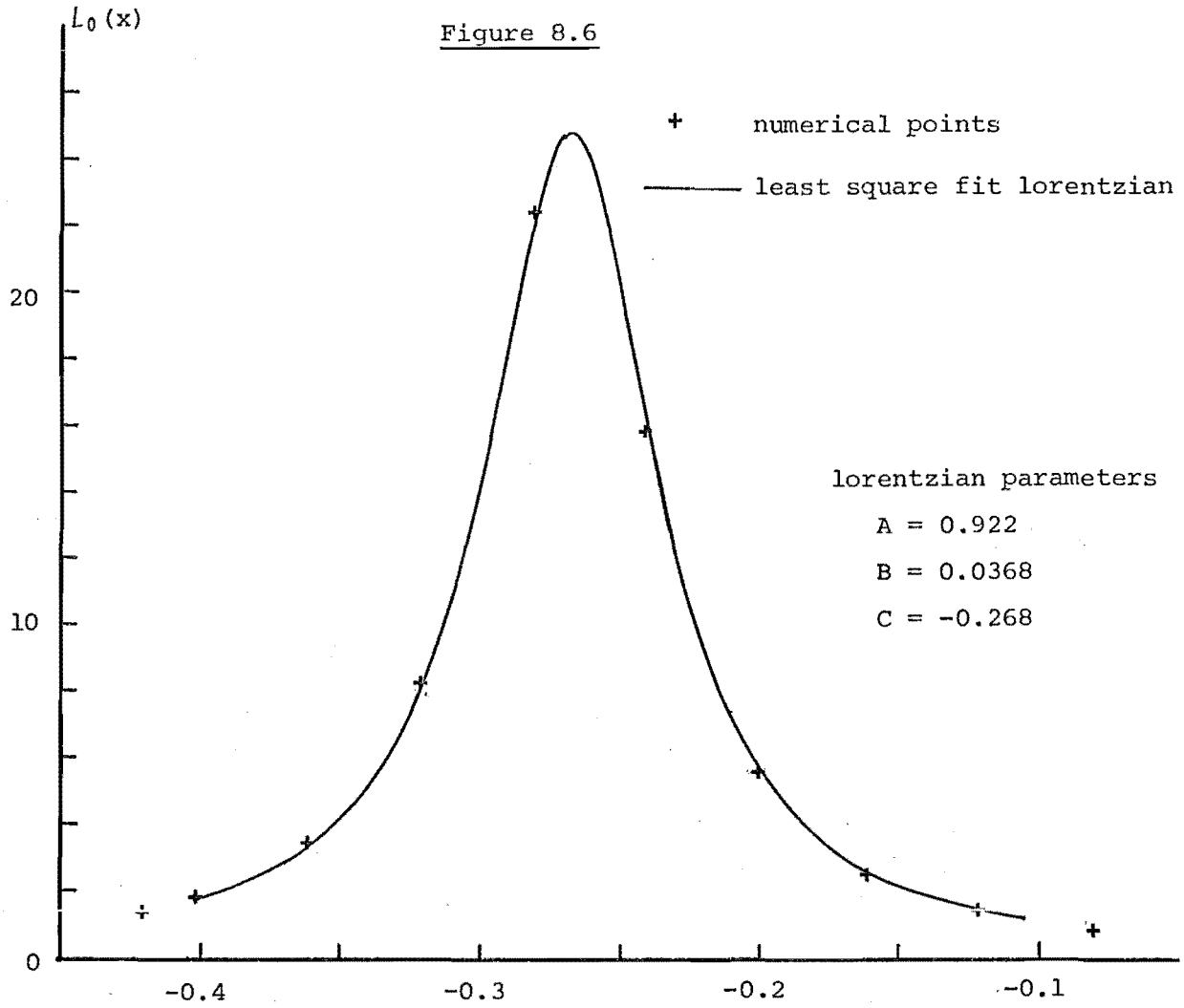
$L_0(x)$
numerical points
least square fit lorentzian
lorentzian parameters
A = 0.922
B = 0.0368
C = -0.268
20
10
0
-0.4
-0.3
-0.2
-0.1

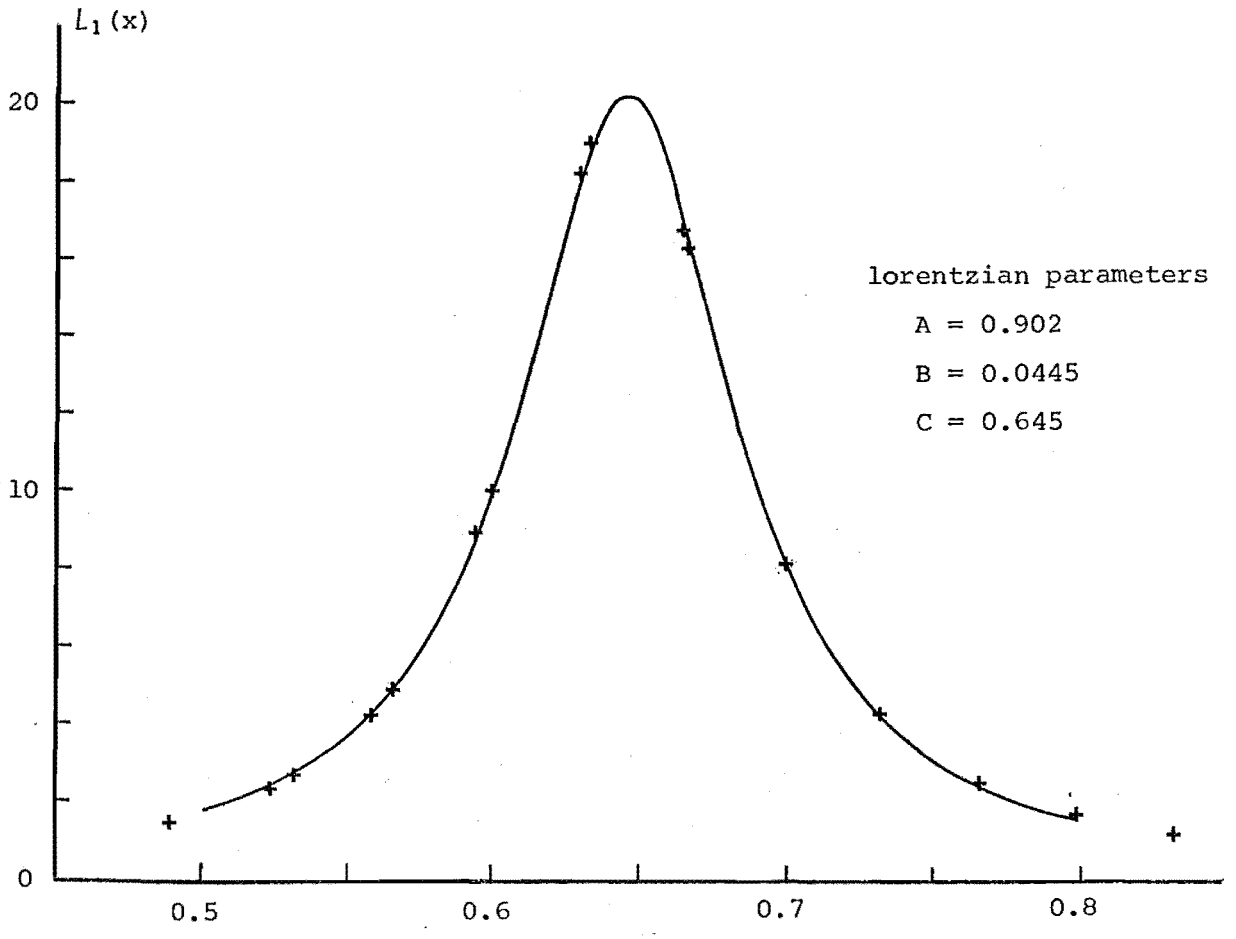
$L_1(x)$
lorentzian parameters
A = 0.902
B = 0.0445
C = 0.645
20
10
0
0.5
0.6
0.7
0.8

We studied the cross terms of $|M_{01}+{}^2P_{01}|^2$ with the structure

$$\int_{-\infty}^{\infty} dx\left[f_D(x) - f_D(x+\omega_0)\right] L_0(x) L_1(x+\omega_0) \left[M_{01}\,{}^2P_{10}\ (x,\omega_0) + {}^2P_{01}(x,\omega_0)\ M_{10}\right] \tag{8.9}$$

This lineshape (8.9) is compared with the previous one by normalizing them and plotting on the same graph (figure 8.7 points ● and O respectively). It is clear that the contribution to the lineshape of these two is essentially identical and has only altered the magnitude and not the shape of the line. The normalization of these is that the original lineshape is multiplied by 8.04 while that arising from (8.9) is multiplied by 3.06 and hence results in a significant contribution to the lineshape.

8.4.2 One-phonon Line

When the convolution giving the basic contribution to the no-phonon line (N.P.L.) ((3.36): diagram 3.13) was evaluated analytically giving the pure lorentzian (3.38), not only was the asymmetrical nature of the lineshape lost but also the one-phonon sidebands. That these should appear is easily seen in figure 8.8 where the self-energy part is used explicitly and compared with the one-phonon sideband diagram (3.21).

Figure 8.8

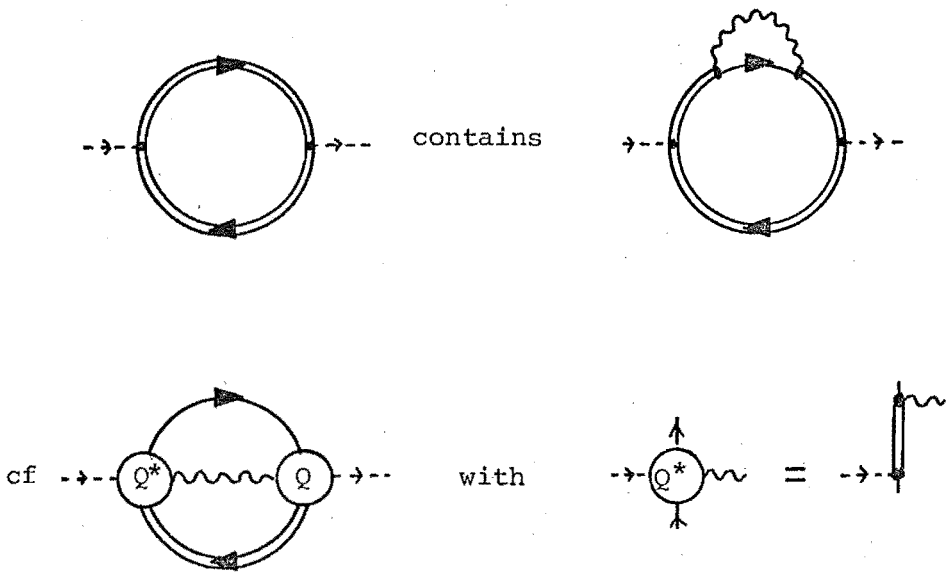

Figure 8.7

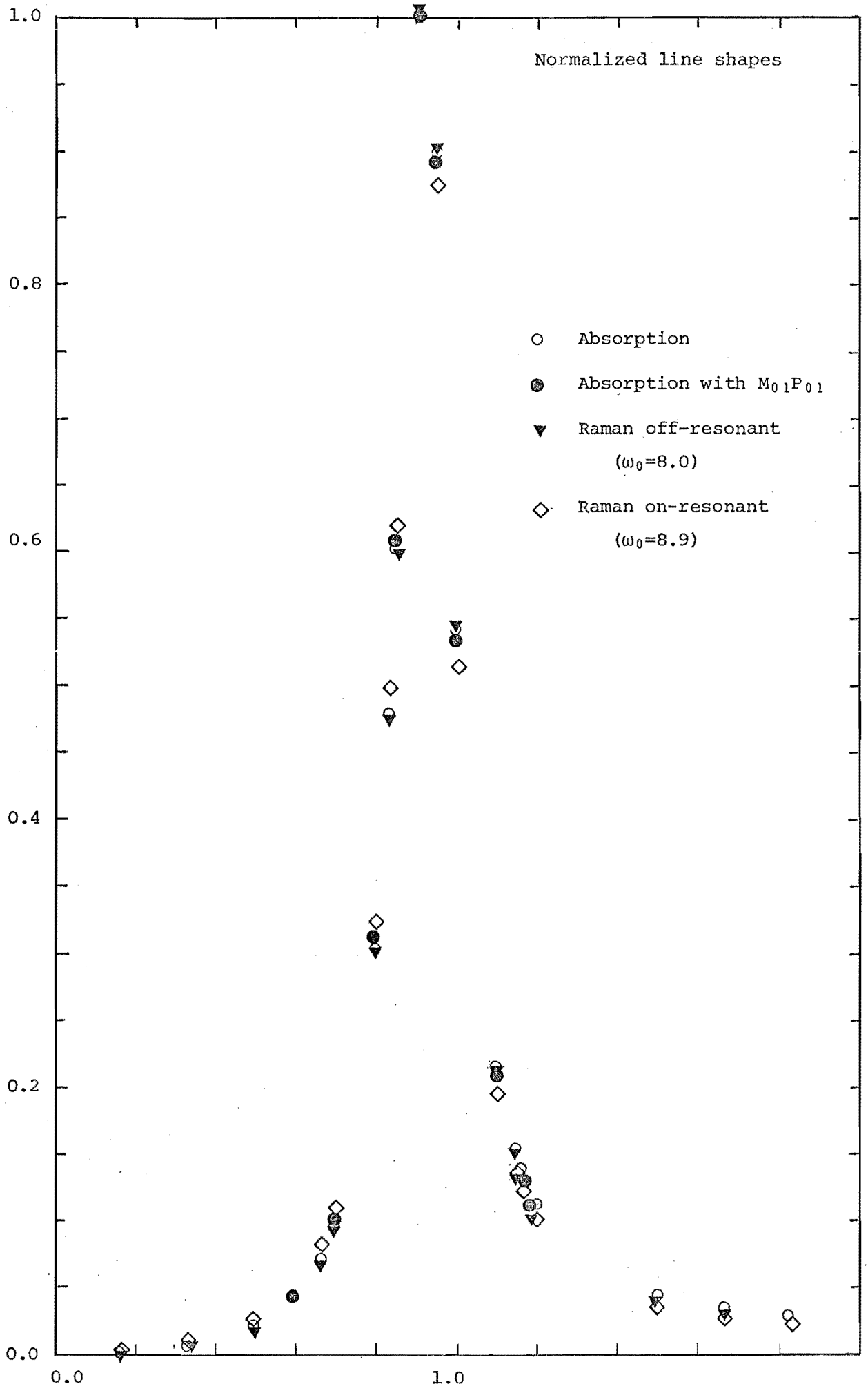
Normalized line shapes
Absorption
Absorption with $M_{01}P_{01}$
Raman off-resonant
(ω_0=8.0)
Raman on-resonant
(ω_0=8.9)
1.0
0.8
0.6
0.4
0.2
0.0
0.0
1.0

The resulting one-phonon sideband is clearly seen in the numerical points as a broad peak to the right of the N.P.L. which reflects the density of states. (Figure 8.9).

This was then generalized by evaluating the leading contribution to 3.45 including the two second-order contributions to $Q(x,\pm\omega_k,\omega_0)$ This contribution is plotted in figure (8.10) where again the broad peak to the right of the N.P.L. is apparent.

8.5 Raman Lineshape

Using the same model of §8.2 we evaluated the convolution (6.13) giving the basic contribution to the Raman lineshape. The integrand in this convolution is not identical to that for the absorption contribution and furthermore depends on the input laser frequency ω_0. This suggests that the absorption and Raman lineshapes could be different, and the purpose of this calculation was to investigate the magnitude of any difference for our model system.

As we chose input laser frequencies ω_0 that were close to resonance with the energy difference $\varepsilon_3 - \varepsilon_1$ we made the approximation discussed in §7.5.1 of considering only the resonant term of (6.14). We evaluated (6.13) for the input laser frequencies, $\omega_0 = 8.9$ (exact resonance) and $\omega_0 = 8.0$ (near resonance) and the normalized lineshapes are plotted in figure 8.7 (plotted as ◇ and ▼ respectively). It is clear that the exact resonance lineshape is identical to the absorption spectrum and the off-resonance lineshape differs only slightly from those. This suggests that the Raman and absorption spectrum are essentially the same for our model system and possibly for systems in general.

The sharply-peaked approximation applied to the convolution (6.13) suggests that the intensity variation with input laser frequency is contained in the function $|P_{01}(\bar{\lambda}_0,\omega_0+i\delta)|^2$ In figure 8.11 we have plotted the numerical intensity dependence taken from the lineshape peak position $\omega = \omega_0 + 0.9$ against the input laser frequency (dotted points).

Figure 8.9

Phonon Sideband

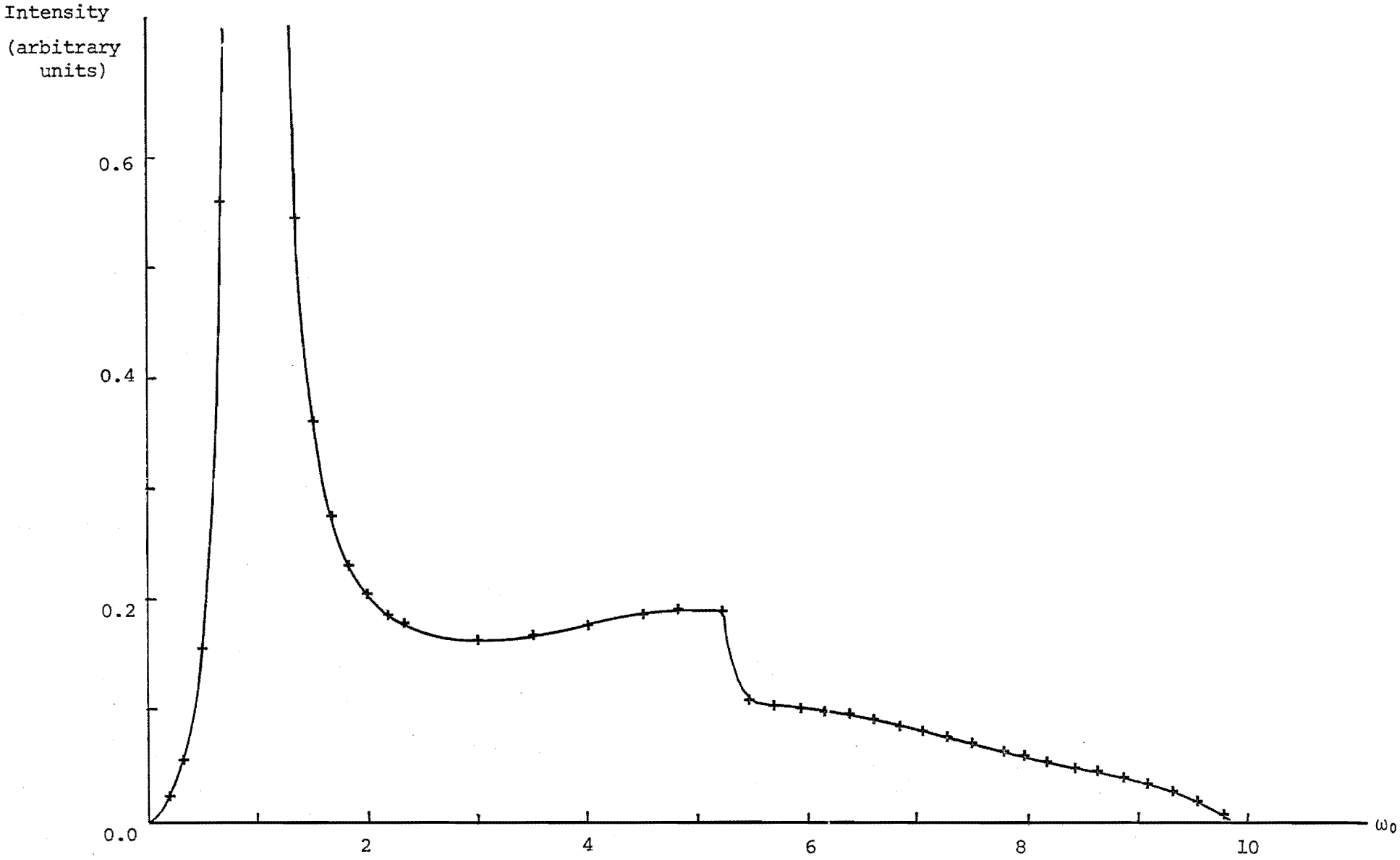

Figure 8.10 One Phonon Sideband

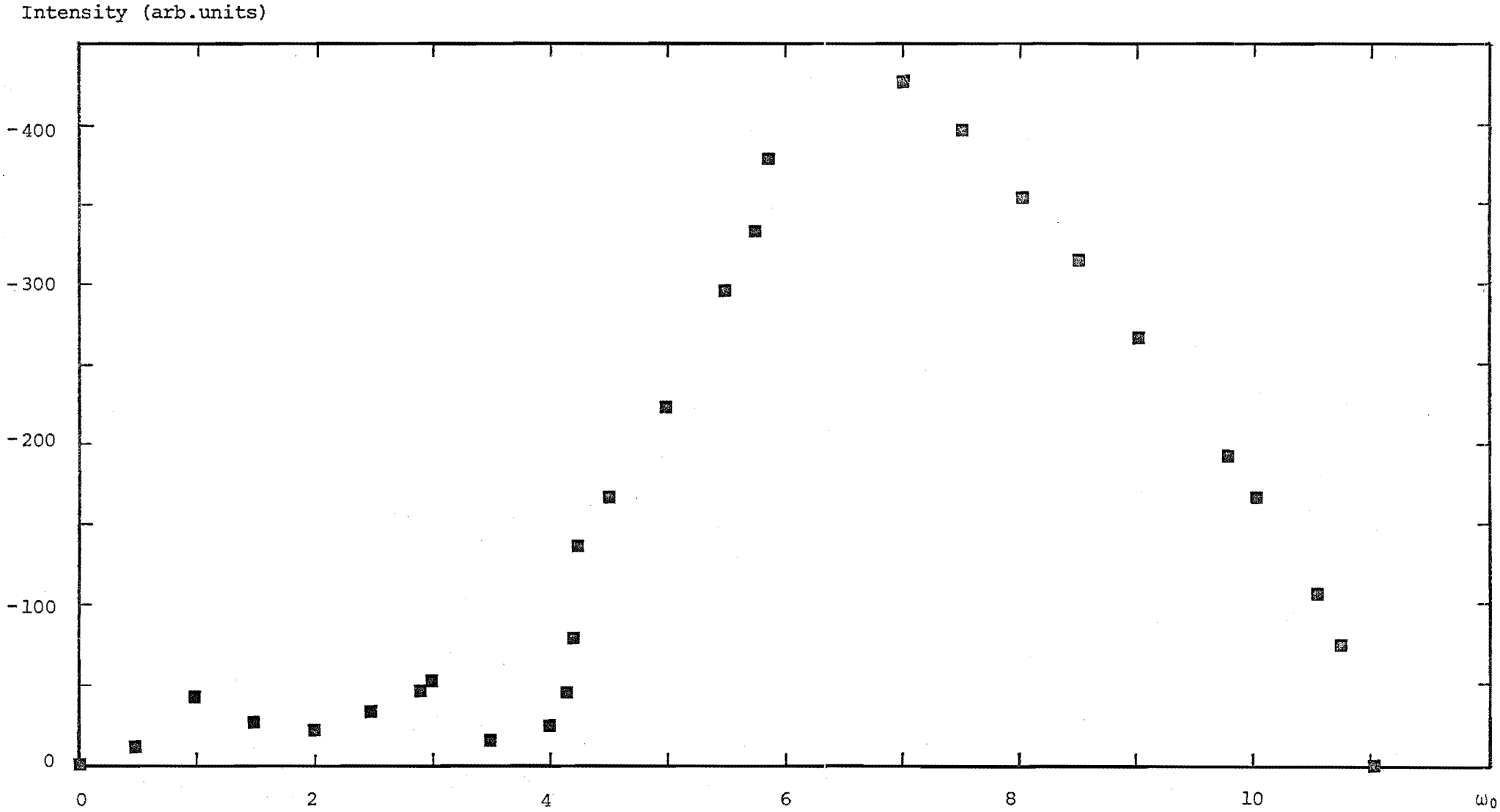

Figure 8.11 Intensity as function of input laser frequency

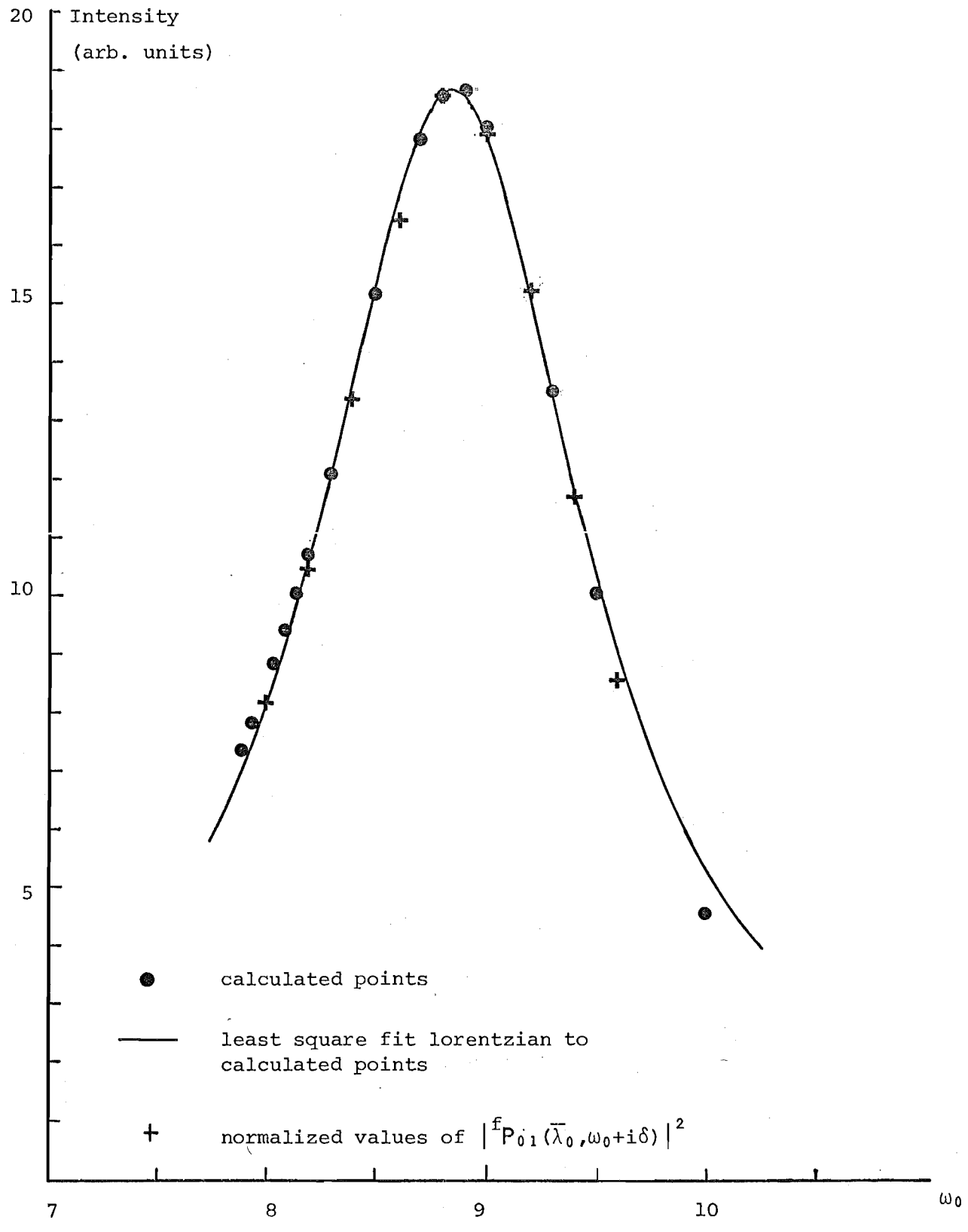

On the same graph is the analytic function $|P_{01}(\bar{\lambda}_0, \omega_0+i\delta)|^2$ (crosses) which is clearly an excellent approximation to the intensity dependence.

Friedman *et.al.* (1976) have compared the intensity of the Raman spectrum as a function of incident laser frequency, which they label the "excitation profile", with the absorption spectrum in a matrix-isolated Br_2 system. They note that these are often quite different.

The present formalism agrees with this observation because in general the analytic function $|P_{mn}(\bar{\lambda}_m, \omega_0+i0^+)|^2$ which describes the excitation profile is not the same as the lorentzian absorption lineshape (3.38). Agreement however is possible if it is a good approximation to neglect all but a single contribution to $|P_{mn}(\bar{\lambda}_m, \omega_0+i0^+)|^2$. As discussed in § 7.5.1 this is possible when the resonant intermediate level is well separated from adjacent levels and we are considering the excitation profile near resonance. For example retaining the resonant term of (6.14) we obtain

$$|P_{mn}(\bar{\lambda}_m, \omega_0+i0^+)|^2 \alpha \left|\frac{1}{\omega_0+\delta_m-\delta_s-i\gamma_s}\right|^2$$

$$\alpha \frac{1}{(\omega_0+\delta_m-\delta_s)^2+\gamma_s^2} \qquad (8.10)$$

while the absorption lineshape for the transition from level m to level s (using 3.38) is

$$\sigma(\omega_0) \alpha \frac{\gamma_m+\gamma_s}{(\omega_0+\delta_m-\delta_s)^2+(\gamma_m+\gamma_s)^2} . \qquad (8.11)$$

These are both peaked at the same position and have approximately the same width if γ_m, (which in Raman experiments is usually the width of the ground state and hence relatively small), can be neglected with respect to the width of the intermediate state γ_s. However we repeat that in general we do not expect such an agreement.

The calculations presented in this chapter give us confidence that the approximations made in the preceeding chapters to obtain analytic results

are reasonable but suggest that for accurate results the numerical convolutions should be performed.

CHAPTER 9 : CONCLUSIONS

9.1 Results of this Work.

In chapter 2 we investigated three possible mappings from spin operators to fermion annihilation/creation operators that allow the retention of the usual fermion Wick's theorem. These were the drones, quasi-spin and iso-spin mappings and their associated projection operations that arise from the difference between the spin and fermion commutation relations. By applying each of these mappings to an interacting spin-phonon system and evaluating the resulting coupled-mode dispersion relation we were able to assess their relative merits. The iso-spin mapping was found to be the most convenient for the types of problem we considered; it had simpler diagram rules and projection operation, required fewer contour integrations in the evaluation of diagrams and allowed both physical and group theoretical interpretations to be attributed to the diagrams. Because of these advantages over the other two mappings, the iso-spin mapping was employed in our formalisms for the evaluation of both the absorption and Raman spectra.

In chapter 3 these techniques were applied to the evaluation of the absorption spectrum of a crystal containing impurity ions. We showed that for low impurity ion concentrations the spectrum can be approximated by the single-ion spectrum. This justified the approach of previous workers who have used, but did not analyse, this approximation. We extended the results of these workers by deriving general expressions for the lineshape of the N.P.L. and one-phonon sideband and indicating the method needed to obtain that of the m-phonon sideband. Within the various approximation schemes we discuss, the N.P.L. has a lorentzian lineshape whose width is the sum of the widths of the initial and final levels participating in the transitions. (This result is in agreement with the standard Wigner - Weisskopf result). We have also discussed further contributions to the N.P.L. width that result from the encroachment of the one-phonon and m-phonon sidebands into the N.P.L. lineshape.

When the crystal contains higher concentrations of impurity ions the single-ion formalism of chapter 2 is no longer sufficient. We have presented in chapter 4 a new formalism that calculates the contribution to the absorption spectrum that results from pairs of impurity ions. The method was illustrated by a simple application to a pair of two-level ions. It was then applied to a more general case involving a pair of Kramers ions which presented some novel results not correctly/fully analysed by previous workers. In the formalism we have developed, the shifts of the four degenerate ground state levels, (and hence the splittings in the absorption spectrum), that result from virtual phonon exchange processes, are related to the eigenvalues of a four dimensional shift matrix. By exploiting time-reversal invariance and hermicity, various symmetries among the matrix elements were found, reducing the number of independent parameters relevant to the splittings to four. Enumerating all the diagrams that contributed to these parameters it was found that no second-order diagrams or diagrams containing trivial vertices could cause splittings (although they would shift the centre of gravity of the four levels). The lowest order non-vanishing contributions to the splittings were found to arise from fourth-order diagrams containing two excited state propagators. These result in a T^9 temperature dependence in the splittings in the low temperature, Debye acoustic phonon model limit.

In Chapters 5 - 7 we derived a formalism that yields the Raman spectrum for a crystal containing low concentrations of impurity ions. This formalism is valid for, and was applied to, both the steady-state and time-dependent scattering regimes. It is also valid both near and far from resonance. We derived expressions containing both the frequency and time dependences of the output Raman intensity for the N.P.L. and the phonon sidebands upon excitation by a short laser pulse. The consequences of the uncertainty principle are automatically built into the theory. Within various approximations we develop, the no-phonon lineshape is identical to the absorption N.P.L. Numerical investigations of a simple model have shown this to be an excellent approximation. The

spectrum time dependence was found to contain both rapid and slow decay/rise time components with rise times related to the laser pulse and the width of the intermediate state(s) respectively. This is in agreement with the experimental results of Williams *et.al.* (1974). The formalism predicts a 'ringing' which would optimally be observed upon scattering from a single ion, or a number of similar localized ions, close to resonance with high temporal resolution.

It should be emphasised that each of the topics investigated requires the formalism developed in chapter 2 such as the Feynman diagram rules, the projection procedure (P) and the diagram interpretation ideas. The methods developed then do not require one to begin from scratch for each new problem but allows the results and techniques used previously to be extended to consider new problems of this type.

9.2 Suggestions for further work

In § 2.2.5 we showed that the iso-spin projection operation was not applicable to the two-particle pseudo-fermion propagators because it did not eliminate unphysical intermediate states. In our applications this was no restriction because P needed only to be applied to either two-particle (absorption) or four-particle (Raman) G.F. However a mapping and/or a projection operation that was not restricted in this manner would be advantageous if it also had all or most of the advantages of the iso-spin mapping. Although preliminary investigationsinto this possibility were instigated, a successful mapping was not found, leaving this a possibility for further study.

In the evaluation of both the absorption and Raman spectrum we neglected a denominator of the form $1 + P(\textcircled{1})$. This was because it did not depend on (incident or emitted) photon energies and hence could contribute only an overall intensity shift to the total spectrum. This factor would be temperature dependent and should result in overall intensity variations with temperature. Calculations of these and comparison with experimental results on such dependences would be a useful

test of the present method.

Finally a detailed test of the predicted time dependences of Chapter 7 could be performed by comparing the theoretical calculations with the results from a simple experimental system. Special attention should be paid to the 'ringing' phenomena predicted and the variations in time dependence across the one-phonon sideband.

APPENDIX 3A

Relating Green's function to spectral representation

Expanding (3.1) in Lehmann representation we obtain

$$\sigma(\omega_0) \sim \omega_0 \sum_{mn} e^{-\beta E_m} \langle m|M|n\rangle\langle n|M|m\rangle F_{mn} \tag{3A.1}$$

where

$$F_{mn} = \int_{-\infty}^{\infty} dt \left\{e^{-i\omega_0 t} - e^{i\omega_0 t}\right\} \cdot e^{i(E_m - E_n)t}$$

Evaluating the time integrals we obtain

$$F_{mn} = \delta(\omega_0 - E_m + E_n) - \delta(\omega_0 + E_m - E_n) \ . \tag{3A.2}$$

The defining equation for the G.F. can be rewritten as

$$G(i\omega_n) = \int_0^{\beta} d\tau \ e^{i\omega_n \tau} \langle T_\tau \{M(\tau)M\}\rangle \tag{3A.3}$$

and expanding this in the Lehmann representation we obtain

$$G(i\omega_n) = \sum_{mn} \ell^{-\beta E_m} \langle m|M|n\rangle\langle n|M|m\rangle H_{mn}(i\omega_n) \tag{3A.4}$$

where

$$H_{mn}(i\omega_n) = \int_0^{\beta} d\tau \ e^{i\omega_n \tau} \ e^{(E_m - E_n)\tau}$$

Evaluating the integral over τ we obtain

$$H_{mn}(i\omega_n) = \frac{e^{\beta(E_m - E_n)} - 1}{(i\omega_n + E_m - E_n)} \tag{3A.5}$$

Defining the function

$$F(\omega_0) = \frac{1}{2\pi i} \{G(\omega_0 + i0^+) - G(\omega_0 - i0^+)\} \tag{3A.6}$$

we obtain using (3.15)

$$F(\omega_0) = - \sum_{mn} e^{-\beta E_m} \langle m|M|n\rangle\langle n|M|m\rangle \ (e^{\beta(E_m - E_n)} - 1)$$

$$\delta(\omega_0 + E_m - E_n) \tag{3A.7}$$

which gives upon interchanging m and n,

$$F(\omega_0) = \sum_{mn} e^{-\beta E_m} \langle m|M|n\rangle\langle n|M|m\rangle \; (\delta(\omega_0 - E_m + E_n)$$

$$-\delta(\omega_0 + E_m - E_n)) \; . \qquad (3A.8)$$

Comparing (3A.8) with (3A.1 - 2) we obtain the required result

$$\sigma(\omega_0) \sim \frac{\omega_0}{2\pi i}\{G(\omega_0 + i0^+) - G(\omega_0 - i0^+)\} \qquad (3A.9)$$

APPENDIX 3B

Convolutions of $L_i(x)$ and $A_i(x)$ functions

Many of the convolutions considered can be expressed in the form

$$\sigma(\omega_0) = \int_{-\infty}^{\infty} dx\ f(x)g(\omega_0-x)\ dx \equiv f*g(\omega_0) \tag{3B.1}$$

where

$$f(x) = f_1(x)f_2(x)f_3(x) \cdots\cdots f_n(x) \tag{3B.2}$$

$$g(x) = g_1(x)g_2(x)g_3(x) \cdots\cdots g_m(x)$$

This convolution can be evaluated by the Faltung theorems (Jennison 1961) giving

$$\sigma\ (\omega_0) = h(\omega_0) \tag{3B.3}$$

where $h(\omega_0)$ is the universe Fourier transform of $H(k)$ defined by

$$H(k) = F(k)\cdot G(h) \tag{3B.4}$$

where $F(h)$, $G(h)$ are the Fourier transforms of $f(x)$, $g(x)$ respectively. To obtain these from (3B.2) we use

$$F(k) = (F_1*F_2* \cdots *F_n)(k) \tag{3B.5}$$

$$G(k) = (G_1*G_2* \cdots *G_m)(k)$$

where $F_i(k)$ $G_i(k)$ are the Fourier transforms of $f_i(x)$, $g_i(x)$ respectively.

We take the $F_i(x)$ and $G_i(x)$ to have the form

$$F_i(k),\ G_i(k) = \begin{cases} a_i\ e^{ik(\lambda_i+i\gamma_i)} & k>0 \\ a_i^*\ e^{ik(\lambda_i-i\gamma_i)} & k<0 \end{cases} \tag{3B.6}$$

which are satisfied by the relevant functions

$$L_i(x) = \frac{\gamma_i/\pi}{(x-\lambda_i)^2+\gamma_i^2} \qquad a_i = a_i^* = 1$$

$$A_i(x) = \frac{(x-\lambda_i)}{(x-\lambda_i)^2+\gamma_i^2} \qquad a_i = -a_i^* = i\pi \tag{3B.7}$$

Let us consider the form of F(k) in (3B.5) for n = 2. We have

$$(F_1 * F_2)(k) = \begin{cases} a_{12}\, e^{ik(\lambda_1+i\gamma_1)} + a_{21}\, e^{ik(\lambda_2+i\gamma_2)} \\ a_{12}^{*}\, e^{ik(\lambda_1-i\gamma_1)} + a_{21}^{*}\, e^{ik(\lambda_2-i\gamma_2)} \end{cases} \tag{3B.8}$$

where

$$a_{ij} = \frac{i}{2\pi}\left[\frac{a_i a_j^{*}}{\omega_{ij}+i\gamma_i+i\gamma_j} - \frac{a_i a_j}{\omega_{ij}+i\gamma_i-i\gamma_i}\right]$$

Note that this is the sum of two functions each of which has the form of (3B.6). This enables us to easily perform a further convolution for n = 3 giving

$$(F_1 * F_2 * F_3)(k) = \begin{cases} a_{(12)3}\, e^{ik(\lambda_1+i\gamma_1)} + a_{(21)3}\, e^{ik(\lambda_2+i\gamma_2)} + a_{(31)2}\, e^{ik(\lambda_3+i\gamma_3)} \\ a_{(12)3}^{*}\, e^{ik(\lambda_1-i\gamma_1)} + a_{(21)3}^{*}\, e^{ik(\lambda_2-i\gamma_2)} + a_{(31)2}\, e^{ik(\lambda_3-i\gamma_3)} \end{cases} \tag{3B.9}$$

where

$$a_{(ij)k} = \frac{i}{2\pi}\left[\frac{a_{ij}\, a_k^{*}}{\omega_{ik}+i\gamma_i+i\gamma} - \frac{a_{ij}\, a_k}{\omega_{ik}+i\gamma_i-i\gamma_k}\right] \tag{3B.10}$$

in an obvious generalization of (3B.8).

This procedure can be continued giving

$$F(k) = \sum_{i=1}^{n} \begin{cases} b_i\, e^{ik(\lambda_i+i\gamma_i)} & k>0 \\ b_i^{*}\, e^{ik(\lambda_i-i\gamma_i)} & k<0 \end{cases}$$

$$G(k) \quad \sum_{j=1}^{m} \begin{cases} c_j\, e^{ik(\lambda_j+i\gamma_j)} & k>0 \\ c_j^{*}\, e^{ik(\lambda_i-i\gamma_j)} & k<0 \end{cases} \tag{3B.11}$$

This gives as the result

$$H(k) = \sum_{i=1}^{n}\sum_{j=1}^{m} \begin{cases} b_i c_j\, e^{ik(\lambda_{ij}+i\gamma_{ij})} & k>0 \\ (b_i c_j)^{*}\, e^{ik(\lambda_{ij}-i\gamma_{ij})} & k<0 \end{cases} \tag{3B.12}$$

where $\lambda_{ij} = \lambda_i + \lambda_j$, $\gamma_{ij} = \gamma_i + \gamma_j$, etc.

Finally taking the inverse Fourier transform of H(k) gives as the result

$$\sigma(\omega_0) = \sum_{ij} \left\{ \text{Real}(b_i c_j) \frac{\gamma_{ij}/\pi}{(\omega_0+\lambda_{ij})^2+\gamma_{ij}} - \text{Imag} \frac{b_i c_j}{\pi} \frac{(\omega_0+\lambda_{ij})}{(\omega_0+\lambda_{ij})^2+\gamma_{ij}^2} \right\}$$

(3B.13)

which consists of a sum of $L_{ij}(\omega_0)$ and $A_{ij}(\omega_0)$ functions multiplied by various coefficients.

For example evaluating the convolution of two lorentzians in (3.37) we have

$$f(x) = f_1(x) = \frac{\gamma_n/\pi}{(x-\delta_n)^2+\gamma_n^2} \quad \therefore \quad a_1=b_1=1, \ \lambda_1=\delta_n, \ \gamma_1=\gamma_n \tag{3B.14}$$

$$g(x) = g_1(x) = \frac{\gamma_m/\pi}{(x+\delta_m)^2+\gamma_m^2} \quad \therefore \quad a_1=c_1=1, \ \lambda_1=-\delta_m, \ \gamma_1=\gamma_m \tag{3B.15}$$

giving $\lambda_{11} = \delta_n-\delta_m$ and $\gamma_{11} = \gamma_n+\gamma_m$ and

$$\sigma(\omega_0) = 1 \cdot \frac{\gamma_{11}/\pi}{(\omega_0+\lambda_{11})^2+\gamma_{11}} - \frac{0}{\pi} \frac{(\omega_0 \ \lambda_{11})}{(\omega_0+\lambda_{11})^2+\gamma_{11}^2} \tag{3B.16}$$

$$= \frac{(\gamma_n+\gamma_m)/\pi}{(\omega_0+\delta_n-\delta_m)^2+(\gamma_m+\gamma_n)^2}$$

APPENDIX 4A

Basic transformations of Hamiltonians

$$\mathcal{H}_{imp} = \sum_m \varepsilon_m (a_{1m}^\dagger a_{1m} + a_{2m}^\dagger a_{2m})$$

$$= \sum_m \varepsilon_m (a_{1m}^\dagger a_{1m} [\sum_n a_{2n}^\dagger a_{2n}] + a_{2m}^\dagger a_{2m} [\sum_n a_{1n}^\dagger a_{1n}])$$

$$= \sum_{mn} \varepsilon_m [(a_{1m}^\dagger a_{2n}^\dagger)(a_{1m} a_{2n}) + (a_{2m}^\dagger a_{1n}^\dagger)(a_{2m} a_{1n})]$$

$$= \sum_{mn} \varepsilon_m (\psi_{mn}^\dagger \psi_{mn} + \psi_{nm}^\dagger \psi_{nm})$$

$$= \sum_{mn} (\varepsilon_m + \varepsilon_n) \psi_{mn}^\dagger \psi_{mn}. \qquad (4A.1)$$

$$\mathcal{H}^{int} = \sum_{mnk} \{V_{mn}^{1k} a_{1m}^\dagger a_{1n} + V_{mn}^{2k} a_{2m}^\dagger a_{2n}\} \phi_k$$

$$= \sum_{mnk} \{V_{mn}^{1k} a_{1m}^\dagger a_{1n} (\sum_\ell a_{2\ell}^\dagger a_{2\ell})$$

$$+ V_{mn}^{2k} a_{2m}^\dagger a_{2n} (\sum_\ell a_{1\ell}^\dagger a_{1\ell})\} \phi_k$$

$$= \sum_{mn\ell} \sum_k \{V_{mn}^{1k} (a_{1m}^\dagger a_{2\ell}^\dagger)(a_{1n} a_{2\ell})$$

$$+ V_{mn}^{2k} (a_{1\ell}^\dagger a_{2m}^\dagger)(a_{1\ell} a_{2n})\} \phi_k$$

$$= \sum_{mn\ell} \sum_k \{V_{mn}^{1k} \psi_{m\ell}^\dagger \psi_{n\ell} + V_{mn}^{2k} \psi_{\ell m}^\dagger \psi_{\ell n}\} \phi_k \qquad (4A.2)$$

$$
\begin{aligned}
M &= \sum_{mn} M^1_{mn}\, a_{1m}^{\dagger} a_{1n} + M^2_{mn}\, a_{2m}^{\dagger} a_{2n} \\
&= \sum_{mn} M^1_{mn}\, a_{1m}^{\dagger} a_{1n} \Big(\sum_{\ell} a_{2\ell}^{\dagger} a_{2\ell}\Big) + M^2_{mn}\, a_{2m}^{\dagger} a_{2n} \Big(\sum_{\ell} a_{1\ell}^{\dagger} a_{1\ell}\Big) \\
&= \sum_{mn\ell} M^1_{mn} \big(a_{1m}^{\dagger} a_{2\ell}^{\dagger}\big)\big(a_{1n}\, a_{2\ell}\big) + M^2_{mn} \big(a_{1\ell}^{\dagger} a_{2m}^{\dagger}\big)\big(a_{1\ell}\, a_{2n}\big) \\
&= \sum_{nm\ell} M^1_{mn}\, \psi_{m\ell}^{\dagger} \psi_{n\ell} + M^2_{mn}\, \psi_{\ell m}^{\dagger} \psi_{\ell n} \\
&= \sum_{mn\ell o} \big(M^1_{m\ell}\, \delta_{no}\, \psi_{mn}^{\dagger} \psi_{\ell o} + M^2_{no}\, \delta_{m\ell}\, \psi_{mn}^{\dagger} \psi_{\ell o} \\
&= \sum_{mn\ell o} \big(M^1_{m\ell}\, \delta_{no} + M^2_{no}\, \delta_{m\ell}\big) \psi_{mn}^{\dagger} \psi_{\ell o} \\
&\equiv \sum_{mn\ell o} M_{mn\ell o}\, \psi_{mn}^{\dagger} \psi_{\ell o} \qquad (4A.3)
\end{aligned}
$$

APPENDIX 4B

Basic transformations

(a) Proof of (4.39):

$$\grave{\psi}^\dagger \equiv (\grave{\Psi})^\dagger = (A\psi)^\dagger = \psi^\dagger A^\dagger \tag{4B.1}$$

(b) Proof of (4.40):

$$\begin{aligned}
\mathcal{H}_{imp} &= \underset{\sim}{\psi}^\dagger \cdot E \cdot \psi \\
&= \underset{\sim}{\psi}^\dagger \cdot (A^\dagger A) \cdot E \cdot (A^\dagger A)\psi \qquad \text{because } A^\dagger A = 1 \\
&= (\underset{\sim}{\psi}^\dagger A^\dagger) \cdot (AEA^\dagger) \cdot (A\psi) \\
&\equiv \grave{\psi}^\dagger \cdot \grave{E} \cdot \grave{\psi} \qquad \text{where } \grave{E} = AEA^\dagger
\end{aligned} \tag{4B.2}$$

(c) Proof of (4.41):

$$\begin{aligned}
\mathcal{H}_{int} &= \sum_k (\underset{\sim}{\psi}^\dagger \cdot V^{1k} \cdot \psi + \psi^\dagger \cdot V^{2k} \cdot \psi)\phi_k \\
&= \sum_k ((\underset{\sim}{\psi}^\dagger A^\dagger)(AV^{1k}A^\dagger)(A\psi) + (\underset{\sim}{\psi}^\dagger A^\dagger)(AV^{2k}A^\dagger)(A\psi))\phi_k \\
&\equiv \Sigma(\grave{\underset{\sim}{\psi}}^\dagger \grave{V}^{1k} \cdot \grave{\psi} + \grave{\underset{\sim}{\psi}}^\dagger \cdot \grave{V}^{2k} \cdot \grave{\psi})\phi_k
\end{aligned}$$

$$\text{where } \grave{V}^{ik} = AV^{ik}A^\dagger \quad i = 1,2 \tag{4B.3}$$

(d) Proof of (4.42):

This result is a consequence of the theorem

Thm 4B.1 If $\underset{\sim}{x} = \begin{pmatrix} x_1 \\ x_2 \\ x_3 \\ \vdots \end{pmatrix}$ is an n-vector, $\underset{\sim}{y} = (y_1, y_2 \cdots)$ an n-tuple and A,B are n x n square matrices then

$$(A\underset{\sim}{x}) \otimes (\underset{\sim}{y}B) = A \cdot (\underset{\sim}{x} \otimes \underset{\sim}{y}) \cdot B \ .$$

Proof:

$$\begin{aligned}
[(A\underset{\sim}{x}) \otimes (\underset{\sim}{y}B)]_{ij,k\ell} &= (A\underset{\sim}{x})_{ik} (\underset{\sim}{y}B)_{j\ell} \\
&= A_{is} x_{sk} y_{jr} B_{r\ell}
\end{aligned}$$

but $x_{sk} = x_s \delta_{ki}$ and $y_{jr} = y_r \delta_{ji}$ and hence

$$[(A\underline{x})\otimes(\underset{\sim}{y}\,B)]_{i,\ell} = A_{is}\, x_s\, y_r\, B_{r\ell}$$

$$= A_{is} \cdot (\underline{x} \otimes \underset{\sim}{y})_{sr}\, B_{r\ell}$$

$$= [A \cdot (\underline{x} \otimes y) \cdot B]_{i,\ell}. \quad \blacksquare$$

Hence we obtain the result

$$\hat{F}(\tau) = \langle T_\tau\{\hat{\psi}(\tau) \otimes \underset{\sim}{\psi}^\dagger(0)\}\rangle$$

$$= \langle T_\tau\{(A\psi(\tau)) \otimes (\underset{\sim}{\psi}^\dagger(0)A^\dagger)\rangle$$

$$= A \cdot \langle T_\tau\{\psi(\tau) \otimes \underset{\sim}{\psi}^\dagger(0)\}\rangle \cdot A^\dagger$$

$$= A\, F(\tau) A^\dagger \qquad (4B.4)$$

Proof of (4.43)

$$\hat{F}(i\omega_n) = A\, F(i\omega_n)\, A^\dagger = A(F^0(i\omega_n) + F^0(i\omega_n)\, \Sigma(i\omega_n) F(i\omega_n))A^\dagger$$

$$\hat{F}(i\omega_n) = A\, F(i\omega_n) A^\dagger \qquad \text{(from 4B.4)}$$

$$= A(F^0(i\omega_n) + F^0(i\omega_n)\, \Sigma(i\omega_n)\, F(i\omega_n))A^\dagger \qquad \text{(using 4.22)}$$

$$= AF^0(i\omega_n)A^\dagger + (A\, F^0(i\omega_n)A^\dagger)(A\, \Sigma(i\omega_n)A^\dagger)(A\, F(i\omega_n)A^\dagger)$$

$$\hat{F}(i\omega_n) = \hat{F}^0(i\omega_n) + \hat{F}^0(i\omega_n)\hat{\Sigma}(i\omega_n)\, \hat{F}(i\omega_n) \qquad (4B.5)$$

where $\hat{\Sigma}(i\omega_n) \equiv A\, \Sigma(i\omega_n)A^\dagger$

APPENDIX 4C

Two level second-order splitting:

Evaluating the contribution of the diagram of figure 4.8 for choice (4.48a) of intermediate states we split up the diagram into the two possible phonon propagator directions explicitly giving (figure 4C.1)

Figure 4C.1

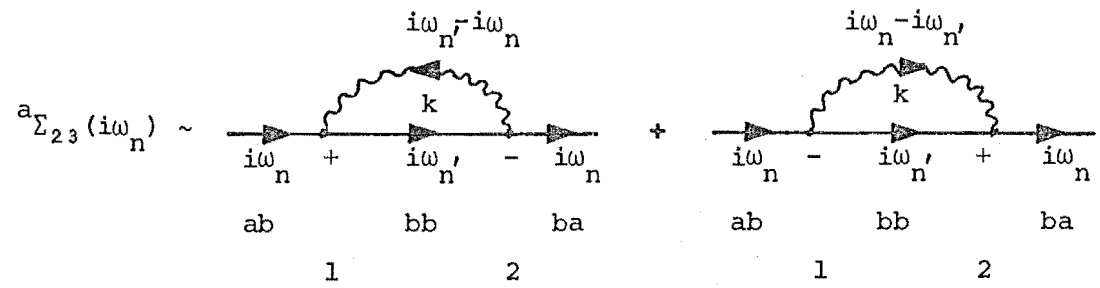

$$a_{\Sigma_{23}(i\omega_n)} = \beta^{-1} \sum_{i\omega_{n'}} F_{bb}(i\omega_{n'}) e^{i\omega_{n'}0^+} \sum_k \left[\frac{V_{ab}^{1k} V_{ba}^{2-k}}{i\omega_{n'} - i\omega_n - \omega_k} + \frac{V_{ab}^{1-k} V_{ba}^{2k}}{i\omega_n - i\omega_{n'} - \omega_k} \right]$$

$$= - \int_C \frac{dz}{2\pi i} F_{bb}(z) \frac{e^{z0^+}}{e^{\beta z}+1} \sum_k \left[\frac{V_{ab}^{1k} V_{ba}^{2-k}}{z - i\omega_n - \omega_k} - \frac{V_{ab}^{1-k} V_{ba}^{2k}}{z - i\omega_n + \omega_k} \right]$$

$$= \sum_k \left[\frac{F_{bb}(i\omega_n+\omega_k)}{e^{\beta\omega_k} - 1} V_{ab}^{1k} V_{ba}^{2-k} - \frac{F_{bb}(i\omega_n-\omega_k)}{e^{-\beta\omega_k} - 1} V_{ab}^{1-k} V_{ba}^{2k} \right]$$

$$= \sum_k V_{ab}^k V_{ba}^k \left\{ \frac{e^{i\underline{k}\cdot\underline{R}} n_k}{i\omega_n + \omega_k - \epsilon_{bb}} + \frac{e^{-i\underline{k}\cdot\underline{R}}(n_{k+1})}{i\omega_n - \omega_k - \epsilon_{bb}} \right\} \qquad (4C.1)$$

where contour C encircles the poles of the Fermi-Dirac function and we have used $e^{\beta(i\omega_n)} = -1$.

Similarly for choice (4.48b) we obtain (figure 4C.2)

Figure 4C.2

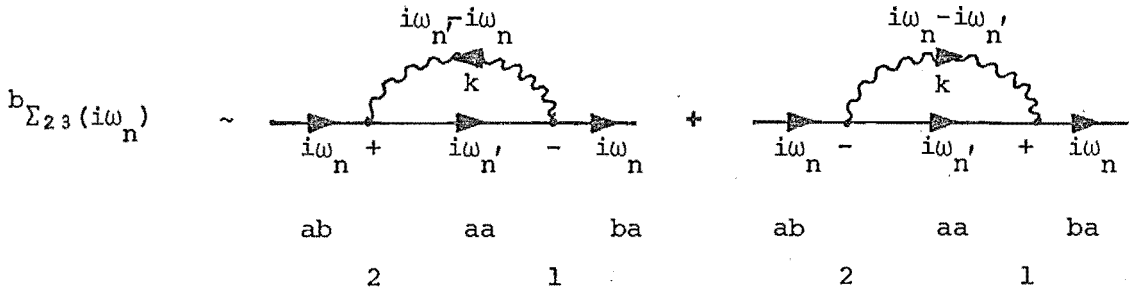

$$b\Sigma_{23}(i\omega_n) = \beta^{-1} \sum_{i\omega_n'} F_{aa}(i\omega_n') e^{i\omega_n' 0^+} \sum_k \left| \frac{V_{ba}^{2k} V_{ab}^{1-k}}{i\omega_n' - i\omega_n - \omega_k} + \frac{V_{ba}^{2-k} V_{ab}^{1k}}{i\omega_n - i\omega_n' - \omega_k} \right|$$

$$= \sum_k \left| \frac{F_{aa}(i\omega_n + \omega_k)}{(e^{\beta\omega_k} - 1)} V_{ba}^{2k} V_{ab}^{1-k} - \frac{F_{aa}(i\omega_n - \omega_k)}{(e^{-\beta\omega_k} - 1)} V_{ba}^{2-k} V_{ab}^{1k} \right|$$

$$= \sum_k V_{ba}^k V_{ab}^k \left\{ \frac{e^{-i\underline{k}\cdot\underline{R}} n_k}{i\omega_n + \omega_k - \varepsilon_{aa}} + \frac{e^{i\underline{k}\cdot\underline{R}} (n_{k+1})}{i\omega_n - \omega_k - \varepsilon_{aa}} \right\} \qquad (4C.2)$$

Obtaining the real part of ${}^a\Sigma_{23}(\varepsilon_{ab} + i0^+) + {}^b\Sigma_{23}(\varepsilon_{ab} + i0^+)$ gives

$$\Delta_{23}(\varepsilon_{ab}) = \sum_k V_{ab}^k V_{ba}^k \left\{ \frac{e^{i\underline{k}\cdot\underline{R}} n_k}{\omega_{ab} + \omega_k} + \frac{e^{-i\underline{k}\cdot\underline{R}} (n_{k+1})}{\omega_{ab} - \omega_k} \right.$$

$$\left. + \frac{e^{-i\underline{k}\cdot\underline{R}} n_k}{\omega_{ab} + \omega_k} + \frac{e^{i\underline{k}\cdot\underline{R}} (n_{k+1})}{\omega_{ba} - \omega_k} \right\}$$

$$= \sum_k V_{ab}^k V_{ba}^k \left\{ \frac{e^{i\underline{k}\cdot\underline{R}}}{\Delta - \omega_k} - \frac{e^{-i\underline{k}\cdot\underline{R}}}{\Delta + \omega_k} \right\} \qquad (4C.3)$$

Where $\Delta = \omega_{ba}$. By converting the sum over $\underline{k}$ to an integral over (k,θ,ϕ) using density of states (den(k)) gives

$$\sum_k f(\underline{k}) = \frac{V}{8\pi^3} \int_0^{k_D} dk\, den(k) \int_{-1}^{+1} d\mu \int_0^{2\pi} d\phi\, f(k,\mu,\phi) \qquad (4C.4)$$

and we obtain

$$= \frac{V}{\pi^2} \int_0^{k_D} dk\ den(k)\ V_{ab}^k\ V_{ba}^k\ \frac{\sin(kR)}{kR}\ \frac{\omega_k}{\Delta^2-\omega_k^2} \qquad (4C.5)$$

To evaluate this further we require the form of the density of states den(k). As this will vary markedly we shall assume a Debye model (den($\underline{k}$) = k^2) distribution. Using (3.8) we obtain

$$\Delta_{23}\ (\varepsilon_{ab}) = -\frac{V_{ab}\ V_{ba}}{c\pi^2 R} \cdot \int_0^{k_D} dk\ \frac{k^3 \sin(kR)}{k^2-k_0^2} \qquad (4C.6)$$

where we defined $k_0 = \Delta/c$.

To evaluate this integral let us consider two limiting approximations

(a) $k_0 << k_D$

$$\Delta_{23}(\varepsilon_{ab}) \simeq -\frac{V_{ab}\ V_{ba}}{c\pi^2 R} \int_0^{k_D} dk\ k\sin(kR)$$

$$= -\frac{V_{ab}\ V_{ba}}{c\pi^2} \left\{ \frac{\sin k_D R}{R^3} - \frac{k_D}{R^2} (\cos k_D R - 1) \right\} \qquad (4C.7)$$

(b) $k_0 >> k_D$

$$\Delta_{23}(\varepsilon_{ab}) \simeq \frac{V_{ab}\ V_{ab}}{ck_0^2\ \pi^2 R} \int_0^{k_D} k^3\ \sin kR$$

$$= -\frac{V_{ab}\ V_{ba}}{ck_0^2\ \pi^2} \left\{ \frac{R^2k_D^2 - 6k_D}{R^4} (\cos k_D R - 1) - \frac{3R^2k_D^2 - 6}{R^5} \sin k_D R \right\}$$

(4C.8)

In analysing similar type integrals, McMahon and Silsbee (1964) found that the oscillatory $\sin k_D R$ and $\cos k_D R$ distance dependance arose because of the pathological nature of the Debye density of states at k_D. They found the distance dependance was better behaved when more realistic density of states were employed, and found an R^{-3} dependance at large R.

APPENDIX 4D

Contribution of diagram 4.12a to self-energy:

$$\Sigma_{mm',nn'}(i\omega_n) \leftarrow \beta^{-1} \sum_{i\omega_{n'}} \beta^{-1} \sum_{i\omega_{n''}} F_{am'}(i\omega_{n'}) \; F_{nm'}(i\omega_{n'}+i\omega_{n''}-i\omega_n)$$

$$F_{nb}(i\omega_{n''}) \sum_{k\ell} \frac{V^{1k}_{ma} V^{1\ell}_{an} V^{2-k}_{m'b} B^{2-\ell}_{bn'}}{(i\omega_{n'}-i\omega_n-\omega_k)(i\omega_{n''}-i\omega_n-\omega_\ell)} \; e^{i\omega_{n'}0^+} \; e^{i\omega_{n''}0^+}$$

$$= \int_C \frac{dz'}{2\pi i} \frac{-e^{z'0^+}}{e^{\beta z'}+1} \int_C \frac{dz''}{2\pi i} \frac{-e^{z''0^+}}{e^{\beta z''}+1} \; F_{am'}(z') \; F_{nm'}(z'+z''-i\omega_n)$$

$$F_{nb}(z'') \sum_{k\ell} \frac{V^{1k}_{ma} V^{1\ell}_{an} V^{2-k}_{m'b} V^{2-\ell}_{bn'}}{(z'-i\omega_n-\omega_k)(z''-i\omega_n-\omega_\ell)}$$

$$= \sum_{k\ell} \left[\frac{-1}{e^{\beta(i\omega_n+\omega_k)}+1}\right]\left[\frac{-1}{e^{\beta(i\omega_n+\omega_\ell)}+1}\right] V^{1k}_{ma} V^{1\ell}_{an} V^{2-k}_{m'b} V^{2-\ell}_{bk'}$$

$$F_{am'}(i\omega_n+\omega_k) \; F_{nm'}(i\omega_n+\omega_k+\omega_\ell) \; F_{nb}(i\omega_n+\omega_\ell)$$

$$= \sum_{k\ell} \frac{n_k n_\ell \; V^{1k}_{ma} V^{1\ell}_{an} V^{2-k}_{m'b} V^{2-\ell}_{bn'}}{(i\omega_n-\varepsilon_{am'}+\omega_k)(i\omega_n-\varepsilon_{nm'}+\omega_k+\omega_\ell)(i\omega_n-\varepsilon_{nb}+\omega_\ell)} \qquad (4D.1)$$

Contribution of diagram 4.12b to self energy:

$$\Sigma_{nn',mm'}(i\omega_n) \leftarrow \beta^{-1} \sum_{i\omega_{n'}} \beta^{-1} \sum_{i\omega_{n''}} F_{nb}(i\omega_{n'}) \; F_{nm'}(i\omega_{n'}+i\omega_{n''}-i\omega_n) F_{am'}(i\omega_{n''})$$

$$\sum_{k\ell} \frac{V^{2\ell}_{n'b} V^{2k}_{bm'} V^{1-\ell}_{na} V^{1-k}_{am}}{(i\omega_{n'}-i\omega_n-\omega_\ell)(i\omega_{n''}-i\omega_n-\omega_k)} \; e^{i\omega_{n'}0^+} \; e^{i\omega_{n''}0^+}$$

$$= \sum_{k\ell} \frac{n_k \; n_\ell \; V^{2\ell}_{n'b} V^{2k}_{bm'} V^{1-\ell}_{na} V^{1-k}_{am}}{(i\omega_n+\omega_\ell-\varepsilon_{nb})(i\omega_n+\omega_k+\omega_\ell-\varepsilon_{nm'})(i\omega_n+\omega_k-\varepsilon_{am'})} \qquad (4D.2)$$

Contribution of diagram 4.12c to self-energy:

$$\underset{\bar{m}m',\bar{n}n'}{\Sigma}(i\omega_n) \leftarrow \beta^{-1}\sum_{i\omega_{n'}}\beta^{-1}\sum_{i\omega_{n''}} F_{\bar{a}m'}(i\omega_{n'})F_{\bar{n}m'}(i\omega_{n'}+i\omega_{n''}-i\omega_n)F_{\bar{n}b}(i\omega_{n''})$$

$$\sum_{\bar{k}\bar{\ell}} \frac{V^{1-k}_{\bar{m}\bar{a}} V^{1-\ell}_{\bar{a}\bar{n}} V^{2k}_{\bar{m}'\bar{b}} V^{2\ell}_{\bar{b}\bar{n}'} e^{i\omega_{n'}0^+} e^{i\omega_{n''}0^+}}{(i\omega_{n'}-i\omega_n-\omega_{\bar{k}})(i\omega_{n''}-i\omega_n-\omega_{\bar{\ell}})}$$

$$= \sum_{k\ell} \frac{n_k n_\ell V^{1-k}_{\bar{m}\bar{a}} V^{1-\ell}_{\bar{a}\bar{n}} V^{2k}_{\bar{m}'\bar{b}} V^{2\ell}_{\bar{b}\bar{n}'}}{(i\omega_n+\omega_k-\varepsilon_{am'})(i\omega_n+\omega_k+\omega_\ell-\varepsilon_{nm'})(i\omega_n+\omega_\ell-\varepsilon_{nb})} \qquad (4D.3)$$

where we have used $\bar{\underline{k}} = -\underline{k}$, $\varepsilon_{\bar{a}} = \varepsilon_a$, and $\omega_{-\underline{k}} = \omega_{\underline{k}}$

APPENDIX 5A

(a) Relationship between G^{II} and G^{III}.

We shall prove (5.14) which relates the two GF's defined by (5.12) and (5.13) namely

$$G^{II}_{\eta\zeta\alpha\beta}(\underline{r}_3,\underline{r}_4;\underline{r}_1,\underline{r}_2;i\omega_1,i\omega_2) = \beta^{-1} \sum_{i\omega_3} G^{III}_{\eta\zeta\alpha\beta}(\underline{r}_3,\underline{r}_4;\underline{r}_1,\underline{r}_2;i\omega_1,i\omega_2,i\omega_3) \tag{5A.1}$$

Proof:

$$\text{R.H.S.} = \beta^{-1} \sum_{i\omega_3} \int_0^\beta d\tau_3\, e^{i\omega_1\tau_3}\, e^{-i\omega_3\tau_3}\, Q(\tau_3) \tag{5A.2}$$

where

$$Q(\tau_3) = \int_0^\beta d\tau_1 d\tau_2\, e^{-i\omega_1\tau_1 - i\omega_2\tau_2} \langle T_\tau \{A_\alpha(\chi_1) A_\beta(\chi_2) A_\eta(\underline{r}_3,\tau_3) A_\zeta(\underline{r}_4)\}\rangle \tag{5A.3}$$

which is related to the L.H.S. by (cf 5.12)

$$\text{L.H.S.} = G^{II}_{\eta\zeta\alpha\beta}(\underline{r}_3,\underline{r}_4;\underline{r}_1,\underline{r}_2;i\omega_1,i\omega_2) = Q(0) \tag{5A.4}$$

It will be noted that (5A.2) contains an expression

$$\beta^{-1} \sum_{i\omega_3} e^{-i\omega_3\tau_3} \equiv \beta^{-1} \sum_{n=-\infty}^{\infty} e^{\frac{-i2n\pi}{\beta}\tau_3} \quad \beta^{-1} \sum_{n=-\infty}^{\infty} e^{in\theta}$$

$$= \beta^{-1}[1 + 2(\cos\theta + \cos 2\theta + \cos 3\theta + \cdots)] = f(\theta) \tag{5A.5}$$

with $\theta = 2\pi\tau_3/\beta$.

This can be written in the form of the Fourier series

$$f(\theta) = \frac{1}{2} a_0 + \sum_{n=1}^{\infty} [a_n \cos(n\theta) + b_n \sin(n\theta)] \tag{5A.6}$$

with Fourier coefficients

$$a_n = 2\beta^{-1} \;\forall_n \quad \text{and} \quad b_n = 0 \;\forall_n$$

It is easy to show that the Dirac delta function $2\pi\beta^{-1}\delta(\theta)$ has identical Fourier coefficients enabling the identification

$$(5A.5) = \beta^{-1} \sum_{i\omega_3} e^{-i\omega_3\tau_3} = \beta^{-1}\, 2\pi\, \delta\left(\frac{2\pi}{\beta}\tau_3\right)$$

$$= \delta(\tau_3)$$

where we have used the property $\delta(ax) = a^{-1}\delta(x)$.

(Schiff 1968).

Using this result in (5A.2) then gives us the required result

$$\text{RHS} = \int_0^\beta d\tau_3 \left[\beta^{-1} \sum_{i\omega_3} e^{-i\omega_3\tau_3}\right] e^{i\omega_1\tau_3}\, Q(\tau_3)$$

$$= \int_0^\beta d\tau_3 \cdot \delta(\tau_3)\, e^{i\omega_1\tau_3}\, Q(\tau_3)$$

$$= Q(0)$$

$$= \text{L.H.S.}$$

This result can also be verified in detail by comparing the Lehmann representation of the two G.F.'s.

(b) Relating $\langle \Delta N(\underline{k})\rangle_t$ to G^{II}

We shall outline the proof of expression (5.15) which relates $\langle \Delta N(k)\rangle_t$ (5.10) to the two-time G.F. G^{II} (5.12). A study of (5.11) reveals that it contains an expression

$$\int_{-\infty}^{0} dt_1 \int_{-\infty}^{t_1} dt_2 \,\langle [[B, A_1(t_1)],\, A_2(t_2)]\rangle \exp\{-i(\xi_1+i\delta)t_1 - i(\xi_2+i\delta)t_2\} \qquad (5A.7)$$

where we define $B \equiv A_\eta(\underline{r}_3)A_\zeta(\underline{r}_4)$, $A_1(t) \equiv A_\alpha(\underline{r}_1, t)$, $A_2(t) \equiv A_\beta(\underline{r}_2, t)$. Expanding the commutations involved in this expression and transforming to the Lehmann representation we can evaluate the integrals over t_1 and t_2 to give

$$(5A.7) = -\sum_{nm\ell} \rho_n \left[\frac{A_2^{nm} A_1^{m\ell} B^{\ell n}}{(E_{nm}-\xi_2-i\delta)(E_{\ell m}-\xi_1-\xi_2-i\delta)} - \frac{A_2^{nm} B^{m\ell} A_1^{\ell n}}{(E_{nm}-\xi_2-i\delta)(E_{\ell m}-\xi_1-\xi_2-i\delta)} \right.$$

$$\left. - \frac{A_1^{nm} B^{m\ell} A_2^{\ell n}}{(E_{\ell n}-\xi_1-i\delta)(E_{\ell m}-\xi_1-\xi_2-2i\delta)} + \frac{B^{nm} A_1^{m\ell} A_2^{\ell n}}{(E_{\ell n}-\xi_2-i\delta)(E_{mn}-\xi_1-\xi_2-2i\delta)} \right] \qquad (5A.8)$$

This term corresponds to that of (5.11) multiplied by $J_\alpha^{ext}(\underline{r}_1)\, J_\beta^{*ext}(\underline{r}_2)$. The other term that is multiplied by $J_\alpha^{*ext}(\underline{r}_1)\, J_\beta^{ext}(\underline{r}_2)$ can similarly be shown to give expression (5.9) also but with ξ_1 and ξ_2 interchanged.

Similarly if (5.12) is reexpressed in the Lehmann representation and the integrals over τ_1 and τ_2 performed we obtain

$$G^{II}_{\eta\zeta\alpha\beta}(\bar{r}_3,\bar{r}_4;\bar{r}_1,\bar{r}_2;i\omega_1,i\omega_2) = \sum_{nm\ell} \rho_n \left[\frac{A_2^{nm} A_1^{m\ell} B^{\ell n}}{(E_{nm}-i\omega_2)(E_{n\ell}-i\omega_1-i\omega_2)} \right.$$

$$- \frac{A_2^{nm} B^{m\ell} A_1^{\ell n}}{(E_{nm}-i\omega_2)(E_{\ell m}-i\omega_1-i\omega_2)} - \frac{A_1^{nm} B^{m\ell} A_2^{\ell n}}{(E_{\ell n}-i\omega_2)(E_{\ell m}-i\omega_1-i\omega_2)} + \frac{B^{nm} A_1^{m\ell} A_2^{\ell n}}{(E_{\ell n}-i\omega_2)(E_{mn}-i\omega_1-i\omega_2)}$$

$$+ \frac{A_1^{nm} A_2^{m\ell} B^{\ell n}}{(E_{nm}-i\omega_1)(E_{n\ell}-i\omega_1-i\omega_2)} - \frac{A_1^{nm} B^{m\ell} A_2^{\ell n}}{(E_{nm}-i\omega_1)(E_{\ell m}-i\omega_1-i\omega_2)} - \frac{A_2^{nm} B^{m\ell} A_1^{\ell n}}{(E_{\ell n}-i\omega_1)(E_{\ell m}-i\omega_1-i\omega_2)}$$

$$\left. + \frac{B^{nm} A_2^{m\ell} A_1^{\ell n}}{(E_{\ell n}-i\omega_1)(E_{mn}-i\omega_1-i\omega_2)} \right] \qquad (5A.9)$$

Comparing (5.9) multiplied by its relevant J^{ext} factors plus the corresponding terms with ξ_1 and ξ_2 interchanged and noting the identity

$$\int_E dr_1 dr_2 \; A_1 A_2 \; J^{ext}_\alpha(\underline{r}_1) J^{*ext}_\beta(\underline{r}_2) = \int_E d\underline{r}_1 d\underline{r}_2 A_2 A_1 J^{*ext}_\alpha(\underline{r}_1) \; J^{ext}_\beta(\underline{r}_2)$$

because α and β are summed over and $\underline{r}_1, \underline{r}_2$ are integrated over the same range then we obtain the desired expression (5.11).

APPENDIX 6A

Contribution of figure 6.18:

This diagram gives a contribution

$$\sum_k \sum_{mn} \sum_{abcd} M_{ma} V^{-k}_{ab} M_{bn} M_{nc} V^{k}_{cd} M_{dm} \beta^{-1} \sum_{i\omega_{n'}} e^{i\omega_{n'} 0^+} F_m(i\omega_{n'}) F_a(i\omega_{n'}+i\omega_1) F_c(i\omega_{n'}-i\omega_2)$$

$$\beta^{-1} \sum_{i\omega_{n''}} e^{i\omega_{n''} 0^+} F_b(i\omega_{n''}) F_n(i\omega_{n''}-i\omega_1+i\omega_3) F_d(i\omega_{n''}-i\omega_1-i\omega_2)$$

$$\frac{1}{i\omega_{n''}-i\omega_{n'}-i\omega_1-\omega_k-\pi_k(i\omega_{n''}-i\omega_{n'}-i\omega_1)} \quad . \tag{6A.1}$$

Evaluating the sums over $i\omega_{n'}$ and $i\omega_{n''}$ by converting to a contour integral about the poles of the Fermi-Dirac function we obtain

$$(6A.1) = \sum_k \sum_{mn} \sum_{abcd} M_{ma} V^{-k}_{ab} M_{bn} M_{nc} V^{k}_{cd} M_{dm} \cdot \int_{-\infty}^{\infty} dx' \, [f_D(x') - f_D(x'+\omega_t)] L_m(x') F_a(x'+i\omega_1) F_c(x'-i\omega_2$$

$$\int_{-\infty}^{\infty} dx'' f_B(x'') L_a(x'') F_b(x''+x'+i\omega_1) F_d(x''+x'-i\omega_2) L_n(x''+x'+\omega_t) \tag{6A.2}$$

Making the sharply peaked approximations and replacing the x'', x' dependances of the f_B, f_D, shift and width functions and also in the vertex functions (F_a, F_b, F_c and F_d) we obtain

$$(6A.1) = \sum_k \sum_{mn} \sum_{abcd} M_{ma} V^{-k}_{ab} M_{bn} M_{nc} V^{k}_{cd} M_{dm} \; (\bar{\rho}_m - \bar{\rho}_n) F_a(\bar{\lambda}_m + i\omega_1) F_c(\bar{\lambda}_m - i\omega_2)$$

$$F_b(\bar{\lambda}_m + \bar{\omega}_k + i\omega_1) F_d(\bar{\lambda}_m + \bar{\omega}_k - i\omega_2) \quad \bar{n}_k$$

$$\int_{-\infty}^{\infty} dx' \, L_m(x') \cdot \int_{-\infty}^{\infty} dx'' \, L_k(x'') L_n(x''+x'+\omega_t) \quad . \tag{6A.3}$$

where $\bar{\omega}_k = \omega_k + \Delta_k(\bar{\omega}_k)$

and $\bar{n}_k = f_B(\bar{\omega}_k)$.

Evaluating the two nested convolutions of (6A.3) we obtain a contribution

$$\sum_{k}\sum_{mn}\bar{n}_{k}(\bar{\rho}_{m}-\bar{\rho}_{n})\left[\sum_{ab}M_{ma}V^{-k}_{ab}M_{bn}F_{a}(\bar{\lambda}_{m}+i\omega_{2})F_{c}(\bar{\lambda}_{m}-i\omega_{2})\right]$$

$$\left[\sum_{cd}M_{nc}V^{k}_{cd}M_{dm}F_{c}(\bar{\lambda}_{m}+\bar{\omega}_{k}+i\omega_{1})F_{d}(\bar{\lambda}_{m}+\bar{\omega}_{k}-i\omega_{2})\right]$$

$$\frac{\gamma_{m}+\gamma_{n}+\gamma_{k}}{(\omega_{0}-\omega+\bar{\omega}_{k}+\delta_{m}-\delta_{n})^{2}+(\gamma_{m}+\gamma_{n}+\gamma_{k})^{2}}\,. \qquad (6A.4)$$

APPENDIX 6B

Momentum conservation in Raman scattering

The creation operator $a^{\dagger}_{im}$ creates a level m on ion i. Let $\underline{r}_i = \underline{N}\cdot\underline{\underline{R}}$ where $\underline{N} = (n_1, n_2, n_3)$ where n_i are integers and $\underline{\underline{R}}$ be the base vectors of the (Bravais) lattice. The matrix elements of the dipole moment operator $M^{\alpha}_{mn}(\underline{r}_i)$ will include a factor $e^{i\underline{k}\cdot\underline{r}_i}$ where $\underline{k}$ is the wavevector of the photon,

e.g. 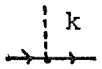

$\equiv M_{mn}(\underline{r}_i) \propto e^{i\underline{k}\cdot\underline{r}_i}$.

The P_{mn} and Q_{mn} functions of electronic and phonon Raman scattering respectively, ((6.9) and (6.19)), would then result in factors of the form:

$$\text{Electronic} \Rightarrow \sum_i e^{i\underline{r}_i\cdot(\underline{k}_s-\underline{k}_0)} = \sum_{\underline{N}} e^{i(\underline{k}_s-\underline{k}_0)\cdot\underline{\underline{R}}\cdot\underline{N}} = \Delta(\underline{k}_s-\underline{k}_0) \qquad (6B.1)$$

$$\text{Phonon} \Rightarrow \sum_i e^{i\underline{r}_i\cdot(\underline{k}_s-\underline{k}_0+\underline{\ell})} = \sum_{\underline{N}} e^{i(\underline{k}_s-\underline{k}_0+\underline{\ell})\cdot\underline{\underline{R}}\cdot\underline{N}} = \Delta(\underline{k}_s-\underline{k}_0+\underline{\ell}) \qquad (6B.2)$$

where $\underline{\ell}$ is the wavevector of the phonon, and Δ is defined as a Dirac delta function (up to a reciprocal lattice vector. cf Kittel p160 (1971)).

For a general n-phonon Raman scattering process a similar analysis gives a factor

$$\Delta(\underline{k}_s-\underline{k}_0+\sum_{i=1}^{n}\underline{\ell}_i) \qquad (6B.3)$$

where $\underline{\ell}_i$ are the wavevectors of the phonons while for an n-phonon absorption process we obtain a factor

$$\Delta(\underline{k}+\sum_{i=1}^{n}\underline{\ell}_i). \qquad (6B.4)$$

APPENDIX 7A

Disproof of Aminov's claims:

Aminov (1975) starts with the contribution to the differential cross-section derived by Shen (1974) and interpreted as R.R.S.,

$$f_{RRS}(\omega_\ell,\omega_s) = \frac{\omega_\ell\,\omega_s^{\,3}}{\pi c^4}\ \mathrm{Im}\ [\,(\omega_\ell-\omega_s-\omega_{fg}-i\Gamma_{fg})\,(\omega_s-\omega_{nt}+i\Gamma_{nf})\,(\omega_\ell-\omega_{ng}-i\Gamma_{ng})\,]^{-1} \tag{7A.1}$$

and RF

$$f_{RF}(\omega_\ell,\omega_s) = -\frac{\omega_\ell\,\omega_s^{\,3}}{\pi c^4}\ \mathrm{Im}\ [\,(\omega_\ell-\omega_{ng}+i\Gamma_{ng})\,(\omega_s-\omega_{nf}+i\Gamma_{nf})\,(\omega_\ell-\omega_{ng}-i\Gamma_{ng})\,]^{-1} \tag{7A.2}$$

In these equations ω_ℓ,ω_s are the incident and emitted frequencies with ω_ℓ close to the resonance frequency ω_{ng} of a three level system ground, intermediate and excited states g, n, and f respectively.

The integrated intensity of (7A.1) over the range of emitted frequencies within Δ of the spectral line at $\omega_s=\omega_{nf}$ gives a quantity

$$\int_{\omega_{nf}-\Delta}^{\omega_{nf}+\Delta} f_{RRS}(\omega_\ell,\omega_s)\,d\omega_s = \mathrm{Im}[\,(\omega_\ell-\omega_{ng}-i\Gamma_{ng})^{-1}(\omega_\ell-\omega_{ng}+i\Gamma_{nf}-i\Gamma_{fg})^{-1}]$$

$$\left\{2i\,\tan^{-1}\left(\frac{\Gamma_{nt}}{\Delta}\right)+\,i\,\tan^{-1}\left(\frac{\Gamma_{fg}}{\omega_\ell+\Delta-\omega_{ng}}\right)\,-i\,\tan^{-1}\left(\frac{\Gamma_{fg}}{\omega_\ell-\Delta-\omega_{ng}}\right)\right.$$

$$\left.+\,\ell n[\,(\omega_\ell-\Delta-\omega_{ng})^2+\Gamma_{fg}^2\,]^{\frac{1}{2}}-\ell n[\,(\omega_\ell+\Delta-\omega_{ng})^2+\Gamma_{fg}^2\,]^{\frac{1}{2}}\right\} \tag{7A.3}$$

Assuming the conditions $\Delta \gg \Gamma_{nf},\Gamma_{fg}$ and the condition $\omega_\ell-\omega_{ng} \ll \Delta$ (i.e. close to resonance) Aminov claimed the part of (7A.3) in curly brackets was of the order Γ/Δ and $(\omega_\ell-\omega_{ng})/\Delta$ and hence that the RRS contribution was negligible.

However it is found that the contribution to RF contains a similarly small quantity and a careful calculation gives, under the above conditions,

the approximations

$$\int_{\omega_{nf}-\Delta}^{\omega_{nf}+\Delta} f_{RRS}(\omega_\ell,\omega_s)\,d\omega_s \simeq \frac{\omega_\ell(\omega_{nf})^3}{\pi c^4}\,\frac{2}{(\omega_\ell-\omega_{ng})^2}\left\{\frac{2\Gamma_{nf}-\Gamma_{ng}}{\Delta}\right\} \tag{7A.4}$$

$$\int_{\omega_{nf}-\Delta}^{\omega_{nf}+\Delta} f_{RF}(\omega_\ell,\omega_s)\,d\omega_s \simeq \frac{\omega_\ell(\omega_{nf})^3}{\pi c^4}\,\frac{2}{(\omega_\ell-\omega_{ng})^2}\left\{\frac{\Gamma_{nf}}{\Delta}\right\} . \tag{7A.5}$$

The ratio of these contributions is then $(2\Gamma_{nf}-\Gamma_{ng})/\Gamma_{nf}$ which is <u>not</u> negligible compared to unity.

Appendix 7B

Raman-time dependent contributions:

In this appendix we calculate the time dependences of $\pi^{\alpha\eta}_{mn}(t,x,\omega')$ using various approximations for the diagrams that contribute to $P_{mn}(x,i\omega_1)$. We are required to evaluate

$$\pi^{\alpha\eta}_{mn}(t,x,\omega') = \int_{-\infty}^{\infty} \frac{d\xi}{2\pi} S(\xi) e^{-i(\xi+\omega_0)(t-\bar{R}/c)} P^{\alpha\eta}_{mn}(x,\xi+\omega_0+i\delta) \qquad (7B.1)$$

which can be expressed using (5.6) as the contour integral

$$\pi^{\alpha\eta}_{mn}(t,x,\omega') = e^{-i\omega_0(t-\bar{R}/c)} (i\Gamma_0/\pi) \int_C d\xi \frac{[e^{-i\xi(t-t_+)} - e^{-i\xi(t-t_-)}]}{(\xi+i\Gamma_0)(\xi-i\delta)}$$

$$P_{mn}(x,\xi+\omega_0+i\delta) \qquad (7B.2)$$

where $t_\pm = t - \bar{R}/c \pm T/2$ and C is one of the contours C_1, C_2 given in figure 7B.1.

Figure 7B.1.

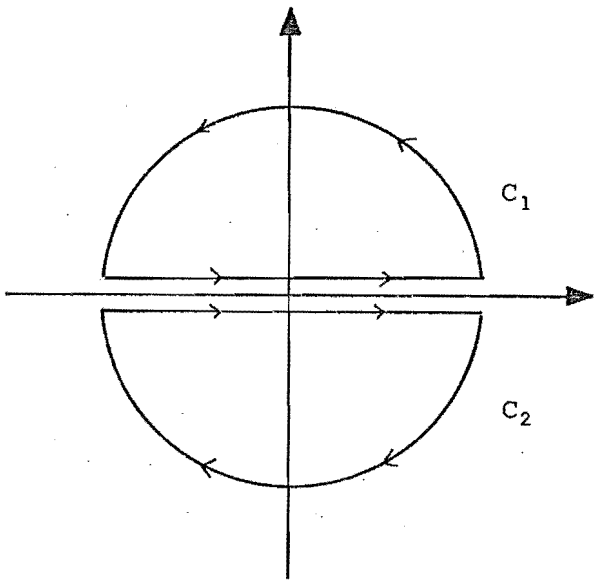

Contours C_1, C_2 are chosen to ensure that the integral around the half-circles (upper, lower respectively) vanish. This is achieved by the choices for the two parts of (7B.2) given in table 7B.1.

TABLE 7B.1

part	$t < t_-$	$t_- < t < t_+$	$t_+ < t$
$e^{-i\xi(t-t_+)}$	C_1	C_1	C_2
$e^{+i\xi(t-t_-)}$	C_1	C_2	C_2

A study of $P^{\alpha\eta}_{mn}(x,\xi+\omega_0+i\delta)$ reveals that, regarded as a function of ξ it contains no poles in the upper half-plane and as a result for $t < t_-$ we obtain

$$\pi^{\alpha\eta}_{mn}(t < t_-,x,\omega') = e^{-i\omega_0(t-\bar{R}/c)}\ 2i[\,e^{\delta(t-t_+)}-e^{\delta(t-t_-)}]$$

$$P_{mn}(x,\omega_0+2i\delta) \tag{7B.3}$$

which vanishes upon taking the limit $\delta \to 0$. This result is equivalent to the casual property (7.21).

Expression (7B.2) for the other time regions $t_- < t < t_+$ and $t_+ < t$ must be evaluated for each particular form of $P_{mn}(x,\xi+\omega_0+i\delta)$.

(a) Dressed Time Dependence:

Using ${}^0P^{\alpha\eta}_{mn}(x,i\omega_1)$ defined by (6.14) results in a time dependence

$${}^0\pi^{\alpha\eta}_{mn}(t,x,\omega') = 2i\ e^{-i\omega_0(t-\bar{R}/c)}$$

$$\Bigg\{ \sum_s \frac{M^{\alpha}_{ms}\ M^{\eta}_{sn}[\,(\Delta_s + i\Gamma_s)G_0(t) - i\Gamma_0\ G_s(t)]}{(\Delta_s+i\Gamma_s)(\Delta_s+i\Gamma_s-i\Gamma_0)}$$

$$+ \sum_s \frac{M^{\eta}_{ms}\ M^{\alpha}_{sn}[\,(\Delta'_s - i\Gamma'_s)G_0(t) + i\Gamma_0\ G'_s(t)]}{(\Delta'_s-i\Gamma'_s)(\Delta'_s-i\Gamma'_s+i\Gamma_0)} \Bigg\} \tag{7B.4}$$

where $\Delta_s = x + \omega_0 - \lambda_s - \Delta_s(x)$

$$\Delta'_s = x + \omega' - \omega_0 - \lambda_s - \Delta_s(x+\omega')$$

$$\Gamma_s = \Gamma_s(x)$$

$$\Gamma'_s = \Gamma_s(x+\omega'). \tag{7B.5}$$

and

$$G_0(t) = \begin{cases} 0 & t < t_- \\ 1 - e^{-\Gamma_0(t-t_-)} & t_- < t < t_+ \\ [1 - e^{-\Gamma_0 T}] e^{-\Gamma_0(t-t_+)} & t_+ < t \end{cases}$$

$$G_s(t) = \begin{cases} 0 & t < t_- \\ 1 - e^{-(\Gamma_s - i\Delta_s)(t-t_-)} & t_- < t < t_+ \\ [1 - e^{-(\Gamma_s - i\Delta_s)T}] e^{-(\Gamma_s - i\Delta_s)(t-t_+)} & t_+ < t \end{cases} \qquad (7B.6)$$

$$G'_s(t) = \begin{cases} 0 & t < t_- \\ 1 - e^{-(\Gamma'_s + i\Delta'_s)(t-t_-)} & t_- < t < t_+ \\ [1 - e^{-(\Gamma'_s + i\Delta'_s)T}] e^{-(\Gamma'_s + i\Delta'_s)(t-t_+)} & t_+ < t \end{cases}$$

Using the lorentzian approximation, $x = \bar{\lambda}_m$, and quasi-steady state approximation $\omega' = \omega_t$ $(= \omega_0 - \omega)$ then parameters (7B.5) become

$$\Delta_s = \omega_0 + \delta_m - \delta_s$$

$$\Delta'_s = \omega + \delta_m - \delta_s \,. \qquad (7B.7)$$

The resonance condition occurs when Δ_s, for some s in the sum of (7B.4), vanishes. Under such conditions the first term in curly brackets, for this s, dominates every other contribution to the sum giving the time dependence (7.16).

(b) Zero-order time dependence

The evaluation of (7B.2) for the zero-order diagrams, where $P^{\alpha\eta}_{mn}(i\omega_1)$ defined by (6.7) is substituted for $P^{\alpha\eta}_{mn}(x,i\omega_1)$, can be obtained from the expression (7B.4) by setting Γ_s and Γ'_s to zero for every term in the sum of making the substitutions $x = \lambda_m$ and $\omega' = \omega_{mn}$ giving

$$
{}^{0}\pi^{\alpha\eta}_{mn}(t,\omega_{nm}) = 2i\, e^{-i\omega_0 (t - \bar{R}/c)}
$$

$$
\left\{ \sum_s \frac{M^{\alpha}_{ms}\, M^{\eta}_{sn} [\Delta_s\, G_0(t) - i\Gamma_0\, {}^{0}G_s(t)]}{\Delta_s(\Delta_s - i\Gamma_0)} \right.
$$

$$
\left. + \sum_s \frac{M^{\eta}_{ms}\, M^{\alpha}_{sn}\, \Delta'_s\, G_0(t) + i\Gamma_0\, {}^{0}G'_s(t)}{\Delta'_s(\Delta'_s + i\Gamma_0)} \right\} \qquad (7B.8)
$$

where

$$
\Delta_s = \omega_0 + \omega_{ms}
$$

$$
\Delta'_s = \omega_{ns} - \omega_0
$$

and

$$
{}^{0}G_s(t) = \begin{cases} 0 & t < t_- \\ 1 - e^{i\Delta_s (t-t_-)} & t_- < t < t_+ \\ [1 - e^{i\Delta_s T}] e^{i\Delta_s (t-t_+)} & t_+ < t \end{cases}
$$

$$
{}^{0}G'_s(t) = \begin{cases} 0 & t < t_- \\ 1 - e^{-i\Delta'_s (t-t_-)} & t_- < t < t_+ \\ [1 - e^{-i\Delta'_s T}] e^{-i\Delta'_s (t-t_+)} & t_+ < t \end{cases} \qquad (7B.9)
$$

(c) A Fourth-Order Raman time-dependent contribution

We shall evaluate the contribution to the time-dependence of (7.20) from the first term of (6.17) namely

$$
{}^{2}P^{\alpha\eta}_{mn}(x,i\omega_1) = \sum_{abc} \sum_k \binom{n_k}{n_k+1} V^{k}_{mn}\, M^{\alpha}_{ab}\, M^{\eta}_{bc}\, V^{k}_{cn}\, A_a\, (x \pm \omega_k)
$$

$$
A_c(x + \omega' \pm \omega_k) \cdot \frac{1}{x + i\omega_1 \pm \omega_k - \lambda_b - \Sigma_b\, (x + i\omega_1 \pm \omega_k)} \cdot \qquad (7B.10)
$$

This results in a time-dependence

$$
{}^{2}\pi^{\alpha\eta}_{mn}(t,\bar{\lambda}_m,\omega') = \sum_{ac} \sum_k \binom{n_k}{n_k+1} V^{k}_{ma}\, M^{\alpha}_{ab}\, M^{\eta}_{bc}\, V^{k}_{cn}
$$

$$A_a(\bar{\lambda}_m \pm \omega_k)\; A_c(\bar{\lambda}_m + \omega' \pm \omega_k)\; .\; 2i\; e^{-i\omega_0(t - \bar{R}/c)}$$

$$\sum_b \frac{[(\Delta_b + i\Gamma_b)G_0(t) - i\Gamma_0 G_b(t)]}{(\Delta_b + i\Gamma_b)(\Delta_b + i\Gamma_b - i\Gamma_0)} \qquad (7B.11)$$

where $\Delta_b = \omega_0 \pm \omega_k + \bar{\lambda}_m - \lambda_b - \Delta_b(\bar{\lambda}_m \pm \omega_k)$

$\equiv \omega_0 \pm \omega_k + \delta_m - \delta_b$

$\Gamma_b = \Gamma_b(\bar{\lambda}_m \pm \omega_k)$

Expression (7B.11) involves both a sum over phonon frequencies (ω_k) and over energy levels (δ_b) and we expect a resonant condition for b and k such that both Δ_b vanishes and k corresponds to a peak in the phonon density of states. On exact resonance the time dependence will be similar to that of (7.16), (cf figure 7.6), but will reflect the width Γ_b. Because of the sum over phonon frequencies we expect this to result in resonances that are less sharp tending to give less distinct time-dependences than the second-order expression (7B.4).

APPENDIX 7C

One-Phonon time dependent contribution

In this approximation we calculate the contribution to $f_{\Theta_{mn}^{\alpha\eta}}(t,\bar{\lambda}_m,\omega',\pm\omega_k)$ by the contribution

$$\varrho_{mn}^{\alpha\eta}(\bar{\lambda}_m,i\omega_1,\pm\omega_k) = \sum_{ab} \frac{M_{ma}^{\alpha} V_{ab}^{k} M_{bn}^{\eta}}{(\bar{\lambda}_m+i\omega_1-\lambda_a-\Sigma_a(\bar{\lambda}_m+i\omega_1))(\bar{\lambda}_m+i\omega_1\pm\omega_k-\lambda_b-\Sigma_b(\bar{\lambda}_m+i\omega_1\pm\omega_k))} \tag{7C.1}$$

which is the contribution calculated by Kushinoki.

Using (5.7) we can re-express (7.23) as

$$f_{\Theta_{mn}^{\alpha\eta}}(t,\bar{\lambda}_m,\omega',\pm\omega_k) = e^{-i\omega_0(t-\bar{R}/c)}(i\Gamma_o/\pi) \int_C d\xi \frac{[e^{-i\xi(t-t_+)} - e^{-i\xi(t-t_-)}]}{(\xi+i\Gamma_0)(\xi-i\delta)} f_{\varrho_{mn}^{\alpha\eta}}(\bar{\lambda}_m,\xi+\omega_0+i\delta,\pm\omega_k) \tag{7C.2}$$

where contour C is chosen in the same manner as discussed in appendix 7B. (cf Table 7B.1 and figure 7B.1).

The function $f_{\varrho.}(\bar{\lambda}_m,\xi+\omega_0+i\delta,\pm\omega_k)$, regarded as a function of ξ only has poles in the lower half-plane and this gives the casual relationship

$$f_{\Theta_{mn}^{\alpha\eta}}(t,\lambda_m,\omega',\pm\omega_k) = 0 \quad \text{if} \quad t < t_- \ . \tag{7C.3}$$

Substituting (7C.1) in (7C.2) gives

$$f_{\Theta_{mn}^{\alpha\eta}}(t,\bar{\lambda}_m,\omega',\pm\omega_k) = 2i\, e^{-i\omega_0(t-\bar{R}/c)} \sum_{ab} M_{ab}^{\alpha} V_{ab}^{k} M_{bn}^{\eta}$$

$$\left[\frac{G_0(t)}{(\Delta_a+i\Gamma_a-i\Gamma_0)(\Delta_b+i\Gamma_b-i\Gamma_0)} + \frac{i\Gamma_0}{\Delta_a-\Delta_b+i\Gamma_a-i\Gamma_b} \left\{ \right.\right.$$

$$\left.\left. \frac{G_a(t)}{(\Delta_a+i\Gamma_a)(\Delta_a+i\Gamma_a-i\Gamma_0)} - \frac{G_b(t)}{(\Delta_b+i\Gamma_b)(\Delta_b+i\Gamma_b-i\Gamma_0)} \right\} \right] \qquad (7C.4)$$

where $\Delta_a = \omega_0+\delta_m-\delta_a$, $\Delta_b = \omega_0+\delta_m-\delta_b\pm\omega_k$, $G_0(t)$ is defined by (7B.6) and for i = a,b we have

$$G_i(t) = \begin{cases} 0 & t<t_- \\ 1 - e^{-(\Gamma_i+i\Delta_i)(t-t_-)} & t_-<t<t_+ \\ [1 - e^{-(\Gamma_i+i\Delta_i)T}]\, e^{-(\Gamma_i+i\Delta_i)(t-t_+)} & t_+<t \end{cases} \qquad (7C.5)$$

Resonance conditions occur when either

(i) $\Delta_a = 0$

and/or

(ii) $\Delta_b = 0$ and there is a peak in the phonon density of states.

The contributions containing the factors $G_0(t)$, $G_a(t)$ and $G_b(t)$ have rise and decay time constants Γ_0, Γ_a and Γ_b respectively. Condition (i) for resonance is identical with that for the ordinary Raman expression (7B.4) and will result in the same time-dependence. Condition (ii) is identical to the resonance condition for the fourth-order Raman contribution (7B.11) and results in the same time-dependence as this term with its corresponding less distinct resonance. If both resonance conditions (i) and (ii) are satisfied simultaneously then we can simplify (7C.4) giving

$$f_{\Theta_{mn}^{\alpha\eta}}(t,\bar{\lambda}_m,\omega',\pm\omega_k) = 2i\, e^{-i\omega_0(t-\bar{R}/C)}$$

$$\frac{M_{ma}^{\alpha} V_{ab}^{k} M_{bn}^{\eta}}{(\Delta_a+i\Gamma_a-(i\Gamma_0)^2} \left[G_0(t) + \frac{i\Gamma_0}{(\Delta_a+i\Gamma_a)^2} G_a(t) \right] \qquad (7C.6)$$

REFERENCES

Abou-Ghantous M., Jaussaud P.C., Bates C.A., Fletcher J.R. and Moore W.S.
1974 Phys. Rev. Lett. 33, 530-3.

Abramowitz M. and Stegun I.A. 1965 Handbook of mathematical functions, with formulas, graphs and mathematical tables. N. Y. Dover Publications.

Abrikosov A.A. 1965 Physics 2, 5-20.
1968a Soviet Physics J.E.T.P. 26, 641-6.
1968b Soviet Physics J.E.T.P. 26, 1192-8.

Abrikosov A.A., Gor'kov L.P. and Dzyaloshinski I.E.
1959 Soviet Physics J.E.T.P. 36, 636-41.
1963 Methods of Quantum Field Theory in Statistical Physics transl. by Silverman R.A. New Jersey Prentice-Hall.

Aharonov Y. and Bohn D. 1961 Phys. Rev. 122, 1649-58.
1964 Phys. Rev. 134, B1417-8.

Aharonov Y. and Safko J. 1975 Annals of Phys. 91, 279-94.

Allen S.J. 1968 Phys. Rev. 166, 530-9.

Allen S.J. and Guggenheim H.J. 1971a Phys. Rev. B 4, 937-50.
1971b Phys. Rev. B 4, 950-68.

Aminov L.K. 1975 Phys. Rev. B 12, 3490.

Anderson P.W. 1958 Phys. Rev. 112, 1900-16.

Anderson R.J., Baker J.M. and Birgeneau R.J.
1971 J. Phys. C : Solid St. Phys. 4, 1620-3

Baker J.M. 1971a Rep. Prog. Phys. 34, 109-73.
1971b J. Phys. C : Solid St. Phys. 4, 1631-4

Baker J.M. and Mau A.E. 1967 Can. J. Phys. 45, 403-28.

Bareiss E.H. and Neuman C.P. 1965 Singular Integrals and Singular Integral Equations with a Cauchy Kernel and the Method of Symmetric Pairing Argonne Nat'l Lab. Report 6988.

Barker A.S. Jr. and Loudon R. 1972 Rev. Mod. Phys. 44, 18-47.

Barnes S.E. 1972 J. Phys. C : Solid St. Phys. 5, L178-80.
1974 Phys. Rev. B 9, 4789-807.

Barrie R. and Rystephanick R.G. 1966 Can. J. Phys. 44, 109-38.

Baym G. and Mermin N.D. 1961 J. Math. Phys. 2, 232-4.

Behringer J. 1974 in Molecular Spectroscopy vol. 2 : A review of the literature published during 1972 and early 1973. London The Chem. Soc.

Berestetskii V.B., Litshitz E.M. and Pitaevskii L.P. 1971 Relativistic Quantum Theory part 1 transl. by Syko J.B. and Bell J.S. Oxford Perganen Press.

Biegala L. 1976 Phys. Lett. 56A, 125-6.

Bjorken J.D. and Drell S.D. 1964 Relativistic Quantum Mechanics. N.Y. McGraw-Hill p.211.

Bloor D. and Copland G.M. 1972 Rep. Prog. Phys. 35, 1173-264.

Bohn D. and Bub J. 1966a Rev. Mod. Phys. 38, 453-69.
1966b Rev. Mod. Phys. 38, 470-5.

Born M. and Huang K. 1954 Dynamical Theory of Crystal Lattices Oxford Clarendon Press ppl99-203.

Bradbury M.I. and Newman D.J. 1968 Chem. Phy. Lett. 2, 495-7.
1971 J. Phys. Chem. Solids 32, 627-36.

Buckbinder I.L. and Westwanskii B. 1975 Journal of Magnetism and Magnetic Materials 1, 11-18.

Callen H.B. 1961 in Fluctuations, Relaxation and Resonance in Magnetic Systems Ed. ter Haar D. Edinburgh Oliver and Boyd ppl5-22.

Cardona M. 1975 Light Scattering in Solids vol.8 of Topics in Applied Physics Ed. M. Cardona N.Y. Springer-Verlag.

Care C.M. and Tucker J.W. 1976 J. Phys. C : Solid St. Phys. 9, 4237-50.

Churchill R.V. 1960 Complex Variables and applications Tokyo McGraw-Hill p.155.

Copland C.M. 1970 Chem. Phys. Lett. 7, 175-7.

Courtens E. and Szöke A. 1977 Phys. Rev. A 15, 1588-1603.

Cuden C.B. 1976 Phys. Rev. B 13, 1993-2002.

Davis P.J. and Rabinowitz P. 1967 Numerical Integration Massachusetts Blaisell Publ. Comp.

Delsart C., Pelletier-Allard N., and Pelletier R.
1974 Opt. Comm. 11, 84-8.

Doniach S. 1966 Phys. Rev. 144, 382-9.

Dyson F.J. 1949a Phys. Rev. 75, 486-502.
1949b Phys. Rev. 75, 1736-55.
1956a Phys. Rev.102, 1217-30.
1956b Phys. Rev.102, 1230-44.

Eliashberg G.M. 1962 Sov. Phys. J.E.T.P. 14, 886-92.

Elliot R.J. and Thorpe M.F. 1968 J.Appl. Phys. 39, 802-7.

Fetter A.L. and Walecka J.D. 1971 Quantum Theory of Many-Particle Systems N.Y. McGraw-Hill.

Feynman R.P. 1949a Phys. Rev. 76, 749-59.
1949b Phys. Rev. 76, 769-89.

Fidler F.B. and Tucker J.W. 1970a Solid St. Comm. 8, 2055-8.
1970b J. Phys. C : Solid St. Phys. 3, 1877-83.
1971 J. Phys. C : Solid St. Phys. 4, 2583-92.

Fogedby H.C. 1972 Phys. Lett. 41A, 103-4.

Fouche D.G. and Chang R.K. 1972 Phys. Rev. Lett. 29, 536-9.

Franken P.A. and Ward J.F. 1963 Rev. Mod. Phys. 35, 23-39.

Friedman J.M. and Hochstrasser R.M.
1974 Chem. Phys. 6, 155-65.

Friedman J.M., Rousseau D.L. and Bondybey V.E.
1976 Phys. Rev. Lett. 37, 1610-3.

Fulton R.L. 1974 J.Chem. Phys. 61, 435.

Galitskii V. and Migdal A.B. 1955 Soviet Phys. J.E.T.P. 7, 96-104.

Giovannini D. 1965 Scientific papers at the College of General Education, University of Tokyo 15, 49.

Gontier Y. and Trahin M. 1971 Phys. Rev. A 4, 1896-906.

Hackett P.A. 1976 Phys. Rev. Lett. 36, 1403-6.

Haberlandt H.and Kühnel A. 1973 phys. stat. sol. (b) 60, 625-32.

Halldorsson T. and Menke E. 1970 Z. Naturforsch 259, 1356.

Hameking H. and Wehrum R.P. 1975 J. Phys. C : Solid St. Phys. 8, 3468-74.

Hayes W. 1975 Contemp. Phys. 16, 69-91.

Heisenberg W. 1927 Z. Physik. 43, 172.

Heitler W. 1954 The quantum theory of radiation, Oxford Clarendon Press.

Hernandez R. and Walker M.B. 1972 Can. J. Phys. 50, 440-74.

Holstein T. and Primakoff H. 1940 Phys. Rev. 58, 1098-113.

Huber D.L. 1970 Phys. Rev. B 1, 3409-16.

Inoue M. and Moriya T. 1970 J. Phys. Soc. Jap. 29, 117-31.

Jacobsen E.H. and Stevens K.W.H.
1963 Phys. Rev. 129, 2036-44.

Jacon M. and Van Labeke D. 1975 Mol. Phys. 29, 1241-59.

Jenkins F.A. and White H.E. 1957 Fundamentals of Optics 3rd edit.
Tokyo McGraw-Hill p452.

Jennison R.C. 1961 Fourier Transforms and convolutions
for experimentalists Oxford Pergamon Press.

Johnstone I.W. 1975 Ph.D. thesis, University of Canterbury.

Judd B.R. 1967 Secound Quantization and Atomic
Spectroscopy Baltimore John Hopkins p41.

Kane-Maquire C. and Konigstein J. A.
1973 J. Chem. Phys. 59, 1899-1904.

Kawabata A. 1970 J. Phys. Soc. Jap. 29, 890-901.
1971a J. Phys. Soc. Jap. 30, 68-85.
1971b Vijnana Parishad Anusandhan Patrika
14, 157-79.

Keiter H. 1968 Z. Physik 213, 466-81.
1971 Phys. Lett. 36A, 257.

Kimble H.J. and Mandel L. 1975 Opt. Comm. 14, 167-72.

Kittel C. 1971 Introduction to Solid State Physics 4th edit. N.Y. Wiley & Sons Fig.12 p214.

Klein M.V. 1973 Phys. Rev. B 8, 919-21.

Klein M.V. and Colwell P.J. 1971 in Proceedings of the Secound International Conference on Light Scattering in Solids Ed. Balkanski M. Paris Flammarion pp65-9.

Kondilenko I.I., Korotkov P.A. and Strizhevskii V. L. 1960 Opt. & Spec. 9, 13-7.

Kramers H.A. 1930 Koninkl. Ned. Akad. Wetenschap, Proc. 33, 959.
1934 Physica 1, 182-92.

Kramers H.A. and Heisenberg W. 1925 Zs. f. Phys. 31, 681.

Krushinskii L.L. and Shorygin P.P. 1961 Opt. & Spec. 11, 12-7.

Kubo R. 1957 J. Phys. Soc. Jap. 12, 570-86.
1966 Rep. Prog. Phys. 29, 255-84.

Kushida T. 1969 Phys. Rev. 185, 500-8.

Kushida T. and Takushi E. 1975 Phys. Rev. B 12, 824-7.

Kusunoki M. 1976 Progr. Theor. Phys. Jap. 55, 692-709

Larson U. 1972 Z. Physik 256, 65-72.

Lindgärd P.A. and Danielsen O.

1974 J. Phys. C : Solid St. Phys. 7, 1523-35

1976 J. Phys. C : Solid St. Phys. 9, 2081-92.

Lipkin H.J. 1965 Lie Groups for Pedestrians Amsterdam North Holland.

Loudon R. 1964 Adv. Phys. 13, 423-82.

1973 The quantum theory of light Oxford Clarendon Press.

Louisell W.H. 1973 Quantum Statistical Properties of Radiation N.Y. John Wiley & Sons.

Low F. 1952 Phys. Rev. 88, 53-7.

Lyness J.N. 1969 J. ACM 16, 483-95.

McKeeman W.M. 1962 J. ACM 5, 604-5.

McKenzie B.J. and Stedman G.E.

1976 J. Phys. A : Math.Gen. 9, 187-95.

1977 J. Phys. C : Solid St. Phys. 10, 589-603

1978 - in preparation.

McMahon D.H. and Silsbee R.H.

1964 Phys. Rev. 135, A91-6.

Maleev S.V. 1957 Zh. eksper teer Fiz. 33, 1010.

Maradudin A.A. 1966 in Solid State Physics vol. 19 Eds. Seitz F. and Turnbull D. N.Y. Academic Press pp38-9.

Martin P.C. and Schwinger J. 1959 Phys. Rev. 115, 1342-73.

Matlak M. 1973a Acta Physica Polonica A43, 475-8.
1973b Acta Physica Polonica A44, 57-66.
1975 Acta Physica Polonica A47, 735-50.

Matsubara T. 1955 Prog. Theor. Phys. 14, 351-78.

Mattis D.C. 1965 The Theory of Magnetism. N.Y. Harper & Row,

Mattuck R.D. 1976 A guide to Feynman diagrams in the many-body problem 2nd edit. N.Y. McGraw-Hill.

Mayants L.S., Yourgrau W. and van der Merwe A.J. 1976 Ann. der Phys. 33, 21-35.

Metiu H., Ross J., and Nitzan A. 1975 J. Chem. Phys. 63, 1289-94.

Moordian A. 1970 Science 169, 20-5.
1972 Raman Spectroscopy of Solids in Laser Handbook Ed. Arecchi F.T. and Schultz-Du Bois E.O. Amsterdam North Holland pp1409-56.

Morozov V.A. and Shorygin P.P. 1966 Opt. & Spec. 20, 115-20.

Mukamel S., Ben-Reuven A. and Jortner J.

1975 Phys. Rev. A 12, 947-58.

1976 J. Chem. Phys. 64, 3971-5.

Mukamel S. and Jontner J. 1975 J. Chem. Phys. 62, 3609-15.

Murata K.K. 1972 Phys. Lett. 42A, 151-2.

Nishikawa K. and Barrie R. 1963 Can. J. Phys. 41, 1135-73.

O Berg J., Langhoff C.A. and Robinson G. W.

1974 Chem. Phys. Lett. 29, 305-9.

Oppermann R. 1973 Z. Physik 259, 524-9.

Pease M.C. 1965 Methods of Matrix Algebra N.Y.
Academic p321.

Personov R.I., Al'Skits E.I. and Bykovskaya L. A.

1972 Opt. Comm. 6, 169-73.

Pinczuk A. and Burstein E. 1975 in Light Scattering in Solids
vol. 8 of Topics in Applied Physics
Ed. M. Cardona N.Y. Springer-Verlag.

Riseberg L.A. 1972 Phys. Rev. Lett. 28, 786.

Rousseau D.L., Patterson G.D. and Williams P.F.

1975 Phys. Rev. Lett. 34, 1306-9.

St.Peters R.L., Silverston S.D., Lapp M. and Penney C.M.

1973 Phys. Rev. Lett. 30, 191-2.

Schaich W.L. and Ashcroft W.W. 1971 Phys. Rev. B 3, 2452-65.

Schiff L.J. 1968 Quantum Mechanics 3rd edit. Tokyo McGraw-Hill p57.

Schrieffer J.R. 1964 Theory of Superconductivity N.Y. Benjamin.

Schultz T. 1964 Quantum Field Theory and the many-body problem N.Y. Gordon & Breach.

Schultz T.D. and Kwok P.C. 1972 Phys. Lett. 39A, 402-4.

Schultz T.D. and Shapero D. 1973 Phys. Rev. B 7, 5090-100

Schwartz S.E. 1975 Phys. Rev. A 11, 1121-2.

Schwinger J. 1965 in Quantum Theory of Angular Momentum Ed. Biedenharn L. and van Dam H. N.Y. Academic

Sheard F.W. and Toombs G.A. 1973a Solid St. Comm. 12, 713-6
1973b J. Phys C : Solid St. Phys. 4 313-23.

Shen Y.R. 1974 Phys. Rev. B 9, 622-6.

Shorygin P.P. 1973 Sov. Phys. USPEKHI 16, 99-120.

Solin J.R. and Merkelo H. 1975 Phys. Rev. B 12, 624-9.

Spencer H.J. 1968 Phys. Rev. 167, 430-3.

Stedman G.E. 1968 Contemp. Phys. 9, 49-69.

1970a J.Phys. C : Solid St. Phys. 3, 1055-70.

1970b J. Phys.C : Solid St. Phys. 3, 2392-401.

1971a J.Phys. C : Solid St. Phys. 4, 1022-35.

1971b Phys.Lett 35A, 425-6.

1972a J.Phys. C : Solid St. Phys. 5, 121-33.

1972b J.Phys. C : Solid St. Phys. 5, 2665-8.

1973 J.Phys. C : Solid St. Phys. 6, 474-8.

1975 J.Phys. A : Math. Gen. 8, 1021-37.

1976a J.Phys. C : Solid St. Phys. 9, 535-51.

1976b J.Phys. A : Math. Gen. 12, 1999-2019.

1977 Submitted to J. Phys. C.

Stedman G.E. and Newman D.J. 1971 J. Chem. Phys. 55, 152-62.

Subramanian P.R. and Devanathan V.

1974 J. Phys. A : Math. Nucl. Gen. 7,1995-2007

Sugihara K. 1959 J Phys. Soc. Jap. 14, 1231-4.

Szabo A. 1970 Phys. Rev. Lett. 25, 924-6.

1971 Phys. Rev. Lett. 27, 323-6.

Takahashi Y. and Shibata F. 1975 J. Phys. Soc. Jap. 38, 656-68.

Toombs G.A. and Sheard F.W. 1973 J. Phys. C : Solid St. Phys. 6, 1467-88.

Trifonov E.D. and Poiker K. 1966 Sov. Phys. - Solid St. 7, 1897-902.

Trimper S. 1973 phys. stat. Sol.(b) 55, 279-85.

Tucker J.W. 1971 J.Phys. C : Solid St.Phys. 4, L266-8.
1972 J.Phys. C : Solid St.Phys. 5, 2064-76.
1973a Phys.Lett. 5, 431-2.
1973b J.Phys. C : Solid St.Phys. 6, 255-61.

Van Vleck J.H. 1937 Phys.Rev. 52, 1178-1198.
1962 Rev.Math.Fis.Theor. Univ. Natn. Tucuman 14, 189-99.

Verwoerd W.S. 1973 Phys. Lett. 43A, 535-6.
1974a Phys. Rev. B 10, 2868-82.
1974b Phys. Rev. B 10, 2883-91.

Wang Y.L. and Callen H.B. 1966 Phys. Rev. 148, 433-8.

Weisskopf V. and Wigner E. 1930a Zs f Phys. 63, 54.
1930b Zs f Phys. 65, 18.

Wick G.C. 1950 Phys. Rev. 80, 268-72.

Witschel W. 1971 Molecular Phys. 22, 869-79.
1975 Z Physik B21, 313-8.

Williams P.F., Rousseau D.L. and Dworetsky S.H.
1974 Phys. Rev. Lett. 32, 196-9.

Wöger W. and Zittartz J. 1973 Z. Physik 261, 59-70.

Wolf W.P. 1964 Proc. Int. Conf.Magnetism, Nottingham London Phys. Soc.
1971 J. Physique 32, suppl. C1, 24-33.

Wolf W.P. and Birgeneau R.J. 1968 Phys. Rev. 166, 376-82.

Woodward L.A. 1967 in Raman Spectroscopy Ed. Szymanski H.A. N.Y. Plenum Press p7.

Wybourne B.G. 1973 Int. J. Quantum Chem. 7, 1117-37.

Yang D. and Wang Y. 1974 Phys. Rev. B 10, 4714-23.
1975 Phys. Rev. B 12, 1057-70.

Yolin E.M. 1965 Proc. Phys. Soc. 85, 759-65.

Yu P.Y. and Shen Y.R. 1974 Phys. Rev.Lett. 32, 939-42.
1975 Phys. Rev. B 12, 1377-94.

Yu P.Y., Shen Y.R. and Petroff Y.
1973 Phys. Rev. Lett. 30, 283-6.

Zawadowski A. 1969 Z. Physik 226, 235-65.

PUBLICATIONS

An account of the work appearing in chapter 2 of this thesis has been published in

Journal of Physics A : Mathematical and General Physics

vol. 9, pp 187-95, (1976)

and the work of chapters 5,6 and 7 has been published in 1977. in

Journal of Physics C : Solid State Physics, 10, 589-603

Both of these have been in collaboration with G.E. Stedman and copies of the scripts are included herein.

A paper on the work of chapter 4 is in preparation and shall be submitted for publication soon.

J. Phys. C: Solid State Phys., Vol. 10, 1977. Printed in Great Britain. © 1977

pp 589–603

A quantum field theoretic formulation of Raman spectral line shapes

B J McKenzie and G E Stedman†
Department of Physics, University of Canterbury, Christchurch 1, New Zealand

Received 13 June 1977, in final form 28 September 1977

Abstract. The Raman spectrum of a solid is formulated using quantum field theory. The photons are assumed to couple via localised electronic states, e.g. paramagnetic impurities. The laser is assumed to be of low power and to have a frequency well away from any electronic resonance. It is shown that the phonon-induced shift and width of each of the lines corresponding to an electronic transition, a first-order phonon line, and a vibronic transition is formally the same whether the transition is studied by absorption or by Raman spectroscopy. Width and shift contributions are given to second order in broadening interactions for the second-order phonon Raman spectrum. These results exhibit complications in some attempts to compare broadening parameters in different experiments. Some consequential adjustments to formulations of the spectrum of resonance fluorescence are suggested.

1. Introduction

Since the renaissance in Raman spectroscopy, following the advent of the laser, the study of elementary excitations of crystals by light scattering has received increasing attention. Now that inhomogeneous broadening can be reduced and even eliminated, a study of the homogeneous width in some detail assumes a new interest. Most of the phenomenological theories of line broadening, used for example in discussions of resonance fluorescence in gases and solids, make assumptions regarding the additivity of single level widths and the equality of broadening parameters in different experiments which are known to be untenable in the simpler case of absorption spectroscopy (Stedman 1977, hereafter referred to as I, and references therein). The more fundamental approach of quantum optics has been implemented only under severe restrictions on the complexity of the system. Often only coupling to one or two reservoir modes is considered. It has been shown both theoretically and experimentally in the problem of the Jahn–Teller effect that consideration of multimode effects can introduce qualitative changes (Abou-Ghantous *et al* 1974). Indeed, some recent papers have discussed the modification of the Raman spectrum occasioned by Jahn–Teller activity. A more thorough formulation and analysis of the Raman spectrum seems opportune.

Our approach builds on the quadratic response theoretic formalism of Raman spectra developed by Kawabata (1971) for metals and applied by Kusunoki (1976) to gas molecules and Cuden (1976) to superconductivity. Our application is to electronic Raman spectra, or electron-mediated phonon Raman spectra, where the laser power is low and in systems in thermal equilibrium for which the electronic states are essentially

† Until June 1978: Clarendon Laboratory, Oxford OX1 3PU, UK.

8313 Solid State Phys. Ms. 557 569–1E 10/12 FL 26.10.77 31 ems 3G

localised, e.g. paramagnetic ions in a diamagnetic host. This necessitates adaptation of the formalism in such a manner as to count the effects of singly occupied states only: the formal consequences can be described as taking an Abrikosov projection of the usual fermion many body theory (e.g. McKenzie and Stedman 1976). An analogous formalism of the absorption spectrum has been given in I. In that case, the spectrum could be related, via the Golden Rule, to the Lehmann spectral representation of a two-particle electronic Green function whose diagram expansion proceeds by standard many-body techniques.

In the case of the light scattering spectrum it is not so straightforward to determine which four-particle electronic Green function has a Lehmann spectral representation reducing to the appropriate Golden Rule expression (Kramers–Heisenberg relation). We shall follow Kawabata's approach, in which attention is focused on the two-particle photon Green function. To avoid undue repetition of his work, we have kept § 2 brief and formal. The identification of particular contributions in § 3 then follows from the relatively simple technique used in I. Some comments on the theory of resonance fluorescence are offered in § 4 in the light of the conclusions of § 3.

2. Green function formulation from quadratic response theory

Consider a source confined to a region V_E sending light onto a sample which scatters it into a detector, confined to a region V_D. The two regions are in the upper half plane ($z > 0$, of figure 1 of Kawabata 1971) and the sample in the lower half plane. The dimensions of V_E, V_D are much greater than optical wavelengths. If $\boldsymbol{A}(\boldsymbol{r})$ is the vector potential at $\boldsymbol{r}$ with Fourier transform $\boldsymbol{A}(\boldsymbol{k})$ where

$$\boldsymbol{A}(\boldsymbol{k}) = \int_{V_D} \mathrm{d}\boldsymbol{r}\, \boldsymbol{A}(\boldsymbol{r}) \exp(-\mathrm{i}\boldsymbol{k}.\boldsymbol{r})$$

we wish to find the potential $\boldsymbol{A}(\boldsymbol{k})$ in the region V_D produced by an external current $\boldsymbol{J}(\boldsymbol{r}, t)$ in V_E. The radiation field–current interaction is written (e.g. Abrikosov *et al* 1963; we set the mass of the charge carriers and $\hbar$ equal to unity)

$$\mathscr{H}^{\mathrm{ext}}(t) = -\int \mathrm{d}\boldsymbol{r}\, \boldsymbol{A}(\boldsymbol{r}).\boldsymbol{J}(\boldsymbol{r}, t). \tag{1}$$

We define a quantity

$$N(\boldsymbol{k}) = (\boldsymbol{e}.\boldsymbol{A}(\boldsymbol{k}))\,(\boldsymbol{e}.\boldsymbol{A}^{+}(\boldsymbol{k})) \tag{2}$$

which is related to the number density of photons of energy ck with polarisation $\boldsymbol{e}$. From quadratic response theory (Kubo 1966, Callen 1961) $N(\boldsymbol{k})$ can be represented by (cf. Kusunoki 1976 equation (2.11))

$$\langle \Delta N(\boldsymbol{k})\rangle_t = -\int_{-\infty}^{t} \mathrm{d}t_1 \int_{-\infty}^{t_1} \mathrm{d}t_2 \int_{V_E} \mathrm{d}\boldsymbol{r}_1\, \mathrm{d}\boldsymbol{r}_2\, J_\alpha(\boldsymbol{r}_1, t_1)\, J_\beta(\boldsymbol{r}_2, t_2)$$
$$\langle [[N(\boldsymbol{k}), A_\alpha(\boldsymbol{r}_1, t_1 - t)], A_\beta(\boldsymbol{r}_2, t_2 - t)]\rangle \tag{3}$$

where a time-dependent operator has the Heisenberg form and angular brackets represent a thermal expectation value with respect to a Hamiltonian $\mathscr{H}$ for the total system.

We write the time dependence of the generating current in the form

$$J(\boldsymbol{r}, t) = J(\boldsymbol{r}) \int_{-\infty}^{\infty} \mathrm{d}\xi\, S(\xi - \omega_0) \exp[-\mathrm{i}(\xi + \mathrm{i}\delta)\, t] + \text{c.c.} \tag{4}$$

where δ is an infinitesimal positive quantity, $\mathrm{d} = \mathrm{d}/2\pi$, ω_0 is the instantaneous laser frequency and the form of S depends on the laser pulse. We assume $S^*(\xi) = S(-\xi)$. After some manipulation and approximation (Kawabata 1971, equation (2.9)) we obtain

$$\langle \Delta N(\boldsymbol{k})\rangle_t = -\int_{-\infty}^{0} \mathrm{d}t_1 \int_{-\infty}^{t_1} \mathrm{d}t_2 \int_{V_E} \mathrm{d}\boldsymbol{r}_1 \mathrm{d}\boldsymbol{r}_2 \int_{V_D} \mathrm{d}\boldsymbol{r}_3 \mathrm{d}\boldsymbol{r}_4 \exp[\mathrm{i}\boldsymbol{k}.(\boldsymbol{r}_4 - \boldsymbol{r}_3)]$$
$$e_\eta e_\zeta \langle [[A_\eta(\boldsymbol{r}_3)\, A_\zeta(\boldsymbol{r}_4), A_\alpha(\boldsymbol{r}_1, t_1)], A_\beta(\boldsymbol{r}_2, t_2)]\rangle \int\int_{-\infty}^{\infty} \mathrm{d}\xi_1\, \mathrm{d}\xi_2$$
$$S(\xi_1 - \omega_0)\, S(\xi_2 + \omega_0) \exp[-\mathrm{i}(\xi_1 + \xi_2 + 2\mathrm{i}\delta)t]\, \{J_\alpha(\boldsymbol{r}_1) J_\beta^*(\boldsymbol{r}_2) \exp$$
$$[-\mathrm{i}(\xi_1 + \mathrm{i}\delta)t_1 - \mathrm{i}(\xi_2 + \mathrm{i}\delta)t_2] + J_\alpha^*(\boldsymbol{r}_1)\, J_\beta(\boldsymbol{r}_2)$$
$$\times \exp([-\mathrm{i}(\xi_1 + \mathrm{i}\delta)\, t_2 - \mathrm{i}(\xi_2 + \mathrm{i}\delta)\, t_1])\}\,. \tag{5}$$

Now let us define the thermal two-photon Green function

$$\mathscr{G}^{\mathrm{II}}_{\eta\zeta\alpha\beta}(\boldsymbol{r}_3, \boldsymbol{r}_4; \boldsymbol{r}_1, \boldsymbol{r}_2; E_1, E_2) = \int\int_0^{\beta} \mathrm{d}\tau_1 \mathrm{d}\tau_2 \exp[-E_1\tau_1 - E_2\tau_2]$$
$$\times \langle T_\tau\{A_\alpha(\chi_1)\, A_\beta(\chi_2)\, A_\eta(\boldsymbol{r}_3)\, A_\zeta(\boldsymbol{r}_4)\}\rangle \tag{6}$$

where $\chi_i = (\boldsymbol{r}_i, \tau_i)$, T_τ is the chronological operator and E_1, E_2 range over all even multiples of $\mathrm{i}\pi/\beta$. This Green function has a Lehmann spectral representation which can be related to that of the expectation value appearing in equation (5) (Kawabata 1971) so that

$$\langle \Delta N(\boldsymbol{k})\rangle_t = \int_{V_E} \mathrm{d}\boldsymbol{r}_1 \mathrm{d}\boldsymbol{r}_2 \int_{V_D} \mathrm{d}\boldsymbol{r}_3 \mathrm{d}\boldsymbol{r}_4 \exp[\mathrm{i}\boldsymbol{k}.(\boldsymbol{r}_4 - \boldsymbol{r}_3)]\, e_\eta e_\zeta \int\int_{-\infty}^{\infty} \mathrm{d}\xi_1\, \mathrm{d}\xi_2\, S(\xi_1 - \omega_0)$$
$$\times S(\xi_2 + \omega_0) \exp[-\mathrm{i}t(\xi_1 + \xi_2 + 2\mathrm{i}\delta)]\, \mathscr{G}^{\mathrm{II}}_{\eta\zeta\alpha\beta}(\boldsymbol{r}_3, \boldsymbol{r}_4; \boldsymbol{r}_1, \boldsymbol{r}_2, \xi_1 + \mathrm{i}\delta,$$
$$\xi_2 + \mathrm{i}\delta)\, J_\alpha(\boldsymbol{r}_1)\, J_\beta^*(\boldsymbol{r}_2) \tag{7}$$

where E_1, E_2 have been analytically continued to the upper half plane.

At this point it would seem possible to expand the traces in $\mathscr{G}^{\mathrm{II}}$ by the usual perturbation expansion of the interactions contained in $\mathscr{H}$, and thus to obtain a diagram expansion of the Raman spectrum. However, the two energies E_1, E_2 are both connected with the source and do not suffice to define the frequencies of both incoming and emitted light. It is necessary to work with a Green function containing three energy variables defined by (E_3 also range over even multiples of $\mathrm{i}\pi/\beta$):

$$\mathscr{G}^{\mathrm{III}}_{\eta\zeta\alpha\beta}(\boldsymbol{r}_3, \boldsymbol{r}_4; \boldsymbol{r}_1, \boldsymbol{r}_2, E_1, E_2, E_3) = \int\int\int_0^{\beta} \mathrm{d}\tau_1 \mathrm{d}\tau_2 \mathrm{d}\tau_3 \exp(-E_1\tau_1 - E_2\tau_2$$
$$- (E_3 - E_1)\,\tau_3) \langle T_\tau\{A_\alpha(\chi_1)\, A_\beta(\chi_2)\, A_\eta(\chi_3)\, A_\zeta(\boldsymbol{r}_4, 0)\}\rangle. \tag{8}$$

This is related to $\mathscr{G}^{\mathrm{II}}$ by

$$\mathscr{G}^{\mathrm{II}}_{\eta\zeta\alpha\beta}(\boldsymbol{r}_3, \boldsymbol{r}_4; \boldsymbol{r}_1, \boldsymbol{r}_2, E_1, E_2) = \beta^{-1} \sum_{E_3} \mathscr{G}^{\mathrm{III}}_{\eta\zeta\alpha\beta}(\boldsymbol{r}_3, \boldsymbol{r}_4; \boldsymbol{r}_1, \boldsymbol{r}_2, E_1, E_2, E_3)\,. \tag{9}$$

The function $\mathscr{G}^{III}$ can then be expanded, the Raman terms identified, and the result substituted into equations (9) and (7) for precise definition of the spectrum.

The zero-order Hamiltonian for the scattering centre is taken to have the form

$$\mathscr{H}_0 = \sum_m E_m a_m^+ a_m + \sum_k \omega_k (b_k^+ b_k + \tfrac{1}{2}) \tag{10}$$

where a_m^+ creates electronic state m of energy E_m, and b_k^+ an excitation in lattice mode k of frequency ω_k. We use fermion statistics for a_m^+, and correct for the unphysical states this introduces by adding a constant λ to each energy to give an energy $\lambda_m = \lambda + E_m$, then projecting out the one-particle contributions after a calculation by the Abrikosov method, allowing λ to become infinite (McKenzie and Stedman 1976). Within the scatterer, as in I, we shall consider interactions between electrons and phonons of all orders of non-linearity

$$\mathscr{H}_{ep} = \sum_{pqk\pm} a_p^+ a_q b_k^{\pm} (V_{pqk\pm} + \sum_{l\pm} b_l^{\pm} V_{pqk\pm l\pm} + \ldots) \tag{11}$$

as well as anharmonic interactions amongst lattice phonons

$$\mathscr{H}_{pp} = \sum_{jkl} \phi_j \phi_k \phi_l (W_{jkl} + \sum_{l'} \phi_{l'} W_{jkll'} + \ldots) \tag{12}$$

($\phi_k = b_k + b_k^+$). A W_{jkl} vertex with signs on the suffices denotes a coefficient of the corresponding $b_k^{\pm}$ rather than ϕ_k. The interaction with the radiation will be written

$$\mathscr{H}_{rad} = -\frac{e}{m} \sum_{imn} M_{mn}^{\alpha}(\mathbf{r}_i)\, a_m^+ a_n A_{\alpha}(\mathbf{r}_i) \tag{13}$$

where in the dipole approximation (Louisell 1973) to the matrix elements of $e\boldsymbol{A} \cdot \boldsymbol{p}/m$, we set $M_{mn}^{\alpha}(\mathbf{r}_i) = \langle m|p_{\alpha}|n\rangle$ and we have ignored terms which are quadratic in the vector potential. Corresponding to the photon, ionic and phonon excitations we define unperturbed single-particle propagators in the standard form

$$\begin{aligned}
\mathscr{D}_{\alpha\alpha'}^{0}(\mathbf{r}, \mathbf{r}', E) &= \int_0^{\beta} d\tau \exp(E\tau) \langle T_{\tau}\{A_{\alpha}(\mathbf{r}, \tau) A_{\alpha'}(\mathbf{r}', 0)\}\rangle_0 \\
\mathscr{G}_{mn}^{i0}(E') &= -\int_0^{\beta} d\tau \exp(E'\tau) \langle T_{\tau}\{a_m(\tau) a_n^+(0)\}\rangle_0 \\
P_{kk'}^{0}(E) &= \int_0^{\beta} d\tau \exp(E\tau) \langle T_{\tau}\{b_k(\tau) b_{k'}^+(0)\}\rangle_0
\end{aligned} \tag{14}$$

represented by broken, solid and wavy lines respectively. E ranges over even multiples, and E' over odd multiples, of $i\pi/\beta$. We take the electronic operators in $\mathscr{G}_{mn}^{i0}$ to be diagonal in the electronic site label i, i.e. we neglect the coupling of ions by phonon interaction. This will be adequate for discussing Raman spectra involving the electronic levels of impurity ions in low concentration (cf. I). Since the photon coupling M_{mn}^{α} (equation 13) is also diagonal in the site label, any connected set of electronic propagators must involve the electronic states at one site only. The electronic and phonon propagators are diagonal in the state or mode indices and have the form $1/(E - X)$ where X is the excitation energy, i.e. λ_m and ω_k respectively.

Inserting these interactions into equation (8), we obtain a diagram expansion (cf. figure 1(*a*)) of the form

$$\mathscr{G}_{\eta\zeta\alpha\beta}^{III}(\mathbf{r}_3, \mathbf{r}_4; \mathbf{r}_1, \mathbf{r}_2; E_1, E_2, E_3) = \mathscr{G}_0^{III} + \frac{\boldsymbol{P}(C_1 + C_2)}{1 + \boldsymbol{P}(D)} \tag{15}$$

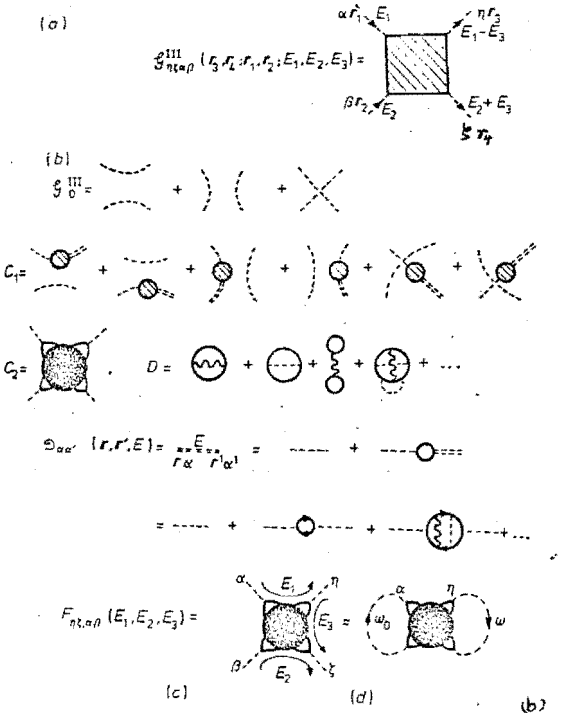

Figure 1. Diagram formulation of the light scattering spectrum. (*a*) Definition of the terms in equation (15) of the text. (*b*) Definition of the ~~phonon propagator and self-energy~~. (*c*), (*d*) Two representations of the Raman scattering kernel: the energy variables are more readily interpreted in (*d*), which however is less specific.

where the various terms are defined in figure 1(*b*). $\boldsymbol{P}$ signifies the Abrikosov projection; if we restrict our applications to essentially single-ion effects we may drop the site label and this projection has the effect of removing diagrams with more than one electronic loop.

The terms in $\mathscr{G}_0^{III}$ and C_1 obviously do not contribute to Raman scattering, and we concentrate on C_2. Apart from the terminal photon propagators these may be written as (cf. figure 1(*c*))

$$\begin{aligned}
F_{\eta\zeta\alpha\beta}(E_1, E_2, E_3) = &\iiint_0^{\beta} d\tau_1 d\tau_2 d\tau_3 \exp[-E_1\tau_1 - E_2\tau_2 - (E_3 - E_1)\tau_3] \\
&\times \langle T_{\tau}\{a_a^+ a_b(\tau_1) a_c^+ a_d(\tau_2) a_e^+ a_f(\tau_3) a_g^+ a_h\}\rangle M_{ab}^{\alpha} M_{cd}^{\beta} M_{ef}^{\eta} M_{gh}^{\zeta}.
\end{aligned} \tag{16}$$

Once this quantity is computed to any desired accuracy, the result is summed over the range of E_3 (equation (9)) or equivalently (Fetter and Walecka 1971) multiplied by the Bose–Einstein factor $f_B(z) = (\exp \beta z - 1)^{-1}$ and integrated around a contour enclosing the imaginary axis of E_3. If the contour is deformed, so that residues are calculated at the poles or cuts of $\mathscr{G}^{III}$ rather than those of f_B, a study of the Lehmann representation of $\mathscr{G}^{III}$ shows that there are four cuts along the lines $\mathrm{Im}(E_3) = 0, E_1, -E_2$,

$E_1 - E_2$. Kawabata (1971) has argued that only the first of these poles is important. His justification consists of comparing values of Bose–Einstein distribution functions, apparently derived on the assumption of black-body radiation distribution (since the photon propagators (equation (14)) are evaluated using a statistical partition function $\exp(-\beta\mathcal{H})$). We have examined the spectral distribution peaks from each cut (at the level of equation (20)) and find the first corresponds to Raman scattering, the second and third to single photon absorption or emission and the last to two-photon absorption or emission processes. Confining ourselves to the first pole, we find then (omitting photon labels)

$$\mathcal{G}^{\mathrm{III}}(E_1, E_2) = \mathrm{P}\int_{-\infty}^{\infty} \mathrm{d}\omega' f_{\mathrm{B}}(\omega') \operatorname*{Lim}_{E\to 0+} [\mathcal{G}^{\mathrm{III}}(E_1, E_2, \omega' + \mathrm{i}E) - \mathcal{G}^{\mathrm{III}}(E_1, E_2, \omega' - \mathrm{i}E)] \tag{17}$$

where P denotes the principal value integral. On substituting this expression into equation (7) and integrating over the volume of the detector with appropriate approximations (Kawabata 1971, Kusunoki 1976) one obtains a general expression for the light scattering spectrum for a general exciting pulse (e.g. equation 4.8 of Kawabata 1971, equation 4.7 of Kusunoki 1976) which we do not reproduce for brevity. The important conclusions are: (1) the pairs (r_1, r_2), (r_3, r_4) are related to incident and emerging photons respectively; (ii) when the photon propagators in $\mathcal{G}^{\mathrm{III}}_{\eta\xi_2\beta}(r_3, r_4; r_1, r_2; E_1, E_2, E_3)$ are integrated over the detector and source volumes in the appropriate manner, the frequency of the scattered radiation becomes equal to $\omega_0 - E_3$; (iii) the remaining variables are deducible from the source spectral distribution. For a steady source, the input spectrum may be written $S(\xi) = 2\pi\delta(\xi)$. Hence from equation (7) $\xi_1 = -\xi_2 = \omega_0$ and $E_1 = \omega_0 + \mathrm{i}\delta$, $E_2 = -\omega_0 + \mathrm{i}\delta$, $\delta = 0+$. The imaginary parts of these variables serve to specify the sign of the imaginary parts of the transition amplitude associated with denominator resonances.

The calculation of the Raman spectrum thus proceeds by use of a simple prescription, which is the goal of this section; diagrams contributing to $\mathcal{G}^{\mathrm{III}}$ are enumerated, the values $E_1 = \omega_0 + \mathrm{i}\delta$, $E_2 = -\omega_0 + \mathrm{i}\delta$ are inserted and the discontinuity (equation (7)) of the expression across the real axis of E_3 at the position $E_3 = \omega_0 - \omega$ evaluated. This last step parallels that in the absorption problem for the one-photon variable ω appropriate to those diagrams, i.e. E_3 plays the same role as ω in I. The parallel is closer if one ignores the imaginary parts of E_1 and E_2 and equates photon mode labels at the source and also at the detector; the various substitutions can then be condensed into two photon energy flows throughout the diagram as in figure 1(*d*). The frequency shift corresponds to the net energy flow through the diagram vertically upwards. (To conform with Kawabata's (1971) figures, the orientation differs from that of the absorption diagrams in I by a $\pi/2$ rotation).

3. Contributions to the Raman spectrum

3.1. Introduction

From § 2 the light scattering spectrum $R_{\omega\eta}(E_1, E_2, E_3)$ can be written as in figure 1(*c*) where $E_1 = \omega_0 + \mathrm{i}\delta$, $E_2 = -\omega_0 + \mathrm{i}\delta$, the discontinuity of the diagram at $E_3 = \omega_0 - \omega$ is taken, and where α, η and ω_0, ω are mode labels and frequencies for incoming and outgoing photons respectively. According to I, a resonance in this expression corresponding to Raman scattering can be identified by a line cutting the appropriate propagators. In this case the cut line should be horizontal so as to intercept the vertical 'flow' of Raman energy shift $\omega - \omega_0$. This is clearer in the slightly cruder representation of figure 1(*d*), which ignores the imaginary parts of E_1 and E_2: the cut line should sever both photon propagators.

The kernel of the diagram may contain only one loop of electronic propagators, dressed in all possible ways with phonon propagators. We ignore radiative dressing in the weak field limit: natural and power broadening are much less than phonon-induced widths in the systems of interest to us. A contribution to the electronic spectrum must have the form of figure 2(*a*), in which the cut line severs two electronic propagators and no phonon propagators; this diagram has a resonance when the Raman frequency shift $\omega - \omega_0$ equals the difference in electronic energies. Similarly the vibronic band as seen in Raman spectroscopy, called the vibroelectronic Raman effect by Kane-Maguire and Koningstein (1973), corresponds to figure 2(*b*). A special case of this diagram (when the

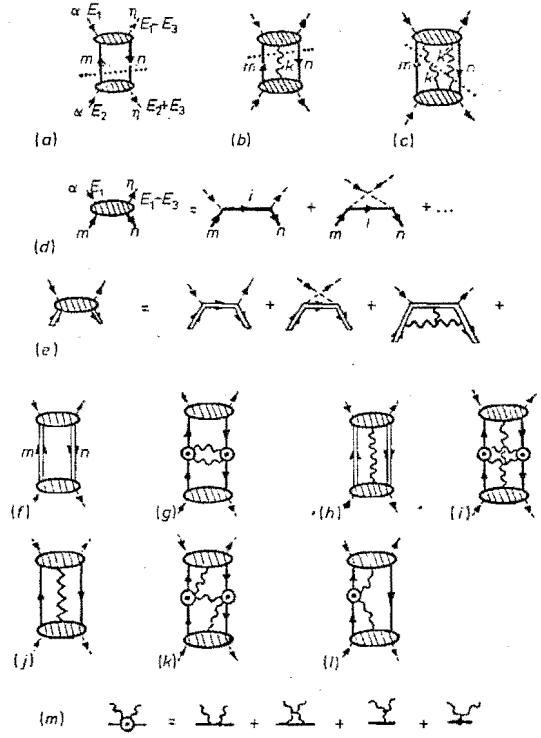

Figure 2. Contributions to the Raman spectrum. (*a*) The electronic Raman effect. (*b*) The vibroelectronic Raman effect (vibronic band). (*c*) The second order phonon Raman spectrum (*d*) Expansion of the polarisability tensor (electron-photon interaction). (*e*) The same expansion with dressed propagators. (*f*), (*g*) Contributions to the shift and width of the electronic Raman line. (*h*)–(*l*) Contributions to the width of the vibronic transition as seen in the Raman spectrum. (*m*) Expansion of the two-electron—two-phonon vertex. In many of these diagrams, similar cases with reflection symmetry have not been exhibited.

electronic states are the same, i.e. $m = n$) corresponds to the first-order phonon Raman spectrum, since this is believed to be mediated by electronic interaction (cf. Loudon 1964). The second-order phonon spectrum as mediated by electronic interaction is represented by figure 2(*c*) (cf. Born and Huang 1954) for the spectrum.

Calculation of the electronic Raman effect (figure 2(*a*)) gives the usual Kramers–Heisenberg expression

$$R_{\alpha\eta} \propto \sum_{mn} (\rho_m - \rho_n)\delta(\omega_0 - \omega + E_m - E_n)\,|P^{\alpha\eta}_{mn}(\omega_0 + i\delta, -\omega_0 + i\delta)|^2 \quad (18)$$

where

$$P^{\alpha\eta}_{mn}(E_1, E_2) \equiv \sum_i \left\{ \frac{M^{\alpha}_{mi} M^{\eta}_{in}}{E_m - E_i + E_1} + \frac{M^{\eta}_{mi} M^{\alpha}_{in}}{E_m - E_i - E_1 + E_2} \right\} + \ldots \quad (19)$$

is the two-electron–two-photon vertex of figure 2(*d*), the polarisability tensor.

The delta-function resonance of equation (18) must now be modified by taking account of the effect of multiple resonance (cf. I); the above form is derived by assuming that only one denominator at a time contributes to the discontinuity of the Green function across the real axis of E_3. For the single particle Green function this is most easily done by summing a geometric progression of diagrams with multiple resonances, to give a Dyson equation for a diagonal electronic propagator of the dressed form $\mathscr{G}^i_m(E) = 1/(E - \lambda_m - \Sigma_m(E))$. The real and imaginary parts of the self-energy $\Sigma_m(E)$, S_m and W_m respectively, give in Lorentzian approximation the shift and width of each electronic state under phonon interaction.

One method of broadening and shifting the resonance of equation (18) is to dress all the electronic propagators in the original diagram. This generalisation of equation (18) may be written in the form

$$\text{Disc}\, R_{\alpha\beta}(E_1, E_2, E_3) \propto \int_{-\infty}^{\infty} d\xi \sum_{mn} f_D(\xi)\mathscr{L}_m(\xi)\mathscr{L}_n(\xi + E_3)\,|\mathscr{P}^{\xi\alpha}_{nm}(\xi, E_1, E_3)|^2. \quad (20)$$

The function $\mathscr{L}_m$ is given by

$$\mathscr{L}_m(\xi) = \frac{W_m(\xi)}{(\xi - E_m - S_m(\xi))^2 + W^2_m(\xi)} \quad (21)$$

and has the form of a Lorentzian for fixed S_m, W_m; $\mathscr{P}^{\xi\alpha}_{nm}$ is the electron–phonon interaction with fully dressed propagators (figure 2(*e*)); ξ is the energy variable appropriate to the electronic integration, and f_D is the Fermi–Dirac distribution function. On assuming that the Lorentzians in equation (20) are sharply peaked, we find a spectrum with $\mathscr{P}^{\xi\alpha}_{nm}(E_m, \omega_0 + i\delta, -\omega_0 + i\delta)$ as the amplitude of the intensity and with a Lorentzian shape whose shift and width are additive combinations of the single particle counterparts for the electronic states m, n. This approach provides the standard formulation of the resonant Raman effect, in that the effect of the finite life of intermediate states is automatically included. However the non-additive components of the line width are not incorporated, since these have to do with repeated resonances in a two-particle, rather than a one-particle, Green function. With the same advantages and limitation one may discuss additive contributions to the shift and width of the vibronic band by dressing all the important propagators, and generalising equation (20) accordingly.

3.2. Width and shift of Raman line spectra

In this section we determine width and shift contributions as in I, that is by testing each diagram for a double resonance that could signify a width or shift contribution and determining the latter by binomial inversion.

3.2.1. Electronic Raman spectrum. The unperturbed spectrum has the form of equations (18) and (19), where in the latter equation (for the electron–photon vertex) we retain only the first two terms. If we ignore resonances within this vertex its structure does not influence the determination of shift and width contributions; there is essentially only one way of cutting a diagram (horizontally) so as to exhibit the Raman resonances. This means the shift and width contributions are equal to those obtained in the absorption case, and the Raman line broadening is identical to the no-phonon line broadening in absorption. The leading contributions comprise the additive parts (figure 2(*f*)) and the non-additive width contribution due to elastic phonon scattering (figure 2(*g*)); the detailed formulae are given in Stedman (1972).

3.2.2. Vibroelectronic Raman effect. Similarly the problem of the shift and width of Raman lines associated with vibronic transitions reduces to the problem of determining the shift and width of the vibronic line in the absorption spectrum. The detailed formulae are given in I. The main contributions arise from the broadening and shift of the parent electronic transition (figure 2(*h*)), including non-additive effects (figure 2(*i*)), anharmonic decay of the phonon (figure 2(*j*)), and approximately a doubling of earlier electronic contributions when the phonon mode involved in its relaxation was identical to that associated with the vibronic transition (figures 2(*k*, *l*)). These conclusions are consistent with the experimental data of Kane-Maguire and Koningstein (1973).

3.2.3. First order phonon Raman spectrum. The contributions to the width and shift of a phonon line seen by Raman spectroscopy have the same form as for a phonon line seen by infrared absorption, assuming the latter to be coupled by electronic interaction with photons. In this case the linewidth should reflect not only the width of the phonon due to anharmonic and electronic decay, but the width of the electronic ground state as well (cf. I).

3.2.4. Second order phonon Raman spectrum. It is possible to see quite sharp features in the second-order (two-phonon) Raman spectrum, because of the stringent restrictions imposed by frequency and wavevector conservation (e.g. Potts *et al* 1973). The theory of the lifetime broadening of these features will again be analogous to the theory for the absorption spectrum; we shall present details here.

To second order in the broadening interactions, the unperturbed spectrum of figure 2(*c*) will be shifted and broadened by the contributions of figure 3. Figure 3(*a*) denotes additive shift and width effects from anharmonic decay of each phonon involved in the transition, (equations (15), (16) of I) and figure 3(*b*) the effect of the finite lifetime of the electronic state. The major effect will come from the electronic ground state, as for the first-order Raman spectrum (equations (10), (11) of I). The interference effects of figure 3(*c*) also have counterparts in the first-order spectrum and are given by equation (19) of I where the phonon label runs over k, k'. The remaining diagrams in figure 3 give contributions to width and shift which are characteristic of the second-order spectrum. If we concentrate on second order in perturbation, only figure 3(*d*) is of interest, repre-

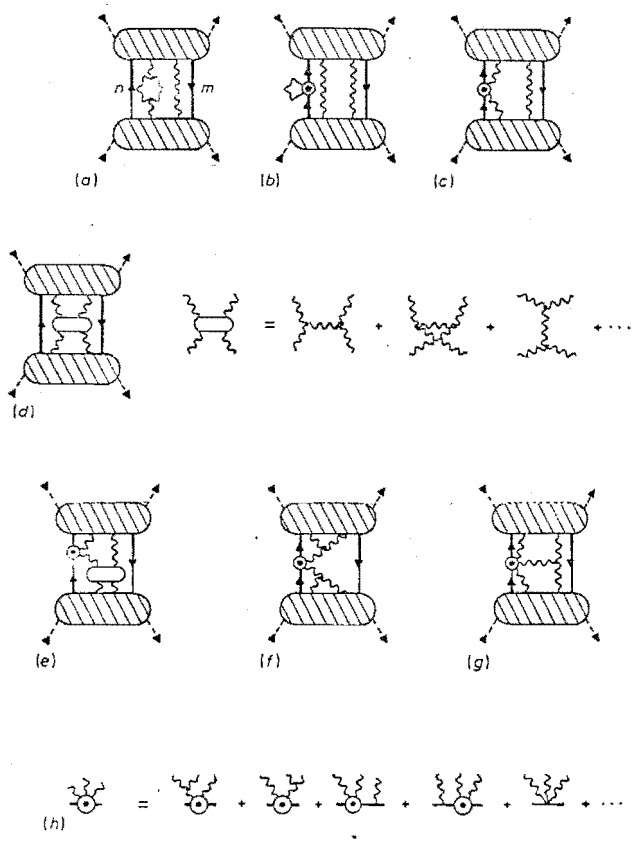

Figure 3. Contributions to the width of the second order phonon Raman spectrum. (*a*)–(*d*) Second order contributions (*e*)–(*g*) Fourth order contributions. (*h*) Expansion of the two-electron—three-phonon vertex. In many of these diagrams, similar diagrams with reflection symmetry are not exhibited.

senting non-additive effects in anharmonic decay of the two phonons. The first term is zero on evaluation and the other terms depicted in figure 3(*d*) give, for a two-phonon creation sideband line,

$$\Lambda_{3d} = \sum_{\ell\pm} |W_{k+k'-l\mp}|^2 (n_{k'} - n_k + 1)/(\omega_{k'} - \omega_k \pm \omega_l) + \sum_{i} |W_{k-k'-l+}|^2 (n_k + n_{k'} + 1)/(\omega_k + \omega_{k'} - \omega_l) \quad (22)$$

and a similar result for widths ($n_k = \langle b_k^+ b_k \rangle$).

This solves the line shape problem for the second-order phonon Raman spectrum to second order in a Lorentzian approximation. Calculation of the remaining figures in figure 3 would provide a result of fourth-order accuracy.

Even at this order, however, one has quite clear departure from the simple rule (e.g. Klein and Colwell 1971) of addition of widths of the phonons participating in a Raman transition. In general there is an electronic component to the width of the spectrum and interference contributions from electron–phonon and phonon–phonon interactions as well.

3.2.5. General. The correspondence drawn in the above cases between the broadening of absorption and Raman lines is initially only formal: the same transition may not be seen unless the selection rules are favourable. In the same manner, the group-theoretical restrictions on the form of the absorption spectrum as developed in Stedman (1976) and in I are formally identical to those for the Raman spectrum.

These conclusions will need modification in the case of the resonant Raman effect. It is then not an adequate approximation to ignore resonances in the electron–photon vertex; within the framework of equation (20), one may not ignore the ξ-dependence of $\mathscr{P}^{\xi z}_{nm}(\xi, E_1, E_3)$. Including this functional dependence has been found to give a useful first step in the discussion of line shapes, which are currently being investigated.

3.3. Applications

In summary, we find the width and shift of lines in the Raman spectrum to be due, not only to the additive contributions arising from single-particle decay using dressed states for the excitations involved in the Raman transition, but also to contributions from the electronic states mediating the transition together with non-additive broadening effects of various types, corresponding to interference between all the excitations involved in the Raman transition or its mediation

In the experiment of Alfano and Shapiro (1971) it was found that the decay of population in the phonon mode excited by Raman scattering had a time constant much greater than that derived from the linewidth of the scattered radiation. The authors mention the relevance of distinguishing longitudinal and transverse relaxation times, T_1 and T_2, in such comparisons. Our formalism has shown that the linewidth of the Raman scattered radiation differs from a population decay time T_1 not only by virtue of elastic scattering effects which normally distinguish T_1 and T_2, but also by the role of electronic linewidths as well.

If the electronic ground state is isolated its broadening may be small in comparison with that of the phonon (in the case of the first-order spectrum). Indeed the temperature dependence of the width and shift of many phonon spectra agree well with the predictions of single-particle anharmonic decay (e.g. Pine and Tannenwald 1969) though exceptions have been noted (Fukumoto *et al* 1973).

As noted in § 3.2, the conclusions of Klein and Colwell (1971) regarding the additivity of widths for n-phonon Raman spectra are modified in an obvious manner.

Two-photon scattering has also been observed in solids (Fritzler and Schaak 1976). A straightforward modification of the analysis (in particular, use of the appropriate term as mentioned in § 2) would cope with this situation, and we may anticipate similar results for the width and shift of the two-photon spectral lines.

The phenomenological expressions normally used for fitting the observed linewidth remain valid provided the electronic broadening terms (direct and Raman) are included. This follows since non-additive terms of all types mimic the temperature dependence of the corresponding conventional contributions (cf. I; for example, equation (22) of this paper and equation (16) of I have a very similar structure).

4. Effects of dissipative interactions on the resonance spectrum

The temporal and spectral properties of light received from an electronic system (a molecule or a solid) when the incident light frequency approximates that of an electronic transition have received much attention. Many discussions and controversies have arisen in various areas of this extensive field. The situation has been clarified as a result of recent data exhibiting the spectrum in the off-resonance case together with the time decay of each peak (Liran *et al* 1977). We offer some comments on the adequacy of existing theory to describe this spectrum, and in particular to predict the widths of the peaks.

First we note that it is incorrect to assume that the parameters characterising the homogeneous broadening of two levels may be added to give the width of the transition between these levels. This assumption has been made in the context of resonance fluorescence by, for example, Beterov *et al* (1973), Shen (1974) and Solin and Merkelo (1975). In fact, the terms which in collision broadening correspond to quasi-elastic phase interruption broadening have analogues in homogeneous broadening; all elastic interactions broaden transitions in a non-additive way (Stedman 1974). While such effects may be small enough to ignore at a first approximation—they will only contribute to the width in the Raman broadening regime—from a formal viewpoint it is just these terms which give rise to the fundamental distinction between longitudinal and transverse relaxation times. Since this distinction was raised by Shen (1976) as a key issue in one of the controversies in the resonance fluorescence literature, the non-additive effects of these terms should be included in such discussions. We note that Eberly (1976) shows that in the strong field case the laser linewidth contributes non-additively for a not dissimilar reason; in his theory the amplitude bandwidth ($S(\xi)$ of § 2) appears only in the longitudinal relaxation rate. In general, the effects of reservoir interaction are too complex by far to be accommodated merely by introducing a one-particle width onto initial, intermediate and final electronic states. However, this approximation has been commonly used in distinguishing resonance fluorescence and resonant Raman scattering (Rousseau and Williams 1976).

The diagram formulation of Kusunoki (1976) exhibits multiparticle effects explicitly, and Kusunoki, like other authors, classifies various contributions under various conventional titles (Raman scattering, collision-induced redistribution scattering). We agree that a diagram formalism is the best formalism for such purposes, since it is general and explicit, but we believe the particular catalogue suggested by Kusunoki to be inadequate in several respects.

Our formalism and that of Kusunoki (1976) are parallel even as regard to the application, though hitherto we have been considering solids and Kusunoki molecules. Kusunoki deals with one molecule and writes its levels in terms of a fermion operator; as a consequence his diagrams should be projected to a physical value by the Abrikosov technique. He also includes the effect of collisions by coupling the fermions to a boson bath, exactly paralleling our phonon interaction. This is a satisfactory approximation for our purpose—we know, as mentioned above, that many results of collision broadening and phonon broadening are analogous. In our notation, Kusunoki catalogues the contributions as in figure 4. Because he is specialising to the resonant situation, he has restricted the diagrams and the intermediate states to those containing the relevant resonance.

A problem with these identifications is that on applying the Abrikosov projection to figure 4(*d*), those terms vanish identically. Two electronic loops, each associated with

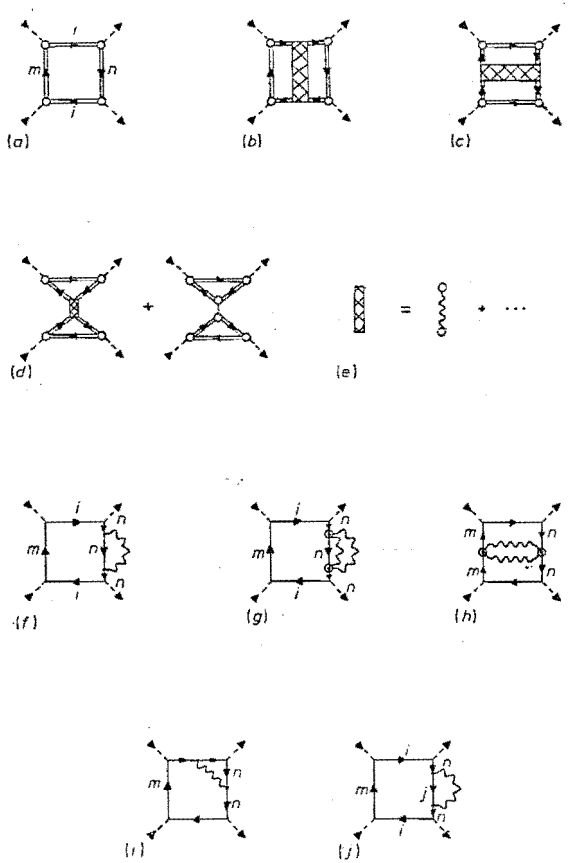

Figure 4. Identification of contributions to the resonance spectrum. The contributions (*a*)–(*d*) are respectively labelled by Kusunoki (1976) Raman scattering, collision-induced redistribution scattering, final-state redistribution scattering and final-state transfer scattering. (*e*) The Born approximation used by Kusunoki. (*f*), (*g*) Contributions to final-state redistribution scattering. (*h*), (*i*) Interference contributions. (*j*) A contribution to final-state transfer scattering.

the states of one molecule, are involved; the Abrikosov prescription allows only one electronic propagator loop per molecule. A minor problem is the omission of non-additive broadening in the Raman spectrum. We note that Kusunoki works within the Born approximation for collisions (figure 4(*e*)) and includes only final-state broadening in many cases; initial-state broadening would also influence the spectrum.

We suggest different diagram identifications for final-state redistribution and transfer scattering. If we define final-state redistribution scattering as the effect on the spectrum of quasiclastic collisions off the final state, the contributions of figure 4(*f, g*) are relevant. Initial-state collisions may also be important, and interference effects with initial and intermediate state collisions (figure 4(*h, i*)) will affect widths and intensities. It is not

clear whether figure 4(*b*), classified by Kusunoki (but not by us) as collision-induced redistribution scattering, would give a width contribution to the fluorescence or Raman spectrum. According to the prescription for widths used in this paper, it would not so contribute to the Raman spectrum; however this prescription may be expected to be inadequate in the case of the resonant spectrum.

If we define final-state transfer scattering as the effect on the spectrum of collisions which take the molecule from the final state n to another level j, a relevant diagram (affecting width and shift of the resonance peaks) is figure 4(*j*). Since Raman scattering includes all such terms we do not support Kusunoki's prescription for distinguishing resonance Raman scattering and absorption followed by emission.

Finally we mention that the work of Friedman *et al* (1976) on the evidence for and against identical absorption and Raman spectral shifts is very relevant to the conclusions of this and the preceding section. While we predicted strong spectral features to occur at the same transition energy these authors give evidence that resonances associated with close-lying electronic or vibrational levels may give spectra which depart from this rule. This arises essentially because of the strong frequency dependence of the photon–electron coupling vertex, when the laser is in near resonance with the transition to the intermediate state.

5. Conclusions

(i) The homogeneous width of a non-resonant Raman spectral line is formally identical to the corresponding width in the absorption spectrum. The various electronic components, from direct (T, $\exp(-\delta/T)$) or Raman (T^5, T^7, T^9) relaxation together with non-additive effects in the latter components, as well as the effects of anharmonicity, are detailed in I and in § 3.2.

(ii) The electronic component of the linewidth should be included when making phenomenological fits to experiment even for phonon Raman lines.

(iii) Distinctions between resonant Raman scattering and resonance fluorescence are inadequate if made within the context of a theory which ignores multiparticle effects (e.g. non-additive linewidth contributions).

(iv) We identify, within a diagram formation incorporating multiparticle effects, contributions to the Raman spectrum from final-state redistribution scattering (figure 4(*f*, *g*)), initial-state redistribution scattering (the same figures reflected about a vertical plane), the interference between these (figure 4(*h*)), final-state transfer scattering (figure 4(*j*)) etc. All such processes contribute to the Raman linewidth.

Acknowledgments

We are grateful to Professor M. Kusunoki for a preprint of his helpful paper. B. J. McKenzie is grateful to the New Zealand University Grants Committee for a Post-graduate Scholarship.

References

Abou-Ghantous M, Jaussaud P C, Bates C A, Fletcher J R and Moore W S 1974 *Phys. Rev. Lett.* 33 530–3
Abrikosov A A, Gor'kov L P and Dzyaloshinski I E 1963 *Methods of Quantum Field Theory in Statistical Physics* (New Jersey: Prentice-Hall).
Alfano R R and Shapiro S L 1971 *Phys. Rev. Lett.* 26 1247–51

Beterov I M, Matyugin Yu A and Chebotaev V P 1973 *Sov. Phys. J.E.T.P.* 37 756–63
Born M and Huang K 1954 *Dynamical Theory of Crystal Lattices* (Clarendon, Oxford)
Callen H B 1961 in *Fluctuation, Relaxation and Resonance in Magnetic Systems* (Ed D ter Haar) (Edinburgh, Oliver & Boyd) pp 15–22
Cuden C B 1976 *Phys. Rev.* B 13 1993–2002
Eberly J H 1976 *Phys. Rev. Lett.* 37 1387–90
Fetter A L and Waleeka J D 1971 *Quantum Theory of Many-Particle Systems* (New York: McGraw-Hill)
Friedman J M, Rousseau D L and Bondybey V E 1976 *Phys. Rev. Lett.* 37 1610–3
Fritzler U and Schaak G 1976 *J. Phys. C: Solid St. Phys.* 9 L23–6
Fukumoto T, Tabuchi K, Nakashima S and Mitsuishi A 1973 *J. Phys. Soc. Japan* 35 622
Kane-Maguire C and Koningstein J A 1973 *J. Chem. Phys.* 59 1899–904
Kawabata A 1971 *J. Phys. Soc. Japan* 30 68–85
Klein M V and Colwell P J 1971 in *Proceedings of the Second International Conference on Light Scattering in Solids* (Ed. M Balkanski) (Paris: Flammarion) pp 65–9
Kubo R 1966 *J. Phys. Soc. Japan* 12 570–86
Kusunoki M 1976 *Progr. Theor. Phys. Japan* 55 692–709
Liran J, Levin L A, Erez G and Jortner J 1977 *Phys. Rev. Lett.* 38 390–3
Loudon R 1964 *Adv. Phys.* 13 423–81
Louisell W H 1973 *Quantum Statistical Properties of Radiation* (New York: Wiley)
McKenzie B J and Stedman G E 1976 *J. Phys. A: Math., Gen* 9 187–95
Pine A S and Tannenwald P E 1969 *Phys. Rev.* 178 1424–30
Potts J E, Walker C T and Nair I R 1973 *Phys. Rev.* B 8 2756–71
Rousseau D L and Williams P F 1976 *J. Chem. Phys.* 64 3519–37
Shen Y R 1974 *Phys. Rev.* B 9 622–6
—— 1976 *Phys. Rev.* B 14 1772–4
Solin J R and Merkelo H 1975 *Phys. Rev.* B 12 624–9
Stedman G E 1972 *J. Phys. C: Solid St. Phys.* 5 121–33
—— 1974 *J. Phys. A: Math., Nucl. Gen.* 7 L48–51
—— 1976 *J. Phys. C: Solid St. Phys.* 9 535–51
—— 1977 *J. Phys. C: Solid St. Phys.* submitted for publication

J. Phys. A: Math. Gen., Vol. 9, No. 2, 1976. Printed in Great Britain.

Drones, quasi-spin or iso-spin? A comparison of many-body techniques for general spin

B J McKenzie and G E Stedman

Department of Physics, University of Canterbury, Christchurch, New Zealand

Received 18 June 1975

Abstract. For an effective-spin system with $2S+1$ levels there are a number of possible mappings of spin onto pseudo-fermion operators. We investigate the relative merits of three of these methods by calculating to second order the dispersion relation for coupled spin-phonon modes in crystals containing $S=1$ effective spin impurities. We find that the drone formalism quickly becomes intractable at higher spin values, as does the related quasi-spin formalism we develop, in contrast with the iso-spin (or Abrikosov projection) formalism.

1. Introduction

The success experienced in the application of the methods of quantum field theory to many-body physics (e.g. see Abrikosov *et al* 1963) is less marked in the field of spin or effective-spin systems (e.g. systems with discrete excitation levels) because of the greater complexity of the rules required. This arises because the spins do not obey either fermion or boson commutation relations and thus the fermion or boson Wick's theorems as such do not apply.

To overcome this difficulty, a number of approaches involving mappings of the spins onto fermion (or boson) operators has evolved. These in general allow Wick's theorem to be recovered at the expense of suitable operations to remove unphysical states that may arise.

We discuss three such mappings which are the simplest known to us (table 1). In each case S obeys spin, and $a_{j\mu}$, $b_{j\mu}$ fermion, commutation rules.

The *iso-spin* mapping, requiring just one fermion, was valuable in nuclear and particle physics (Lipkin 1965). It was introduced to many-body theory by Abrikosov (1965); for later work on the formalism see Oppermann (1973), Verwoerd (1974) and

Table 1. Spin-fermion mappings. μ ranges from $-S$ to $+S$ for iso-spin and 1 to $2S$ for drones and quasi-spin; $\mathcal{S}=[S(S+1)-\mu(\mu+1)]^{1/2}$; $S^{-}\equiv(S^{+})^{+}$.

	Iso-spin	Drone	Quasi-spin
S_j^z	$\sum_\mu \mu a_{j\mu}^+ a_{j\mu}$	$\sum_\mu (a_{j\mu}^+ a_{j\mu} - \frac{1}{2})$	$\sum_\mu \frac{1}{2}(a_{j\mu}^+ a_{j\mu} + b_{j\mu}^+ b_{j\mu} - 1)$
S_j^+	$\sum_\mu \mathcal{S} a_{j\mu+1}^+ a_{j\mu}$	$\sum_\mu a_{j\mu}^+ (b_{j\mu} + b_{j\mu}^+)$	$\sum_\mu a_{j\mu}^+ b_{j\mu}^+$

references therein. Unphysical states (in the fermion Fock space) may be removed by extending Abrikosov's projection method (see § 2).

The *drone* formalism was introduced by Mattis (1965) and generalized by Spencer (1968) and Barnes (1972). For applications, especially to coupled spin–phonon systems, see Toombs and Sheard (1973) and their references.

The *quasi-spin* mapping (Lipkin 1965) has not previously been used to generate a diagram technique for spin systems. It arises in superconductivity (Anderson 1958), atomic physics (Judd 1967) and crystal field theory (Wybourne 1973). In § 2, we develop the diagram method for general spin, using Barnes' (1972) formulation for drones as a guide.

In the following sections we discuss violation of the linked cluster theorem and calculation of $S=1$ spin–phonon modes for all methods, concluding that in general the Abrikosov method is preferable to either drones or quasi-spin for $S>\frac{1}{2}$.

2. Formalism for general spin

Barnes' (1972) contribution to generalizing the drone method was to recognize that an arbitrary physical spin-space may be written as a direct sum of product drone–fermion spaces. This enabled him to find the trace over the spin states of an arbitrary spin operator in terms of traces over the product spaces multiplied by suitable factors to correct for the unphysical states. Finally he was able to show that if one used a diagram approach, the diagram value for arbitrary spin could be obtained by multiplying the appropriate $S=\frac{1}{2}$ diagram by a number of factors $K_S(l)$ where l is the number of drone–fermion loops labelled with the same site label. We now give a parallel analysis of quasi-spin.

For quasi-spin the operators for $S=\frac{1}{2}$ at a specific site (a_1^+, a_1, b_1^+, b_1) generate a two-dimensional space spanned by basis vectors $|11\rangle, |10\rangle, |01\rangle, |00\rangle$ where the first and second labels give the eigenvalues of the number operators $a_1^+a_1$, $b_1^+b_1$ respectively. Now by considering the operation of S^z, S^2 expressed in terms of the fermion operators acting on these basis vectors, one finds that $|11\rangle$, $|00\rangle$ correspond to $|S=\frac{1}{2}\, M_S=\frac{1}{2}\rangle$, $|S=\frac{1}{2}\, M_S=-\frac{1}{2}\rangle$ respectively and both $|10\rangle$, $|01\rangle$ correspond to $|S=0\, M_S=0\rangle$. Thus the fermion space contains *one* spin $\frac{1}{2}$ subspace and *two* spin zero subspaces. We write this as $\tilde{S}_{1/2}=S_{1/2}\oplus 2S_0$, where the tilde refers to the fermion space representation. Following Barnes, we find the spin states contained in any product space $(\otimes\tilde{S}_{1/2})^n$ and by inverting these, we obtain the physical spin spaces as a direct sum of fermion spaces. For example:

$$S_{1/2}=(\otimes\tilde{S}_{1/2})^1\ominus 2S_0$$

$$S_1=(\otimes\tilde{S}_{1/2})^2\ominus 4(\otimes\tilde{S}_{1/2})^1\oplus 3S_0$$

$$S_{3/2}=(\otimes\tilde{S}_{1/2})^3\ominus 6(\otimes\tilde{S}_{1/2})^2\oplus 10(\otimes\tilde{S}_{1/2})^1\ominus 8S_0$$

with the notation $(\otimes\tilde{S}_{1/2})^2=\tilde{S}_{1/2}\otimes\tilde{S}_{1/2}$ etc.

One obtains for an arbitrary spin operator θ,

$$\langle\theta\rangle_{S=1/2}=Y_{1/2}(1)\langle\theta\rangle_{\tilde{1}}$$

$$\langle\theta\rangle_{S=1}=Y_1(2)\langle\theta\rangle_{\tilde{2}}-4Y_1(1)\langle\theta\rangle_{\tilde{1}}$$

etc, where $\langle\theta\rangle_{S=1}$, $\langle\theta\rangle_{\tilde{n}}$ denote the unperturbed thermal average of θ with respect to the

spin 1 states and the states of the nth-fermion product space $(\otimes\vec{S}_{1/2})^n$ respectively, and

$$Y_S(n) = \mathrm{Tr}_{\vec{n}} \exp(-\beta\mathscr{H}_S)/\mathrm{Tr}_S \exp(-\beta\mathscr{H}_S).$$

If the zero-order spin Hamiltonian has the form $\mathscr{H}_S = \omega_0\Sigma_j S_j^z$, the multiplicative factors are $Y_S(n) = [(f^+f^-)^n Z_S]^{-1}$ with $f^\pm = [1+\exp(\pm\beta\omega_0/2)]^{-1}$ and where Z_S is the true partition function for the S spin state.

The value of the Feynman diagram corresponding to arbitrary spin S is to be evaluated by multiplying the value of the corresponding $S=\frac{1}{2}$ diagram by suitable factors:

$$\langle\text{diagram}\rangle_S = K_S(l, p)K_S(m, q)\ldots\langle\text{diagram}\rangle_{S=1/2}$$

where, for each diagram involving several sites, there is a factor $K_S(l, p)$ for each distinct site with l loops and p 'free' spin-state labels. For example $K_1(l, p) = Y_1(2)l^p - 4\,Y_1(1)$. We shall find that, for certain diagrams, p is not necessarily equal to the power of the product space as stated by Barnes.

In the Abrikosov formalism, the approach for removing the effect of unphysical states is somewhat different. Because the spaces considered here are not powers of $S=\frac{1}{2}$ spaces one cannot apply a method like that used for drones and quasi-spin except for the case $S=\frac{1}{2}$. (This is effectively the approach of Yolin (1965) when he multiplies his diagrams by a factor $Y^p = [(1+\cosh\beta\omega_0)/\cosh\beta\omega_0]^p$, where p is the number of distinct spins represented in the diagram.) The conventional approach is to add an energy λ to each fermion and then remove the effect of the unphysical multiparticle states at the end of the calculation by means of the projection

$$\boldsymbol{P} = \frac{1}{\mathrm{Tr}\exp(-\beta\mathscr{H}_S)} \lim_{\lambda\to\infty} \mathrm{e}^{\beta\lambda}. \tag{1}$$

3. Linked cluster theorem

Keiter (1968, 1971) pointed out that the Abrikosov 'freezing-out' procedure (equation (1)) destroys the linked cluster theorem (LCT). We express this by

$$\mathscr{D} = \mathscr{D}^0 + \frac{\boldsymbol{P}\{C\} + \boldsymbol{P}\{CD\}}{1+\boldsymbol{P}\{D\}} \tag{2}$$

where $\mathscr{D}$, $\mathscr{D}^0$ are the perturbed and unperturbed phonon propagators respectively. C represents the connected diagrams with the exception of $\mathscr{D}^0$ and D the vacuum diagrams with the exception of 1.

Equation (2) is also valid for drones and quasi-spin with the exception that $\boldsymbol{P}$ now has the significance of multiplying the diagram by the appropriate $K_S(l, p)$ factors. The LCT fails in these cases also because the factors multiplying the disconnected diagrams (e.g. CD) do not factorize into the parts that multiply the corresponding connected (C) and vacuum (D) diagrams.

In a weak-coupling problem such as the spin–phonon coupled-modes problem to be considered in § 4, $(1+\boldsymbol{P}\{D\})^{-1}$ can be expanded using the binomial theorem. Because the diagram factors do not factorize appropriately, the disconnected diagrams that result (e.g. $\boldsymbol{P}\{CD\} - \boldsymbol{P}\{C\}\,.\,\boldsymbol{P}\{D\}$) do not cancel. As an example of this, consider the approach of Yolin (1965) who was criticized by Schultz and Kwok (1972) for assuming

LCT. As we have already mentioned, dealing with the Abrikosov technique for $S=\frac{1}{2}$ enabled Yolin to remove the effect of unphysical states by multiplying his diagrams by a factor Y^p. The first disconnected diagram to appear in the expansion arises in the fourth order and is indicated in figure 1 (using Yolin's conventions). Although the similar diagrams with $n_1 \neq n_2$ cancel, the one with $n_1 = n_2$ does not, and must be multiplied by a factor $(Y - Y^2)$; Yolin in his work presumably did not realize this. However, the diagram does not affect his calculation of the lifetime of the coupled modes as it contributes no imaginary part, and thus his calculation agrees with other published results for the lifetime (e.g. see Toombs and Sheard 1973, Fidler and Tucker 1970). This diagram would affect only the fourth-order frequency shift.

In the case of drones, for $S=\frac{1}{2}$, the LCT is recovered; the $K_{1/2}(l, p)$ factors are all unity and hence the required factorization results.

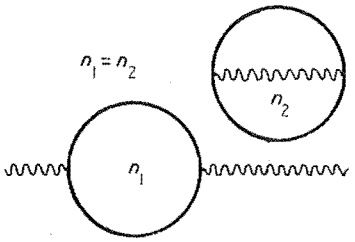

Figure 1. A fourth-order unlinked diagram arising in the problem of Yolin. Full lines represent A^0 propagators (equation (4)) and wavy lines the phonon propagator.

4. Example: spin–phonon coupled modes for $S=1$

The relative usefulness of the previous three methods for $S>\frac{1}{2}$ may be assessed by applying each to a specific problem, namely the coupled-modes dispersion relation for $S=1$.

Our model Hamiltonian is chosen as follows:

$$\mathcal{H} = \mathcal{H}_s + \mathcal{H}_p + \mathcal{H}_{sp}$$

$$\mathcal{H}_s = \omega_0 \sum_j S_j^z \qquad \mathcal{H}_p = \sum_k \omega_k c_k^+ c_k$$

$$\mathcal{H}_{sp} = N^{-1/2} \sum_{k,j} B_k \exp(i\boldsymbol{k} \cdot \boldsymbol{R}_j)\psi_k[S_j^x + \xi(S_j^+ S_j^+ + S_j^- S_j^-)] \tag{3}$$

where $B_k = \frac{1}{3}\epsilon(\omega_0\omega_k)^{1/2}$ is the coupling coefficient and $\psi_k = c_k + c_{-k}^+$ is a lattice mode amplitude operator. The interaction term with coefficient ξ is required to enable a phonon mode to couple all second-order states (e.g. Fidler and Tucker 1971).

We require the poles of the perturbed phonon propagator defined (following Toombs and Sheard 1973, in their notation) by

$$D_{kk'}(\tau) = -\langle T_\tau\{\psi_k(\tau)\psi_{-k'}(0)\}\rangle.$$

The corresponding unperturbed phonon propagator has Fourier coefficients diagonal in $\boldsymbol{k}, \boldsymbol{k}'$:

$$\mathscr{D}_k^0(\mathrm{i}\omega_n) = \frac{2\omega_k}{(\mathrm{i}\omega_n)^2 - \omega_k^2}.$$

For the procedures needed to develop a diagram expansion for $\mathscr{D}_k(\mathrm{i}\omega_n)$ see Abrikosov *et al* (1963).

Below we evaluate the diagrams generated for the drone, quasi-spin and Abrikosov techniques individually.

4.1. Drones

We define propagators,

$$\begin{aligned} \Delta^0_{j\mu;j'\mu'}(\tau) &= -\langle T_\tau\{\phi_{j\mu}(\tau)\phi_{j'\mu'}(0)\}\rangle_0 \\ A^0_{j\mu;j'\mu'}(\tau) &= -\langle T_\tau\{a_{j\mu}(\tau)a^+_{j'\mu'}(0)\}\rangle_0 \end{aligned} \tag{4}$$

where $\phi_{j\mu} = b_{j\mu} + b^+_{j\mu}$, which have Fourier coefficients diagonal in μ, μ' and in j, j':

$$\Delta^0(\mathrm{i}\omega_n) = 2/\mathrm{i}\omega_n \qquad A^0(\mathrm{i}\omega_n) = 1/(\mathrm{i}\omega_n - \omega_0).$$

One obtains the second-order diagrams shown in figure 2 where the propagators $\mathscr{D}^0_k$, Δ^0 and A^0 are represented by wavy, broken and full lines respectively.

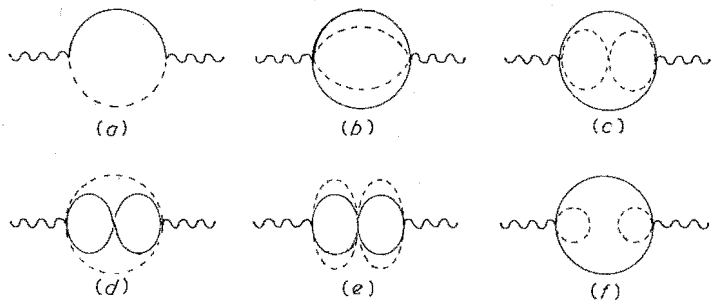

Figure 2. Second-order diagrams in the drone and quasi-spin formulation. Diagram (*f*) should be omitted for quasi-spin.

It is necessary to distinguish figures 2(*b*, *c*) in this manner because, although the diagrams themselves all have the same value, the $K_S(l, p)$ factors multiplying them are different both in magnitude and sign. This arises from the contraction of factors of the form

$$\sum_{jj'}\sum_{\mu_1\mu_1'}\sum_{\mu_2\mu_2'}\langle T_\tau\{a_{j\mu_1}(\tau_1)\phi_{j\mu_1}(\tau_1)a_{j\mu_1'}(\tau_1)\phi_{j\mu_1'}(\tau_1)\phi_{j\mu_2'}(\tau_2)a_{j\mu_2'}(\tau_2)\phi_{j'\mu_2'}(\tau_2)a_{j'\mu_2'}(\tau_2)\}\rangle_0.$$

Depending on the pairs one chooses to contract, one can obtain products of Kronecker deltas like $\delta_{jj'}(\delta_{\mu_1\mu_2})^2(\delta_{\mu_1'\mu_2'})^2$ (figure 2 (*b*)), $\delta_{jj'}[\delta_{\mu_1\mu_2'}]^2[\delta_{\mu_1'\mu_2}]^2$ (figure 2(*e*)), which result in a single sum over j and a double sum over μ_1, μ_1'; or like $\delta_{jj'}\delta_{\mu_1\mu_2}\delta_{\mu_1'\mu_2}\delta_{\mu_1\mu_2'}\delta_{\mu_1'\mu_2}$ (figures 2(*c*, *d*)), which leave only single sums over j and μ. Thus figures 2(*b*, *e*) have

factors like $K_1(1,2)$ multiplying them while figures 2(*c*, *d*) have a factor $K_1(1,1)$ and also a different sign.

The diagram convention used in figure 2 is to label the outgoing stubs (μ_1, μ_1') and ingoing stubs (μ_2, μ_2') in the same order at each vertex (see figure 3), and introduce the twists to connect them. Evaluating the diagrams and their K factors, one obtains the contribution to $\mathscr{D}_k(i\omega_m)$ given in table 2.

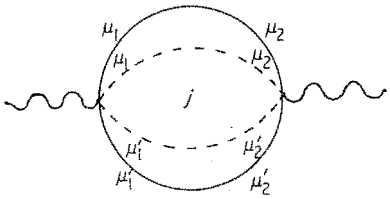

Figure 3. Labelling conventions for figure 2.

Table 2. Diagram contributions for drones. For brevity we define $G_\pm(\omega_0) = \exp(\beta\omega_0) \pm \exp(-\beta\omega_0)$, $H_\pm(\omega_0) = \exp(\beta\omega_0) \pm 1$, $I(\omega_0) = H_+(\omega_0)H_+(-\omega_0)$, $Z(\omega_0) = G_+(\omega_0)+1$.

Figure	Diagram	K factor
2(*a*)	$\dfrac{\frac{1}{2}\epsilon^2\omega_0^2\omega_k G_-(\omega_0)}{[(i\omega_m)^2-\omega_0^2]I(\omega_0)}$	$2\dfrac{I(\omega_0)}{Z(\omega_0)}$
2(*b*–*e*)	$\dfrac{\xi^2\epsilon^2\omega_0^2\omega_k}{(i\omega_m)^2-4\omega_0^2}\dfrac{G_+(\omega_0)H_-(2\omega_0)H_-(-\omega_0)}{G_-(\omega_0)H_+(2\omega_0)H_+(-\omega_0)}$	$-4\dfrac{I(\omega_0)}{Z(\omega_0)}$
2(*f*)	0	$2\dfrac{I(\omega_0)}{Z(\omega_0)}$

4.2. *Quasi-spin*

We define propagators $A^0_{j\mu;j'\mu'}(\tau)$ by equation (4) and also

$$E^0_{j\mu;j'\mu'}(\tau) = -\langle T_\tau\{b_{j\mu}(\tau)b^+_{j'\mu'}(0)\}\rangle_0.$$

Again the Fourier coefficients are diagonal in j and μ labels, but they have different values since $\mathscr{H}_s$ has a different fermion representation:

$$A^0(i\omega_n) = E^0(i\omega_n) = \frac{1}{i\omega_n - \omega_0/2}.$$

The diagrams obtained can again be represented by those of figure 2 except that the broken and full lines now represent the A^0 and E^0 propagators respectively, and figure 2(*f*) does not appear. The evaluated diagrams and their factors are given in table 3.

4.3. *Abrikosov*

We define the propagator $A_{j\mu,j'\mu'}(\tau)$ using equation (4). The corresponding unperturbed propagator has Fourier coefficients diagonal in j, j' and μ, μ', but now a function

Table 3. Diagram contributions for quasi-spin. Abbreviations are defined in the caption to table 2; $X \equiv \{[\exp(\frac{3}{2}\beta\omega_0) - \exp(-\omega_0/2)][\exp(\beta\omega_0) - \exp(-\frac{1}{2}\beta\omega_0)]\}/H_+(\frac{3}{2}\omega_0)$.

Figure	Diagram	K factor
2(*a*)	$\dfrac{-\frac{1}{2}\epsilon^2\omega_0^2\omega_k}{(i\omega_m)^2-\omega_0^2}\dfrac{G_-(\frac{1}{2}\omega_0)}{I(\frac{1}{2}\omega_0)}$	$-2\dfrac{I(\frac{1}{2}\omega_0)G_+(\frac{1}{2}\omega_0)}{Z(\omega_0)}$
2(*b–e*)	$\dfrac{+\xi^2\epsilon^2\omega_0^2\omega_k}{[(i\omega_m)^2-4\omega_0^2]}\dfrac{G_-(\frac{1}{2}\omega_0)X}{I(\frac{1}{2}\omega_0)H_+^2(-\frac{1}{2}\omega_0)H_-(\omega_0)}$	$-4\dfrac{I^2(\frac{1}{2}\omega_0)}{Z(\omega_0)}$

of μ:

$$A_\mu^0(i\omega_n) = \frac{1}{i\omega_n - \mu\omega_0} \qquad \mu = 0, \pm 1. \tag{5}$$

If one adds energy λ to each fermion, $\mu\omega_0 \to \mu\omega_0 + \lambda$, in equation (5). One obtains the diagrams shown in figure 4 in which the propagators A_1^0, A_0^0 and A_{-1}^0 are represented by full lines above, on or below the level of the phonon propagator respectively. Figures 4(*a*, *b*) correspond to figure 2(*a*), and figure 4(*c*) corresponds to figures 2(*b–e*).

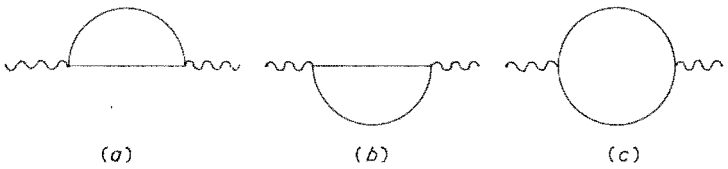

Figure 4. Diagrams for the Abrikosov formulation. Different orientations of the full line distinguish the A_μ^0 (see text).

Evaluating these but before having applied the limiting procedure of equation (1), we obtain

$$\begin{aligned} &\text{figures } 4(a, b): \quad \frac{\epsilon^2\omega_0^2\omega_k}{(i\omega_m)^2-\omega_0^2}U(\lambda) \\ &\text{figure } 4(c): \quad \frac{4\xi^2\epsilon^2\omega_0^2\omega_k}{(i\omega_m)^2-4\omega_0^2}U(\lambda) \end{aligned} \tag{6}$$

where $U(\lambda) = 1/[\exp(-\beta\omega_0)\exp(-\beta\lambda)+1] - 1/[\exp(\beta\omega_0)\exp(-\beta\lambda)+1]$. Applying the limiting procedure described in § 2 to the factor $U(\lambda)$ in equation (6), one obtains

$$Q(\omega_0) \equiv G_-(\omega_0)/Z(\omega_0) \tag{7}$$

precisely the factor obtained when the contributions from the diagrams and K factors in tables 2 and 3 are combined.

In § 5 we will explain why the method of § 4.3 (Abrikosov) is preferable to those of §§ 4.1 (drones) and 4.2 (quasi-spin). First we complete the derivation of the coupled-mode dispersion relation. Considering the second-order diagrams calculated as contributing to a self-energy $\Pi_k(i\omega_m)$

$$\mathscr{D}_k(i\omega_m) = \frac{1}{[\mathscr{D}_k^0(i\omega_m)]^{-1} - \Pi_k(i\omega_m)} \tag{8}$$

then $\mathscr{D}_k(i\omega_n)$ is given correct to second order. Thus, to second order,

$$\Pi_k(i\omega_m)=\epsilon^2\omega_0^2\omega_k Q(\omega_0)\left(\frac{1}{(i\omega_m)^2-\omega_0^2}+\frac{4\xi^2}{(i\omega_m)^2-4\omega_0^2}\right).$$

This is substituted into equation (8), $i\omega_m$ is analytically continued to ω, and then the poles are obtained by equating the denominator to zero. This gives

$$(x-y)(x-4)(x-1)-\epsilon^2 yQ(\omega_0)[(x-4)+4\xi^2(x-1)]=0 \tag{9}$$

where $x=(\omega/\omega_0)^2$, $y=(\omega_k/\omega_0)^2$. By obtaining the three roots of equation (9) for x as a function of y one obtains the dispersion curve for the coupled spins. In figure 5 curves are given for $\epsilon^2=0{\cdot}1$ and $\epsilon^2=0{\cdot}01$, with $\xi=1$ and with β chosen such that $Q(\omega_0)=1$.

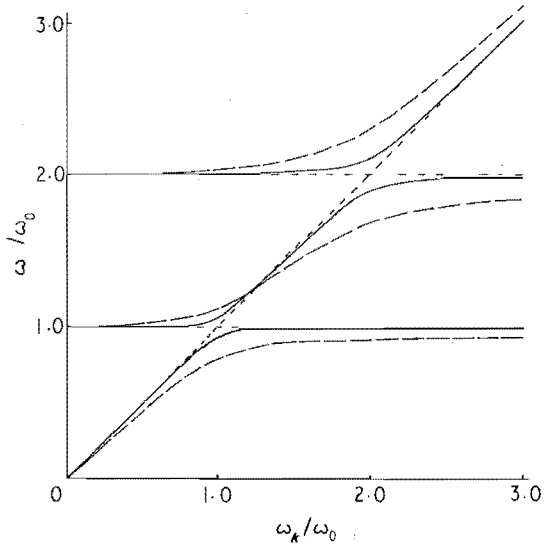

Figure 5. Coupled-mode dispersion relation for $S=1$, evaluated for two strengths of coupling. The full curve represents the solution for $\epsilon^2=0{\cdot}01$, and the broken curve for $\epsilon^2=0{\cdot}1$.

5. Comparison of techniques

The main advantage of using the Abrikosov technique is that, in the evaluation of figure 4(c), only one integration is required. The equivalent diagrams for drones and quasi-spin (figures 2(b–e)) require three nested integrations. For general S, the Abrikosov approach would yield $S(2S+1)$ diagrams, each requiring one integration; the drone or quasi-spin technique would give $2S$ diagrams, but a number of free integration variables ranging from 1 (for the first diagram) to $4S-1$ (for the last). The Abrikosov technique also avoids the necessity of differentiating the diagrams (and the K factors) in figures 2(b–e). If one took a perturbation linear in spin ($\xi=0$ in equation (3)) these comments would not apply, and the three methods would be comparable; however this choice of interaction is less realistic for general spin in the physical problems we have in mind.

The standard basis operator technique of Yang and Wang (1974) could be a serious competitor to the Abrikosov method at higher spin values. However, this method is much different in structure to the methods considered in this paper.

We conclude that although drones, quasi-spin and Abrikosov projection techniques are comparable for $S=\frac{1}{2}$, the first two methods quickly become intractable with increasing spin for realistic choices of the interaction Hamiltonian, and the advantages of the Abrikosov technique render it the most attractive method.

Acknowledgment

B J McKenzie is grateful to the New Zealand University Grants Committee for a Postgraduate Scholarship.

References

Abrikosov A A 1965 *Physics* **2** 5–20
Abrikosov A A, Gor'kov L P and Dzyaloshinskii I Y 1963 *Methods of Quantum Field Theory in Statistical Physics*, 2nd edn (Oxford: Pergamon Press)
Anderson P W 1958 *Phys. Rev.* **112** 1900–16
Barnes S E 1972 *J. Phys.* C: *Solid St. Phys.* **5** L178–80
Fidler F B and Tucker J W 1970 *Solid St. Commun.* **8** 2055–8
—— 1971 *J. Phys.* C: *Solid St. Phys.* **4** 2583–92
Judd B R 1967 *Second Quantization and Atomic Spectroscopy* (Baltimore: Johns Hopkins) p 41
Keiter H 1968 *Z. Phys.* **213** 466–81
—— 1971 *Phys. Lett.* **36A** 257
Lipkin H J 1965 *Lie Groups for Pedestrians* (Amsterdam: North Holland)
Mattis D C 1965 *Theory of Magnetism* (New York: Harper and Row)
Oppermann R 1973 *Z. Phys.* **259** 285–300
Schultz T D and Kwok P C 1972 *Phys. Lett.* **39A** 402–4
Spencer H J 1968 *Phys. Rev.* **167** 430–3
Toombs G A and Sheard F W 1973 *J. Phys.* C: *Solid St. Phys.* **6** 1467–88
Verwoerd W S 1974 *Phys. Rev.* B **10** 2868–82
Wybourne B G 1973 *Int. J. Quantum Chem.* **7** 1117–37
Yang D H and Wang Y 1974 *Phys. Rev.* B **10** 4714–23
Yolin E M 1965 *Proc. Phys. Soc.* **85** 759–65